Vibration Analysis of MR Fluid Sandwich Plates and Identification of Optimal MR Fluids Treatments

Mehdi Eshaghi

A Thesis

In the Department

of

Mechanical and Industrial Engineering

Presented in Partial Fulfillment of the Requirements

For the Degree of

Doctor of Philosophy (Mechanical Engineering) at

Concordia University

Montreal, Quebec, Canada

June 2015

CONCORDIA UNIVERSITY

School of Graduate Studies

This is to certify that the thesis was prepared

By :   **Mehdi Eshaghi**

Entitled: **Vibration Analysis of MR Fluid Sandwich Plates and Identification of Optimal MR Fluids Treatments**

and submitted in partial fulfilment of the requirements for the degree of

DOCTOR OF PHILOSOPHY (Mechanical Engineering)

complies with the regulations of the University and meets the accepted standards with respect to originality and quality.

Signed by the final examining committee:

_____	Chair
Dr. Yousef R.Shayan	
_____	External Examiner
Dr. Mehdi Ahmadian	
_____	External to Program
Dr. P. Pillay	
_____	Examiner
Dr. M. Packirisamy	
_____	Examiner
Dr. J. Dargahi	
_____	Co-supervisor
Dr. R. Sedaghati	
_____	Co-supervisor
Dr. S. Rakheja	

Approved by

              Dr. A. Dolatabadi, Graduate Program Director

June 29, 2015

              _____

              Dr. Robin A.L. Drew, Dean
              Faculty of Engineering & Computer Science

ii

ABSTRACT

Vibration Analysis of MR Fluid Sandwich Plates and Identification of Optimal MR Fluids Treatments

Mehdi Eshaghi, Ph.D.
Concordia University, 2015.

The MR fluids can change their rheological behavior rapidly and reversibly under an applied magnetic field. Due to their unique characteristics, these promising controllable fluids can be effectively utilized in devices and structures in a reliable and fail-safe manner to suppress vibration with minimal power requirement. While modeling of MR dampers and their integration in systems and structures to control vibration have been widely studied, there are relatively few studies on MR based sandwich structures. MR sandwich structures can provide better vibration control capability as their damping and stiffness characteristics can be simultaneously varied. Considering this, the main objectives of this dissertation are to develop accurate models to predict the vibration characteristics of MR based sandwich plates under varying magnetic field and also develop design optimization strategies to identify optimal MR fluids treatments.

MR fluids typically experience low shear strain in sandwich structures and thus they operate in pre-yield region and behave like visco-elastic materials. In this study, first MR fluids have been accurately characterized in pre-yield region. Particularly new frequency-magnetic flux dependent constitute models for both loss and storage moduli have been proposed. To accomplish this, an experiment is conducted on a sandwich beam structure with aluminum face layer and MR fluid as the core layer, under different magnetic field densities. The frequency response characteristics of the sandwich cantilevered beam are subsequently measured under harmonic base excitations. Dynamic responses of the structure are also obtained using the developed finite element (FE) model. The frequency and field dependent complex shear moduli of the MR fluids (MRF 132DG and MRF 122EG) are then identified by minimizing the error between natural frequency and damping parameters obtained by experiment and FE model. The validity of the proposed constitute

models is demonstrated by comparing the FE model results with the experimental data for a copper sandwich structure comprising the two MR fluids.

Next, the characterized MR fluids have been used as the core layer in the fully and partially treated sandwich plates. The goal is to predict the dynamic responses of the MR sandwich plates under different levels of magnetic field. To accomplish this, finite element and Ritz models based on the classical plate theory are formulated to obtain governing equations of motion of the multi-layer rectangular and circular sandwich plates fully and partially treated with MR fluids as the core layer under different boundary conditions. Extensive experimental studies have been conducted to validate the developed models. Then, the validated models have been effectively utilized to conduct comprehensive investigation on the effect of MR fluid properties, geometry of the face layers, thickness of the core layers and magnetic flux density on vibration suppression capability of the sandwich plate structures. Finally, an optimization problem is formulated based on genetic algorithm (GA) to identify optimal locations for the MR fluid treatments, resulting in maximum variations in the stiffness and damping of the structure, corresponding to the lower three modes of flexural vibration in response to the applied magnetic field. The effects of shear deformation on the vibration properties of fully and partially treated sandwich structures are discussed, comprehensively.

Dedication

This dissertation work is dedicated to my parents

for their endless love, support and encouragement

Acknowledgment

LIST OF CONTENT

CHAPTER 1

INTRODUCTION AND SCOPE OF THE DISSERTATION

CHAPTER 2

DYNAMIC CHARACTERISTICS AND CONTROL OF MR/ER SANDWICH STRUCTURES: A STATE-OF-THE ART REVIEW

CHAPTER 7

CONTRIBUTION, CONCLUSIONS AND FUTUR WORK

LIST OF FIGURES

LIST OF TABLES

Nomenclature

B	Magnetic flux density
CPT	Classical Plate Theory
CSR	Constant shear rate
CSS	Constant shear stress
E	Electric field strength
ER	Electro-Rheological
FG	Functionally graded
G'	Storage modulus
G''	Loss modulus
G^*	Complex shear modulus
G_r	Shear modulus of rubber
MR	Magneto-Rheological
MRE	Magneto-Rheological Elastomer
mT	Millitesla
Oe	Oersted
η	Loss factor
τ	Shear stress
γ	Shear strain
τ_y	Yield stress
μ	Fluid viscosity
rf_i	Natural frequency ratio
f_{io}	Natural frequency ratio at $E = 0$
η_d	Structural loss factor
ϕ	Mode shape vector
ν	Poisson's ratio
$\{\lambda\}$	Modal coordinate
ω	Natural frequency
ξ	Damping ratio
$\tilde{\tau}$	Shear stress amplitude
$\tilde{\gamma}$	Shear strain amplitude
φ	Phase difference between shear stress and shear strain
G_0	Linear shear modulus

CHAPTER 1

INTRODUCTION AND SCOPE OF THE DISSERTATION

1.1. Introduction

Effectiveness of solid viscoelastic materials in sandwich structures for control of vibration has been well-established, especially for their ease of application and low cost. These materials, however, exhibit superior vibration attenuation performance in a specific narrow range of frequency, due to their fixed damping properties. Alternatively, smart fluids/elastomers offer attractive potential for realizing vibration control over a wide frequency range since these can change their rheological properties in response to a controllable applied field. It has been reported that adaptive structures with active constrained layer damping (ACLD) and active control (AC) yield superior vibration attenuation performance compared to sandwich structures with passive constrained layer damping (PCLD) (Huang et al., 1996). The ACLD is generally achieved by replacing or supplementing the constraining layer with an actuator such as piezoceramic. Nearly 30% improvement in the vibration attenuation performance has been reported for a cantilever sandwich beam containing a smart elastomer as the core layer, where compared to that of the structure with a viscoelastic material (Nayak et al., 2011). Moreover, smart elastomer based structures also exhibit greater stability region under axial load compared to that of a sandwich beam with viscoelastic core layer.

Mgnetorheological (MR) fluids exhibit varying rheological properties (elasticity, plasticity and viscosity) from free-flowing condition to semi solid state rapidly and reversibly in response to an applied magnetic field. MR fluid is a suspension of micron sized ferromagnetic particles in a carrier fluid, which is generally a silicon oil. With the application of an external magnetic field, the suspended microscopic particles tend to align along the lines of the magnetic flux due to polarization. The resulting chains of particles restrict movement of fluid perpendicular to the flux direction and thereby yield higher apparent viscosity of the fluid. In the presence of a magnetic flux, the shear stress-strain properties of MR fluid may be described in two distinct regions, referred to as pre- and post-yield regions. In structural applications, the fluid generally remains in the pre-yield region, where it behaves viscoelastically. The shear stress is thus proportional to the

shear strain in terms of the complex shear modulus. The post-yield region, is generally the dominant operational mode for some MR devices such as MR dampers, clutches and brakes. MR elastomers (MRE) are another class of smart materials comprising of magnetic particles suspended in a matrix of foam like material, which prevents the particles to settle down. Hence, they show superior magnetic properties compare to that of MR fluids. The potential performance of MR elastomers has been widely explored analytically and experimentally for a range of applications such as sandwich beam structures (Zhou and Wang, 2005; Choi et al., 2008) and tunable vibration absorbers (Gandhi and Thompson, 1990; Ginder et al., 2001).

Electro-rheological fluids (ER) exhibit varying rheological properties under varying electric field. Conventionally, these materials are fabricated by suspending semiconducting solid particles in a dielectric carrier liquid. Although, functionality of the MR fluids subjected to the magnetic field and the ER fluids subjected to the electric field is similar to some extent, these fluids exhibit distinct characteristics which distinguish their performances and potential applications. For instance, MR fluids can provide greater changes in the rheological properties and higher yield stress in the presence of a magnetic field compared to the ER fluids subjected to an electric field. Weiss et al. (1993) reported that the shear yield stress of MR fluids may change from 2-3 kPa in the absence of magnetic field to 100 kPa under a magnetic field of 3000 Oe. On the other hand, the ER fluids show maximum shear yield stress of 5 kPa for an applied electrical field strength of $4 \, \text{kV mm}^{-1}$ (Weiss et al., 1994). Yalcintas and Dai (1999) reported that, for the same applied field strength and size of a typical sandwich beam structure, the shift in the natural frequencies of MR based beam were almost two times higher than those of the ER sandwich beam. Moreover, the ER fluids applications might be limited due to sedimentation of the solid particles, sensitivity to impurities and temperature, variations in the material response in electric-time conditions and requiring high voltage to exhibit variations in the rheological properties (Yalcintas and Dai, 1998, 1999). Yalcintas and Dai (1999) suggested MR fluids for vibration suppression of the structures under high applied frequency while ER materials were recommended for vibration suppression of the structures with low operational frequency.

The present study aims to characterize two types of MR fluids (MRF 122EG and MRF 132DG) in the pre-yield regime, particularly the frequency dependent loss and storage moduli as a function of the magnetic flux density. The characterized MR fluids are applied in the fully and partially

treated sandwich plates to identify dynamic responses of the MR sandwich plates under different levels of magnetic field. The dynamic responses of the sandwich plates are evaluated experimentally and analytically. Then, the effect of MR fluid properties, geometry of the face layers, thickness of the core layers and magnetic flux density on the vibration suppression capability of the sandwich plate structures are comprehensively investigated. Subsequently, the dynamic characteristics of sandwich plates partially treated with the MR fluids are studied, numerically and experimentally, considering different boundary conditions and intensities of the magnetic flux. Finally, an optimization problem is formulated based on genetic algorithm (GA) to seek optimal locations for the MR fluid treatments, which results in maximum variations in the natural frequency, loss factor and energy dissipation of the structures in response to magnetic field.

1.2. Motivation and Objectives

The reported studies on sandwich structures containing MR and ER fluids have employed widely different analytical and experiment methods for characterizing the fluids and dynamic responses of the adaptive structures. Although a few studies have presented the state-of-the-art developments in sandwich structures (Librescu and Hause, 2000), ER fluids applications (Stanway et al., 1996) and MR dampers (Wang and Liao, 2011), a similar review of developments in vibration analysis of multi-layered MR/ER structures could not be found. A critical review of studies reporting vibration analysis and control of MR and ER fluids sandwich structures including beam, plate, shell and panel structures, is thus considered vital to acquire the existing knowledge in the field and to identify the research gaps. .

While several studies have addressed characterization of MR fluids in the post yield region, only a few studies have attempted characterization in the pre-yield region (Mohammadi et al., 2010). Operation in the post-yield region tends to disrupt the motion of particles suspended in the carrier fluid. Considering that the MR fluid in sandwich structures generally functions within the pre-yield regime, an accurate characterization of the pre-yield properties of fluid is vital for the development of numerical models to accurately predict the response of MR based adaptive structures. The MR/ER fluids characterization methods are generally based on four primary methods, namely, the oscillatory shear strain, rheometery, treating MR sandwich beam as a SDOF system and the standardized test method described in ASTM E756. The rheometery and the oscillatory shear strain approaches typically cause the MR fluid to operate in the post-yield region,

while the method employing the MR sandwich beam as a SDOF system is considered more effective for relatively moderate magnetic flux density due to flexibility of the host structure. Moreover, such a model does not consider the effect of excitation frequency on the complex shear modulus. The standardized ASTM E756 method may also yield errors since it neglects contributions of viscoelastic properties of the sealant. Considering above, this research dissertation aims to develop a frequency-magnetic field dependent phenomenological model for accurate pre-yield characterization of MR fluids over a wide range of magnetic flux density (0-90 mT) and excitation frequency (10-500 Hz).

The reported studies in the field of adaptive structures have generally focused on ER- or MR-treated sandwich beams, while the studies on vibration behaviors of plates have been mostly limited to ER-treated sandwich plates. Only a few studies have investigated dynamic properties of MR sandwich plates. The experimentally measured characteristics of MR sandwich plates, in-particular, have not been reported. Considering this, the present research study also aims at conducting a comprehensive fundamental investigation on dynamic responses of rectangular and annular circular sandwich plates containing MR fluid through experiments and theory. Furthermore, it focuses on dynamic response analyses of partially treated MR sandwich plates and identifications of optimal treatment locations to achieve greater vibration attenuation.

Accordingly, the specific goals of this research dissertation can be summarized as follows:

(i) To conduct a comprehensive review of reported studies on applications of MR/ER fluids for realizing active and semi-active vibration suppression in sandwich structures;

(ii) To characterize MR fluids in the pre-yield regime, particularly the frequency dependent loss and storage moduli as a function of the magnetic flux density;

(iii) To investigate dynamic characteristics of rectangular sandwich plates containing MR fluid as the core layer, through experiments and finite element analyses;

(iv) To analyze vibration properties of multi-layered annular circular sandwich plates with a MR fluid layer, through experiments and Ritz method;

(v) To formulate a design optimization strategy for identifying optimal locations and sizes of MR fluid segments in the partially treated sandwich plates to maximize vibration suppression capability of the structure;

1.3. Organization of the Manuscript-Based Dissertation

This manuscript based dissertation has been compiled on the basis of requirements described in "Thesis Preparation and Thesis Examination Regulation" booklet of the School of graduate Studies at Concordia University. The dissertation includes seven chapters addressing the objectives illustrated in the previous sections. Chapter 1 presents an introduction to the dissertation research including motivations, objectives and organization of the dissertation. Chapters 2 to 6 present the state of the art review, formulation, methods and results of studies addressing MR fluid characterization, experimental and analytical methods, vibration properties of multi-layered MR-fluid plate structures and optimization for realizing optimal partially treated MR fluid structures. Finally the main conclusions of the dissertation research are summarized in chapter 7 together with recommendations for future work. The articles extracted from the dissertation research, which have been either published or submitted to peer-reviewed accredited journals and presented in Chapters 2 to 6, are summarized as below:

Chapter 2 presents the following article:

M. Eshaghi, R. Sedaghati, S. Rakheja. "Dynamic characteristics and control of MR/ER sandwich structures: A state-of-the-art review". *Journal of Intelligent Material Systems and Structures*, 2015.

This paper presents a comprehensive review of reported studies on applications of MR/ER fluids for realizing active and semi-active vibration suppression in sandwich structures. The review focuses on methods of characterizing the MR/ER fluids in the pre-yield region; magnetic/electric field-dependent phenomenological models describing the storage and loss moduli of fluids; experimental and analytical methods developed for vibration analysis of sandwich structures with MR/ER fluid treatments; analysis of structures with partial MR/ER fluids treatments and optimal treatment locations; and developments in control strategies for vibration suppression of MR/ER sandwich structures. The studies on dynamic responses of fully and partially treated MR/ER based sandwich beams, plates, shells and panels are also discussed, including the mathematical modeling methods and associated assumptions, methods of solutions, and experimental methods.

Chapter 3 presents following article:

M. Eshaghi, S. Rakheja, R. Sedaghati. "An accurate technique for pre-yield characterization of MR fluids". *Smart Materials and Structures*, 2014, 24: 65018-31.

This study concerns with characterization of two different types of magneto-rheological fluids (MR 122EG and MR 132DG) in the pre-yield region. A phenomenological model is proposed for characterizing complex shear moduli of the MR fluids as a function of both the magnetic flux density and the excitation frequency using experimental data acquired for both the fluids. The experiments were conducted with a sandwich beam structure with aluminum face layer and MR fluid as the core layer. A nearly uniform magnetic field was applied across the sandwich beam using two ceramic permanent magnet bars. The frequency response characteristics of the sandwich cantilevered beam were subsequently measured under harmonic excitations swept in the 0 to 500 Hz frequency range considering different densities of the applied magnetic flux, ranging from 0 to 90 mT. Dynamic responses of the structure were also obtained through analysis of a finite element (FE) model developed using the classical plate theory. The frequency and field dependent complex shear moduli of the two MR fluids were identified from both the experimental data and the FE model results. The validity of the proposed methodology is demonstrated by comparing the FE model results with the experimental data for a copper sandwich structure comprising the two MR fluids.

Chapter 4 presents the following article:

M. Eshaghi, R. Sedaghati, S. Rakheja. "The effect of magneto-rheological fluid on vibration suppression capability of adaptive sandwich plates: Experimental and finite element analysis". *Journal of Intelligent Material Systems and Structures*, 2015, Special Issue Article 1-16.

This paper presents an experimental and theoretical study of vibration analysis of a magneto-rheological (MR) fluid-based sandwich plates. Two sandwich plates consisting of polyethylene terephthalate (PET) face layers were fabricated with two different MR fluids (MRF 132DG and MRF 122EG) as the core layer and silicon rubber spacer as the sealant. The dynamic responses of the cantilever sandwich plate were experimentally characterized. A finite element model based on the Classical Plate Theory was formulated to obtain governing equations of motion of the multi-layer MR plate. The complex shear modulus of each MR fluid in the pre-yield region was described

6

by a phenomenological model as a function of the magnetic flux density and excitation frequency, as described in the previous chapter. The results clearly showed enhanced vibration suppression properties of the MR sandwich plate over a broad frequency range through variations in both the stiffness and damping under varying magnetic field density.

Chapter 5 presents the following article:

M. Eshaghi, R. Sedaghati, S. Rakheja. "Analytical and experimental free vibration analysis of multi-layer MR-fluid circular plates under varying magnetic flux". *Journal of Sound and Vibration*, 2015.

Free vibration characteristics of sandwich annular circular plates comprising magneto-rheological (MR) fluid as the core layer are evaluated analytically and experimentally. An analytical model of the sandwich annular plate was formulated using Ritz method based on the classical plate theory. The numerical analyses were performed to study the free vibration responses of the sandwich plate in terms of resonant frequencies and loss factors considering variations in the magnetic flux and boundary conditions. The experiments were conducted on a free-free sandwich circular plate comprising two PETG (Polyethylene Terephthalate Glycol) face layers constraining the MR fluid core layer. A hollow-core electromagnet was developed for inducing variable magnetic flux over the structure. The free vibration properties of the sandwich plate were measured using MEscop VES modal analyzer. The measured data were analyzed to determine natural frequencies of the MR sandwich plate under different levels of the magnetic flux, which were subsequently used to examine validity of the analytical model. Furthermore, the effects of plate parameters such as radius ratio and core layer thickness on the natural frequencies and damping of the structure were investigated. The results suggested that increasing the flexibility of the face layers and MR fluid volume yields more pronounced effect of magnetic flux on the structure stiffness properties.

Chapter 6 presents the following article:

M. Eshaghi, R. Sedaghati, S. Rakheja." Vibration analysis and optimal design of multi-layer plates partially treated with the MR fluid". *Mechanical Systems and Signal Processing*, 2015.

The vibration characteristics of a sandwich plate partially treated with the magnetorheological (MR) fluid are investigated numerically and experimentally considering different boundary conditions and intensities of the magnetic flux. A cantilevered sandwich plate consisting of an aluminum host layer with nine equal cavities for the MR fluid treatments and a constraining layer was fabricated for experimental characterizations and validations of the finite-element (FE) model. The dynamic responses of the untreated plate and the partially treated plate, where only one of the nine cavities in the core layer was filled with the MR fluid (MRF 132DG), were measured under harmonic excitation applied at the fixed support. The finite element model of the sandwich plate, developed using the classical plate theory considering the effect of slippage between the top and bottom layers of the structure, is verified using the experimental data. The validated FE model is subsequently used to investigate the effects of partial MR fluid treatments, magnetic flux intensity and boundary conditions on the dynamic response characteristics of the structure. The effect of shear deformation on the vibration properties of the MR sandwich plate is further highlighted. Finally, an optimization problem is formulated to identify optimal locations for the MR fluid treatments so as to maximize the variations in the natural frequencies and damping ratios in response to magnetic field. The solution of the optimization problem, attained using the genetic algorithm (GA) suggested that the MR fluid applied to locations with noticeable shear strain can maximize the stiffness variations and damping of the structure, irrespective of the boundary condition and the mode of vibration.

CHAPTER 2

DYNAMIC CHARACTERISTICS AND CONTROL OF MR/ER SANDWICH STRUCTURES: A STATE-OF-THE ART REVIEW

2.1. Introduction

During past four decades, applications of MR and ER fluids in adaptive sandwich structures have been widely studied, primarily for the purpose of vibration control. The rapid response time of controllable MR/ER fluids to an applied magnetic/electric field and reversible variations in their stiffness and damping properties have been the key motivations for adaptive structures applications. Vibration and control analysis of MR/ER sandwich structures necessitate accurate characterization of the core layer in the pre-yield region (Weiss et al., 1994). Operating in the post-yield region disrupts the particles suspended in the carrier fluid, which results in sedimentation of the particles. This phenomenon degrades the properties of the smart fluids. Weiss et al. (1994) reported 20-30% reduction in the storage modulus of the ER fluid, in the strain level of 1-10%, due to repetitive test on the adaptive structure. Moreover, Vaičaitis et al. (2008) reported that although ER materials reduce displacement amplitude of sandwich beams in the linear region significantly, they cannot effectively suppress nonlinear vibration of the structures in response to the applied electric field. While the MR/ER fluids were accurately characterized in the pre-yield region, they might be employed fully or partially in the adaptive structures. Partially treated MR or ER based sandwich structures may provide superior damping performance compared with the fully treated ones while having less weight (Yalcintas and Coulter, 1998; Rajamohan et al., 2010). Then, a control synthesis to achieve vibration suppression of the sandwich structures through application of a controlled magnetic/electric field might be formulated and applied to the structure. Although there are some review papers addressing the behavior of sandwich structures (Librescu and Hause, 2000), ER fluids applications (Stanway et al., 1996) and MR dampers (Wang and Liao, 2011), no study has been reported reviewing the articles on vibration and control analysis of the sandwich beam, plate, shell and panel structures incorporating MR/ER fluids as the core layer. This study summarizes and critically reviews the reported articles on characterization of magneto- and electro-rheological fluids in the pre-yield regime, particularly the frequency dependent loss and storage moduli as a function of the magnetic/electric field density, dynamic characteristics of

fully and partially treated adaptive sandwich structures containing controllable ER/MR fluids, optimization strategies and design of controller to realize vibration suppression of the structures corresponding to selected modes of vibration. A comprehensive review and comparison of the considered assumptions, mathematical modeling and methods of solution, experimental procedures and results presented in the literature are particularly emphasized.

2.2. Characterization of MR/ER fluids

The properties of MR/ER fluids strongly depend upon applied magnetic/electric field. In the absence of applied field, the suspended particles are randomly dispersed within the carrier fluid. The MR/ER fluid may thus be regarded as a Newtonian fluid, since it exhibits constant viscosity. Moreover, the fluid shows linear relationship between the stress and the strain rate at any point. In the presence of magnetic/electric field, the suspended particles align themselves in the direction of applied filed and restrict the motion of MR/ER fluid. The net effect is development of yield stress and apparent viscosity of the fluid. The MR/ER fluid in the presence of magnetic/electric field thus may not be regarded as a Newtonian fluid. In this case, shear stress-shear strain properties of the fluid may be investigated in two regions, referred to as pre-yield and post-yield regions. In the pre-yield region, MR/ER fluid behaves viscoelastically and shear stress and shear strain are proportional in terms of the complex modulus G^* given by (Li et al., 1999)

$$G^* = G' + iG''$$
(2.1)

where G' is the storage modulus, which determines average energy stored per unit volume of the material over a deformation cycle, and G'' is the loss modulus, which is defined as dissipated energy per unit volume of material in a deformation cycle (Rajamohan et al., 2010). The post-yield regime, generally, may be regarded as a dominant operational mode for some MR/ER devices such as dampers, clutches and brakes (Coulter et al., 1993). In the post-yield regime, the shear stress is typically described by the Herschel Bulkley equation (Wang and Gordaninejad, 1999):

$$\begin{cases} \tau = \tau_y + k|\partial u/\partial z|^n & |\tau| \geq \tau_y \\ \partial u/\partial z = 0 & |\tau| \leq \tau_y \end{cases}$$
(2.2)

where τ, τ_y, k and u denote shear stress, yield stress, plastic viscosity and velocity of the fluid, while the exponent n is a flow behavior index. As depicted in Figure 2.1, the above relation describes the Newtonian fluid, when $\tau_y = 0$ and $n=1$ and dynamic viscosity of the fluid is constant.

The Herschel Bulkley model reduces to the Bingham plastic model for *n*=1. The equation demonstrates shear thinning and shear thickening fluids, for *n*<1 and *n*>1, respectively.
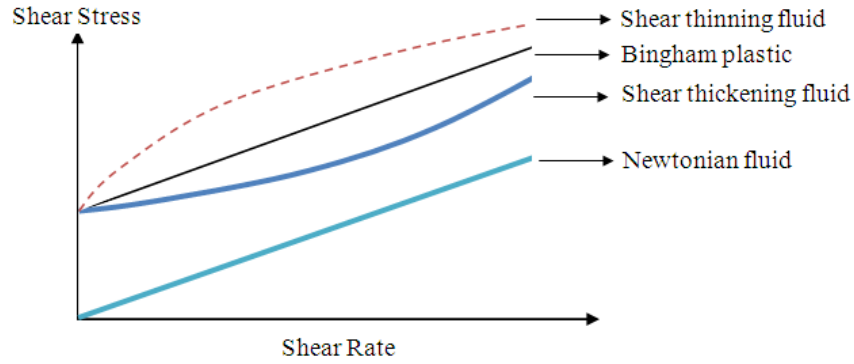
Figure 2.1 Shear stress variations of different fluids against shear rate

MR/ER fluids may be also subjected to oscillatory shear strain, $\gamma = \tilde{\gamma} \sin(\omega t)$, in some applications. The Fourier transformation technique is the most common method to characterize the behavior of the fluids under oscillatory shear in the pre- and post-yield regions. Based on this technique, the stress response under harmonic shear strain may be expressed as (Wilhelm, 2002):

$$\tau = \tilde{\gamma} \sum_{m=1,odd}^{\infty} \left[G'_m \sin(m\omega t) + G''_m \cos(m\omega t) \right] \tag{2.3}$$

where G'_m and G''_m are the *m*-th storage and loss moduli, respectively. It is worth noting that reversing the coordinate system does not change the stress response (Bird et al., 1987), thus only the odd harmonic terms are considered in Eq. (2.3). The first harmonic storage and loss moduli are represented in terms of the shear strain amplitude, $\tilde{\gamma}$, shear stress amplitude, $\tilde{\tau}$ and the phase difference φ between the shear stress and strain at the fundamental frequency, such that:

$$G'(\omega, field, \tilde{\tau}) = \frac{\tilde{\tau}}{\tilde{\gamma}} \cos(\varphi), \qquad G''(\omega, field, \tilde{\tau}) = \frac{\tilde{\tau}}{\tilde{\gamma}} \sin(\varphi) \tag{2.4}$$

where *field* denotes the magnetic flux density (MR fluid) or electric field strength (ER fluid). In the linear region, G'_1 and G''_1 are significantly higher than other coefficients and do not depend on the shear stress amplitude. The shear stress response may thus be expressed as:

$$\tau = \tilde{\gamma} \left(G'(\omega, field) \sin(\omega t) + G''(\omega, field) \cos(\omega t) \right) \tag{2.5}$$

2.2.1. Pre-yield Characterization of MR/ER fluids

The adaptive structures containing MR/ER fluids tend to work in the pre-yield region (Weiss et al., 1994). While the shear strain amplitude experienced by the MR/ER fluids is considered as an important factor which yields the fluids to operate in the pre- or post-yield region, the applied field strength can also change their operation regions. In fact, intensifying the applied field may cause the MR/ER fluids or elastomers to operate in the post-yield region (Hu et al., 2011).
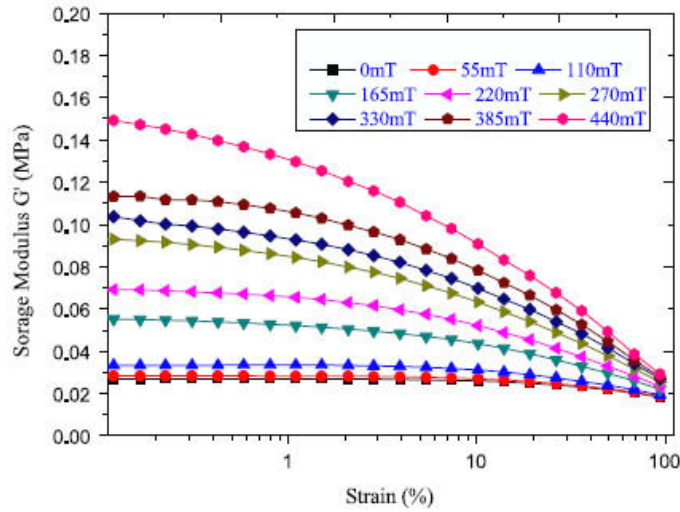
Figure 2.2 Variations in the storage modulus of MRE with shear strain amplitude, under different levels of magnetic flux density. (Hu et al., 2011)
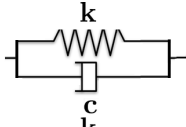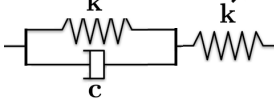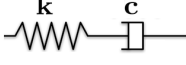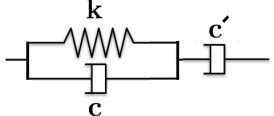
Hu et al. (2011) reported that in the low range of strain amplitude (less than 0.5%, which is near the yield strain of typical MR fluids) the storage modulus of a typical MR elastomer is nearly constant by increasing the strain rate, and the MR elastomer is in the linear (pre-yield) region. This was particularly more evident for magnetic flux density up to 110 mT. Increasing the magnetic flux density, however, caused the MR elastomer to work in the non-linear post-yield region, even in very low range of the shear strain amplitude, as depicted in Figure 2.2.

2.2.1.1. Viscoelastic models representing rheological properties of MR/ER fluids in the pre-yield region

Several models have been developed to identify the storage and loss moduli of the MR/ER fluids in terms of applied field and frequency. Depending on characteristics of these smart fluids, different phenomenological constitutive models have been employed to describe their rheological behavior in the pre-yield regime. It should be noted that, so far, no comprehensive model has been developed to describe pre-yield behavior of these smart fluids (Mohammadi et al., 2010). That is,

depending on the frequency range of interest, applied external field and properties of the smart fluid, different models should be employed to describe fluids behavior. Viscoelastic models are the most common models to account for rheological properties of the smart fluids in the pre-yield regime (Ghandi and Bullough, 2005). These models may be described as a combination of springs and viscous dashpots. Viscoelastic models are categorized into two main groups; that is, solid-like models and fluid-like models.

Table 2.1 Viscoelastic models employed for characterization of MR and ER fluids

Model	Configuration	Storage modulus	Loss modulus
Solid models			
Kelvin-Voight Solid		$G' = k$	$G'' = c\omega$
Three-parameter Solid		$G' = \dfrac{k'\left[(k+k')k+(c\omega)^2\right]}{(k+k')^2+(c\omega)^2}$	$G'' = \dfrac{k'^2 c\omega}{(k+k')^2+(c\omega)^2}$
Fluid models			
Maxwell Fluid		$G' = \dfrac{k(c\omega)^2}{k^2+(c\omega)^2}$	$G'' = \dfrac{k^2 c\omega}{k^2+(c\omega)^2}$
Three-parameter Fluid		$G' = \dfrac{k(c'\omega)^2}{k^2+\left((c+c')\omega\right)^2}$	$G'' = \dfrac{\left(k^2+(c+c')c\omega^2\right)c'\omega}{k^2+\left((c+c')\omega\right)^2}$

The most common solid-like models representing the pre-yield behavior of the MR/ER fluids are Kelvin-Voight Solid (Yen and Archon, 1991; Mohammadi et al., 2010; Sapiński et al., 2010) and Three-parameter Solid (Zener Element) models (Gamota and Filisco, 1991), while those of the fluid-like models are Maxwell Fluid (Sims et al., 2004) and Three-parameter Fluid models (Kamath and Wereley, 1997), as illustrated in Table 2.1. Recently, Li et al. (2010) developed a four-parameter model to illustrate viscoelastic properties of MR elastomers under harmonic loading. The storage and loss moduli of the model, which comprised of Three-parameter Solid model in parallel with a spring (k''), were expressed as:

$$G' = \frac{\left(k'k''+kk''+kk'\right)\left[(k+k')^2+c^2\omega^2\right]+c^2\omega^2 k'^2}{(k+k')\left[(k+k')^2+c^2\omega^2\right]}$$

$$G'' = \frac{c\omega k'^2}{\left[(k+k')^2+c^2\omega^2\right]}$$

(2.6)

In order to determine whether the solid or fluid models can identify pre-yield characteristics of a typical MR or ER fluid accurately, the experimental behavior of the fluid in terms of energy dissipation in a cycle of deformation (Yen and Archon, 1991), stress-strain hysteresis data (Tang and Conard, 1996), stress-strain response under constant strain rate amplitude (Sprecher et al.,1987) or variations in the storage and loss moduli with excitation frequency (Claracq et al., 2004) can be monitored and compared with those of the developed models. Yen and Archon (1991) investigated the loss and storage moduli of an ER fluid in the pre-yield regime, in the range of 1-100 Hz. Their experiment reported modest change in the storage modulus with frequency, which suggests solid type behavior of the ER fluid. In this case, the Kelvin-Voight solid model could describe complex shear modulus of the ER fluid, accurately. They also investigated pre- and post-yield behaviors of ER fluid under low and high amplitude oscillatory vibrations. Figure 2.3 illustrates the pre- and post-yield shear stress responses (solid lines) of the ER based device under oscillatory strain input (dashed line), conducted by Yen and Archon (1991). It was observed that under low amplitude strain, the stress-strain has a linear relation. However, increasing the strain amplitude leads the ER fluid into the post-yield region and stress response is nonlinear. Furthermore, the shear stress and strain responses are in phase, suggesting negligible damping and predominant elastic behavior of the ER fluid. Yen and Archon (1991) also observed linear variations in the dissipated energy per cycle of ER device with frequency, which again verified the validity of Kelvin-Voight Solid model to represent pre-yield characteristics of the ER fluid. It should be noted that in the Kelvin-Voight Solid model the dissipated energy per cycle varies linearly with the applied frequency.

(a) Pre-yield region   (b) Post-yield region
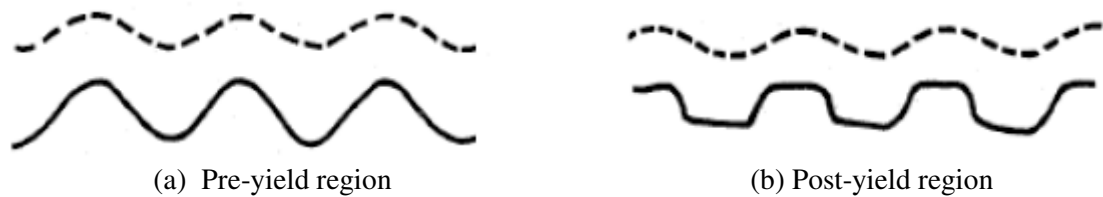
Figure 2.3 Pre- and post-yield shear stress responses (solid lines) of an ER based device under oscillatory strain input (dashed line). (Yen and Archon, 1991)

Claracq et al. (2004) employed a rheometer to determine variations in the loss and storage moduli of a typical MR fluid with frequency. The results suggested insignificant variations in the storage modulus with frequency while the loss modulus varied linearly. This behavior could be represented by Kelvin-Voight Solid model comprising of a strong spring in parallel with a weak

14

dashpot. Tang and Conard (1996) and Sprecher et al. (1987) used variations in the shear stress with shear strain to identify rheological behavior of MR and ER fluids, respectively, in terms of excitation frequency and applied field. Their findings showed linear variations in the shear stress with shear strain in the pre-yield region. In these studies, the rheological behaviors of the fluids suggested application of the solid models such as three-parameter model to represent the storage and loss moduli. Simes and Werely (2003) employed the Maxwell fluid model to characterize an ER fluid in the pre-yield regime. In the Maxwell model, the loss and storage moduli approach zero in small values of the excitation frequency, while in practice, the pre-yield region is an elastic region and stiffness never fades out. In order to compensate this error, they employed a bi-viscous element for the damper in the model. This model, however, was not a physical model and represented behavior of the fluid mathematically. Considering different aspects of solid and fluid models, Ghandi and Bullough (2005) suggested that the solid models are more appropriate to identify pre-yield characteristics of the MR/ER fluids.

2.2.1.2. The methods of characterizing MR/ER fluids in the pre-yield region

The MR/ER fluids characterization methods reported in the literature are generally based on four primary methods, namely, the oscillatory shear strain (Wilhem, 2002; Mohammadi and Sedaghati, 2012), rheometery (Sun et al., 2003; Mohammadi et al., 2010), treating MR sandwich beam as a SDOF system (Choi et al., 1990; Rajamohan et al., 2010) and standardized test method described in ASTM E756 (Choi et al., 1992; Leng et al., 1997; Allahverdizadeh et al., 2013). Review of the studies on characterization of the MR/ER fluids reveals that rheometers have been widely used to characterize the fluids in terms of frequency and applied field. These devices, which work in either oscillatory or rotational mode, comprise two parallel plates and the MR/ER fluids fill the gap between two the plates, as depicted in Figure 2.4.

(a)   (b)
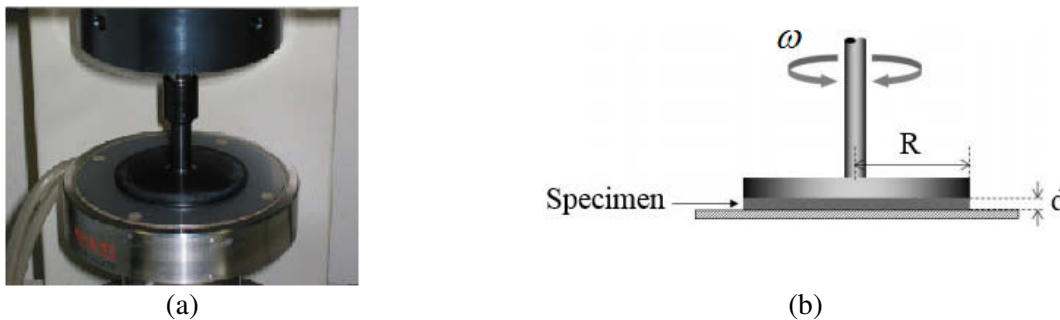
Figure 2.4 (a) Real image and (b) schematic diagram of a rotational rheometer (Murata, 2012).

15

In rotational mode, the lower plate is fixed and the upper one rotates and a sensor measures the torque and related external forces (Mohammadi et al., 2010). The fluid experiences a constant shear strain across the gap, while the strain varies with radial displacement. The pre-yield storage and loss moduli of the fluids are measured at the edge of the top plate (Hirunyapruk et al., 2010). In the oscillation mode, an oscillating plate connected to the shaker is placed between two parallel plates containing the MR/ER fluid. This symmetric arrangement prevents unwanted coupling between the in-plane and transverse motion of the central plate (Sun et al., 2003). Dynamic signal analyzer uses the measured central plate displacement and axial forces on the fixed plates to identify the storage and loss moduli of the fluids in terms of frequency and applied field (Mohammadi and Sedaghati, 2012). The measurements may be performed in two different modes, namely, amplitude sweep mode and frequency sweep mode (Mohammadi et al., 2010). The amplitude sweep test varies the amplitude of strain under constant excitation frequency to identify the maximum shear stress corresponding to linear behavior of the fluid. Then, frequency sweep test is employed to find the storage and loss moduli of the fluid in terms of frequency. It is worth noting that the frequency sweep test may be conducted in constant shear rate (CSR) or constant shear stress (CSS) modes (Mohammadi et al., 2010).

Application of sandwich structure as SDOF for pre-yield characterization of MR/ER fluids is preferable to the rheometer (Shiang and Coulter, 1996), which is due to smaller strain amplitude of the fluid in the sandwich structure compared to the rheometer. Choi et al. (1990) investigated free vibration of a hollow beam of polystyrene filled by ER fluid to find the complex shear modulus of the fluid. The composite beam was considered as a viscoelastic element and modeled as a single-degree-of-freedom system. Considering small thickness of polystyrene employed to fabricate hollow beam, the shear modulus of the structure was considered to be equal to that of the ER fluid. Employing free vibration analysis and obtaining the natural frequencies and logarithmic decrement of the structure, the loss and storage moduli of the fluid were obtained. The developed model, however, could not capture frequency dependent behaviors of the storage and loss moduli. Rajamohan et al. (2010) employed the same procedure on MR sandwich beam of aluminum face layers to characterize the fluid, but the effect of face layers was not taken into account. They designed an optimization problem to update the loss and storage moduli obtained from the experiment to achieve better agreement with experimental results, in terms of resonant frequencies.

ASTM E756 (ASTM, 2002) is a standard test for characterizing viscoelastic materials in the linear region. The standard employs cantilever sandwich beam to predict rheology of polymer materials sandwiched in the core layer. Choi et al. (1992) employed this standard to identify rheological behavior of the ER fluid. They outlined poor accuracy of the method for demonstrating rheological behavior of the sandwich beam structures with ER fluid. Their study suggested a decrease in the derived moduli of the composite beam with increase of the applied field. They related this anomalous behavior to deviation of beam deformation from the assumptions considered in the ASTM equations. Allahverdizadeh et al. (2013, 2013b) also employed this technique to characterize ER fluid in the pre-yield region. They reported that the standardized ASTM E756 method provides a rough estimation of the storage and loss moduli of the fluid and is not accurate, which is in part attributed to neglecting contribution due to the sealant. Furthermore, this method cannot capture frequency dependent behavior of the fluid and is more applicable for sandwich structures with solid viscoelastic materials as the core layer. Allahverdizadeh et al. (2013, 2013b, 2013c) suggested that the ASTM method should be accompanied by an optimization process to update and modify the extracted data. Consequently, they employed particle swarm optimization (PSO) technique to seek optimal storage modulus of the ER fluid by matching the resonant frequencies obtained by theory and experiment. Then, the optimum loss modulus was obtained by matching the theoretical resonance amplitudes with those of experiment.

2.2.1.3. Mathematical representation of the loss and storage moduli

It has been widely reported that the storage (G') and loss moduli (G'') of the MR/ER fluids, prior to saturation, can be described by quadratic functions in the magnetic flux density/electric field (*B/E*) (Choi et al., 1990; Mohammadi et al., 2010; Rajamohan et al., 2010, 2010b, 2010c; Allahverdizadeh et al., 2013b). This is attributed to rheological behaviors of the MR/ER fluids which depend on the dipole-dipole interactions. These interactions are proportional to the product of *B/E* and the dipole moment, *P*. The dipole moment is also proportional to *B/E* prior to the saturation of the MR/ER fluids; consequently, the rheological properties of the MR/ER fluids such as loss and storage moduli, and yield stress are quadratic functions of *B/E* (Choi et al., 1990). Mohammadi et al. (2010) identified rheological properties of two smart fluids including a ferromagnetic nano-particle fluid and a MR fluid using rheometer. In the frequency domain,

17

Kelvin-Voigt solid and the three-parameter fluid models were employed to represent the pre-yield behaviors of the ferromagnetic nano-particle and MR fluids, respectively. They also suggested quadratic polynomials to represent storage modulus of the fluids in terms of magnetic field strength. This model was developed for a limited range of frequency in which the storage modulus no longer depends on the excitation frequency. Since no value of magnetic field was found for which the loss modulus was independent of frequency, they could not present explicit functions representing the loss factors in terms of magnetic field density.

Ginder et al. (1995) reported that, although at very low levels of applied magnetic field the rheological properties of the MR fluid may be represented by a quadratic function in terms of magnetic field strength, at flux density above linear region but lower than what is needed for complete saturation of the MR fluid, the rheological properties of the fluid are proportional to $B^{3/2}$. The properties of the magnetically saturated MR fluid, however, do not depend on the magnetic flux density. Yalcintas and Dai (2004) and Mikhasev et al. (2011) proposed linear functions in terms of magnetic flux density to represent complex shear modulus of the MR fluids. Yanju et al. (2001) suggested Hyperbl functions $\left((aE)\big/(b+E)\right)$ to represent the storage and loss moduli of a typical ER fluid, where a and b were parameters related to the material and excitation frequency and E represented the electric field strength. Hirunyapruk et al. (2010) proposed two exponential functions to identify the storage modulus and loss factor of a typical MR fluid (MRF 140CG) in the pre-yield region. The frequency independent equations, which predicted the storage modulus and loss factor up to magnetic saturation, were expressed as:

$$G' = G'_z + (G'_\infty - G'_z)\left(1 - e^{-\alpha_1 B^{\alpha_2}}\right)$$
$$\eta = \eta_\infty + (\eta_z - \eta_\infty)e^{-\alpha_3 B^{\alpha_4}}$$

(2.7)

where G' and η represent the storage modulus and loss factor, respectively. $\alpha_1, \alpha_2, \alpha_3, \alpha_4, G'_z, G'_\infty, \eta_z, \eta_\infty$ are the empirical constants identified by fitting the models to the experimental data. Figure 2.5 illustrates variations in the storage modulus and loss factor of the fluid with the magnetic flux density (Hirunyapruk et al., 2010). The experimental results obtained by rheometer were shown by bullet points while those obtained by the developed model were depicted by solid lines. The results suggest saturation of the fluid around 250 mT. Furthermore, the storage modulus and loss factor indicate quadratic variations with the magnetic flux density, in the pre-saturation region.
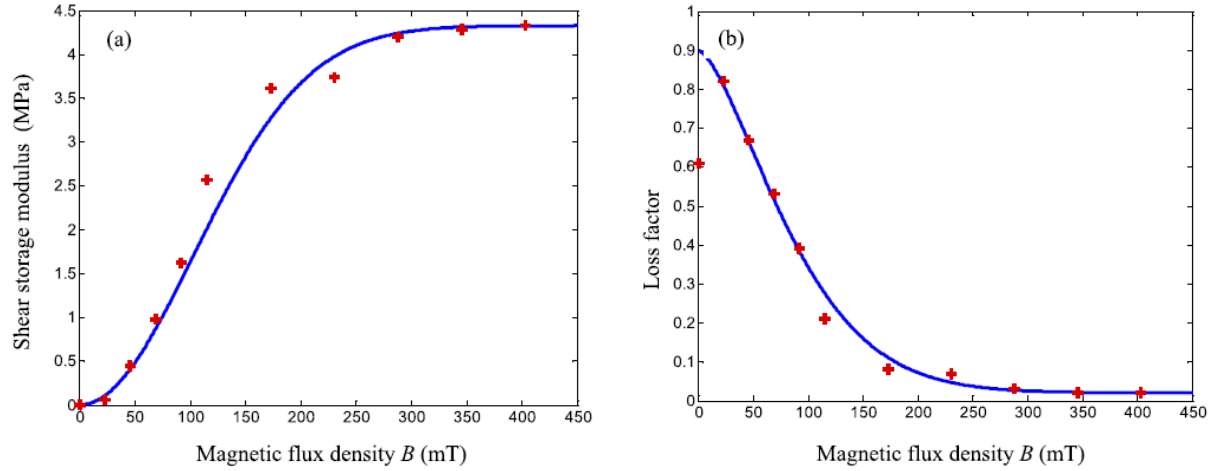
Figure 2.5 Variations in the (a) shear storage modulus and (b) loss factor of MRF 140CG with magnetic flux density. Measurement (+) and empirical models (-) (Hirunyapruk et al., 2010).

Equivalent linearized complex moduli of the ER/MR fluids may be employed to represent the fluids behavior in the post-yield region (Lee, 1995; Lee and Cheng, 1998; Allahverdizadeh et al., 2014). The experiments conducted by Stevens et al. (1987) suggested a constitutive relationship for the ER fluid under quasi-static shearing as:

$$\tau = G_0 \gamma \left(1 - e^{-(\gamma_0 / \gamma)}\right) + \mu \dot{\gamma} \qquad (2.8)$$

where τ and γ denote shear stress and shear strain, respectively. G_0 represents linear shear modulus of infinitesimal shear strain. γ_0, which is a model parameter, and G_0 are electric field dependent functions and normally represented in a quadratic form (Lee and Cheng, 2000; Allahverdizadeh et al., 2013b, 2014). It should be noted that the shear stress due to viscosity of the fluid, μ, was much lower than that of the exponential function, thus the effect of viscosity neglected from the equation (Lee, 1995; Allahverdizadeh et al., 2013b). In order to obtain the pre-yield equivalent moduli at different amplitude of strain, the hysteresis loop of ER fluid under sinusoidal strain excitation was constructed. The linear equivalent storage and loss moduli of the ER fluid in cyclic loading were obtained to yield the same strain energy and dissipated energy of the fluid. Having found the equivalent pre-yield storage and loss moduli of the fluid, the viscoelastic models could be employed to investigate dynamic responses of ER/MR sandwich structures (Lee, 1995; Allahverdizadeh et al., 2013b). It is worth noting that the pre-yield behavior of MR/ER fluids may be predicted using post-yield characterization of these fluids. Choi et al. (1992) and Mohammadi and Sedaghati (2012) extrapolated the post-yield characteristics of ER

19

fluid to identify pre-yield properties. Genc and Phule (2002) conducted the same analysis for the MR fluids.

2.3. Dynamic characteristics of fully treated MR/ER sandwich beam structures

2.3.1. Fabrication and experimental study

The concept of sandwich structures containing ER and MR fluids as the core layer were introduced in the patents issued by Carlson et al. (1990) and Weiss et al. (1996), respectively. The primary studies on dynamic characteristics of MR/ER sandwich structures were conducted on the multi-layer sandwich beam, which was due to its relatively simple mechanical model (Lara-Prieto et al., 2010). Furthermore, the experimental studies on MR/ER sandwich beam structures have been mostly conducted on the cantilever sandwich beams (Gandhi et al., 1989; Chen et al., 1994; Don and Coulter, 1995; Berg et al., 1996; Phani and Venkatraman, 2003, 2005; Rajamohan et al., 2010, 2010b, 2010c; Wei et al., 2011) although some studies on clamped-clamped (Haiqing and King, 1997) and simply supported structures (Yalcintas and Coulter, 1995; Yalcintas et al., 1995; Lee and Cheng, 1998; Sun et al., 2003) have also been reported. The MR/ER sandwich beam, as depicted in Figure 2.6, consists of two elastic layers, MR/ER fluid core layer and spacer, which provides a gap between face layers and prevent fluid from leakage. It is worth noting that Qiu et al. (1999) conducted an experiment on five-layer sandwich structure comprising of three elastic and two ER core layers to increase the effect of fluid in vibration suppression.

Figure 2.6 Sketch of a sandwich beam structure (Lara-Prieto et al., 2010)

2.3.1.1. Face layers

Review of literature shows that the elastic layers employed in the MR sandwich structures were typically chosen from aluminum strips (Yalcintas and Dai, 1999, 2004; Sun et al., 2003; Yeh and

Shih, 2006; Zhou et al., 2006; Sapiński and Snamina, 2009; Bishay et al., 2010; Rajamohan et al., 2010, 2010b, 2010c; Lara-Prieto et al., 2010; Hu et al., 2011; Joshi, 2012). It is attributed to low damping properties and relatively high stiffness of aluminum compared to that of the MR fluid. Furthermore, relative magnetic permeability of aluminum is equal to one, which ensures uniform distribution of the magnetic field applied to the structure (Sun et al., 2003). The face layer materials, however, have no effect on uniformity of the electric field applied to the core layer of ER sandwich structures; hence different materials such as aluminum (Choi et al., 1992, Don and Coulter, 1995; Yalcintas and Coulter, 1995b; Shiang and Coulter, 1996; Wei et al., 2011), steel (Berg et al., 1996; Haiqing and King, 1997; Phani and Venkatraman, 2003), polystyrene (Choi et al., 1992) and FGM (Allahverdizadeh et al., 2013) have been employed to fabricate the ER based sandwich structures. MR sandwich beams also could employ some other materials such as conductive (Nayak et al., 2010; Choi et al., 2010) and polyethylene based materials (Hirunyapruk et al., 2010; Lara-Prieto et al., 2010) as the face layers. Hirunyapruk et al. (2010) and Lara-Prieto et al. (2010) utilized non-metallic materials of perspex and polyethylene (PET) as the elastic layers, respectively. These materials were transparent and ensured that no bubble were left within the fluid during the fabrication process (Lara-Prieto et al., 2010). Joshi (2012) fabricated an adaptive structure consist of a cantilever hollow pipe of stainless steel which encompassed inner wooden layer and an embedded layer of MR fluid. Due to rigidity of the structure, the MR fluid was not subjected to significant shear deformation; hence no noticeable variations in the dynamic responses of the structure was reported, in response to the applied magnetic field.

Choi et al. (2010) employed steel skins and MRE as the core layer to fabricate an adaptive sandwich beam. They investigated the effect of steel skin face layers on disturbing homogeneity of the magnetic flux applied to the structure. The results illustrate that the sandwich beam with thick steel skins induces higher value of magnetic field than that with thin steel face layer, under the same external conditions. Furthermore, under dynamic deformation of conductive skins, motion-induced eddy current is generated on the face layers so that the magnetic field closed to the face layers is disturbed and magneto-elastic load is applied to the face layers (Zhou and Wang, 2006b). The magneto-elastic load consists of Lorenz body force and the surface force caused by the Maxwell's stress applied on the surface of the conductive skins. However, the results suggest insignificant effect of magneto-elastic loads on the dynamic properties of the sandwich beam. It should be noted that the bulk magnetic permeability of the MR fluids is in the range of 3-9, which

is significantly lower than that of steel (around 500). Therefore, the magneto-elastic force applied to the MR fluid has no significant effect on the vibration analysis of the MR based sandwich structures (Zhou and Wang, 2006b).

2.3.1.2. Sealant and spacer

In order to maintain uniform gap between face layers and contain the fluid as the core layer, spacer and sealant are required to adhere around the edges. To this purpose, applications of plastic spacer (Sun et al., 2003; Wei et al., 2008), silicon rubber (Choi et al., 1992; Yalcintas and Coulter, 1995; Berg et al., 1996; Allahverdizadeh et al., 2013, 2014), latex materials (Don and Coulter, 1995; Shiang and Coulter, 1996), polycarbonate (Yalcintas et al., 1995; Don and Coulter, 1995; Shiang and Coulter, 1996), perspex (Phani and Venkatraman, 2003, 2005) and Buna-N rubber (Rajamohan et al., 2010, 2010b, 2010c) have been widely reported in the literature, which is due to flexibility and oil resistance properties of these materials. Bishay et al. (2010) employed aluminum frame to provide a uniform gap between the face layers of MR based sandwich beam. The high flexural rigidity of the aluminum frame prevented the structure to experience significant shear deformation in the core layer; hence the effect of MR fluid on the dynamic characteristics of the structure was insignificant, in response to applied magnetic field. Application of PET frame and tape for sealing the MR fluid have also been reported by Lara-Prieto et al. (2010) and Hirunyapruk et al. (2010), respectively. Some studies have considered the effect of the sealant and spacer in the mathematical modeling (Lee, 1995; Kang et al., 2001; Rajamohan et al., 2010, 2010b, 2010c; Bishay et al., 2010; Allahverdizadeh et al., 2013, 2014). They employed rule-of-mixture to account for the effect of silicon rubber on the complex shear modulus of the core layer. Based on rule-of-mixture, the homogenized complex shear modulus of the middle layer can be expressed as:

$$\bar{G} = G_r \left(\frac{b_r}{b} \right) + G^* \left(1 - \frac{b_r}{b} \right) \tag{2.9}$$

where G_r and G^* are the shear moduli of the rubber and fluid, respectively, while b_r and b are the associated widths of the rubber and sandwich beam, respectively. The material properties of the rubber may be provided by experiment (Lee and Cheng, 1998) or supplier (Rajamohan et al., 2010).

2.3.1.3. Applying magnetic/electric field over MR/ER sandwich structures

While application of magnetic field over MR sandwich structure was accompanied with some complexities which limited maximum applied field and coverage area, the electric field over ER sandwich structures could be provided easily. The face layers of ER sandwich structures served as the electrodes for the applied electric field through high-voltage power supply (Choi et al., 1993, 1994; Wei et al., 2007, 2011). The maximum electric field strength reported in the literature is in order of 4 kV mm^{-1}. A thorough review of the reported studies shows that the permanent magnets were widely used to generate magnetic flux over the MR sandwich structures. Different intensities of the magnetic field were realized by varying the vertical position of the permanent magnets with respect to the sandwich structure. The vast majority of the reported studies using permanent magnets with MR sandwich beam structures have considered substantially low field density, well below the magnetic saturation of the fluids (around 700 mT). Rajamohan et al. (2010, 2010b, 2010c) characterized the fluid properties and evaluated responses of an MR sandwich beam under the field up to 50 mT. Joshi (2012), Yalcintas and Dai (1999, 2004), Sun et al. (2003), Bishay et al. (2010) and Hu et al. (2011) conducted similar studies with fields up to 55 mT, 70 mT, 90 mT, 100 mT and 100 mT, respectively. It is very difficult to achieve a uniform field density of higher magnitude with permanent magnets, partly due to limited clearance between the structure and the magnets, although it would be possible to realize a stronger field locally at some points on the structure. Choi et al. (2010) and Lara-Prieto et al. (2010) used somewhat higher field density in the order of 300 and 320 mT, respectively. The magnetic flux distributions over the structures in these two studies were non-homogenous, which was attributed to the usage of several magnets to generate the magnetic flux. In these studies, the magnets were located inside aluminum housings at top and bottom of the MR beam. Since the magnets located in each housing had the same polarity, they repelled each other resulting in gaps between the magnets and thereby non-homogenous magnetic field. Hirunyapruk et al. (2010) employed electromagnet to generate a local magnetic flux of 205 mT over small portion of a tunable MR-filled beam-like vibration absorber.

2.3.1.4. The experiment methods

Three main experiments have been conducted to characterize dynamic responses of the MR/ER multi-layer beam structures in terms of natural frequency and damping properties: free vibration (Gandhi et al., 1989; Choi et al, 1990; Leng et al., 1997; Lara-Prieto et al., 2010; Rajamohan et al.,

2010; Joshi, 2012), impact hammer (Lu and Li, 2007; Lara-Prieto et al., 2010) and shaker excitation (Zhou and Li, 2003; Sun et al., 2003; Hirunyapruk et al., 2010; Bishay et al., 2010; Choi et al., 2010; Rajamohan et al., 2010, 2010b, 2010c; Joshi, 2012; Allahverdizadeh et al., 2013, 2014). Lara-Prieto et al. (2010) employed three mentioned methods to investigated dynamic responses of MR sandwich beam. Their results suggest that although the applied force in each case was different and the structure vibrated at different amplitudes, the acquired natural frequencies of the structure were almost the same. Furthermore, pure forces could not be applied to the structure without any interaction between the exciter and structure. In other words, the mass and stiffness effects of the hammer tip and shaker attachment caused some discrepancies between theoretical and experimental results. The acceleration responses of the MR/ER sandwich structures were measured by accelerometers mounted on the face layers. Although single-axis accelerometers were widely used to measure vibration responses of the structures (Rajamohan et al., 2010, 2010b, 2010c; Allahverdizadeh et al., 2013, 2014), application of laser sensors (Choi et al., 2010) and eddy current probe (Lee and Cheng, 1998; Wei et al., 2007, 2011) for measuring vibration displacement and laser vibrometer (Lara-Prieto et al., 2010) for measuring velocity have also been reported. The measured signals were analyzed in the signal analyzer and the natural frequencies and damping properties of the sandwich beam structures were subsequently identified from the peaks in the frequency response functions. Figure 2.7 shows schematic of a typical experimental setup up representing shaker excitation of a cantilever MR sandwich beam.
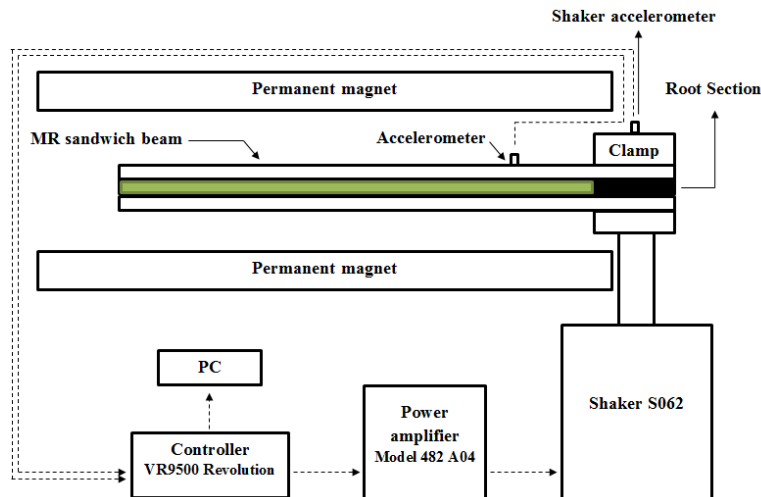
Figure 2.7 Schematic experimental setup conducting based vibration excitation on MR sandwich beam

2.3.2. Mathematical modeling

In the view of viscoelastic behavior of MR/ER fluids in the pre-yield region, all the models demonstrating vibration characteristics of viscoelastic sandwich structures are also potentially applicable to MR/ER adaptive structures. The first model, demonstrating dynamic responses of viscoelastic sandwich structures, was proposed by Rose et al. (1959). This model, which is known as RKU, is based on a modified Euler-Bernoulli beam equation and was expressed as:

$$m(x)\frac{\partial^2 w}{\partial t^2} + \frac{\partial^2}{\partial x^2}\left(EI\frac{\partial^2 w}{\partial x^2} \right) = 0 \tag{2.10}$$

where $m(x)$ is the mass per unit length and *EI* denotes the flexural rigidity of the structure, which is presented in terms of material properties and geometry of the viscoelastic sandwich beam. DiTaranto et al. (1965) presented a sixth order differential equation to characterize governing equations of motion of a three-layer viscoelastic beam structure. Subsequently, Mead and Markus (1969, 1970) modified the DiTaranto model and took the effects of beam transverse inertia into account. Furthermore, in contrast to DiTaranto model, which was applicable to simply supported boundary condition under special class of forced vibration, the Mead and Markus (MM) model could investigate the sandwich structures under different geometry boundary conditions. The MM model can be expressed as:

$$\frac{\partial^6 w}{\partial x^6} - g(1+Y)\frac{\partial^4 w}{\partial x^4} + \frac{m(x)}{EI}\left(\frac{\partial^4 w}{\partial x^2 \partial t^2} - g\frac{\partial^2 w}{\partial t^2} \right) = \frac{1}{EI}\left(\frac{\partial^2 q(x,t)}{\partial x^2} - gq(x,t) \right) \tag{2.11}$$

where $m(x)$ is the mass per unit length and *g, Y* and *EI* are defined based on geometry and material properties of the sandwich beam. $q(x,t)$ also represents the harmonic loading over the sandwich structure.

Coulter et al. (1989) and Coulter and Duclos (1990) employed RKU model to investigate dynamic responses of ER sandwich beam structures. Application of DiTaranto and MM models for characterizing vibration behavior of the MR/ER based sandwich beams have also been widely reported (Yalcintas and Coulter, 1995, 1995c, 1998; Yalcintas and Dai, 1999; Yeh and Shih, 2005; Hu et al., 2006). Mahjoob et al. (1993) provided a comparison between the results obtained by RKU and MM models and those of the experiment on an ER based sandwich beam. They suggested more realistic dynamic behavior of the structure predicted by MM model. It is worth

noting that since these models have been developed for viscoelastic materials, they might show some inaccuracies in the analysis of MR/ER fluid structures. For instance, Coulter and Duclos, (1989) conducted an experiment on ER sandwich structure and realized that application of RKU underestimates both modal frequencies and damping of the structure. They attributed this discrepancy to deviation between the theoretical assumptions and the experimental model. Don and Coulter (1995) suggested that the RKU and MM models can adequately predict dynamic behavior of ER based adaptive structure, if the core layer thickness is uniform and strain in the sandwiched layer is uninhibited.

Finite element method is the most reported approach in vibration analysis of the MR/ER sandwich structures (Lee, 1995; Zhou et al., 2006; Rezaeepazhand and Pahlavan, 2008; Bishay et al., 2010; Hirunyapruk et al., 2010; Rajamohan et al., 2010, 2010b, 2010c, 2013; Wei et al., 2011; Allahverdizadeh et al., 2012, 2013, 2013b, 2014; Nayak et al., 2012; Mohanty, 2013). Furthermore, application of Hamilton energy method (Sun et al., 2003;Yeh et al, 2004; Chen and Hansen, 2005; Rezaeepazhand and Pahlavan, 2008; Choi et al., 2010; Dwivedy and Srinivas, 2011) and Ritz method (Rajamohan et al., 2010, 2010b, 2010c; Rajamohan and Ramamoorthy, 2012) have been widely reported. The solutions assumed that the normal stress in the core layer was neglected which was due to negligible Young's modulus of the MR fluid compared to the elastic layers. The fluid layer thickness was assumed to be very small compared to its length and the slippage between the elastic and fluid layers was neglected. The shear strain and stress components in the elastic layers were considered to be negligible and CPT assumptions were applicable which was due to very small thickness of the elastic layers compared to the length of the beam. The transverse displacement through the structure was considered uniform and the damping due to elastic layers was also assumed to be negligible (Yalcintas and Dai, 1999, 2004; Sun et al., 2003; Rajamohan et al., 2010, 2010b, 2010c; Bishay et al., 2010).

Some studies however have not implemented aforementioned assumptions and modeled the sandwich structures with less simplifications. Choi et al. (2010) employed higher order sandwich beam theory and assumed that the applied load could change thickness of the core layer and core layer cross section may not remain planar. Nayak et al. (2012) presented a vibration analysis on the MR sandwich beam using two different assumptions and compared the results. In the first case, the classical theory was employed and only the potential energy due to shear deformation of the

26

core layer was considered. In the second case, higher order theory was used to derive governing equations of motion of the structure and in addition to shear deformation, the potential energy due to transverse and axial deformations in the core layer was considered. The results suggested an insignificant increase in the stiffness and damping properties of the structure under second assumptions compared to those of the first assumptions. Furthermore, the response amplitudes in the second case were found to be less than that of the classical plate theory. Allahverdizadeh et al. (2013c) suggested that the fourth natural frequency of an ER sandwich beam, obtained by Timoshenko and Euler–Bernoulli theories, showed 3 and 16% deviation from the experiment, respectively, when the thickness ratio (thickness to length) of the face layers increased up to 0.1.

2.3.3. Observations and findings

2.3.3.1. The effect of applied field on the natural frequencies of MR/ER sandwich beams

The reported studies on the dynamic responses of MR/ER multi-layer sandwich beams suggest increase in the natural frequencies of the structures with increasing the magnetic/electric field. This phenomenon, which was reported in several studies (Choi et al., 1989, 1989b, 1989c; Choi and Park, 1994; Yalcintas and Coulter, 1995, 1995b, 1995c; Yeh and Shih, 2005; Rajamohan et al., 2010, 2010b, 2010c; Sepehrinour and Nezami, 2012; Allahverdizadeh et al., 2012, 2013, 2013b, 2014) can be attributed to increase in the complex shear modulus of the MR/ER fluids with increasing the applied field. However, few studies (Bishay et al., 2010; Choi et al., 2010; Lara-Prieto et al., 2010; Hu et al., 2011) reported decrease in the natural frequencies of the MR based sandwich beam structures with increase of the applied magnetic field. Bishay et al. (2010) believed that drop in the natural frequencies was attributed to the damping effect of MR fluid which was higher than its stiffness effect. Choi et al. (2010) reported that decrease in the natural frequencies was due to the magnetic preload. The magnetic preload increased flexibility of the sandwich structure and decreased the natural frequencies (Yin et al., 2006). Lara-Prieto et al. (2010) illustrated that shifting to the lower frequencies in response to increasing the applied magnetic field was attributed to non-uniform magnetic field over the structure, which would also lead to non-uniform concentration of the magnetic particles and stiffening effect of the MR fluid along the sandwich beam. However, the last justification seems more realistic, since no study has reported decrease in the natural frequencies of fully treated ER sandwich beam in response to

increasing the electric field which might be attributed to uniform electric field applied to the ER based structures.

The variations in the natural frequencies of ER sandwich structures subjected to an electric field are less significant than those of the MR based structures in response to the magnetic field (Yalcintas and Dai, 1999). Some studies reported insignificant variations in the resonant frequencies of ER sandwich structures in response to the electric field (Wei et al, 2007; Rezaeepazhand and Pahlavan, 2008). Based on the study conducted by Phani and Venkatraman (2005), although ER fluid filled beam with starch particle concentration of 30% showed no significant variations in the resonant frequencies, in response to the applied electric field, a linear relationship between these two items could be observed in an ER based sandwich beam with 40% starch particle concentration. It is widely reported that variations in the resonant frequencies of MR/ER based sandwich beam structures with applied magnetic/electric field are almost linear (Coulter and Duclos, 1990; Choi et al., 1992; Rajamohan et al., 2011; Allahverdizadeh et al., 2013b). Don and Coulter (1995) announced that although experimental results indicated linear variations in the resonant frequencies of ER sandwich beam with respect to the applied electric field, the theoretical results showed a parabolic relationship. They believed that linear resonance-electric relationship reported in the experiment was due to overfilling of the core layer. Lu and Li (2007) proposed an exponential function to relate the resonant frequencies of ER based sandwich beam to the applied electric field as:

$$rf_i = rf_o + Ae^{E/t} \tag{2.12}$$

where $rf_i = f_i / f_{io}$ represents the ratio of ith natural frequency of the sandwich beam under electric field of E to that of the structure with no electric filed, f_{io}. rf_o, A and t are regression coefficients.

2.3.3.2. *The effect of applied field on the loss factors and deflection of MR/ER sandwich beams*

Damping properties of adaptive sandwich structures have been widely studied in terms of loss factor (Yalcintas and Dai, 1999, 2004; Sun et al., 2003; Yeh and Shih, 2006, 2006b; Bishay, 2010; Choi et al., 2010; Rajamohan et al., 2010, 2010b, 2010c, 2013; Nayak et al., 2010, 2012, 2012b). The loss factor is defined as the ratio of imaginary to real component of complex eigenvalues (Sun et al., 2003; Rajamohan et al., 2010). The loss factor relates to the dissipated energy as proportion of the stored energy of a material per radian. Although qualitative trend of variations in the natural

frequencies of MR/ER sandwich structures in response to the magnetic/electric field is predictable, the structural loss factors exhibit different behaviors. Variations in the loss factors of MR/ER sandwich beam structures under magnetic/electric field depend on both the loss and storage moduli of the fluids. Depending on behaviors of these moduli, the structural loss factor may be subject of decrease (Haiqing et al., 1993; Yalcintas and Coulter, 1995b, 1995c) or increase (Choi et al., 1992; Yalcintas and Coulter, 1995c; Wei et al., 2007) with increasing the applied field. In addition to the fluid moduli, the excitation frequency and beam geometry significantly contribute in variations in the loss factor of the structures under applied field. Lara-Prieto et al. (2010) reported 41% increase in the damping ratio of a MR based sandwich beam with PET face layers, while the applied magnetic field reached up to 110 mT. The study conducted by Joshi (2012) suggested 59% increase in the damping ratio of a MR multi-layer beam structure with aluminum elastic layers while the magnetic flux density increased from 30 to 55 mT. The more significant increase in damping of aluminum sandwich structure compared to PET one might be attributed to negligible damping of aluminum face layers, while in PET sandwich beam the face layers contributed in damping properties of the structure, significantly. Therefore, application of magnetic field caused more significant variations in the damping of AL sandwich beam compared to PET one.

It is widely reported that the loss factors corresponding to lower modes of MR/ER based sandwich structures increase with increasing the applied field and this trend is reversed as the applied field increases further (Haiqing et al., 1993; Yalcintas and Coulter, 1995c; Rajamohan et al., 2010; Allahverdizadeh et al., 2012). This might be attributed to variations in the storage modulus and loss modulus of MR/ER fluids with magnetic/electric field. Li et al. (2005) employed rheometer to investigate pre-yield dynamic properties of a typical MR fluid under different levels of magnetic flux. They identified four field-induced regions, I, II, III and IV, in the system. These regions were defined by three values of critical magnetic flux density, Bc_1, Bc_2 and Bc_3, as depicted in Figure 2.8. In the first region the fluid, which was subjected to very low magnetic flux, exhibited Newtonian behavior and experienced coexisting of particles and random chains. The storage modulus was almost constant, while the loss factor increased slightly with magnetic flux. The storage modulus and loss factor increased significantly in the second region in which the MR fluid was a mixture of chains and random clusters. In the third region the fluid experienced coexisting of the clusters and chains and the storage modulus and loss factor sharply increased and decreased, respectively. The last region contained saturated MR fluid and rheological properties of the fluid

showed no variation with the applied magnetic field. In this region the particle chains formed stable clusters in direction of applied magnetic field. These four regions may interpret variations in the storage modulus and loss factor of the MR/ER sandwich structures with respect to applied field.
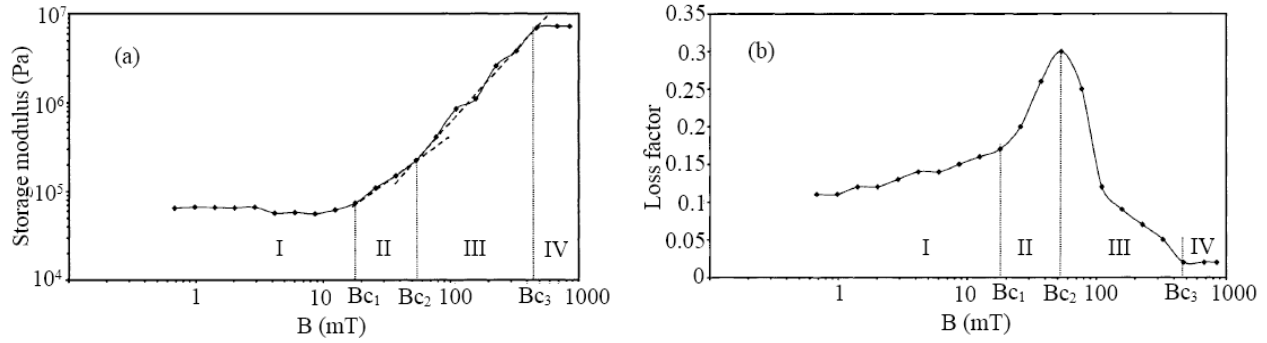
Figure 2.8 Variations in the (a) storage modulus (Pa) and (b) loss factor of a typical MR fluid with magnetic flux density (Li et al., 2005).

The adjustable stiffness and damping properties of MR/ER fluids enables adaptive sandwich structures to suppress unwanted vibration and decrease instability (Tylikowski, 2002; Dwivedy and Srinivas, 2008). Hu et al. (2006) suggested significant decrease in the displacement amplitude and notable rightward shift in the resonant frequencies of MR based sandwich beam structures, in response to the applied magnetic field. Both the stiffness and damping of the sandwich structures could be substantially varied by varying the applied magnetic field. The monotonic decrease in the displacement amplitude could be directly attributed to increase in both the stiffness and damping of the structure with increasing magnetic field. It has been also reported that higher magnetic flux reduces sharpness of the peaks in frequency response function of the structure, which is attributed to increase in the damping of the sandwich beam (Sun et al., 2003). Ying and Ni (2009) employed a cantilever sandwich beam with MR elastomer core and supplemental mass under stochastic support motion excitation to model a smart composite wall with floor and equipment. The results show significant effect of the core layer in minimizing the velocity response of the sandwich beam.

2.3.3.3. The effects of different parameters on dynamic responses of MR/ER sandwich beams

Irrespective of applied magnetic/electric field, some other parameters such as material and thickness of the face layers (Choi et al, 1992; Rezaeepazhand and Pahlavan, 2008; Allahverdizadeh et al., 2012, 2013b, 2014), fluid thickness (Yeh et al., 2004; Rezaeepazhand and Pahlavan, 2008; Mohanty 2013), boundary conditions (Yalcintas and Coulter 1995, 1995b, 1995c; Lee and Cheng

1998; Allahverdizadeh et al., 2013b), external disturbances (Wei et al., 2007; Allahverdizadeh et al., 2012), modes of vibration (Yalcintas and Coulter 1995; Lu and Li, 2007) and temperature (Gandhi et al., 1989) may also change the natural frequencies, loss factors and vibration amplitude of the MR/ER based sandwich structures. Yeh and Shih (2005) suggested an increase in the loss factor of the ER sandwich structures with core layer thickness. The study of Rezaeepazhand and Pahlavan (2008) showed that increasing the core layer thickness increased the settling time in transient response of the sandwich beam structure, which was attributed to increasing mass of the structure and decreasing the shear deformation in the core layer. This behavior might be attributed to low applied electric field employed in the study. It is worth noting that, irrespective of boundary condition, the region of instability for the MR/ER sandwich beam under axial load starts at a higher frequency compared with the untreated structure (Dwivedy et al., 2009; Dwivedy and Srinivas, 2011; Nayak et al., 2012b). It should be noted that, in these studies the structure was subjected to an axial load consisting of constant static and harmonic variable loads. Furthermore, increasing MR/ER core layer thickness may increase critical dynamic loading of the sandwich structures (Yeh et al., 2004; Yeh and Shih, 2005; Yeh and Shih, 2006, 2006b; Dwivedy et al., 2009; Dwivedy and Srinivas, 2011; Nayak et al., 2012b; Tabassian and Rezaeepazhand, 2011, 2013). The instability region decreases with application of the static magnetic field over the structure (Yeh and Shih, 2006, 2006b; Nayak et al., 2012b).

Allahverdizadeh et al. (2012) investigated the effect of face layer materials on dynamic characteristics of ER sandwich beam. They conducted a vibration analysis on the rotating ER sandwich beam with face layers of functionally graded (FG) material, which was a mixture of ceramic and metal. Their study showed that increasing the FGM volume fraction index at constant rotating speed decreased (increased) the natural frequencies (loss factors) of the structure. It was attributed to lower stiffness of the metallic part compared to ceramic component. In fact, increasing the FGM volume fraction enhanced contribution of metallic part in face layer material and decreased stiffness of the structure. They also reported an increase and decrease in the natural frequencies and loss factors of the structure, respectively, as the rotating speed increased. This was also reported by Rajamohan (2013) and Rajamohan and Natarajan (2012) for rotating MR sandwich beam structures. Wei et al. (2006, 2007) related this phenomenon to increasing stiffness of the sandwich beam and instability of the suspended particles at higher rotor speed. It is worth noting that the vibration suppression capability of rotating ER fluid decreases by increasing the

rotational speed, while it is not affected by rotating acceleration (Wei et al., 2007). The schematic and real image of a rotating ER fluid is shown in Figure 2.9. Yalcintas and Coulter (1995) investigated the effect of geometry boundary condition on the natural frequencies and loss factors of ER sandwich beam and realized that the higher constrained boundary conditions elevated the natural frequencies and reduced the loss factors of the structure, which was due to small shear deformation experienced by the core layer. The similar results were also reported for MR sandwich beam by Rajamohan et al. (2010).

<div align="center">(a)   (b)</div>
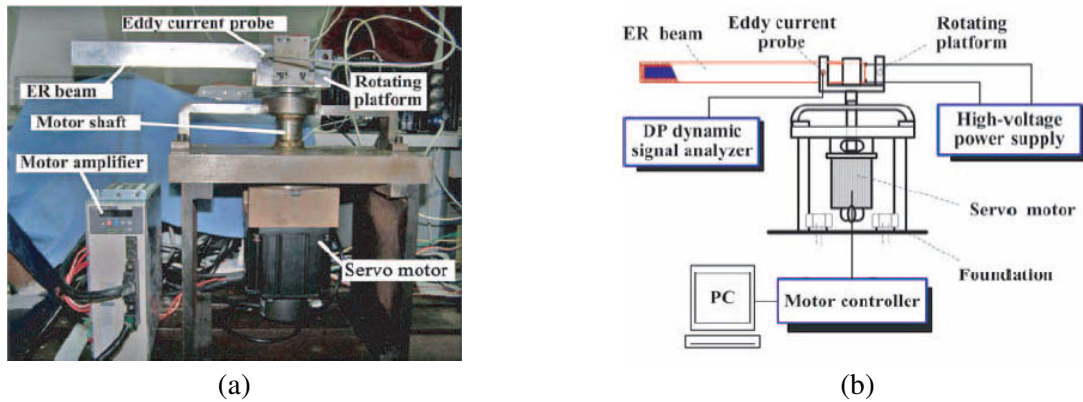
Figure 2.9 (a) Real image and (b) schematic diagram of a rotating ER fluid (Wei et al., 2007)

Choi et al. (2010) illustrated frequency dependent behavior in the loss factors of a MRE sandwich beam, experimentally and theoretically. They suggested relatively stronger influence of excitation frequency on the loss factors, under low level of magnetic flux density compared to that of higher magnetic flux. This might be attributed to relatively stronger adhesion of magnetic particles under the higher magnetic flux, where the vibration frequency effect became less significant (Li et al., 1999). Yalcintas and Dai (1999) reported a decrement in the loss factors of a MR based sandwich structure with increasing the mode numbers. It was believed that the loss factor reduction was attributed to low shear deformation of the structure in higher frequencies. The results presented by Yalcintas and Coulter (1995b), however, show some exceptions in the clamped-free ER sandwich beam so that the loss factors corresponding to the first two modes were smaller than those of other modes. They attributed it to the mode shapes of the sandwich beam structure. The wavelength of clamped-free sandwich beam corresponding to the first mode was smaller than those of the other end conditions, which resulted in reducing the shear deformation of the core layer. It is widely reported that the loss factors corresponding to lower modes of MR/ER based sandwich structures increase initially with the excitation frequency and then decrease as the

32

excitation frequency increases further (Yalcintas and Coulter, 1995b, 1995c). The dynamic responses of ER sandwich structures is also highly temperature dependent. Gandhi et al. (1989) outlined less significant increment of the resonant frequencies and damping ratios of ER sandwich beam with respect to the applied electric field at higher temperature, which was attributed to adverse effect of the temperature on electro-viscous phenomenon of the ER fluids.

2.3.3.4. Non-linear analysis of MR/ER sandwich beam structures

While most of the studies on dynamic characteristics of MR/ER sandwich structures assumed the core layer to operate in the pre-yield region, the non-linear behaviors of the MR/ER sandwich structures have also been reported. (Lee and Cheng, 1998; Qiu et al., 1999; Phani and Venkatraman, 2005; Rezaeepazhand and Pahlavan, 2008; Allahverdizadeh et al., 2014). Lee and Cheng (1998) showed that the effect of applied electric field on the non-linear natural frequencies and loss factors of the ER sandwich structure decreased with increasing the vibration amplitude. Phani and Venkatraman (2005) suggested a decrease in the loss factors of ER sandwich beam with vibration amplitude, in the non-linear region. They believed that the inverse relation between the loss factor and vibration amplitude indicated coulomb friction type of damping in the core layer. Rezaeepazhand and Pahlavan (2008) employed Bingham model to investigate transient response of a sandwich beam with ER core layer in the post-yield regime. Their results showed negligible contribution of the viscous damping component of the core layer in the damping properties of the structure, compared to the damping component associated with applying electric field (coulomb damping). Allahverdizadeh et al. (2014) compared dynamic characteristics of an ER sandwich beam assuming ER fluid in the pre- and post-yield regions. They reported an increase in the non-linear frequency ratio ($\omega_{non-linear}/\omega_{linear}$) of the ER sandwich beam with increasing vibration amplitude, while the structure was under electric field of 2 kV mm^{-1}. They attributed this trend to typical hardening behavior of the structure in large vibration amplitude. Furthermore, they suggested a decrease in the loss factor ratio of the structure by increasing the vibration amplitude, which was due to the smaller force required to break chains of dielectric particles in the ER fluid. Their study showed that the non-linear frequency or loss factor ratios were not equal to one, even at very low range of vibration amplitude. This verifies non-linear behavior of MR/ER fluids under high magnetic/electric field, irrespective of shear strain amplitude.
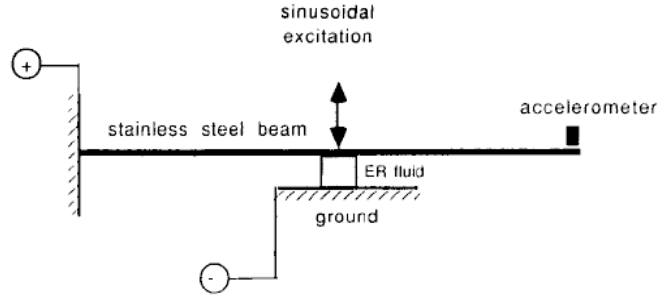
Figure 2.10 ER fluid as complex spring applied to a cantilever beam (Haiqing et al., 1993)

Haiqing et al. (1993) employed ER fluid as a complex spring under a cantilever beam, as depicted in Figure 2.10. The results showed that increasing the applied electric field increased the stiffness and damping properties of the structure in non-linear fashion so that the frequency response function curve changed its shape in different amplitudes of excitation force. This study illustrated that vibration characteristics of ER based sandwich structure could be considered to be linear in very low (E=0 kV mm^{-1}) and high (E=5 kV mm^{-1}) electric field strengths, while behavior of the system was non-linear at medium range of electric field (E=3 kV mm^{-1}). They related the non-linearity to simultaneous contributions of the pre-yield and post-yield deformations on the system vibration. Phani and Venkatraman (2005) outlined that the linear behavior of the structure in low electric field strength indicates dominate contribution of the elastic face layers in the flexural dynamics relative to the ER fluid core layer.

2.3.3.5. Disagreements between the theoretical and experimental results

In the study of MR/ER sandwich beam structures some discrepancies between theoretical and experimental results may be observed. Don and Coulter (1995) attributed discrepancy of the results to overfilling of the core layer. Their study on ER sandwich beam showed that overfilling increased mass of the structure and reduced the effective electric field, which was due to increase in the sandwiched layer spacing. Furthermore, they found that extensive testing caused the liquid component of the ER material to seep through corners of the structure and increase the volume fraction of particles suspended in the fluid which resulted in changing rheological behavior of the fluid in response to the electric field. Lee and Cheng (1998) considered complexities in accurate modeling of the boundary condition as a source of error in their study. Several studies have considered inaccurate characterization of MR/ER fluids as a source of error in the experimental studies (Coulter and Duclos, 1990; Coulter et al., 1989; Don, 1993; Yalcintas and Coulter, 1995b).

Yalcintas and Dai (2004) related the disagreement between theory and experiment to neglecting the effect of sealant in the mathematical modeling, non-uniformity of magnetic/electric field and additional unwanted constraints existing in the experimental setup. The sealant increases the stiffness and damping of the structure. Choi et al. (2010) attributed the discrepancies to coupling between the sandwich beam and the test rig, bonding between skin and core layers and possible non-linearity in the sandwiched layer.

The study conducted by Sun et al. (2003) on MR sandwich beam involved significant disagreement between the theoretical and experimental results. This deviation was more noticeable, when the structure vibrated in the low vibrational modes. They believed that deviation of the results might be attributed to different layouts of the sandwich beam in the experiment and theory. In the theoretical analysis, it was assumed that, the structure was placed between two permanent magnets horizontally. In the experiment, in order to eliminate the effect of bending of the beam due to its weight, the structure was placed perpendicularly between permanent magnets. Figure 2.11 shows the horizontal and vertical configurations of MR sandwich beams. Yalcintas and Dai (2004) and Lara-Prieto et al. (2010) have also addressed the concerns regarding horizontal position of the MR sandwich structure. Wei et al. (2007) employed ER fluid to attenuate vibrations of the robot arm for IC packaging. They modelled the arm as a rotating sandwich beam containing ER fluid. Their study revealed that although there was a qualitative agreement between theoretical and experimental results, the predicted resonant frequencies and loss factors were higher and lower than experimental results, respectively. They attributed these differences to fabrication of the test beam and inaccuracies in the boundary conditions. Although theory assumes uniform thickness of three layers, it was not achievable in the experiment due to bending of the elastic layers and non-uniform adjustments of the sealant material.

(a)   (b)

Figure 2.11 (a) Horizontal and (b) vertical positions of MR sandwich beam (Lara-Prieto et al., 2010)

2.4. Dynamic characteristics of fully treated MR/ER sandwich plates and shells

2.4.1. MR/ER sandwich plates with rectangular face layers

Compared to multi-layer MR/ER beam structures, fewer studies have been reported on sandwich plates containing MR/ER fluids as the core layer. The studies on vibration behavior of sandwich plates have been mostly limited to ER treated ones (Coulter et al., 1993c; 1993b; Yeh and Chen, 2004, 2005; Rezaeepazhand and Pahlavan, 2008b) and very few studies have investigated dynamic properties of MR sandwich plates (Pranoto et al., 2004; Ying et al., 2012, 2014; Yeh, 2013). So far no experimental study has been reported on the vibration analysis of MR based sandwich plates, which is perhaps due to various challenges associated with providing a uniform magnetic flux over the structure. Review of literature shows that appropriate applications of MR/ER core layers increase controllability (Cho et al., 2005) and stability (Rahiminasab and Rezaeepazhand, 2013) and decrease vibration amplitude (Hasheminejad and Maleki, 2009) of the sandwich plates, remarkably. Rahiminasab and Rezaeepazhand (2013) employed ER fluid to change flutter boundaries of sandwich structures. They reported significant effect of ER core layer on aerodynamic stability of the sandwich plates. In fact, application of electric field caused flutter to occur at higher aerodynamic pressure, which was mostly attributed to increasing stiffness of the structure. The similar study was conducted by Hasheminejad and Motaaleghi (2014) to investigate active flutter suppression of sandwich shell containing ER fluid, under axial supersonic gas flow.

2.4.1.1. Fabrication and experimental study

MR/ER sandwich plate, as depicted in Figure 2.12, comprises of base layer, sealant spacer, constraining layer and MR/ER fluid as the core layer. Similar to sandwich beam structures, aluminum was widely used as the face layers of multi-layer MR/ER plates (Oyadiji, 1996; Choi, 2000; Choi et al., 2001). Although the two face layers were mostly chosen from the same material, Choi et al. (1999) contained ER fluid between the composite laminate and aluminum as the base and constraining layers, respectively. Aluminum can serve as the electrodes for the applied electric field through high-voltage power supply (Choi et al., 1999). Cho et al. (2005) and Lu and Meng (2006) employed glass–epoxy laminate as the face layers and a copper-clad laminate as electrode to provide electric field over the structure.
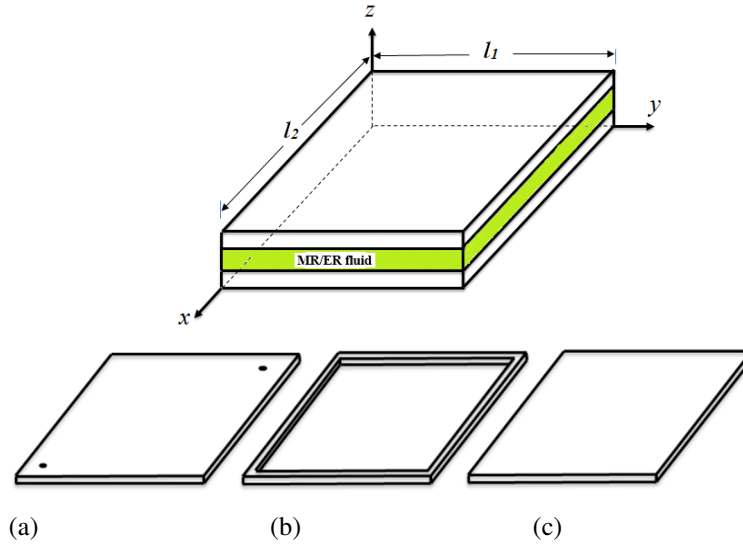
Figure 2.12 A sandwich plate with MR/ER fluid core layer consisting of (a) constraining top layer, (b) sealant spacer, (c) base layer

Silicon rubber has been used in the sandwich plates to serve three purposes. It provided a gap between two face layers, sealed the ER fluid and served as an electrical insulator for ER sandwich plates (Choi et al., 1999, 2001; Choi, 2000; Cho et al., 2005). The forced vibration conducted on the sandwich plate has been mainly performed using shaker excitation (Oyadiji 1996; Choi et al., 1999; Choi, 2000) and impact hammer test (Kim et al., 1992; Cho et al., 2005). Lu and Meng (2006) conducted two experiments (laser holographic interference experiment and modal testing) to identify dynamic responses of an ER based sandwich plate. They reported some discrepancies between the results obtained by two the methods, which was attributed to poor fixing situation in the frequency response test. In general, the experimental studies on ER sandwich plates show disagreement with theoretical results, to some extent. Choi et al. (1999) attributed the minor discrepancy between experiment and theory to neglecting the effects of fixture, silicone rubber spacer and the thin aluminum or copper foils employed for electrodes in the finite element model.

2.4.1.2. Mathematical modeling

The assumptions employed in the analysis of adaptive sandwich beams (no slippage between the layers, uniform transverse displacement through the thickness and negligible normal stress and transverse shear strain in the core and face layers, respectively) are also applicable for the analysis of the MR/ER plate structures (Choi et al., 1999; Lu and Meng, 2006; Narayana and Ganesan, 2007; Hasheminejad and Maleki, 2009). Due to small thickness ratio of the face layers, classical

plate theory was widely employed to identify displacement field in the face layers (Yeh and Chen, 2004, 2005, 2007; Hasheminejad and Maleki, 2009). The displacement profile of the core layer was also obtained using compatibility conditions of three layers. Application of finite element method has been extensively reported to derive governing equations of motion of MR/ER sandwich plates under different geometry boundary conditions (Cho et al., 2005; Lu and Meng, 2006; Yeh et al., 2009; Yeh, 2007b, 2010, 2011). Hasheminejad and Maleki (2009) developed an exact closed form solution to identify dynamic responses of an ER sandwich plate. The solution was only applicable for simply supported structures.

Developing theoretical model representing dynamic characteristics of adaptive sandwich plates requires accurate characterization of MR/ER fluids contained in the core layer. Cho et al. (2005) and Choi et al. (1999) employed rheometer to characterize ER fluids employed in the sandwich ER plate structures. Choi (2000) adopted the model developed by Choi et al. (1990), which was based on treating cantilever beam as a single-degree-of-freedom system, to analyze ER sandwich plate. The ER models developed by Don (1993) and Yalcintas and Coulter (1995c) have been widely used to identify the complex shear modulus of ER fluids employed in the core layer of the sandwich plates (Hasheminejad and Maleki, 2009; Yeh and Chen, 2004, 2005, 2006, 2007). Yeh (2013) utilized the quadratic functions proposed by Rajamohan et al. (2010) to investigate dynamic characteristics of MR sandwich plate.

2.4.1.3. Dynamic responses of MR/ER sandwich plates

The studies on MR/ER sandwich plates suggest an increase in the resonant frequencies of the structures with increasing the applied magnetic/electric field (Choi et al., 1999, 2001; Cho et al., 2005; Yeh 2007, 2007b, 2013; Hasheminejad and Maleki, 2009). In particular, the effect of applied field strength on the lower modes resonant frequencies were more pronounced compared to those of the higher modes (Hasheminejad and Maleki, 2009). While the natural frequencies of the MR/ER based sandwich plates increase with applied magnetic/electric field, variations in the loss factors with respect to the applied field do not follow the same trend. Figure 2.13(a) shows that, similar to sandwich beams, the loss factor of ER sandwich plates increase at low electric field strength, reach a peak at intermediate field magnitude, and subsequently decrease as the field strength is further enhanced (Hasheminejad and Maleki, 2009). This behavior has also been reported for MR sandwich plate (Yeh, 2013).
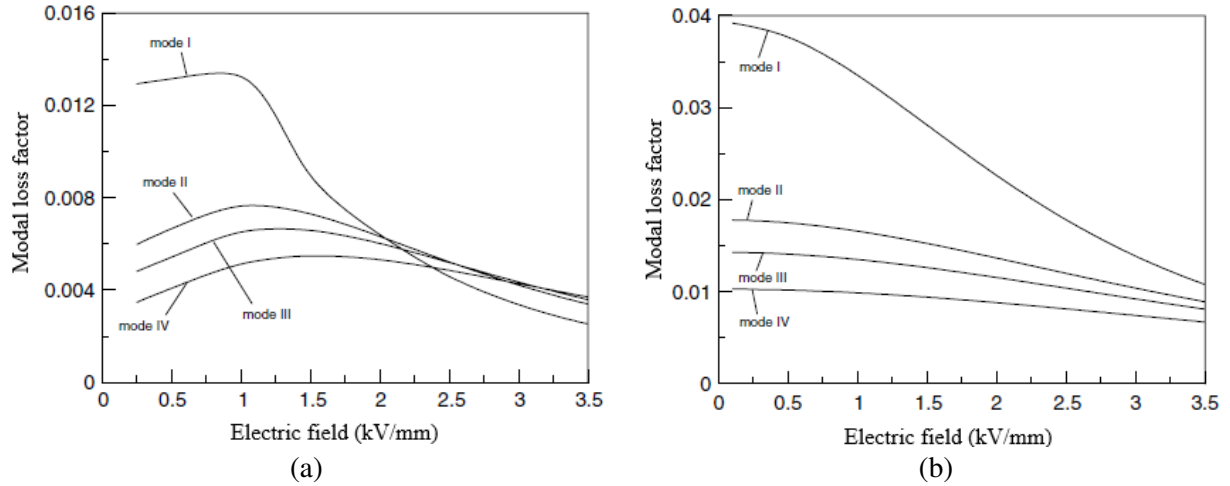
Figure 2.13 Variations in modal loss factors corresponding to lower four modes of a sandwich plate with two different ER fluids (a & b) (Yeh and Chen, 2007)

The loss factor peak may shift to the higher or lower magnetic/electric field amplitude in the structures with different face or core layer thicknesses, aspect ratios, MR/ER fluids and excitation frequencies. For instance, Hasheminejad and Maleki (2009) illustrated that higher aspect ratio of an ER based sandwich plate shifted the loss factor peak to the higher electric field magnitudes. Yeh and Chen (2007) observed a drop in the loss factor of ER plate as the electric field increased, as depicted in Figure 2.13(b). In this case the loss factor peak shifted to low electric field strength. It is worth noting that although it is expected that application of magnetic/electric field over the MR/ER sandwich plates always enhances the stiffness and damping properties of the structures and suppress undesired vibration, Hasheminejad and Maleki (2009) concluded that applying an electric field does not necessarily lead to improving vibration response of an ER sandwich plate. In fact, corresponding to a specific frequency of excitation there was an optimal electric field which caused minimum displacement amplitude. In other words, vibration suppression capability of MR/ER sandwich plates are frequency dependent (Lu and Meng, 2006). On the other hand, an anti-optimal electric field could result maximum displacement amplitude in the structure. Accordingly, inappropriate application of magnetic/electric field may degrade vibration control performance of the MR/ER sandwich plates, significantly (Yalcintas and Coulter, 1995b).

While magnetic/electric field strength highly affects the resonant frequencies and loss factors of sandwich plates, some other parameters such as face layer geometry (Narayana and Ganesan, 2007; Hasheminejad and Maleki, 2009), core layer thickness (Yeh 2007, 2007b, 2013), boundary conditions (Narayana and Ganesan, 2007) and excitation frequency (Lu and Meng, 2006) influence

modal parameters of the structures, remarkably. The significance of these factors on dynamic responses of the sandwich plates are relatively different. Hasheminejad and Maleki (2009) reported more noticeable effect of electric field strength on vibration suppression of ER sandwich structure in comparison with increasing the ER core layer thickness. They also suggested direct and inverse effect of aspect ratio on the natural frequencies and loss factors of ER sandwich plate, respectively. In other words, the natural frequencies (modal loss factors) increase (decrease) with increasing the aspect ratio. Narayana and Ganesan (2007) investigated the effect of boundary condition on dynamic responses of sandwich plate containing ER fluid. They concluded that increasing constraints on the four edges of sandwich plate increased natural frequencies and decreased modal loss factors. Cantilever and all clamped edge plate showed the maximum and minimum loss factors, respectively. They also found that the sandwich plate with viscoelastic as the core layer was stiffer and showed superior damping properties compared to ER based sandwich plate, under all boundary conditions except CFFF and CCFF. In these cases the conventional viscoelastic core exhibits poor damping for the first few modes, when compared to the ER plate. It should be noted that C and F represent clamped and free ends, respectively.

Core layer thickness plays significant role on dynamic characteristics of the sandwich plate. The core thickness might significantly enhance vibration controllability of the structure, under high levels of applied field (Vaicaitis et al., 2007). Increasing the core layer thickness may decrease the natural frequencies (Yeh and Chen, 2004) and increase the modal loss factors (Narayana and Ganesan, 2007). Decrease in the resonant frequencies signifies that the effect of thickening the core layer on mass of the structure is more significant than its stiffness (Mohammadi and Sedaghati 2012c). Yeh and Chen (2004) suggested that application of strong electric field may cause the natural frequencies of the ER sandwich plate to increase continuously as the thickness ratio of the ER layer increases. Furthermore, Yeh and Chen (2007) showed that, under high electric field strength, the modal loss factor of ER sandwich plate increased with increasing ER layer thickness. However, under low electric field strength, it decreased initially and then increased, by further increase of ER layer thickness. Yeh and Chen (2005) reported decrease in the dynamic stability regions of the sandwich plate with increasing ER layer thickness. Rahiminasab and Rezaeepazhand (2013) suggested decrease in the critical aerodynamic pressure of sandwich ER plate with increase of ER core thickness, while increasing of constraining layer thickness caused a reverse effect.

2.4.2. Sandwich structures with annular plate, skew plate and shell face layers

Although rectangular sheets have been widely employed to serve as the constraining and base layers for MR/ER sandwich plates, application of annular (Yeh, 2007, 2007b, 2010, 2010b, 2011, 2012; Yeh et al., 2009) and skew plates (Narayana and Ganesan, 2007) have also been reported. The effects of different parameters such as magnetic/electric field, core layer thickness, aspect ratio and boundary condition on the annular or skew plates are similar to those of the rectangular sandwich plate structures. Furthermore, few studies have addressed dynamic characteristics of sandwich shells with MR/ER fluids as the core layer (Tylikowski, 2000; Yeh, 2011b; Mikhasev et al., 2011; Mohammadi and Sedaghati, 2012b, 2012c; Hasheminejad and Motaaleghi, 2014). Mohammadi and Sedaghati (2012b) presented non-linear vibration analysis of a sandwich shell with ER fluid as the core layer. They proposed a new notation referred to as H-notation in the finite element analysis to reduce computational costs. The results demonstrated hardening type in the non-linear behavior of the sandwich structure so that increasing the amplitude of excitation increased the resonant frequency ratio ($\omega_{non-linear}/\omega_{linear}$). The rate of variations, however, depended on boundary condition and core layer thickness, significantly. Yeh (2011b) adopted finite element method to identify dynamic characteristics of multi-layer shell structure with ER fluid. The dynamic responses of the shell structure, however, follow the same trend as sandwich plate structures (Yeh, 2013), under different electric field levels, core layer thicknesses and modes of vibration. So far no experimental study on MR based sandwich shell has been reported, which might be related to challenges in providing magnetic flux over the structure. Mikhasev et al. (2011) presented the only theoretical study on dynamic characteristics of non-circular cylindrical shell with MR fluid as the core layer. The structure consisted of *N* transversely isotropic layers and MR core layers were sandwiched between the elastic layers. Although the results demonstrated the correlation between vibration suppression capability of the structure and material properties of layers, the effect of MR layer thickness in vibration control of the structure was highlighted.

2.4.3. Applications of MR/ER sandwich plates

While the main application of adaptive MR/ER based sandwich plates was to provide adjustable stiffness and damping properties to suppress unwanted vibration of the base layer, review of literature also suggests some other applications (Choi et al., 2001; Pranoto et al., 2004). Choi et al. (2001) investigated the effect of ER sandwich plate on noise control. They proposed an acoustic

cavity comprised of five acrylic sheets and ER plate as the sixth face of the cavity. A loud speaker generated sound pressure from outside of the cabin. The speaker was excited with sweep sine signals from the function generator through the power amplifier. A microphone was used to measure the sound level inside the cavity through a small hole in the bottom of cavity. The fuzzy control algorithm was adopted to attenuate sound transmission from the speaker into the cabin.
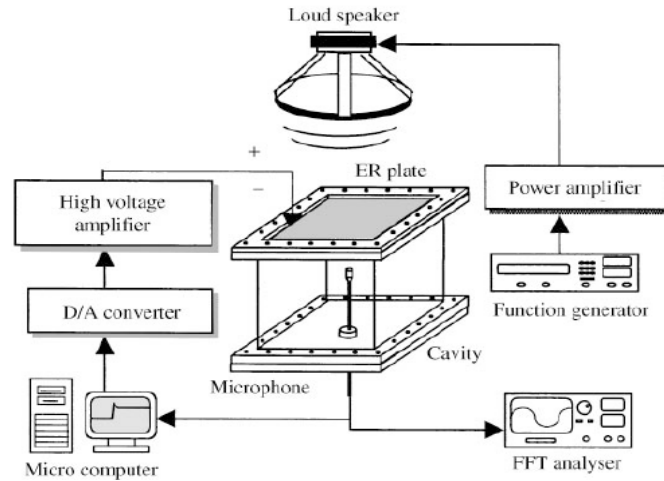
Figure 2.14 Experimental setup for noise control (Choi et al., 2001)

The experimental set up is shown in Figure 2.14. The results signified remarkable effect of ER plate on sound pressure attenuation in the cabin. Application of controlled electric field reduced the pressure level by 20 and 19 dB at 62 and 98 Hz, respectively. Hasheminejad and Shabanimotlagh (2010) investigated the effect of MR elastomer on sound insulation improvement of a sandwich plate containing MR elastomer as the core layer. Although application of magnetic field caused no significant improvement in sound insulation at low frequencies, the effect on intermediate and high frequency regions were noticeable.

Harland et al. (2001) inserted ER sandwich plate into a part of vibrating structure to attenuate vibration transmission. In their experiment, a sandwich ER plate was glued between two sections of a clamped-clamped perspex beam to suppress vibration transmission, as depicted in Figure 2.15. The advantage of proposed insert over traditional passive dampers was to provide variable properties and have negligible effect on integrity and mass of the structure. The perspex beam was excited on one side of the insert while the vibration was measured on both sides of the sandwich insert. The results suggested significant effect of the insert in reducing vibration transmission in the main structure.

42
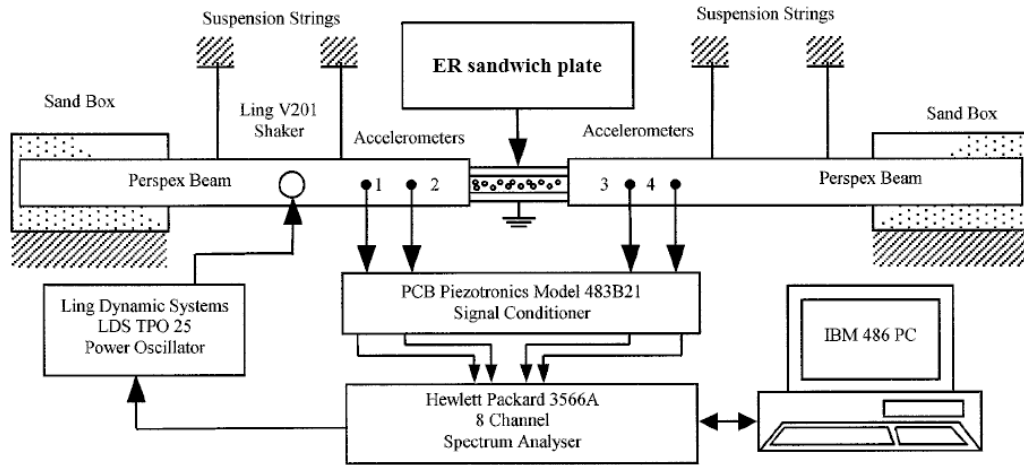
Figure 2.15 Experimental setup (Harland et al., 2001)

Figure 2.16 shows a shear mode MR damper designed by Pranoto et al. (2004), which is applicable for vibration suppression of large flexible structures such as aircraft wings. The damper comprised a thin rectangular box, number of thin plates with slits and MR fluid which was contained in the box. Permanent magnets attached to the box surface provided magnetic flux over the structure and solidified the MR fluid to resist against shear deformation due to plates sliding. The advantage of proposed damper over ordinary hydraulic damper was to work for small displacement. In contrast to rubber damper, which shows poor performance in low frequency region, the proposed damper could generate large damping force in the low frequencies. The resisting force due to shear motion was almost constant and frequency independent, which was the main difference of the proposed damper with piston-type ones. The proposed thin and light damper worked passively and needed no energy for activation. Pranoto et al. (2004) applied the damper on a vibrating wing and reported 90% reduction in amplitude of vibration corresponding to the first (bending) and second (torsional) modes of the wing.
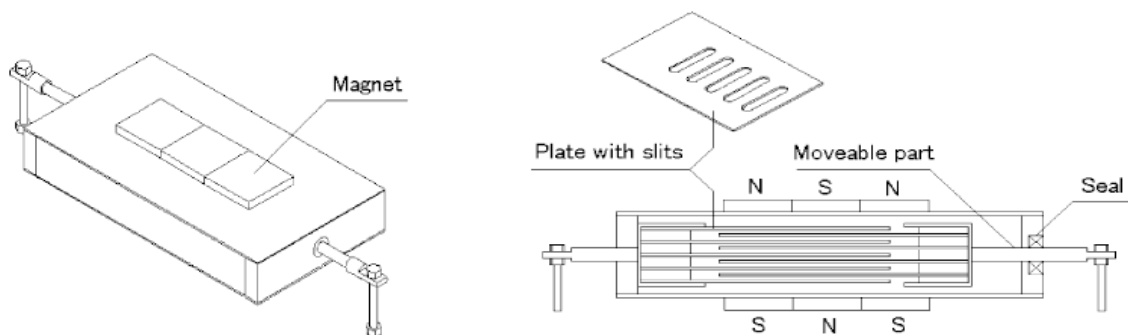
Figure 2.16 Geometry of MR damper (Pranoto et al. 2004)

43

2.5. Dynamic characteristics and optimum design of partially treated MR/ER sandwich structures

2.5.1. Partially treated sandwich beam, plate and shell structures

A survey of literature shows substantial increase in the stiffness and damping properties of the sandwich structures, fully treated with the MR/ER fluid layer, with increasing applied field. The fully treated sandwich structures, however, result in higher mass due to high weight density of the fluid, and pose some practical challenges in implementing the MR/ER fluid layer (Kciuk and Turczyn, 2006). Furthermore, application of a uniform magnetic/electric field over the entire structure poses difficult challenges. Partial MR/ER fluid treatments would thus be desirable, particularly when applied to optimal locations to achieve maximum controllability with relatively small size treatment and low energy consumption. Partially treated sandwich structures comprise elastic face layers and partial MR/ER segments as the core layer. Those parts of the core layer where not covered by the MR/ER treatments (untreated regions) may be filled by other materials. Haiqing and King (1997) and Lu and Li (2007) considered untreated parts in the core layer of partially treated ER sandwich beam to be filled by air. Oyadiji (1996) and Choi et al. (1999) employed the same layout of the core layer to fabricate partially treated sandwich plate. Rajamohan et al. (2010b) proposed a sandwich beam of aluminum face layers and partially treated MR fluid as the core layer. The remaining segments of the core layer were considered to be of aluminum material. In order to suppress vibration amplitude of a cross-ply elastic composite laminate, Panah and Hasheminejad (2010) proposed a partial ER fluid segment attached to the base layer. The top layer was assumed to be as the same size of the ER segment. Mohammadi and Sedaghati (2012c) investigated dynamic responses of a partially treated sandwich shell structure. Unconstrained viscoelastic material was employed at boundaries and untreated locations to seal electrorheological fluid. The thickness of the viscoelastic layer was considered to be equal to thickness of the ER core and constraining layers. The logic behind choosing unconstrained viscoelastic material was to achieve more dependency of the structural loss factor on the constrained ER fluid.

2.5.1.1. Dynamic responses of partially treated sandwich structures

The properties of partially treated MR/ER sandwich structures are strongly affected by different fluid and structural related parameters such as core layer thickness, complex shear modulus of the

fluid, applied field strength, face layer geometry and boundary conditions. Furthermore, the number and location of the fluid treatments contribute significantly in the dynamic responses of the sandwich structures. In the absence of applied magnetic/electric field, partial treatments yield relatively lower natural frequencies of the sandwich structure compared to those of untreated ones, irrespective of the configuration, end conditions and modes of vibration (Rajamohan et al., 2010b). That is simply due to higher mass of the fully treated structure. Increasing the applied field generally results in increase in the natural frequencies (Oyadiji 1996; Choi et al., 1999). Haiqing and King (1997) reported reduction in the resonant frequencies of a partially treated sandwich ER beam in response to the electric field. The partial treatment was located at the middle of the clamped-clamped beam. They attributed decrease in the natural frequencies of the structure to solidification of ER fluid subjected to the electric field, which resulted in transmission of vibration energy applied to the upper steel face layer to the lower one. Oyadiji (1996) investigated the effect of ER segments locations on the natural frequencies of a cantilever partially treated ER plate. Silicon rubber was employed to partition the core layer to five cavities parallel to the clamped edge. A constant electric field strength of 2 kV mm^{-1} was provided over the structure. Treating the first cavity (closed to the clamped edge) increased the natural frequencies, compared to those of the untreated structure. The increase was attributed to significant effect of electric field on the stiffness of the ER fluid compared to the mass effect. Treating the second cavity decreased the resonant frequencies which signified significance of the mass effect. This study suggested that treating 60% of the core layer by ER fluid resulted in minimum vibration amplitude of the structure. Panah and Hasheminejad (2010) suggested that the natural frequencies of partially treated sandwich plate subjected to low electric field strength (1 kV mm^{-1}) was lower than untreated structure. Applying high electric field (3 kV mm^{-1}), however, enhanced the resonant frequencies compared to the untreated plate.

It is widely reported that the loss factors of fully treated sandwich structures are generally higher than those of the partially treated ones (Rajamohan et al., 2010b; Joshi, 2012). That is attributed to lower dissipated energy of the latter structure. However, some studies reported higher loss factor of partially treated sandwich structures compared to fully treated ones, under specific boundary conditions and geometries (Haiqing and King, 1997; Rajamohan et al., 2010b; Panah and Hasheminejad, 2010; Mohammadi and Sedaghati, 2012c). Haiqing and King (1997) suggested less significant effect of partial treatments on the loss factor of partially treated ER beam compared to

45

natural frequencies. Panah and Hasheminejad (2010) illustrated the effects of electric field strength and ER patch size on the loss factors of a partially treated ER plate. They showed that employing a large ER segment under high electric filed or small segment under low electric field strength increased the loss factors of the structure. The results also showed noticeable effect of shear deformation in vibration suppression capability of the ER sandwich structures. In other words, the MR/ER fluid segments may adjust the stiffness and damping properties of the partially treated structure in a wide range, if they experience noticeable shear strain. Tylikowski (2000) analyzed vibration responses of a cylindrical shell partially treated with ER fluid, under different boundary conditions. The study concluded more significant variations in the modal parameters of the free-free structure, compared to those of sandwich shell with fixed-free boundary condition, in response to the electric field, which was due to higher shear deformation in the former structure.

2.5.2. Partially activation of the core layer

The effects of partially activation of MR/ER fluids on dynamic responses of the sandwich structures have been investigated in some studies (Yalcintas and Coulter, 1998; Choi et al., 1999; Cho et al., 2005; Lara-Prieto et al., 2010). Choi et al. (1999) fabricated a four-partitioned ER plate to investigate the effect of intensity and area of applied field on the natural frequencies and mode shapes of the structure. The sandwich plate was fully treated by ER fluid and each quarter of the core layer could be activated individually. The results suggested that energizing larger area of the core layer resulted in noticeable suppression of the mode shapes. Cho et al. (2005) proposed an ER based sandwich plate with multi-electrode configuration to provide partially activation of the ER fluid. In other words, the structure was fully treated by ER fluid while the electric field was applied to partial area of the core layer. The study suggested an increase in the natural frequencies and loss factors of the structure as the area of active electrodes increased. Furthermore, activation of regions experiencing significant shear deformation yielded noticeable variations in the modal parameters of the structure. The study concluded that optimal activation of the fluid provided superior ratio of vibration suppression to consumed energy compared to a fully activated ER plate. Lara-Prieto et al. (2010) conducted an experiment to investigate the effect of partial activation of core layer on dynamic characteristics of a cantilever sandwich PET beam structure containing MR fluid as the core layer. It was observed that the natural frequency of beam decreased as the activated area moved away from the clamped end of the cantilever structure. This results were in agreement

with the theoretical study conducted by Yalcintas and Coulter (1998) in which they reported decrease in the resonant frequencies of a simply supported ER beam when only the central region of the beam was activated.

2.5.3. Optimum design of partially treated sandwich structures

The advantage of partially treated over fully treated sandwich structure is to realize an appropriate layout with minimum treatments to obtain almost the same performance as the fully treated one. Design of a partially treated MR/ER sandwich structure requires finding an appropriate configuration of the treatments so that yields the maximum controllability and vibration suppression capability of the structure in terms of stiffness and damping. To this purpose, different optimization problems on MR/ER sandwich structures have been formulated (Rajamohan et al., 2010c; Snamina 2011; Mohammadi and Sedaghati 2012c). Rajamohan et al. (2010c) proposed three optimization problems to investigate the effect of MR layout on dynamic responses of partially treated MR beam. In the first case, the objective function was formulated to find the optimal locations of MR treatments resulting in maximum modal damping factors corresponding to the first five individual modes of vibration, such that:

$$\text{Case 1: } \textit{Maximize } f_1(X) = \eta_d \frac{\sum_{e=1}^{n} \phi_e^{(r)} k_e \phi_e^{(r)}}{\phi^{(r)T} K \phi^{(r)}}, \quad r = 1,..,5 \text{ subjected to } 0 < X \leq N \quad (2.13)$$

where $\phi^{(r)}$ is the rth mode shape vector, $\phi_e^{(r)}$ is the vector extracted from $\phi^{(r)}$ representing the displacement of eth MR fluid element in the core layer, K and k_e denote system and element stiffness matrices, respectively, η_d is the structural loss factor of MR fluid and n and N are the number of MR fluid segments and finite elements of sandwich beam, respectively. The design variable, X, is location of the MR fluid segments in the core layer of the sandwich beam. The objective function corresponding to case 2 was considered to maximize summation of the modal damping factors associated with first five modes.

$$\text{Case 2: } \textit{Maximize } f_2(X) = \sum_{r=1}^{5} \left\{ \eta_d \frac{\sum_{e=1}^{n} \phi_e^{(r)} k_e \phi_e^{(r)}}{\phi^{(r)T} K \phi^{(r)}} \right\} \quad (2.14)$$

Since the modal loss factor corresponding to the fundamental mode of sandwich beam overweighed those of other modes, it was observed that the results obtained in case 2 were identical

to those obtained in case 1. Consequently, the third objective function was considered to be logarithmic damping factors corresponding to the first five modes, such that:

$$\text{Case 3: } \textit{Maximize } f_3(X) = \sum_{r=1}^{5} \ln\left\{ \eta_d \frac{\sum_{e=1}^{n} \phi_e^{(r)} k_e \phi_e^{(r)}}{\phi^{(r)T} K \phi^{(r)}} \right\} \tag{2.15}$$

The above optimization problems were solved using the genetic search algorithm (GA) and sequential quadratic programming (SQP) techniques. This study concluded significant effect of modes of vibration on optimum locations of the MR fluid segments. Furthermore, it was realized that treating the pockets experiencing significant shear deformation could maximize the loss factor. For instance, the MR fluid treatments closed to the supports of simply supported and clamped sandwich beams yielded higher modal damping factors corresponding to all the modes.

Snamina (2011) employed the classical plate theory and energy method to find optimal number and locations of the MR segments in the core layer of a sandwich plate to maximize the energy dissipation of the structure. The objective function was considered as:

$$\textit{Maximize } P = \frac{1}{2} \omega A^2 \, \text{Im}(G) \int_{V} \left(\gamma_{xy}^2 + \gamma_{xz}^2 + \gamma_{yz}^2 \right) dV \tag{2.16}$$

where P is the average power dissipated from the plate, ω and A denote the frequency and amplitude of excitation, respectively, $\text{Im}(G)$ is the imaginary part of the complex shear modulus of the MR fluid and γ represents shear strain of the MR fluid. This study revealed greater number of optimal MR fluid treatments for the higher modes of vibration. Mohammadi and Sedaghati (2012c) formulated an optimization problem to maximize damping corresponding to first two modes of a sandwich panel partially treated with ER fluid. They considered locations of the ER segments, thickness ratios of the face and core layers and electric field intensity as the design variables and employed GA and SQP techniques to find optimal design. Furthermore, a constraint was defined so that the total mass of the sandwich structure should not increase mass of the base layer more than 50%. The optimization results showed that the maximum electric field intensity would yield the highest loss factor, irrespective of boundary condition. Ni et al. (2010) fabricated a sandwich beam with MR elastomer as the core to suppress micro vibration of equipment under stochastic support vibration. They formulated an optimization problem and considered velocity response spectra and the RMS velocity responses of the structure as the objective functions, while

the applied magnetic field was assumed as the design variable. The results accentuated significant effect of optimal MR elastomer on reducing RMS velocity responses of the structure.

2.6. Vibration control of MR/ER sandwich structures

Application of smart fluids in the structures enables to develop semi-active controller to attenuate unwanted vibration in wide range of frequency. This is due to tunable stiffness and damping characteristics of MR/ER based sandwich structures in response to the applied field. Semi-active controllers pose the simplicity and reliability of the passive controllers as well as effectiveness and adaptability of the active ones. Kim et al. (1992) compared performance of semi-active controller with that of passive system, under critical and maximum damping, on a cantilever ER sandwich beam and reported superior functionality of former controller. Furthermore their study indicated that semi-active system was not sensitive to spillover problem comparing with fully active system. Active controllers require force and torque inputs from actuator to suppress vibration, thus application of these controllers is limited due to high cost and power requirements. Moreover, they are prone to instability. Although control study of the MR and ER dampers has been widely investigated, control analysis of the sandwich structures incorporating MR and ER fluids have been addressed only in few studies. Semi-active controllers have been applied to the MR/ER sandwich structures through various control strategies such as ON-OFF control law (Sapiński and Snamina, 2008; Liao et al., 2012), linear quadratic regulator (Rajamohan et al., 2011), sliding mode (Kim et al., 1992; Allahverdizadeh et al., 2013; Hasheminejad et al., 2013) and real time control (Zhang and Li, 2009; Kim et al., 2011). The performance of the controllers were demonstrated by suppressing external disturbances such as sinusoidal signal (Choi et al., 1996; Fukuda et al., 2000; Liao et al., 2012), random signal (Han et al., 1994; Choi et al., 1996; Liao et al., 2012; Allahverdizadeh et al., 2013), impulse (Rajamohan et al., 2011; Liao et al., 2012; Allahverdizadeh et al., 2013) and white noise (Rajamohan et al., 2011). Furthermore, some studies investigated the effects of semi-active controllers on free vibration of sandwich structures (Cho et al., 2005; Rajamohan et al., 2011).

2.6.1. Semi- active control of sandwich structures

Vibration control in the adaptive structures is directly connected to control of their modes, therefore the governing equations of motion of the structures are generally expressed in the modal

form using modal coordinates (Rajamohan et al., 2011; Allahverdizadeh et al., 2013). In view of uniform distributed variable damping properties of the sandwich structures, which are provided by MR/ER fluid core layers, proportional damping assumption can be employed in the vibration analysis of the structures. Employing modal coordinate system yields uncoupled governing equations of motion for the sandwich structure in the following form (Rajamohan et al., 2011; Allahverdizadeh et al., 2013):

$$\{\ddot{\lambda}_i\}+[2\xi_i\omega_i]\{\dot{\lambda}_i\}+\{\omega_i^2\}\{\lambda_i\}=\{f_i\}, \quad i=1,2,...,n \tag{2.17}$$

where $\{\lambda\}$ and $\{f\}$ denote modal coordinate and force vectors, respectively. ω_i and ξ_i are the natural frequency and corresponding modal damping ratio for the ith normal mode, respectively. The modal parameters of the MR/ER based sandwich structures show significant variations in response to applied field; hence the natural frequencies and modal damping factor of the structures can be represented as a function of controlled magnetic/electric field, u_i:

$$\{\ddot{\lambda}_i\}+C(u_i)\{\dot{\lambda}_i\}+K(u_i)\{\lambda_i\}=\{f_i\}, \quad i=1,2,...,n \tag{2.18}$$

where $K(u_i)=\left[\omega_i^2\right]$ and $C(u_i)=[2\xi_i\omega_i]$. In order to realize an appropriate controller over the structure, variations of $K(u_i)$ and $C(u_i)$ with applied field should be identified. It is widely reported that these two parameters vary linearly with respect to the applied field (Kim et al., 1992; Choi et al., 1993; Rajamohan et al., 2011; Allahverdizadeh et al., 2013). However, the approximation is valid in limited range of frequency and applied field. The field dependent equation presented in Eq. (2.18) can be used to develop different semi-active controllers such as LQR (Rajamohan et al., 2011) and sliding mode (Allahverdizadeh et al., 2013) for the sandwich structures.

Liao et al. (2012) presented mathematical model of a MRE based vibration isolation system as a single-degree-of-freedom-system, as depicted in Figure 2.17. The MR elastomers worked in the shear mode and provided adjustable stiffness in the structure and support the mounting plate. The controllable magnetic flux was generated by the magnetic coil and transferred to the MR elastomers through magnetic conductor. The voice coil motor received the velocity feedback of the mounting plate and base to generate appropriate damping force.

50
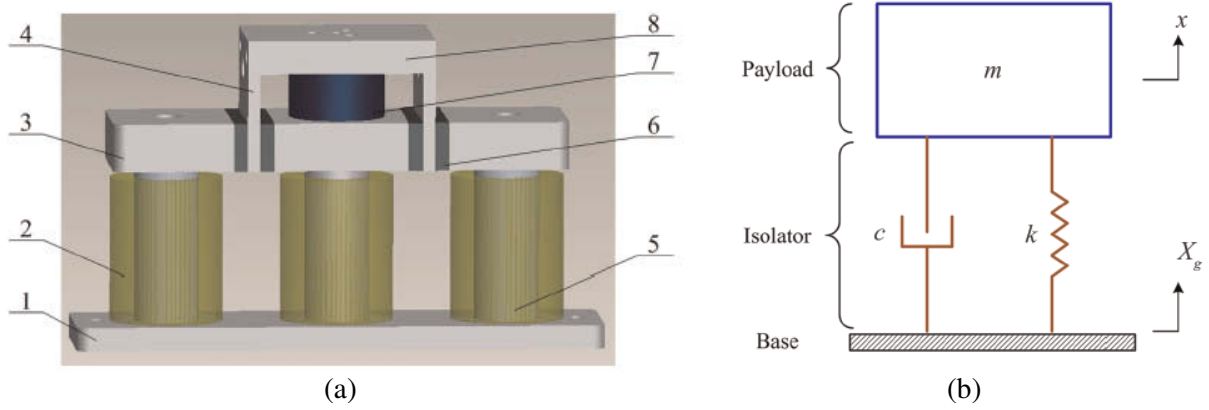
Figure 2.17 (a) MRE based vibration isolator including 1: base, 2: magnetic excitation coil, 3: magnetic conductor, 4: shear plate, 5: iron core, 6: MRE, 7: voice coil motor and 8: mounting plate and (b) equivalent single-degree-of-freedom-system (Liao et al., 2012).

Liao et al. (2012) designed a simple ON-OFF controller for the structure under sinusoidal excitation, as follows:

$$\begin{cases} k = k_{max} \ and \ c = c_{max} & if \ \omega \leq \sqrt{2}\omega_0 \\ k = k_{min} \ and \ c = c_{min} & if \ \omega > \sqrt{2}\omega_0 \end{cases} \tag{2.19}$$

where k_{max} and k_{min} denote the maximum and minimum stiffness of the MRE based vibration isolator, respectively and c_{max} and c_{min} represent maximum and minimum damping of the structure, respectively. ω_0 is the natural frequency of equivalent SDOF system and ω represents excitation frequency. They also employed following control law to attenuate vibration of the structure under random excitation:

$$\begin{cases} k = k_{max} \ and \ c = c_{max} & if \ x_r \dot{x}_r \geq 0 \\ k = k_{min} \ and \ c = c_{min} & if \ x_r \dot{x}_r < 0 \end{cases} \tag{2.20}$$

where x_r and $\dot{x}_r$ are the displacement and velocity of the payload with respect to the base, respectively. The results presented in the study suggested significant vibration suppression of the payload in different load cases. Furthermore, they showed that although energy dissipation in the structures generally occurs through damping elements, the stiffness element under proper ON-OFF controller can dissipate energy, as depicted in Figure 2.18.
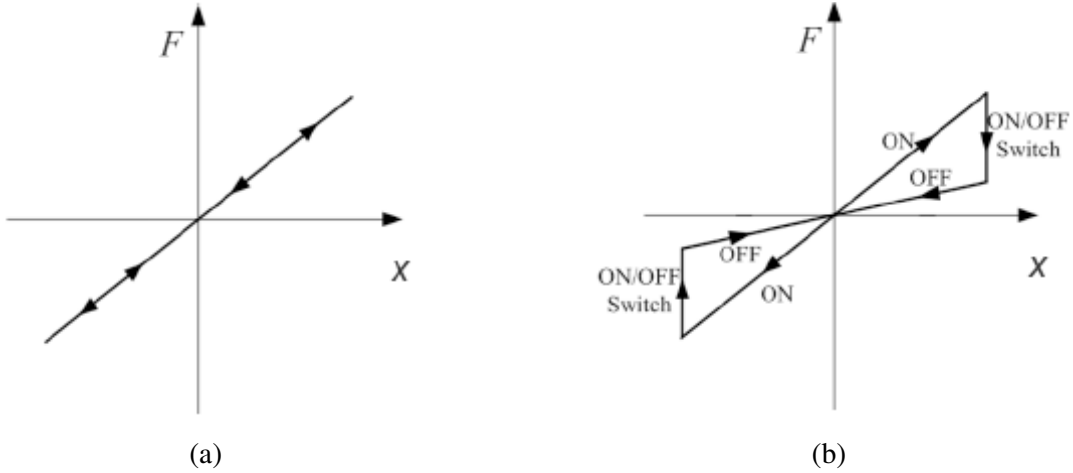
Figure 2.18 Variations of elastic force with displacement (a) without and (b) with controller

(Liao et al., 2012)

Sapiński and Snamina (2008) demonstrated the concept of switched stiffness in vibration analysis of a cantilever beam with MR fluid as the core layer. They considered free end displacement and velocity of the sandwich beam to design the controller. Their results revealed that switching stiffness to low value, while displacement reached the maximum, dissipated energy from the structure. The control low was also given as:

$$
\begin{cases}
k = k_{max} & if \ w\dot{w} \geq 0 \\
k = k_{min} & if \ w\dot{w} < 0
\end{cases}
\tag{2.21}
$$

where w and $\dot{w}$ are displacement and velocity at the free end of sandwich beam, respectively.

While most of the studies on control of sandwich structures with MR/ER fluids developed controller over fully treated sandwich structures under fully activation of the core layer, there are few studies addressing control synthesis of partially treated sandwich structures or partially activation of the MR/ER fluids. Rajamohan et al. (2011) presented full-state observer- based and limited state LQR controller to suppress free and forced vibration of a cantilever beam, comprising of two elastic layers and MR fluid as the core layer. Application of full-state observer-based LQR control decreased tip displacement as well as settling time of the free vibration. The study showed that, vibration control of the partially treated beam might be as well as fully treated one, if the MR treatments were located near free end of the beam. For instance, the settling time of the fully treated controlled beam was 0.59 s while that of passive structure was in order of 4.3s. Interestingly, the settling time of controlled partially treated beam was measured to be 0.53 s, which was lower than

that of fully treated beam. Park et al. (1998) investigated dynamic responses and shape control of a sandwich plate containing ER fluid as the core layer. The host layer was partitioned to provide four cavities. The results illustrated that application of controlled partial ER fluids, tuned structural mode shapes and elasto-dynamic properties of the structure, significantly. Cho et al. (2005) reported that application of partially activated ER fluid under sliding mode controller resulted in much less energy consumption than fully activated structure, while almost the same vibration attenuation was acquired. Although, it is widely reported that application of controller increases the natural frequencies of the sandwich structures with MR/ER fluids, Rajamohan et al. (2011) suggested no significant shift in the lower three resonant frequencies of the controlled partially treated MR sandwich beam.

2.6.2. Active controllers

While application of semi-active controller on adaptive structures is popular and the semi-active controller is less sensitive to spillover than active controller (Kim et al., 1992), the active controller should be applied, once complete vibration suppression of the adaptive structure is desired (Shaw, 2000). The semi-active controllers can effectively mitigate vibration of the structure in the neighborhood of the resonance frequencies (Choi and Park, 1994). However, non-zero deflection in the structures with semi-active controllers may be observed in different frequencies of excitations. Application of active controllers to mitigate undesired vibration of MR/ER based sandwich structures have been reported in the literature (Choi et al., 1996; Jianting and Jiesheng, 2003). Choi et al. (1996) involved the actuator characteristics into governing equations of motion of a cantilever sandwich beam containing ER fluid to design an active controller. Fukuda et al. (2000) employed ER fluid core layer and piezoceramic actuator to realize an active controller and suppress deflection at the free end of the cantilever composite beam. Four types of feedback control strategies including deflection feedback control (DFC) and velocity feedback control (VFC) through or not through a relay element for both of the ER fluid and piezoceramic actuator were considered. The relay element provided a comparison between control effect of the sinusoidal and rectangular waves as the input to the actuators. In other words, four types of control strategies were applied to ER fluid and piezoceramic actuator and the amounts of the control input signals based on DFC and VFC were measured. The results suggested that VFC without a relay element for ER

fluid and piezoceramic actuator showed optimal performance in vibration attenuation of the structure, under sinusoidal excitation.

The Lyapunov stability theory has been employed in some studies to apply active controllers for vibration mitigation of sandwich beam structures with ER (Rahn and Joshi, 1998) and MR (Chen and Hansen, 2005; Chen and Tian, 2006) fluids, respectively. Shawn (2000) developed two-stage hybrid controller to attenuate vibration of an ER based adaptive beam under harmonic disturbances. This controller combined fuzzy logic-based semi-active controller with an active force controller. The semi-active controller tuned the resonant frequencies and improved transient response of the structure, while the active controller eliminated external disturbances and improved steady state responses. The results highlighted superior performance of hybrid controller over semi-active and active controllers in suppressing undesired vibration. Furthermore, the results reported beating phenomenon in response to active control of the structure which was due to small damping of the structure and negligible deviation of the excitation and natural frequencies of the structure. Hasheminejad et al. (2013) developed an active controller to control supersonic flutter motion of sandwich plate with ER fluid as the core layer. An arbitrary flow with various yaw angles was applied to the structure mounting on a Winkler–Pasternak elastic foundation.

2.6.3. Adaptive tunable vibration absorbers

Dynamic vibration absorbers are designed to operate in the shear mode and suppress undesired vibration of vibrating parts (main systems). To operate effectively, the natural frequency of the vibration absorber should coincide with that of the main system (Li et al., 2005b). Since traditional vibration absorbers employ passive elements, their stability and damping effects are limited and they only control unwanted vibrations of the vibrating objects in narrow range of frequency (Kela and Vähäoja, 2009). In order to alleviate this problem, applications of adaptive tuned vibration absorbers (ATVA) for vibration suppression of the vibrating systems have been widely reported (Deng and Gong, 2007; Sinko et al., 2012). They typically employ MR elastomer to provide variable complex shear modulus in response to applied magnetic field (Deng et al., 2006, 2006b; Deng and Gong, 2007, 2008). They also utilize semi-active (Deng et al., 2006; Dong et al., 2009) or active (Liao et al., 2011) controllers to reduce vibration of the main structures at different excitation frequencies. Kim et al. (2011b) developed a tunable vibration absorber to suppress vibration of cryogenic coolers applied in the observation satellite, as shown in Figure 2.19.

<center>(a)   (b)</center>
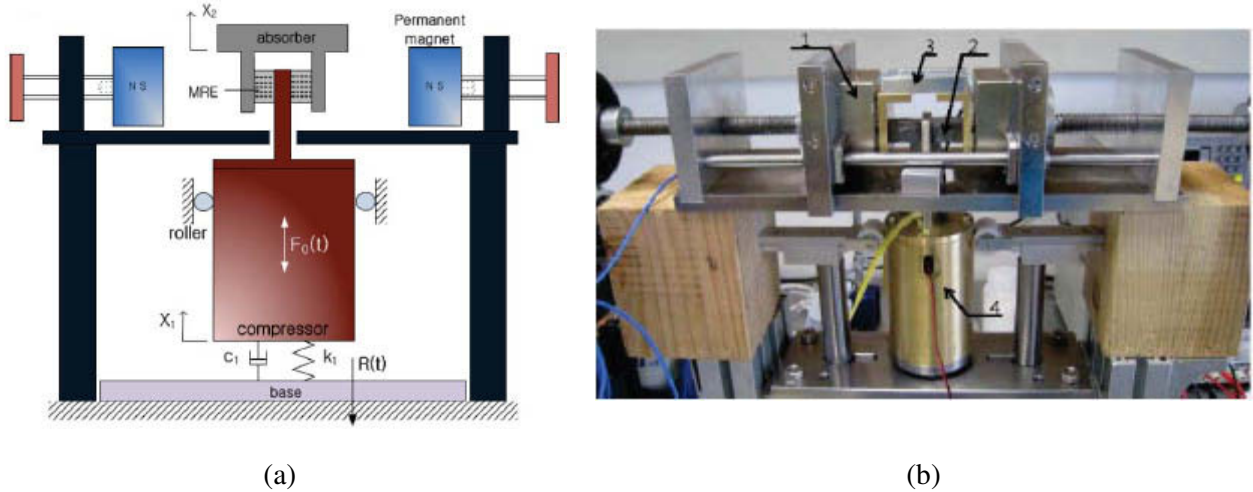
Figure 2.19 (a) Cryogenic cooler system with an MRE TVA diagram and (b) experimental setup; 1: Permanent magnet, 2: MRE, 3: Absorber mass and 4: Compressor (Kim et al., 2011).

These coolers decreased temperature of image sensors during the operation. The disturbances generated by coolers were transmitted to the sensors and yielded poor image quality. Variable stiffness of the vibration absorber in response to the magnetic field enabled to develop a real time controller to suppress vibration of the coolers. The results revealed that the absorber could tune its resonant frequency up to 87% and suppressed vibration of the coolers significantly. It is worth noting that a survey on passive, adaptive and active vibration absorbers was presented by Sun et al. (1995).

2.7. Conclusions

This paper mainly summarizes the studies on pre-yield characterization of MR/ER fluids, dynamic responses of partially and fully treated sandwich beams, plates, shells and panels containing MR/ER fluids as the core layer and control strategies applied to the structures. A comprehensive review on different fabrication techniques, experimental methods, mathematical modeling and methods of solution were presented and the results based on different assumptions were compared. The effects of different parameters such as applied field, geometry, elastic layer material, boundary conditions, excitation frequency, temperature and external disturbances on dynamic responses of the structures were thoroughly investigated. Furthermore, the complexities associated with experimental studies and the sources of disagreement between theoretical and experimental studies were addressed. Although most of the studies on sandwich structures employed MR/ER fluids to attenuate undesired vibration and instability of the base layers,

<center>55</center>

applications of these structures as shear mode dampers and vibration absorbers have been also reported. The results suggested that although rheometers have been widely used to characterize MR/ER fluids in terms of applied field and excitation frequency, treating MR/ER sandwich beam structures as SDOF systems ensured pre-yield characterization of the fluids which was due to smaller strain amplitude of the fluids in the sandwich structures compared to the rheometers. Moreover, solid models were more appropriate to identify pre-yield characteristics of the MR/ER fluids. It was further noted that application of MR/ER fluids in sandwich structures subject to magnetic/electric field could significantly alter the stiffness and damping properties of the structures under a noticeable shear strain. Although, fully treated sandwich structures generally yielded more significant performance compared to partially treated ones, optimal design of the partially treated MR/ER based sandwich structures, in some cases, could provide superior damping properties compared with the fully treated ones, while having less weight. The performance of the partially and fully treated structures, however, could be enhanced by developing appropriate semi-active or active controllers over the structures. The results highlighted that semi-active controllers could suppress resonant deflection of the structures while active controllers ensured complete vibration suppression of the adaptive structures in a wide range of frequency.

CHAPTER 3

AN ACCURATE TECHNIQUE FOR PRE-YIELD CHARACTERIZATION OF MR FLUIDS

3.1. Introduction

The magnetorheological (MR) fluids, owing to their rapidly varying and reversible rheological properties under an external magnetic field, have been widely explored for active vibration control in systems and structures (Chen and Hansen, 2005; Jolly et al., 1998). A range of vibration control devices employing MR fluid in either flow (Yao et al., 2002) or shear (Lee and Kim, 1999) or squeeze mode (Farjoud et al., 2009) has evolved over the past two decades. These have shown that MR fluids exhibit distinctly different characteristics depending on their operational mode. Applications of MR fluids in sandwich structures necessitate accurate characterization of the fluids. A number of phenomenological constitutive models have been reported for characterizing the storage and loss moduli of the magneto- as well as electro-rheological (ER) fluids in the pre- and post-yield regimes. The reported models tend to differ substantially, which may in part be attributed to differences in the characterization methods, type of fluid and the base structure used in the reported studies. It has been suggested that a generalized model specifically describing the pre-yield behavior of smart fluids has not yet been reported (Mohammadi et al., 2010). The reported models, however, consistently show strongly nonlinear dependence of fluid properties on the excitation frequency and the applied external field.

The post-yield regime may be regarded as the dominant operational mode for the MR fluids in many applications such as MR dampers, clutches and brakes. A number of models have thus been proposed to accurately characterize the MR fluid in the post-yield regime. The widely used Bingham plastic model considers the fluid as a rigid body, when shear stress of the fluid is lower than the yield stress, assuming Newtonian behavior in the post-yield and constant plastic viscosity of the fluid (Philips, 1969). The Bingham plastic model for shear thinning and thickening fluids may thus yield considerable errors. A generalized model, referred to as the Herschel Bulkley model, has been applied to describe non-Newtonian behavior of the fluids in the post-yield regime (Wang and Gordaninejad, 1999).

The ER and MR fluids experience oscillatory shear strain in many applications. Consequently, a number of studies have investigated their dynamic properties under oscillatory shear strain (Wilhem, 2002; Li et al., 2003; Mohammadi and Sedaghati, 2012). Wilhelm (2002) employed Fourier transform technique to formulate shear stress of smart fluids in terms of shear strain in the non-linear region. The study showed negligible magnitudes of higher order harmonics of the Fourier series compared to that of the first harmonic in the linear region (Li et al., 2003). Mohammadi and Sedaghati (2012) proposed a more efficient model to quantify the stress response and dynamic properties of an ER fluid composed of cornstarch and corn oil.

The adaptive structures containing ER and MR fluids tend to work in the pre-yield regime. Operation in the post-yield regime may disrupt the particles suspended in the carrier fluid leading to sedimentation of the particles and thus potential degradation of the fluid properties. Weiss et al (Weiss et al., 1994) reported 20-30% reduction in the storage modulus of the ER fluid in the 1-10% strain range in repeated tests on an adaptive ER-fluid structure. Viscoelastic models have been commonly used for characterizing rheological properties of smart fluids in the pre-yield regime (Ferry 1980). These include the solid-like models such as Kelvin-Voight (Gavin, 2001; Whittle et al., 1995) and Zener Element models (Gamota and Filisko, 1991), and fluid-like models such as Maxwell (Sims and Wereley 2003; Sims et al., 2004) and three parameter fluid models (Kamath and Wereley, 1997). Yen and Archon (1991) experimentally investigated the loss and storage moduli of an ER fluid in the pre-yield regime, in the 1 to 100 Hz frequency range and concluded only modest change in the storage modulus with the excitation frequency. This suggested a solid-like behavior of the ER fluid, which may occur under a high intensity electric field leading to stronger adherence of the semi-conducting particles in the direction of the applied field (Mohammadi et al., 2010). The complex shear modulus of the ER fluid in this case may be effectively described by a Kelvin-Voigt solid model (Gamota and Filisko, 1991). Simes and Werely (2003) proposed a Maxwell fluid model to characterize an ER fluid in the pre-yield regime, where the loss and storage moduli approached nearly zero values at low frequencies. A bi-viscous element was thus employed to describe the expected elastic behavior in the pre-yield region. Choi et al. (1990) estimated complex shear modulus of an ER fluid from free vibration response of a composite polystyrene beam filled with the ER fluid. The loss and storage moduli of the fluid were estimated considering the beam as a viscoelastic element in a single degree of freedom system. A similar method was employed by Rajamohan et al. (2010) for characterizing the shear modulus of

a MR fluid through measurements with an aluminum sandwich beam with MR fluid, although the contribution due to elastic properties of the face layers was neglected. The damping properties of materials in the linear region may also be characterized through the standardized test method defined in ASTM E756, which has been reported to yield acceptable responses in the 50 to 5000 Hz frequency range.

Although several studies have addressed characterization of the MR fluids in the post yield region, the characterizations in the pre-yield region have been addressed in relatively fewer studies. The MR/ER fluids characterization methods are generally based on four primary methods, namely, the oscillatory shear strain (Wilhem, 2002; Li et al., 2003; Mohammadi and Sedaghati, 2012), rheometery (Mohammadi et al., 2010), treating MR sandwich beam as a SDOF system (Choi et al., 1990) and the standardized test method described in ASTM E756. The rheometery and the oscillatory shear strain approach cause the MR fluid to operate in the post-yield region, while the method employing the MR sandwich beam as a SDOF system is considered more effective for low ranges of magnetic flux density due to flexibility of the host structure (Choi et al., 1990). Moreover, such a model does not consider the effect of excitation frequency on the complex shear modulus. ASTM E756 method may also yield errors since it neglects contributions due to the sealant.

The present study proposes a phenomenological model to characterize two types of MR fluids (MR 122EG and MR 132DG) in the pre-yield region over ranges of magnetic flux density (0-90 mT) and excitation frequency (10-500 Hz). Experiments were performed to determine frequency response characteristics of MR sandwich beam with aluminum face layer. The governing equations of motion of the sandwich beam structure were obtained in the finite element form using the classical plate theory. The shear modulus model of the MR fluids is subsequently formulated as a function of both the magnetic flux density and excitation frequency using the measured data. The identified shear modulus model is subsequently employed in the FE analysis, and the model validity is demonstrated over the ranges of magnetic flux density and frequency for both the MR fluids by comparing the FE model results with the experimental data for a copper sandwich structure comprising the two MR fluids.

3.2. Model formulations

Figure 3.1 illustrates the cantilever sandwich beam structure used in the study, which comprises two elastic material face layers and a core layer of the MR fluid. The fluid is contained within the

structure through a silicon rubber sealant. h_1, h_3 and h_2 define the thickness of the top and bottom face layers, and the fluid layer, respectively, which are very small compared to the length of the beam.

(a)
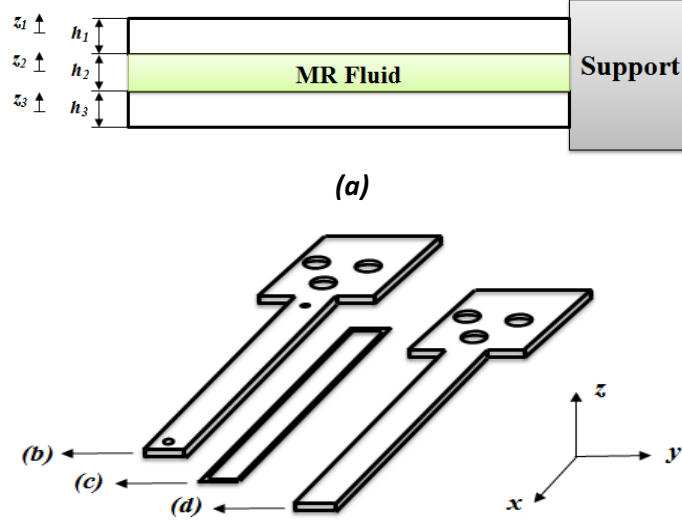
Figure 3.1 Schematic of the (a) sandwich beam, (b) top layer (constraining layer), (c) silicon rubber spacer, (d) bottom layer (host layer)

The classical plate theory (CPT) could thus be used to formulate the governing equations of motion for the sandwich beam. It is assumed that the slippage between the core and elastic layers, normal stress in the core layer and transverse shear strain in the elastic layers are negligible, and the transverse displacement of the structure through the thickness is uniform. The displacement field of an arbitrary point in the face layers can thus be expressed in the following form (Brush and Almroth, 1975):

$$u^{(i)}(x,y,z,t) = u_0^{(i)}(x,y,t) - z_i \frac{\partial w(x,y,t)}{\partial x},$$

$$v^{(i)}(x,y,z,t) = v_0^{(i)}(x,y,t) - z_i \frac{\partial w(x,y,t)}{\partial y}, \quad i=1,3 \tag{3.1}$$

$$w(x,y,z,t) = w(x,y,t)$$

where u and v are longitudinal displacements along the x and y directions, respectively. w represents the transverse displacement, and u_0 and v_0 denote the displacements of the mid layer along the x and y directions, respectively. In the above equations, superscripts $i = 1$ and 3 refer to the top and bottom layers, respectively and z_i is the transverse coordinate in the local coordinate system of each layer, which is located at the mid layer. Considering negligible slippage between

60

the core and face layers, the displacement field of the sandwich structure is uniform through the thickness, namely:

$$u^{(1)}\Big|_{z_1=-h_1/2} = u^{(2)}\Big|_{z_2=h_2/2} \quad \& \quad v^{(1)}\Big|_{z_1=-h_1/2} = v^{(2)}\Big|_{z_2=h_2/2}$$

$$u^{(2)}\Big|_{z_2=-h_2/2} = u^{(3)}\Big|_{z_3=h_3/2} \quad \& \quad v^{(2)}\Big|_{z_2=-h_2/2} = v^{(3)}\Big|_{z_3=h_3/2}$$

(3.2)

The superscript, $i=2$, in the above equations refers to the core layer. The displacement field of the MR fluid is formulated based on the continuity of the displacements between the core and face layers. The transverse shear strains (γ_{xz} and γ_{yz}) and shear stresses (τ_{xz} and τ_{yz}) in the core layer may be subsequently formulated as:

$$\gamma_{xz}^{(2)} = \frac{d}{h_2}\frac{\partial w}{\partial x} + \frac{u_0^{(1)} - u_0^{(3)}}{h_2}; \quad \gamma_{yz}^{(2)} = \frac{d}{h_2}\frac{\partial w}{\partial y} + \frac{v_0^{(1)} - v_0^{(3)}}{h_2}; \quad \tau_{xz}^{(2)} = G^* \gamma_{xz}^{(2)}; \quad \tau_{yz}^{(2)} = G^* \gamma_{yz}^{(2)}$$

(3.3)

where $d = h_1/2 + h_2 + h_3/2$ and G^* represents complex shear modulus of the core layer.

In the absence of a magnetic field, the MR fluid may be regarded as a Newtonian fluid, and it exhibits a linear relationship between the stress and the strain rate at any point. The fluid, however, deviates from the Newtonian behavior in the presence of magnetic field. In this case, the shear stress-shear strain properties of the MR fluid may be investigated in two regions, referred to as pre-yield and post-yield regions. The fluid exhibits viscoelastic behavior in the pre-yield region, and its shear stress and shear strain are proportional in terms of the complex modulus G^* given by (Li et al., 1999):

$$G^* = G' + iG''$$

(3.4)

where G' and G'' are the storage and loss moduli, which describe the average energy stored and dissipated, respectively, per unit volume of the material over a deformation cycle. In the post-yield regime, the shear stress is typically described by the Herschel Bulkley equation (Wang and Gordaninejad, 1999):

$$\begin{cases} \tau = \tau_y + k|\partial u/\partial z|^n & |\tau| \geq \tau_y \\ \partial u/\partial z = 0 & |\tau| \leq \tau_y \end{cases}$$

(3.5)

where τ, τ_y, k and u denote shear stress, yield stress, plastic viscosity and velocity of the fluid, while the exponent n is a flow behavior index. As depicted in Figure 3.2, the above relation describes the Newtonian fluid, when $\tau_y = 0$ and $n=1$ and dynamic viscosity of the fluid is constant.

The Herschel Bulkley model reduces to the Bingham plastic model for $n=1$. The equation demonstrates shear thinning and shear thickening fluids, for $n<1$ and $n>1$, respectively.
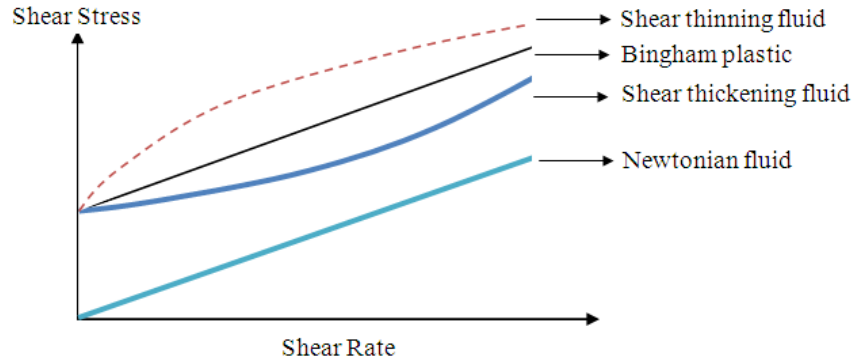
Figure 3.2 Shear stress variation of different fluids against shear rate

MR fluids may be also subjected to oscillatory shear strain, $\gamma = \tilde{\gamma}\sin(\omega t)$, in some applications. The Fourier transformation technique is the most common method to characterize the behavior of the fluids under oscillatory shear in the pre- and post-yield regions. Based on this technique, the stress response under harmonic shear strain may be expressed as (Wilhem, 2002):

$$\tau = \tilde{\gamma}\sum_{m=1,odd}^{\infty}\left[G'_m\sin(m\omega t)+G''_m\cos(m\omega t)\right]$$ (3.6)

where G'_m and G''_m are the m-th storage and loss moduli, respectively. It is worth noting that reversing the coordinate system does not change the stress response (Bird et al., 1987), thus only the odd harmonic terms are considered in Eq. (3.6). The first harmonic storage and loss moduli are represented in terms of the shear strain amplitude, $\tilde{\gamma}$, shear stress amplitude, $\tilde{\tau}$ and the phase difference φ between the shear stress and strain at the fundamental frequency, such that:

$$G'(\omega,B,\tilde{\tau})=\frac{\tilde{\tau}}{\tilde{\gamma}}\cos(\varphi), \qquad G''(\omega,B,\tilde{\tau})=\frac{\tilde{\tau}}{\tilde{\gamma}}\sin(\varphi)$$ (3.7)

where B is magnetic flux density. In the linear region, G'_1 and G''_1 are significantly higher than other coefficients and do not depend on the shear stress amplitude. The shear stress response may thus be expressed as:

$$\tau = \tilde{\gamma}\left(G'(\omega,B)\sin(\omega t)+G''(\omega,B)\cos(\omega t)\right)$$ (3.8)

3.2.1 Finite Element Model

A finite element model of the sandwich structure is formulated using the sandwich plate elements, each with four nodes and seven DOF per node including longitudinal displacements, transverse displacement and slopes, as shown in Figure 3.3. The transverse and longitudinal displacements of the element can be expressed in terms of nodal displacement vector, $q(t) = \{u_{1j}, v_{1j}, u_{3j}, v_{3j}, w_j, w_{,xj}, w_{,yj}\}^T$, $j=1,...,4$ and shape function vectors, such that:

$$u_i^{(0)}(x, y, t) = N_{ui}(x, y) q(t)$$

$$v_i^{(0)}(x, y, t) = N_{vi}(x, y) q(t), \qquad i = 1, 3 \tag{3.9}$$

$$w(x, y, t) = N_w(x, y) q(t)$$

The shape function vectors, $N_{u1}(x, y)$, $N_{v1}(x, y)$, $N_{u3}(x, y)$, $N_{v3}(x, y)$ and $N_w(x, y)$, derived for the sandwich structure are presented in the Appendix.
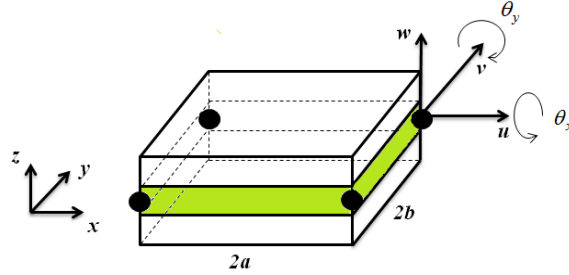
Figure 3.3 Two-dimensional sandwich plate element

For the $2a \times 2b$ plate element, the total potential and kinetic energies, V and T, are the sum of those of the three layers, as:

$$V = V_1 + V_2 + V_3$$

$$T = T_1 + T_2 + T_3 \tag{3.10}$$

where V_1 and V_3 are the total strain energies of the top and bottom layers, respectively, and V_2 is the shear strain energy of the core layer. T_1 and T_3 denote the kinetic energy associated with the transverse motion and axial deformations of the top and bottom layers, respectively, while T_2

quantifies the kinetic energy due to rotational deformation of the core layer. The strain and kinetic energy functions are formulated as:

$$V_i = \frac{1}{2} \int_{-a}^{a} \int_{-b}^{b} \int_{-h_i/2}^{h_i/2} \left(\sigma_x^{(i)} \varepsilon_x^{(i)} + \sigma_y^{(i)} \varepsilon_y^{(i)} + \tau_{xy}^{(i)} \gamma_{xy}^{(i)} \right) dz\, dy\, dx$$

$$V_2 = \frac{1}{2} \int_{-a}^{a} \int_{-b}^{b} \int_{-h_2/2}^{h_2/2} \left(\tau_{xz}^{(2)} \gamma_{xz}^{(2)} + \tau_{yz}^{(2)} \gamma_{yz}^{(2)} \right) dz\, dy\, dx \tag{3.11}$$

$$T_i = \frac{1}{2} \int_{-a}^{a} \int_{-b}^{b} \int_{-h_i/2}^{h_i/2} \rho_i \left(\left(\dot{u}_0^{(i)} \right)^2 + \left(\dot{v}_0^{(i)} \right)^2 + \left(\dot{w} \right)^2 \right) dz\, dy\, dx, \qquad i = 1,3$$

$$T_2 = \frac{1}{2} \int_{-a}^{a} \int_{-b}^{b} \left(\rho_2 h_2 \left(\dot{w} \right)^2 + I_2 \left(\left(\dot{\gamma}_{xz}^{(2)} \right)^2 + \left(\dot{\gamma}_{yz}^{(2)} \right)^2 \right) \right) dy\, dx$$

where ρ_i and ρ_2 are densities of the face and core layers, respectively, and $I_2 = \rho_2 h_2^3 / 12$. σ and ε denote the normal stress and strain components, respectively.

The governing equations of motion of the sandwich plate element are subsequently obtained in the finite element form using the Lagrange's energy method:

$$\frac{d}{dt} \left(\frac{\partial T}{\partial \dot{q}_l} \right) - \frac{\partial T}{\partial q_l} + \frac{\partial V}{\partial q_l} = Q_l, \qquad l = 1,...,n \tag{3.12}$$

where n is number of degrees of freedom of the element, which is 28 in this study. The governing equations of motion for the MR sandwich plate element in the finite element form can be expressed as:

$$\left[m^e \right] \{ \ddot{q} \} + \left[k^e \right] \{ q \} = \{ f^e \} \tag{3.13}$$

where $[m^e]$ and $[k^e]$ are the element mass and stiffness matrices, respectively, and $\{ f^e \}$ is the element nodal force vector. The system governing equations of motion for the fully treated MR sandwich plate structure, obtained by assembling the elemental mass, stiffness and force matrices, can be expressed in terms of the system mass $[M]$ and stiffness $[K]$ matrices, and the force vector $\{F\}$, as:

$$\left[M \right] \{ \ddot{d} \} + \left[K \right] \{ d \} = \{ F \} \tag{3.14}$$

where $\{d\}$ is the global displacement vector. The natural frequencies of the sandwich structure can be computed from the complex eigenvalues of the system of equations, Eq. (3.14).

3.3. Experiments and methods

Two prototype MR sandwich beams (effective length 150 *mm*; width=12 *mm*) with aluminum and copper face layers were fabricated for the study. The aluminum and copper materials were chosen considering their negligible magnetic permeability and damping property (Yalcintas and Dai, 1999). Three different experiments were conducted to characterize the properties of the face layers, the silicon rubber sealant and two MR fluids (MRF 132DG and MRF 122EG). The measurements obtained with the aluminum structure were used to identify the pre-yield shear moduli of the two MR fluids. The data acquired with the copper sandwich structure were applied for verification of the pre-yield model of the MR fluids. The initial experiment involved the identification of Young's modulus and Poisson's ratio of the 1*mm* thick aluminum (6061 alloy; density =2650 kg/m^3) and 0.8 *mm* thick copper (110 sheet; density=8900 kg/m^3) face layers. Although such parameters are readily available, accurate estimates were obtained so as to reduce the contributions of possible differences in these parameters to the measured properties of the MR fluids. Each beam layer was firmly clamped to a support so as to achieve a cantilever condition. A miniature accelerometer (PCB Piezotronics, model: 356A01), weighing 1.5 grams, was installed on the beam, about 30 *mm* from the support. The natural frequencies of the beam were identified from the frequency response characteristics obtained under hammer tests using the ME'scopVES. The half power bandwidth corresponding to each natural frequency was also identified from the frequency response.

Subsequently, the experiments were performed to identify density and complex shear modulus of the silicon rubber sealant. The aluminum face layers were used to fabricate a sandwich structure of two elastic layers, with 2 *mm* gap, using the silicon rubber sealant on the edges. Each face layer comprised a 40×40 *mm* root section, as seen in Figure 3.1(b) and 3.1(d), which is required to simulate a cantilever boundary condition, as per ASTM E756. The hollow sandwich structure was clamped to an electrodynamic vibration exciter. The miniature accelerometer, weighing 1.5 grams, was installed on the top face layer and another single-axis accelerometer was installed on the support, which also served as the feedback to the vibration controller (VR 9500). The frequency response characteristics of the structure were acquired under harmonic vibration in the 1 to 600 *Hz* frequency range, swept at a rate of 1 octave/min. The natural frequencies and the corresponding half power bandwidths of the structure were identified using the frequency response function.

3.3.1 Identification of properties of the face layers and silicon rubber

A finite element model for thin plate structure was also developed to identify the natural frequencies. The Young's modulus and Poisson's ratio of the material were adjusted so as to match the computed natural frequencies with the measured data. The Young's moduli and Poisson's ratios of aluminum and copper were subsequently identified as 65 Gpa, 0.33 and 95 Gpa, 0.35, respectively. The first five natural frequencies of the aluminum beam (34.5, 208.9, 428.8, 533.1, 1036.1 Hz) obtained from the FE analysis were quite close to those obtained experimentally (34.2, 205, 420.1, 510, 1010 Hz). Similarly, the first five natural frequencies of the copper beam obtained from FE analysis (18.9, 116.9, 294.1, 608.3, 1036.1 Hz) were comparable with the measured ones (19.5, 115, 308, 604, 1030 Hz).

The finite element model of the sandwich structure based on classical plate theory was formulated assuming negligible Young's modulus of the silicon rubber compared to that of face layers. The density of the silicon rubber (1460 kg/m^3) was obtained through direct measurements of the volume and the weight. The model used the face layer material properties, identified from the aforementioned experiments. The complex shear modulus of the silicon rubber was thus the only unknown parameter of the model. The loss and storage moduli of the silicon rubber were adjusted to achieve good agreements in computed and measured natural frequencies and the half power bandwidth corresponding to the first three modes. It should be noted that the natural frequencies of the sandwich structure are strongly related to the storage modulus of the silicon rubber, while the half power bandwidth relates to both the loss and storage moduli. The results suggested a constant value of the storage modulus ($G_r' = 1340000\,\text{Pa}$), while the loss modulus (Pa) revealed a quadratic relation with the excitation frequency ω (Hz), such that:

$$G_r^* = G_r' + i\,G_r''$$

$$G_r'' = 152511 + 68.31\,\omega + 0.475\,\omega^2$$

(3.15)

Table 3.1 compares the computed three lower natural frequencies and corresponding half-power bandwidths of the aluminum sandwich beam with the sealant with the measured data. The results show reasonably good agreements between the computed and measured values. The validity of the identified shear modulus was further examined through its application to the cantilever sandwich beam structure comprising two copper face layers and the silicon rubber spacer. The spacer provided a gap of 2 *mm* between the face layers. The natural frequencies and bandwidths of the

66

copper sandwich beam were also obtained from the FE analysis employing the rubber shear modulus model, presented in Eq. (3.15). The comparisons of the model and experimental results of the copper sandwich beam are also compared in Table 3.1. Good agreements between the model and measured data are evident, suggesting that the model presented in Eq. (3.15) accurately describes the shear modulus of the silicon rubber sealant.

Table 3.1 Comparisons of the computed and measured first three natural frequencies (Hz) and corresponding half power bandwidths of the two sandwich structures with the silicon rubber sealant

Material	Method	First Mode		Second Mode		Third Mode	
		Frequency	HP	Frequency	HP	Frequency	HP
Aluminum	EXP	49.01	0.080	217.40	0.030	520.40	0.020
	FE	49.07	0.080	217.70	0.030	526.40	0.020
Copper	EXP	29.83	0.080	131.50	0.034	327.80	0.018
	FE	29.86	0.084	130.66	0.032	322.60	0.017

HP – Half power bandwidth

3.3.2 Identification of MR fluid properties

The final experiments were performed for characterizing the properties of two different MR fluids with carbonyl iron particles: MRF 132DG (viscosity = 0.112 Pa-s, solid content by weight =80.98%, mass density = 3500 kg/m^3); and MRF 122EG (viscosity = 0.042 Pa-s, solid content by weight =72%, mass density = 2350 kg/m^3). The strain amplitude experienced by the core layer of sandwich structures was considered to be substantially lower than the yielding strain of the MR fluids, which is in the range of 0.2% to 0.8% (Li et al., 1999). The MR fluids are thus considered in the pre-yield region, and assumed as viscoelastic materials.

The hollow aluminum sandwich beam structure, realized in the previous experiment, was filled with each MR fluid. For this purpose, two small holes were drilled on the constraining layer near the support and the tip, which permitted fluid injection using a hypodermic syringe and venting of the air from the beam. The holes were subsequently blocked using an aluminum adhesive tape. The aluminum sandwich beams with two different fluids were used for characterization of the fluid properties, while the experiments with the copper sandwich beams permitted the validation of the identified fluid properties. Each sandwich structure was firmly clamped to the vibration exciter. Two ceramic rectangular permanent magnet bars (266 *mm* long, 50 *mm* wide and 25 *mm* thick) were positioned beneath the host layer and slightly above the constraining layer using a specially designed fixture. The permanent magnets were carefully aligned so as to achieve nearly uniform

magnetic field along the span of the beam, which was verified through measurements along the beam length using a Gauss meter. All the test fixtures were fabricated using aluminum and brass so as to reduce the disturbances to the magnetic field. The large size of the magnets compared to the sandwich beam structure also helped to achieve a very uniform magnetic flux over the structure. The measurements revealed less than 5% variations in the magnetic flux over the length of the structure. The horizontal level of the permanent magnets was also verified to ensure that the magnetic flux occurs perpendicular to the beam surface. The fixture was designed so as to vary the distance between the beam surface and the magnet to achieve variations in density of the magnetic flux applied to the structure. The magnetic flux density across the sandwich beam thickness was measured using the Gauss meter.
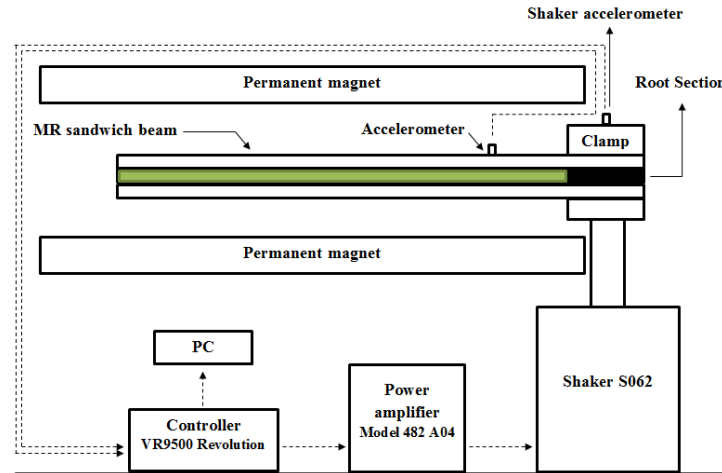
Figure 3.4 Experimental setup

A miniature three-axis accelerometer, weighing 1.5 grams, was installed on the sandwich structure, 30 *mm* from the support, for measurement of the beam response. A single-axis accelerometer was also installed at the support to measure the acceleration due to excitation. The structure was excited using constant acceleration (0.5 m/s^2 peak) harmonic vibration swept in the 1 to 500 Hz frequency at the rate of 1 octave/min, using a vibration controller (VR 9500). The test setup is schematically illustrated in Figure 3.4. The H_1 function was used to characterize the frequency response function (FRF) of the structure. The experiments were conducted under four different levels of magnetic flux density: 0, 30, 50 and 90 mT. For this purpose, the positions of the permanent magnets were varied to achieve the desired magnetic flux density. The experiments were repeated with two aluminum and two copper sandwich beams containing two MR fluids considered in the study. The natural frequencies and the corresponding half-power bandwidths

were extracted from the measured FRF for each experimental condition. The data acquired for the aluminum sandwich beams alone were used for identifying the fluid properties.

A finite element model of the MR based sandwich beam structure is developed for identifying the complex shear moduli of the MR fluids. The properties of the aluminum face layers and silicon rubber sealant, identified from the earlier experiments, were used in the model. The model thus lacked precise knowledge of the complex shear modulus of the fluid. The effect of accelerometer mass was also considered in the model by introducing its effective mass on the beam structure at the appropriate position. Furthermore, the storage and loss moduli of the silicon rubber were slightly lowered (0.20% and 25%, respectively) to account for the effect of the MR fluid on the silicon rubber (Ferry, 1980). Considering that the storage and loss moduli of the MR fluid are strongly dependent upon the excitation frequency and magnetic flux density, repeated simulations were performed to identify the fluid moduli under different magnetic flux densities at several discrete frequencies in the 1 to 500 Hz frequency range. The loss and storage moduli of the fluid were adjusted under each magnetic field and vibration excitation combination so as to achieve reasonably good agreements (less than 2% error) with the corresponding measured data in terms of natural frequencies and half-power bandwidths. The identification process was limited to the frequencies and half-power bandwidths corresponding to the first three modes. The resulting moduli, expressed as functions of the magnetic flux density and excitation frequency, were applied to determine the responses of the copper sandwich beam structure models to examine the validity of the identified properties.

3.4. Results and discussion

3.4.1 Identification of the complex shear moduli models

It has been widely reported that the storage (G') and loss moduli (G'') of the MR fluids could be described by quadratic function in the magnetic flux density (B) (Choi et al., 1990). This is attributed to this fact that the rheological behavior of the MR fluids depends on the dipole-dipole interactions, which are proportional to the product of the magnetic flux density, B, and the dipole moment, P. The dipole moment is proportional to B prior to the saturation of the MR fluid, consequently, the rheological parameters of the MR fluid such as loss and storage moduli, and yield stress are quadratic functions of B (Choi et al., 1990). The moduli are also known to depend on the excitation frequency (Gamota and Filisko, 1991). The results obtained from the measured

data and the finite element model, however, revealed saturation of the moduli with frequency above 300 Hz. In this study, the storage or loss moduli are formulated as a composition of two independent functions in B (mT) and ω (Hz), where the frequency dependence is described by an exponential function, such that:

$$\bar{G} = (a_0 + a_1 B + a_2 B^2)\left(1 - e^{-a_3 \omega}\right) \tag{3.16}$$

where $\bar{G}$ represents the storage or loss modulus (Pa) and a_0, a_1, a_2, and a_3 are unknown constants, which are identified through solutions of an error minimization problem. The minimization problem is formulated as the sum of squared errors between the moduli evaluated from Eq. (3.16) and those established from the FE model tuned to the measured data over the ranges of magnetic flux density and frequency considered in the experiment:

$$E(X) = Minimize\left[\sum_{\omega}\sum_{B}\left(\bar{G} - \bar{G}_{exp}\right)^2\right] \tag{3.17}$$

where E is the minimization function of the design vector X of the constant coefficients, $\bar{G}_{exp}$ is the modulus obtained from the measured data corresponding to three lower mode resonance frequencies and four levels of magnetic flux density (0, 30, 50 and 90 mT), and $\bar{G}$ is the modulus computed from Eq. (3.16). The minimization function thus incorporated 12 data corresponding to different combinations of magnetic flux densities and frequencies. The least-squared minimization technique is employed to compute the constant coefficients for both the storage and loss moduli models. The identified coefficients for the MRF 122EG and MRF 132DG are summarized in Table 3.2. The degree of fit of the models with the experimental data was also evaluated in terms of the R-squared coefficient, R^2. The R^2 values of the storage and loss moduli of the MRF 122EG were obtained as 0.987 and 0.887, respectively, while those for the MRF 132DG were 0.983 and 0.992, respectively.

Table 3.2 The identified coefficients of the storage and loss moduli models of MRF 122EG and MRF 132DG fluids

MR fluid	Modulus	a_0	a_1	a_2	a_3
MRF 122EG	Storage	97905.69	6744.595	92.75970	0.007328
	Loss	41281.45	1807.337	8.470100	0.006500
MRF 132DG	Storage	192160.6	30663.56	243.6247	0.004080
	Loss	45524.40	6757.977	6.441200	0.007416

The shear and loss moduli models, described in Eq. (3.16) and Table 3.2, are subsequently applied in the FE models of the sandwich structures to compute their natural frequencies and half-power bandwidths. Table 3.2 illustrates comparisons of the computed first three natural frequencies and the corresponding half power bandwidths (HP) of the aluminum sandwich beam with MR fluid (MRF 122EG) with the measured data for the range of magnetic flux density considered in the experiments.

Table 3.3 Comparisons of the computed and measured values of the first three natural frequencies (Hz) and corresponding half power bandwidths of the aluminum sandwich beam with MR fluid (MRF 122EG) for different magnetic flux densities (B).

Flux density (mT)	Method	First Mode		Second Mode		Third Mode	
		Frequency	HP	Frequency	HP	Frequency	HP
0	EXP	38.35	0.071	178.00	0.030	444.80	0.024
	FE	38.35	0.077	177.73	0.032	441.77	0.018
30	EXP	38.90	0.090	182.10	0.042	446.10	0.026
	FE	39.48	0.089	183.28	0.041	448.64	0.023
50	EXP	39.68	0.120	189.00	0.042	460.30	0.027
	FE	40.58	0.098	188.64	0.047	455.27	0.028
90	EXP	43.85	0.250	203.00	0.059	471.00	0.029
	FE	43.73	0.105	202.77	0.059	473.21	0.036

The comparisons suggest reasonably good agreements between the computed and the measured values for the entire range of magnetic flux densities. The results reveal that the natural frequencies of the structure increase with increasing magnetic field. This phenomenon, has also been reported in many studies (Yalcintas and Dai, 1998; Sun et al., 2003; Rajamohan et al., 2010), can be attributed to increase in the complex shear modulus of the MR fluid with increasing magnetic flux density. The half power bandwidths corresponding to all the three modes of the structure also increase with increasing magnetic flux. In a similar manner, Table 3.4 illustrates comparisons of the first three natural frequencies and corresponding half power bandwidths of the aluminum sandwich beam model with MRF 132DG fluid with the corresponding measured data. The comparisons show very good agreement between the model and the measured results for the three lower vibration modes, irrespective of the magnetic flux density. It was noted that the MRF 132DG is composed of relatively larger magnetic particles compared to the MRF 122EG. The application of this fluid was thus expected to show more significant changes in the complex shear modulus with varying magnetic flux density. This is evident from relatively greater increases in the natural

frequencies and the half-power bandwidth of the structure compared to those observed for the structure with MRF 122EG fluid.

Table 3.4 Comparisons of the computed and measured values of the first three natural frequencies (Hz) and corresponding half power bandwidths of the aluminum sandwich beam with MR fluid (MRF 132DG) for different magnetic flux densities (B).

Flux density (mT)	Method	First Mode		Second Mode		Third Mode	
		Frequency	HP	Frequency	HP	Frequency	HP
0	EXP	35.28	0.060	167.30	0.028	412.50	0.019
	FE	35.61	0.068	165.91	0.029	414.78	0.016
30	EXP	36.22	0.078	178.30	0.060	436.30	0.031
	FE	37.95	0.120	179.70	0.062	436.22	0.034
50	EXP	37.86	0.130	196.90	0.077	453.50	0.038
	FE	39.98	0.152	191.42	0.078	454.42	0.043
90	EXP	44.56	0.180	223.60	0.084	492.70	0.050
	FE	45.10	0.181	218.57	0.089	498.36	0.056

During the experiments, an opposite trend in the natural frequencies was observed when only one permanent magnet was used to produce the magnetic flux. This suggested that increasing the magnetic flux density would result in shifting of the natural frequencies to lower frequencies, although with higher damping ratios. This behavior has also been reported by Lara-Prieto et al (Lara-Prieto et al., 2010), and is attributed to the concentration of the magnetic particles in the core layer of the structure. Furthermore, applying a single permanent magnet tends to generate a non-uniform magnetic field over the structure, which would also lead to non-uniform concentration of the magnetic particles and stiffening effect of the MR fluid along the sandwich beam.

3.4.2 Frequency and magnetic field dependence of loss and storage moduli

Figures 3.5 and 3.6 illustrate variations in the loss and storage moduli of MRF 122EG and MRF 132DG, obtained by the experiment and model, with increasing the magnetic flux density and excitation frequency. It is evident that the storage and loss moduli of the MR fluids are relatively more sensitive to the magnetic flux density compared to the frequency. Both the moduli increase substantially with increasing field, which can be attributed to increases in the shear stiffness of the fluid. The results also show that for a given value of B, the moduli of the fluids increase with frequency but tend to saturate at higher frequencies.
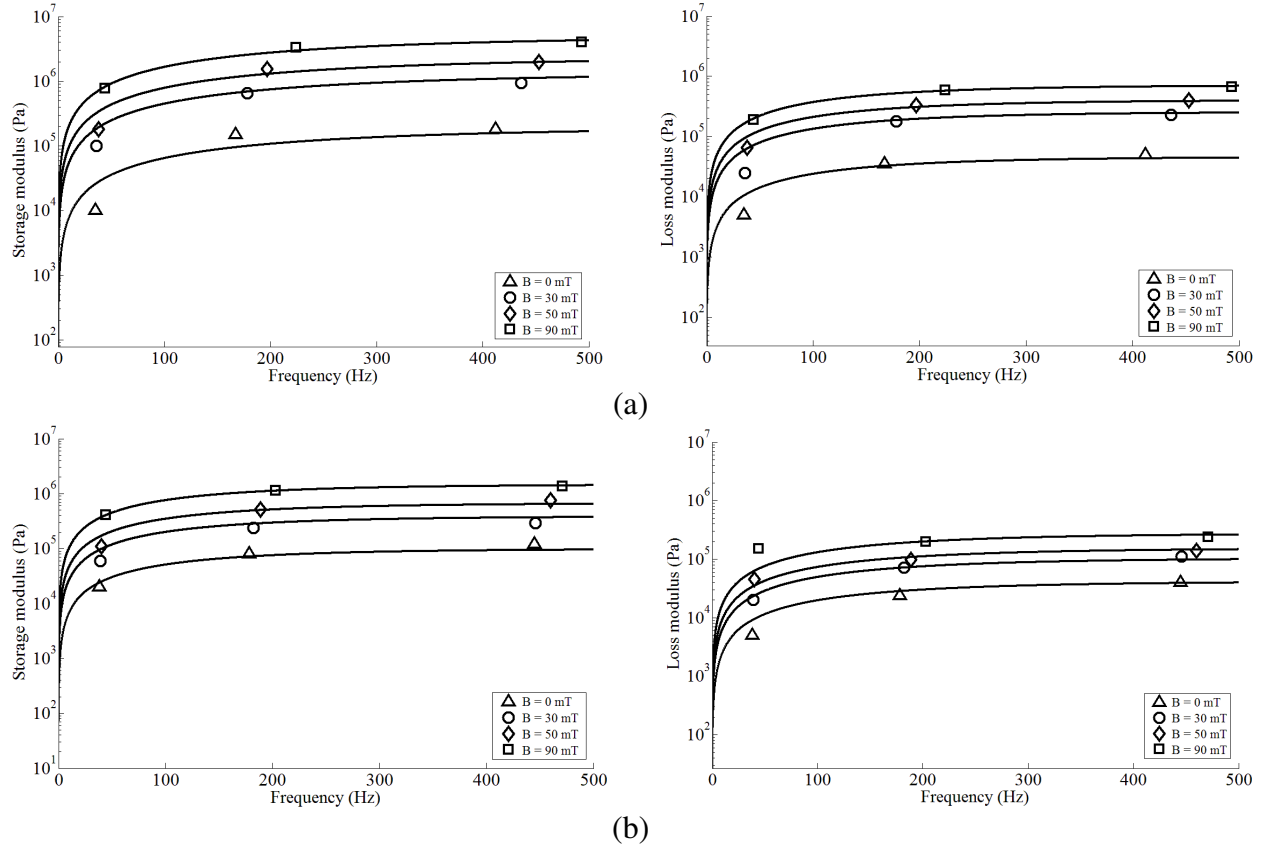
Figure 3.5 Variations in the storage and loss moduli of the (a) MRF 132DG and (b) MRF 122EG fluids with increasing frequency and magnetic flux density. (The moduli obtained from the model are shown by the solid lines).

For a given excitation frequency, on the other hand, both the storage and loss moduli increase with the magnetic flux density in a nearly quadratic manner. For instance, the storage and loss moduli of MRF 122EG at 90 mT are nearly 8 and 5 times, respectively, of those at 10 mT, when the excitation frequency is 100 Hz. Furthermore, the storage modulus of the MR fluids are substantially higher than the loss modulus. The rates of changes in both the moduli with frequency for the MRF 132DG are substantially higher, which causes the saturation at a relatively lower frequency. The rate of change of the moduli with respect to magnetic flux density is also higher for the MRF 132DG. The relatively larger variations in the moduli with the magnetic flux is due to relatively larger particle size and volume fraction of the MRF 132DG. Increasing the magnetic flux density from 10 mT to 90 mT yields nearly 10-fold increase in the storage modulus of MRF 132DG at 100 Hz, while the loss modulus increased 6-fold.
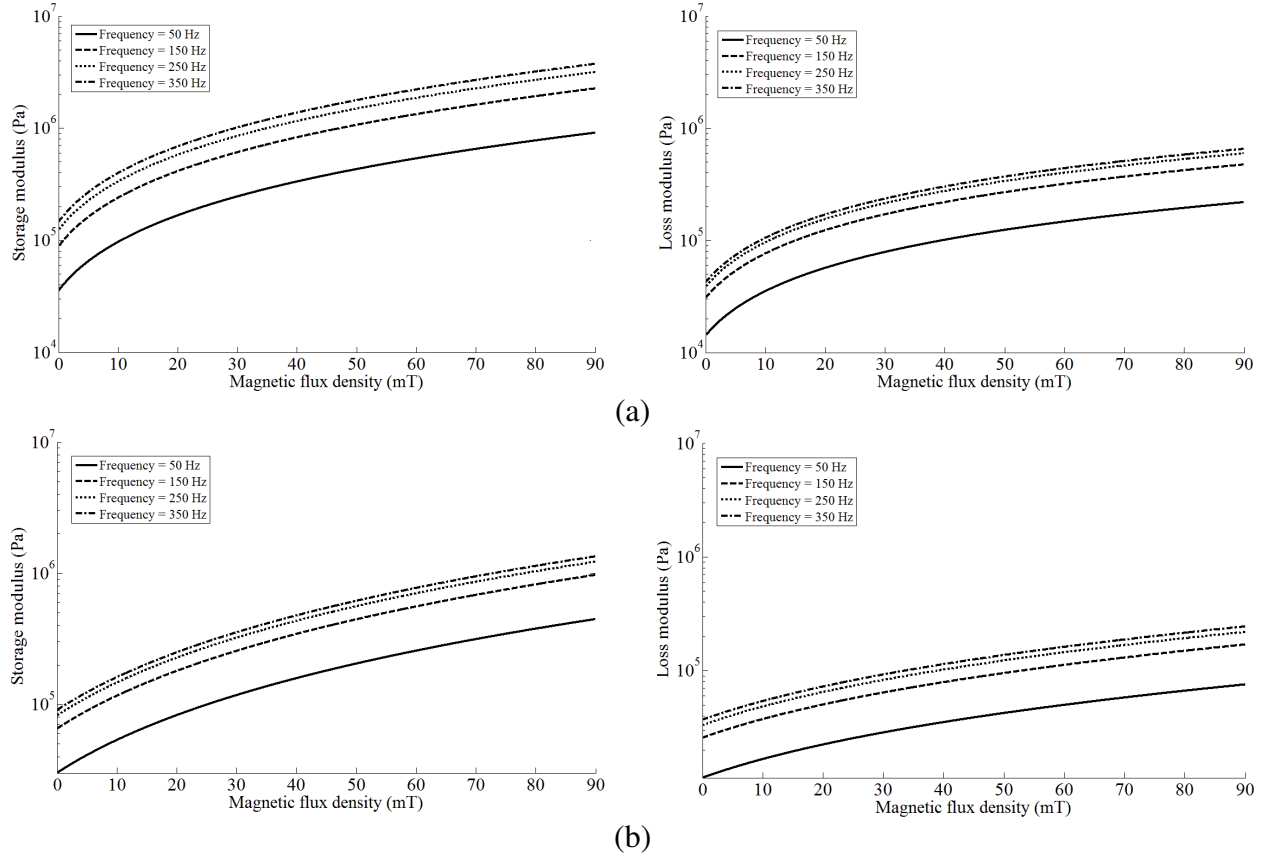
Figure 3.6 Variations in the storage and loss moduli of the (a) MRF 132DG and (b) MRF 122EG fluids with increasing magnetic flux density, under different excitation frequencies.

Figure 3.7 illustrates the variations in the loss factors, defined as the ratio of the loss modulus to the storage modulus, of the two fluids with the excitation frequency and the magnetic flux density. The loss factor relates to the dissipated energy as proportion of the stored energy of a material per radian. The results suggest relatively stronger influence of frequency under the low level magnetic flux density compared to that observed under the higher magnetic flux. This may be attributed to relatively stronger adhesion of magnetic particles under the higher magnetic flux, where the vibration frequency effect becomes less significant. Increasing the magnetic flux density results in a lower loss factor since the effect of magnetic field on the storage modulus is far more pronounced compared to the loss modulus. This behavior has also been reported by Li et al. (1999). The higher storage modulus of MRF 132DG results in relatively lower loss factor compared to that of MRF 122EG.

74

(a)

(b)
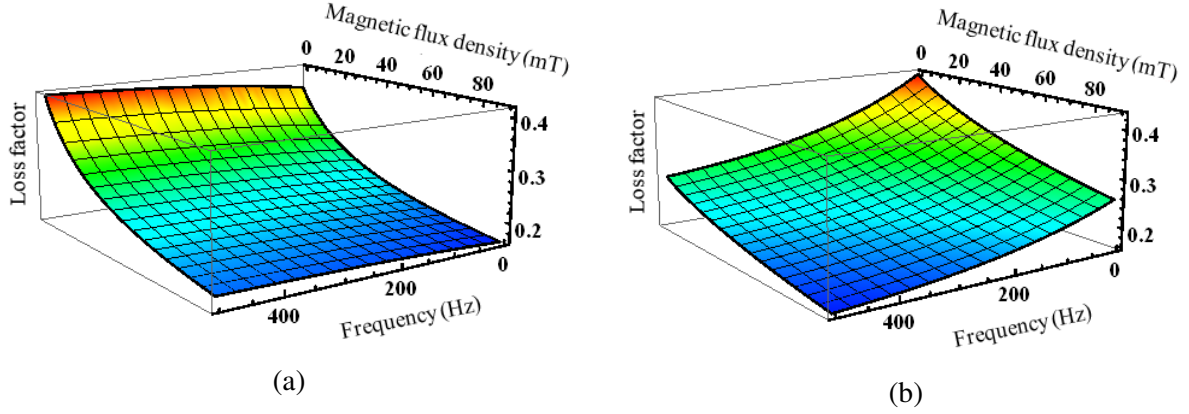
Figure 3.7 Influences of frequency and magnetic flux density on the loss factor of (a) MRF 122EG
and (b) MRF 132DG

3.4.3 Verifications of the complex shear moduli models

The validity of the proposed complex shear modulus model, Eq. (3.16), for the two MR-fluids together with the identified coefficients, is examined through application of the model to the copper sandwich structure. The FE model of the copper sandwich beam with the MR fluid models is analyzed to determine its natural frequencies and the corresponding half-power bandwidths, which are compared with the measured values in Table 3.5 for both the fluids. The results, in-general, show very good agreements between the model results and the measured values for the entire range of magnetic flux density (0 to 90 mT) considered in the study. The results thus suggest that the proposed characterization model, Eq. (3.16), can effectively describe loss and storage moduli of the MR fluids over the frequency and magnetic flux density ranges considered in the study.

The results in Table 3.5 show lower frequencies of the copper beam structure with the MRF 132DG compared to those obtained with the MRF 122EG in the absence of magnetic flux. An identical tendency is also evident for the aluminum beam (Tables 3.3 and 3.4). This tendency is attributable to the relatively higher mass density of the MRF 132DG compared to the MRF 122EG. The MRF 132DG, however, exhibits more significant effects on the natural frequencies under the application of magnetic field. For example, the fundamental frequency of the MRF 132DG-based aluminum sandwich beam increases from 35.28 to 44.56 Hz (26.3%) when the magnetic flux density is increased from 0 to 90 mT. The MRF 122EG, however, yields an increase of 14.3% in the fundamental frequency of the aluminum sandwich beam subject to the same change in the

75

magnetic flux density. This is due to relatively larger size and volume fraction of magnetic particles of the MRF 132DG, which enhances the magnetic permeability of the MR fluid leading to higher density of the magnetic flux in the fluid, and thus greater changes in its rheological property (Mazlan et al., 2007).

Table 3.5 Variations in first three natural frequencies (Hz) and corresponding half power bandwidths of the copper sandwich beam with the two MR fluids against the magnetic flux density (B).

Flux density (mT)	Method	First Mode		Second Mode		Third Mode	
		Frequency	HP	Frequency	HP	Frequency	HP
MRF 122EG							
0	EXP	25.78	0.072	117.00	0.029	298.40	0.017
	FE	25.65	0.080	116.68	0.032	292.90	0.017
30	EXP	25.90	0.084	119.20	0.037	299.10	0.020
	FE	26.21	0.088	120.02	0.041	297.77	0.023
50	EXP	26.08	0.093	122.30	0.042	301.90	0.025
	FE	26.80	0.094	123.27	0.047	302.53	0.027
90	EXP	28.34	0.230	131.90	0.062	310.50	0.030
	FE	28.42	0.100	132.11	0.059	315.49	0.037
MRF 132DG							
0	EXP	24.65	0.076	113.70	0.031	285.50	0.018
	FE	24.59	0.068	112.20	0.031	282.35	0.016
30	EXP	25.23	0.094	118.20	0.054	294.20	0.031
	FE	25.83	0.111	120.35	0.062	296.77	0.035
50	EXP	25.70	0.110	130.00	0.080	308.00	0.060
	FE	26.91	0.143	127.50	0.080	309.27	0.047
90	EXP	30.75	0.210	158.90	0.094	345.80	0.055
	FE	29.59	0.170	144.80	0.097	340.12	0.061

It has been reported that a MR fluid with higher magnetic permeability would yield greater changes in the rheological properties, which is mostly attributed to the stronger magnetic flux formed within the fluid (Jolly et al., 1999; Simon et al., 2001). The results further show relatively small effect of the magnetic flux on the higher modes frequencies. For instance, the third natural frequency of the MRF 122DG based aluminum sandwich beam increases by only 6%, when the magnetic flux density increased from 0 to 90 mT. This increase is substantially lower than 14.3% increase observed in the fundamental frequency. Similarly, for the MRF 132DG, the third mode frequency increased by 19% compared to 26.3% for the fundamental mode. This is mostly due to

greater shear deformations in the sandwich beam structure near the fundamental mode compared to the higher modes.
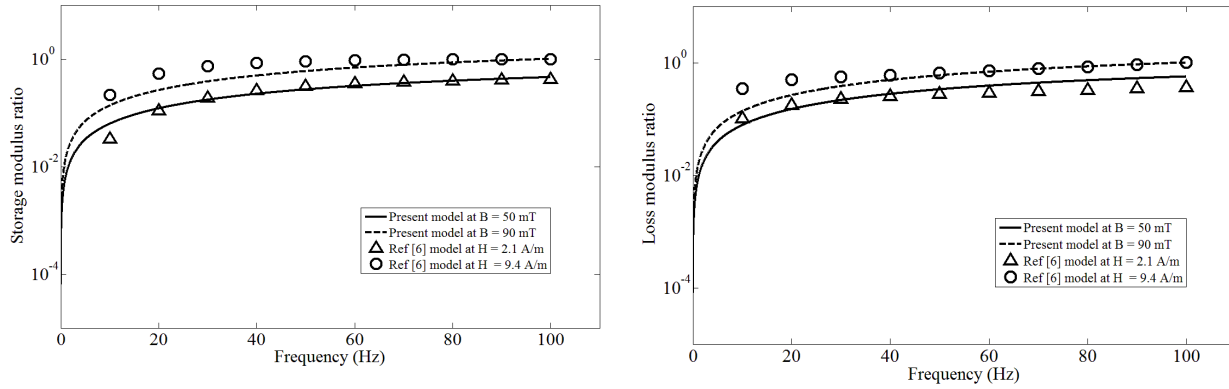
Figure 3.8 Variations of the storage and loss moduli ratios of MRF 132DG (lines obtained by the present model) and MRHCCS4-A (discrete marks obtained by oscillation shear rheometer (Mohammadi et al., 2010)) with frequency, under different magnetic field levels.

The loss and storage moduli of the MR fluids, more or less, follow similar trends with variations in the applied magnetic field and excitation frequency. The rates of variations in the rheological properties, however, may depend on the physical properties of the fluid such as volume fraction, magnetic particle size and carrier fluids. The validity of the proposed model was further attempted by comparing the results obtained for the MRF 132DG fluid with the pre-yield characteristics reported in (Mohammadi et al., 2010) for the MRHCCS4-A fluid using the oscillation shear rheometer. Figure 3.8 compared the storage and loss moduli of MRF132DG with the results reported in (Mohammadi et al., 2010) in the 0-100 Hz frequency range, and two different magnitudes of flux density (50 and 90 mT). The results are presented in terms of the storage and loss modulus ratio, defined as the ratio of the storage or loss modulus at a given frequency and magnetic field to that at the maximum frequency of 100 Hz and the magnetic field levels ($B = 90$ mT for MRF 132DG and $H = 9.4$ A/m for MRHCCS4-A). The comparisons suggest very similar trend, although the storage and loss moduli obtained for the two MR fluids differ.

3.5. Conclusions

The loss and storage moduli of the MR fluids in the pre-yield region vary with the magnetic flux density and the excitation frequency in a nonlinear manner. Both the moduli can be characterized through composition of independent exponential function in frequency and quadratic

function in magnetic flux density. More accurate pre-yield complex shear model of the MR fluid could be identified on the basis of the measurement-based moduli as opposed to the sandwich structure response, namely the natural frequencies and/or the frequency response magnitude peaks. The finite-element model of the sandwich structure in conjunction with the measured frequency responses could provide the target storage and loss moduli for model parameters identification. Furthermore, accurate characterization and integration of the sealant rubber properties in the finite element model is essential to minimize its potential contributions to the MR fluid properties. In this study, the proposed loss and storage moduli models of two different MR fluids (122EG and 132DG) were identified through measurements with an aluminum sandwich beam. From the application of the models to an alternate material (copper) sandwich beam, it is concluded that the proposed models can yield accurate predictions of the structure response in both the resonance frequencies and the corresponding half-power bandwidths over relatively wide ranges of the magnetic flux density. The model results revealed that the pre-yield loss and storage moduli of the MR fluids increase with frequency but approach saturation at frequencies above 200 to 300 Hz. Both the moduli, however, increase with the magnetic flux density in a quadratic manner. Both the fluids showed increase in the resonance frequencies and the half-power bandwidths with increasing magnetic flux, while the increase was considerably larger for the 132DG fluid. Moreover, the stiffening effect of the magnetic field was far more pronounced in the fundamental mode frequency.

CHAPTER 4

THE EFFECT OF MR FLUID ON VIBRATION SUPPRESSION CAPABILITY OF ADAPTIVE RECTANGULAR SANDWICH PLATES

4.1. Introduction

Applications of solid viscoelastic materials in the sandwich structures have been widely investigated for vibration attenuation in a low-cost and reliable manner (Nashif et al., 1985). The vibration control performance of such passive structures is generally limited to a specific frequency range due to fixed damping and stiffness properties of these structures. While low damping viscoelastic materials yield greater attenuation of vibration in the high frequency ranges, higher damping materials are more desirable for control of low frequency vibration. Smart fluids such as magneto-rheological (MR) and electro-rheological (ER) fluids that yield variable rheological properties from free-flowing condition to semi-solid state in response to controlled magnetic/electric field could be employed as the core layer in sandwich structures to achieve improved vibration suppression in a wide frequency range.

Vibration analyses of sandwich plate structures have been widely reported for varying industrial applications. The pioneering study by Ross et al. (1959) presented the effects of viscoelastic material layers on the vibration suppression of the sandwich plate structures. DiTaranto and McGraw (1969) illustrated a strong correlation between the loss factor and excitation frequency through free vibration analysis of a three-layered viscoelastically coupled plate structure considering transverse inertia effect and simply supported boundary condition. Abdulhadi (1971) further reported the forced vibration analysis of the structure. Mirza and Singh (1974) analyzed the axisymmetric vibration responses of circular sandwich plates comprising elastic plates with a low-strength and low-density viscoelastic layer. The effects of rotary inertia and transverse shear were taken into account, while the longitudinal stress in the core layer was neglected. Roy and Ganesan (1993) proposed a finite element solution for the analysis of a three layer circular sandwich plate with viscoelastic material, and presented the effects of thickness and shear modulus of the core layer on the natural frequencies and loss factors.

The applications of the MR and ER fluids in the adaptive beams (Rajamohan et al., 2010, 2010b), plates (Yeh and Chen, 2004, 2005, 2006, 2007) and shells (Mohammadi and Sedaghati,

2012, 2012b) have been widely explored during the past three decades, although the vast majority has focused on beam structures. Choi et al. (1999) experimentally investigated the vibration properties of a clamped-clamped sandwich plate consisting of two aluminum face layers, a rubber spacer and ER fluid as the core layer, and showed a significant shift in the natural frequencies (up to 55%) under a 1 kV/mm electric field. Yeh and Chen (2004, 2005, 2006, 2007) studied the dynamic responses of the isotropic and orthotropic rectangular sandwich plate structures with ER fluid using the finite element methods. The models considered linear stress-strain relationship in terms of the complex shear modulus considering that the ER fluid operates in the pre-yield regime. Yeh (2007) also employed the Rayleigh-Ritz method to study dynamic responses of three-layered annular plates with ER fluid, and concluded that the rectangular and circular plates exhibit similar trends in loss factor and natural frequencies under an applied electric field. Hasheminejad and Maleki (2009) developed an exact closed form solution for the free and forced vibration responses of a simply supported rectangular ER fluid sandwich plate using the classical plate theory. The study showed that the loss factor of the structure approaches its maxima under increasing electric field, but decreases with further increase in the field. It was suggested that an optimal electric field magnitude could be identified to achieve maximum loss factor corresponding to a specific excitation frequency. Furthermore, increasing the ER fluid thickness or face layer aspect ratio resulted in slightly lower vibration magnitude of the structure. Lu and Meng (2006) investigated the vibration analysis of a cantilever sandwich plate comprising two fiberglass laminates and ER fluid core layer. The study concluded more pronounced effect of the electric field intensity on the first and second vibration modes.

Compared to the ER-fluid sandwich structures, relatively fewer studies have presented the vibration analyses of MR fluid structures. Rajamohan et al. (2010, 2010b) investigated the free and forced vibration of a sandwich beam with total and partial MR fluid core layers using finite element and Ritz methods, and concluded that both the natural frequencies and damping ratios of the structure increase with increasing magnetic field intensity. Similar findings have also been reported in other studies on the MR sandwich beams. The effect of magnetic flux on the damping properties of a MR based sandwich beam was experimentally investigated by Lara-Prieto et al. (2010), which showed significant increase in the damping ratio in the presence of a magnetic field. Sun et al. (2003) characterized the complex shear modulus of a MR fluid in the pre-yield region using oscillatory rheometry and investigated dynamic properties of a MR sandwich beam. Another

study demonstrated enhanced capability of a MR adaptive beam in vibration minimization (Chen and Hansen, 2005).

Aforementioned studies have generally focused on ER- or MR-treated sandwich beams, while the studies on vibration behaviors of plates have been mostly limited to ER-treated sandwich plates. Only a few studies have investigated dynamic properties of MR sandwich plates. The experimentally measured characteristics of MR sandwich plates, in-particular, have not been reported. For instance, Ying et al. (2014) employed a magneto-rheological visco-elastomer (MRVE) as the core layer of a sandwich plate to suppress stochastic micro vibration of the plate. Yeh (2013) presented vibration analysis of a MR based sandwich plate using the finite element approach and the phenomenological model of the MRF 122EG fluid reported in (Rajamohan et al., 2010). The study concluded that an increase in the magnetic field increases the storage and loss moduli of the MR fluid, and the resonant frequencies of the structure.

This study investigates the dynamic responses of a MR fluid sandwich plate using experimental and theoretical methods. A cantilever sandwich plate consisting of two polyethylene terephthalate (PET) face layers and MR fluid core layer was fabricated for experimental characterizations in terms of natural frequencies and half power bandwidths. The experiments were conducted with two different MR fluids, MRF 122EG and MRF 132DG, which are characterized in the pre-yield region in terms of the magnetic flux density and excitation frequency. A finite element (FE) model is subsequently developed to derive the governing equations of motion of the structure based on the classical plate theory together with phenomenological complex shear model of the fluids. The validity of the FE model is demonstrated through comparison of the results with the laboratory-measured responses. The measured data are further used to highlight a few important aspects that have not been addressed in the reported studies (Hasheminejad and Maleki, 2009; Yeh, 2013). A systematic parametric study is subsequently performed to investigate the effects of aspect ratio, core layer thickness and boundary conditions on the natural frequencies and damping ratios of the structure as a function of the magnetic flux.

4.2. Formulations

Consider a sandwich plate consisting of an elastic material base layer, rubber sealant spacer, a constraining layer and a MR fluid core layer, as shown in Figure 4.1. In the figure, l_1 and l_2 are the

length and width of the sandwich plate, respectively, while h_1, h_2 and h_3 denote thickness of the top, core and bottom layers, respectively.
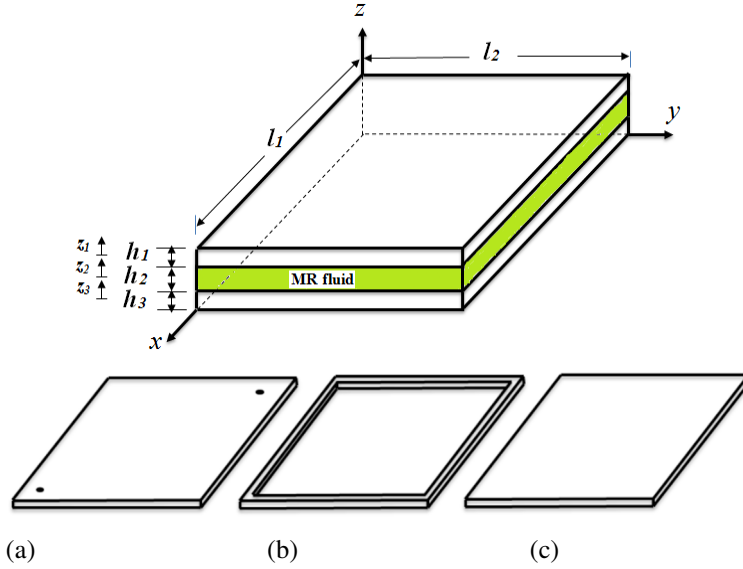
Figure 4.1 A sandwich plate with MR-fluid core layer consisting of (a) constraining top layer, (b) sealant spacer, (c) base layer

4.2.1. Displacement, strain and stress fields

Considering very low thickness to length ratio of the face layers, classical plate theory of Kirchhoff-Love is applied to derive the displacement field of an arbitrary point in the plate domain. Assuming negligible contributions due to the transverse shear deformation and rotary inertia, the displacement field of a Kirchhoff plate may be expressed as (Brush and Almroth, 1975):

$$u^{(i)}(x, y, z, t) = u_0^{(i)}(x, y, t) - z_i \frac{\partial w^{(i)}(x, y, t)}{\partial x}$$

$$v^{(i)}(x, y, z, t) = v_0^{(i)}(x, y, t) - z_i \frac{\partial w^{(i)}(x, y, t)}{\partial y}, \qquad i = 1 \, and \, 3 \qquad (4.1)$$

$$w^{(i)}(x, y, z, t) = w^{(i)}(x, y, t)$$

where u and v denote the longitudinal displacements along the x- and y-directions, respectively. u_0 and v_0 are the longitudinal displacements of the mid-plane along the x- and y-directions, and w represents the transverse displacement. The superscripts $i = 1$ and 3 refer to the top constraining and the bottom layers, respectively, and z_i is the transverse coordinate in the local coordinate system of each layer, as shown in Figure 4.1. The reported studies on sandwich plates generally

consider identical transverse displacement along the thickness of the plate (Hasheminejad and Maleki, 2009; Yeh, 2013). Above formulations, however, consider varying transverse displacement through each layer thickness. Furthermore, a continuous displacement profile through the thickness is considered assuming negligible slippage between the plate layers, which yields the following compatibility relations:

$$
u^{(1)}\Big|_{z_1=-h_1/2} = u^{(2)}\Big|_{z_2=h_2/2} \quad \& \quad v^{(1)}\Big|_{z_1=-h_1/2} = v^{(2)}\Big|_{z_2=h_2/2} \quad \& \quad w^{(1)}\Big|_{z_1=-h_1/2} = w^{(2)}\Big|_{z_2=h_2/2}
$$

$$
u^{(2)}\Big|_{z_2=-h_2/2} = u^{(3)}\Big|_{z_3=h_3/2} \quad \& \quad v^{(2)}\Big|_{z_2=-h_2/2} = v^{(3)}\Big|_{z_3=h_3/2} \quad \& \quad w^{(2)}\Big|_{z_2=-h_2/2} = w^{(3)}\Big|_{z_3=h_3/2}
$$

(4.2)

In the above equations, the superscript (2) refers to the core layer. Considering Eqs. (4.1) and (4.2), the displacement field of the core layer can be formulated in terms of those of the top and bottom layers, as:

$$
u^{(2)}(x,y,z,t) = \frac{u_0^{(1)}+u_0^{(3)}}{2} + \frac{1}{4}\left(h_1\frac{\partial w^{(1)}}{\partial x} - h_3\frac{\partial w^{(3)}}{\partial x}\right) + z_2\left(\frac{u_0^{(1)}-u_0^{(3)}}{h_2} + \frac{h_1}{2h_2}\frac{\partial w^{(1)}}{\partial x} + \frac{h_3}{2h_2}\frac{\partial w^{(3)}}{\partial x}\right)
$$

$$
v^{(2)}(x,y,z,t) = \frac{v_0^{(1)}+v_0^{(3)}}{2} + \frac{1}{4}\left(h_1\frac{\partial w^{(1)}}{\partial y} - h_3\frac{\partial w^{(3)}}{\partial y}\right) + z_2\left(\frac{v_0^{(1)}-v_0^{(3)}}{h_2} + \frac{h_1}{2h_2}\frac{\partial w^{(1)}}{\partial y} + \frac{h_3}{2h_2}\frac{\partial w^{(3)}}{\partial y}\right)
$$

(4.3)

$$
w^{(2)}(x,y,z,t) = \frac{w^{(1)}+w^{(3)}}{2} + z_2\frac{w^{(1)}-w^{(3)}}{h_2}
$$

The normal and in-plane shear strains in the face layers, and the transverse shear strain in the core layer, are subsequently obtained from Eqs. (4.1) and (4.3), as:

$$
\varepsilon_x^{(i)} = \frac{\partial u_0^{(i)}}{\partial x} - z_i\frac{\partial^2 w^{(i)}}{\partial x^2}; \quad \varepsilon_y^{(i)} = \frac{\partial v_0^{(i)}}{\partial y} - z_i\frac{\partial^2 w^{(i)}}{\partial y^2}; \quad \gamma_{xy}^{(i)} = \frac{\partial u_0^{(i)}}{\partial y} + \frac{\partial v_0^{(i)}}{\partial x} - 2z_i\frac{\partial^2 w^{(i)}}{\partial x\partial y}; \quad i=1 \, and \, 3
$$

$$
\gamma_{xz}^{(2)} = \frac{u_0^{(1)}-u_0^{(3)}}{h_2} + \left(\frac{h_1+h_2+2z_2}{2h_2}\right)\frac{\partial w^{(1)}}{\partial x} + \left(\frac{h_3+h_2-2z_2}{2h_2}\right)\frac{\partial w^{(3)}}{\partial x}
$$

(4.4)

$$
\gamma_{yz}^{(2)} = \frac{v_0^{(1)}-v_0^{(3)}}{h_2} + \left(\frac{h_1+h_2+2z_2}{2h_2}\right)\frac{\partial w^{(1)}}{\partial y} + \left(\frac{h_3+h_2-2z_2}{2h_2}\right)\frac{\partial w^{(3)}}{\partial y}
$$

where ε_x and ε_y refer to normal strains along the x- and y-directions, respectively, and γ_{xy}, γ_{xz} and γ_{yz} denote the in-plane and transverse shear strains. It should be noted that in-plane shear

strain in the core layer is negligible (Yeh and Chen, 2007). The above strain equations may be expanded and re-written in a matrix form, as:

$$
\begin{Bmatrix} \varepsilon_x^{(1)} \\ \varepsilon_y^{(1)} \\ \varepsilon_x^{(3)} \\ \varepsilon_y^{(3)} \\ \gamma_{xy}^{(1)} \\ \gamma_{xy}^{(3)} \\ \gamma_{xz}^{(2)} \\ \gamma_{yz}^{(2)} \end{Bmatrix} =
\begin{bmatrix}
\partial/\partial x & 0 & 0 & 0 & -z_1 \partial^2/\partial x^2 & 0 \\
0 & \partial/\partial y & 0 & 0 & -z_1 \partial^2/\partial y^2 & 0 \\
0 & 0 & \partial/\partial x & 0 & 0 & -z_3 \partial^2/\partial x^2 \\
0 & 0 & 0 & \partial/\partial y & 0 & -z_3 \partial^2/\partial y^2 \\
\partial/\partial y & \partial/\partial x & 0 & 0 & -2z_1 \partial^2/\partial x \partial y & 0 \\
0 & 0 & \partial/\partial y & \partial/\partial x & 0 & -2z_3 \partial^2/\partial x \partial y \\
1/h_2 & 0 & -1/h_2 & 0 & \left(\left(h_1+h_2+2z_2\right)/2h_2\right)\partial/\partial x & \left(\left(h_3+h_2-2z_2\right)/2h_2\right)\partial/\partial x \\
0 & 1/h_2 & 0 & -1/h_2 & \left(\left(h_1+h_2+2z_2\right)/2h_2\right)\partial/\partial y & \left(\left(h_3+h_2-2z_2\right)/2h_2\right)\partial/\partial y
\end{bmatrix}
\begin{Bmatrix} u_0^{(1)} \\ v_0^{(1)} \\ u_0^{(3)} \\ v_0^{(3)} \\ w^{(1)} \\ w^{(3)} \end{Bmatrix}
\quad (4.5)
$$

Using the Hooke's law, the corresponding stress components in the face and core layers are obtained as (Brush and Almroth, 1975):

$$
\sigma_x^{(i)} = \frac{E_i}{\left(1-v_i^2\right)}\left(\varepsilon_x^{(i)} + v_i \varepsilon_y^{(i)}\right) = \frac{E_i}{\left(1-v_i^2\right)}\left(\frac{\partial u_0^{(i)}}{\partial x} - z_i \frac{\partial^2 w^{(i)}}{\partial x^2} + v_i\left(\frac{\partial v_0^{(i)}}{\partial y} - z_i \frac{\partial^2 w^{(i)}}{\partial y^2}\right)\right)
$$

$$
\sigma_y^{(i)} = \frac{E_i}{\left(1-v_i^2\right)}\left(\varepsilon_y^{(i)} + v_i \varepsilon_x^{(i)}\right) = \frac{E_i}{\left(1-v_i^2\right)}\left(\frac{\partial v_0^{(i)}}{\partial y} - z_i \frac{\partial^2 w^{(i)}}{\partial y^2} + v_i\left(\frac{\partial u_0^{(i)}}{\partial x} - z_i \frac{\partial^2 w^{(i)}}{\partial x^2}\right)\right)
$$

$$
\tau_{xy}^{(i)} = G\gamma_{xy}^{(i)} = G\left(\frac{\partial u_0^{(i)}}{\partial y} + \frac{\partial v_0^{(i)}}{\partial x} - 2z_i \frac{\partial^2 w^{(i)}}{\partial x \partial y}\right), \qquad i = 1 \, and \, 3 \qquad (4.6)
$$

$$
\tau_{xz}^{(2)} = G^* \gamma_{xz}^{(2)} = G^*\left(\frac{u_0^{(1)} - u_0^{(3)}}{h_2} + \frac{h_1}{2h_2}\frac{\partial w^{(1)}}{\partial x} + \frac{h_3}{2h_2}\frac{\partial w^{(3)}}{\partial x} + \frac{\partial w^{(2)}}{\partial x}\right)
$$

$$
\tau_{yz}^{(2)} = G^* \gamma_{yz}^{(2)} = G^*\left(\frac{v_0^{(1)} - v_0^{(3)}}{h_2} + \frac{h_1}{2h_2}\frac{\partial w^{(1)}}{\partial y} + \frac{h_3}{2h_2}\frac{\partial w^{(3)}}{\partial y} + \frac{\partial w^{(2)}}{\partial y}\right)
$$

where E, v and G are the Young's modulus, Poisson's ratio and shear modulus of the face layers, respectively. σ and τ denote the normal and shear stresses, respectively and G^* is the complex shear modulus of the core layer. This study assumes that the MR fluid operates within the pre-yield region and behaves viscoelastically. The shear stress and shear strain are thus assumed proportional in terms of the complex shear modulus G^*, given by (Li et al., 1999):

$$G^* = G' + iG'' \tag{4.7}$$

where G' is the storage modulus that determines the average energy stored per unit volume of the material over a deformation cycle, and G'' is the loss modulus that relates to the dissipated energy per unit volume of material in a deformation cycle.

4.2.2 Finite element model of the MR based sandwich plate

A finite element model of the plate is formulated for analysis of the sandwich plate structure considering the complex shear moduli of the sealant rubber and the MR fluid. Figure 4.2 illustrates the element used in the formulations, which consists of four nodes with 10 degrees-of-freedom (longitudinal displacements, transverse displacement and slopes about x- and y-axis for the top and bottom layers). Since the displacement field of the core layer is obtained from those of the top and bottom layers, the degrees-of-freedom (DOF) of each node are associated with those at the top and bottom layers.
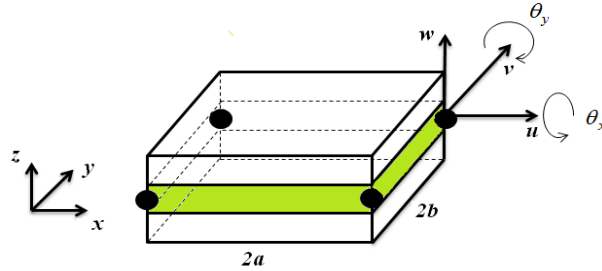
Figure 4.2 Two-dimensional sandwich plate element

The transverse and longitudinal displacements of the element can be expressed in terms of the nodal displacement vector, $q(t) = \left\{ u_{0i}^{(1)}, v_{0i}^{(1)}, u_{0i}^{(3)}, v_{0i}^{(3)}, w_i^{(1)}, w_i^{(3)}, \theta_{xi}^{(1)}, \theta_{xi}^{(3)}, \theta_{yi}^{(1)}, \theta_{yi}^{(3)} \right\}^T$ for $i=1,2,3,4$, and the shape function vectors, $N_{u1}(x,y), N_{v1}(x,y), N_{u3}(x,y), N_{v3}(x,y), N_{w1}(x,y)$ and $N_{w3}(x,y)$, such that:

$$w^{(i)}(x,y,t) = N_{wi}(x,y)q(t); \quad u_0^{(i)}(x,y,t) = N_{ui}(x,y)q(t); \quad v_0^{(i)}(x,y,t) = N_{vi}(x,y)q(t) \tag{4.8}$$

where $\theta_x = \partial w/\partial x$, $\theta_y = \partial w/\partial y$ and $i=1$ and 3. The shape function vectors used in the formulation are listed in the Appendix.

The total potential and kinetic energy of the $2a \times 2b$ plate element is expressed as the sum of those of the individual layers, such that:

$$V = V_1 + V_2 + V_3; \qquad\qquad T = T_1 + T_2 + T_3 \tag{4.9}$$

where V_1 and V_3 represent the total strain energy of the top and bottom layers, respectively, and V_2 is the shear strain energy in the core layer. Similarly, T_1 and T_3 denote the kinetic energy associated with the transverse and axial deformations of the top and bottom layers, respectively, and T_2 is the kinetic energy due to rotational deformation of the core layer. The energy functions for individual layers are obtained as:

$$V_i = \frac{1}{2} \int_{-a}^{a} \int_{-b}^{b} \int_{-h_i/2}^{h_i/2} \left(\sigma_x^{(i)} \varepsilon_x^{(i)} + \sigma_y^{(i)} \varepsilon_y^{(i)} + \tau_{xy}^{(i)} \gamma_{xy}^{(i)} \right) dz \, dy \, dx$$

$$V_2 = \frac{1}{2} \int_{-a}^{a} \int_{-b}^{b} \int_{-h_2/2}^{h_2/2} \left(\tau_{xz}^{(2)} \gamma_{xz}^{(2)} + \tau_{yz}^{(2)} \gamma_{yz}^{(2)} \right) dz \, dy \, dx \tag{4.10}$$

$$T_i = \frac{1}{2} \int_{-a}^{a} \int_{-b}^{b} \int_{-h_i/2}^{h_i/2} \rho_i \left(\left(u_0^{(i)} \right)^2 + \left(v_0^{(i)} \right)^2 + \left(w^{(i)} \right)^2 \right) dz \, dy \, dx, \qquad i = 1 \, and \, 3$$

$$T_2 = \frac{1}{2} \int_{-a}^{a} \int_{-b}^{b} \left(\rho_2 h_2 \left(\dot{w}^{(2)} \right)^2 + I_2 \left(\left(\dot{\gamma}_{xz}^{(2)} \right)^2 + \left(\dot{\gamma}_{yz}^{(2)} \right)^2 \right) \right) dy \, dx$$

where ρ_i is the weight density of face layer i (i =1, 3) and $I_2 = \rho_2 h_2^3 / 12$. Although the top and bottom layers of the sandwich plate structure could move independently, the silicon rubber sealant ensures more uniform deformations of the edges of the two face layers. This constraint is implemented in the FE model in the matrix form, as:

$$D = \left[A^e \right]_{n \times m} \{ q \}_{m \times 1} = 0 \tag{4.11}$$

where $[A^e]$ is the constraint coefficient matrix, n is the number of constraints and m is the element DOF, taken as 40 (element includes four nodes and ten DOF per node).

The governing equations of motion for the sandwich plate structure are subsequently obtained using the Lagrange's energy equation as:

$$\frac{d}{dt} \left(\frac{\partial L}{\partial \dot{q}_i} \right) - \frac{\partial L}{\partial q_i} = Q_i, \qquad i = 1, ..., m \tag{4.12}$$

where L is the Lagrangian and Q_i is the generalized force component. The constraints, defined in Eq. (4.11), are incorporated in the finite element model using the Lagrange multipliers λ_i, such that:

$$L = T - U + \sum_i \lambda_i D_i \tag{4.13}$$

Upon substituting for the energy functions in Eq. (4.10) and the constraints from (4.11) into the Lagrangian Eq. (4.12), and satisfying the stationary conditions, the governing equations of motion for the sandwich plate element are obtained, as:

$$[m^e]_{m \times m} \{\ddot{q}\}_{m \times 1} + [k^e]_{m \times m} \{q\}_{m \times 1} + [A^e]_{m \times n}^T \{\lambda\}_{n \times 1} = \{f^e\}_{m \times 1}$$

$$[A^e]_{n \times m} \{q\}_{m \times 1} = \{0\}_{n \times 1}$$

(4.14)

where $[m^e]$ and $[k^e]$ are the elemental mass and stiffness matrices, respectively, and $\{f^e\}$ is the nodal force vector. The governing equations of motion for the fully treated MR sandwich plate structure are subsequently obtained by assembling the above elemental matrices, such that:

$$[M]_{p \times p} \{\ddot{d}\}_{p \times 1} + [K]_{p \times p} \{d\}_{p \times 1} + [B]_{p \times r}^T \{\lambda\}_{r \times 1} = \{F\}_{p \times 1}$$

$$[B]_{r \times p} \{d\}_{p \times 1} = \{0\}_{r \times 1}$$

(4.15)

In the above equation, $[M]$ and $[K]$ are the system mass and stiffness matrices, respectively, $[B]$ is the constraint coefficient matrix, and $\{F\}$ and $[d]$ are the global force and displacement vectors, respectively. p and r denote the total DOF of the structure and the number of constraints, respectively. The natural frequencies of the sandwich structure were obtained from the complex eigenvalues of the system of equations, given by:

$$\begin{bmatrix} -[M]\omega^2 + [K] & [B]^T \\ [B] & 0 \end{bmatrix} \begin{Bmatrix} d \\ \lambda \end{Bmatrix} = \begin{Bmatrix} 0 \\ 0 \end{Bmatrix}$$

(4.16)

4.3. Experimental methods – identification of material properties

An accurate analysis of the MR sandwich plate necessitated thorough characterizations of the complex shear moduli of the sealant rubber and the MR fluid. In this study, two different series of experiments were performed. In the first series, the experiments were designed to characterize the loss and storage moduli of the sealant rubber and the two MR fluids. The second series of experiments involved characterizations of vibration properties of the two MR fluid plates in terms of natural frequencies and half power bandwidths as a function of the applied magnetic flux, which were subsequently used to examine the validity of the FE model. Two fabricated cantilever MR fluid sandwich plates, each consisting of two 100 $mm \times$ 100 $mm \times$ 2 mm polyethylene terephthalate (PET) face layers separated by 1 mm thick silicon rubber spacer are constraining two different MR

87

fluids (MRF 132DG and MRF 122EG) as the core layer. The choice of PET material (density= 1400 kg/m^3; Young's modulus = 2.2 GPa) was motivated by its negligible magnetic permeability and thereby insignificant effect on the homogeneity of the magnetic flux applied to the structure. The 3 *mm* wide silicon rubber spacer was carefully bonded around the periphery of the top and bottom layers to provide a uniform gap of 1 *mm* between the face layers, and to contain the MR fluid within the core layer. A 100 *mm* by 20 *mm* root section was designed so as to simulate the cantilever boundary condition. The root section consisted of a 1 *mm* thick aluminum spacer located between roots of the two face layers. The physical properties of the MR fluids were taken as those reported by the manufacturer, Lord Corporation. The viscosity at room temperature, solid content by weight and density of the MRF 132DG were taken as 0.112 Pa-s, 80.98% and 3500 kg/m^3, respectively, and those of the MRF 122EG were 0.042 Pa-s, 72% and 2500 kg/m^3, respectively. The MR fluid contained in the core layer was typically subjected to a low shear strain (less than 0.4%) and was thus considered to operate within the pre-yield region.

4.3.1 Identification of the silicon rubber property

The studies reporting the vibration properties of MR- or ER-fluid sandwich beams and plates have mostly neglected the possible effect of the rubber spacer on the vibration characteristics (Hasheminejad and Maleki, 2009; Yeh, 2013). The visco-elastic properties of the rubber spacer, however, may affect the overall stiffness and damping properties of the sandwich structures. The initial experiment within the first series was thus designed to identify properties of the silicon rubber spacer through measurements of the PET sandwich plate without the MR fluid. For this purpose, the hollow sandwich plate with 1 *mm* thick silicon rubber spacer was mounted on an electrodynamic shaker in a cantilever configuration. A lightweight accelerometer (PCB Piezotronics, model 356A01), weighing 2.5 *grams*, was installed at one of the free corners of the sandwich plate to measure the vibration response. A single-axis accelerometer was also installed at the fixed support to measure the support excitation. The hollow sandwich plate was subjected to a harmonic vibration swept in the 1 to 550 Hz frequency range at the rate of 1 octave/min. The support and response acceleration signals were analyzed to obtain the frequency response function (FRF) of the structure using the H_1 method, which was used to identify the first six natural frequencies and the corresponding half power bandwidths of the structure.

The properties of the rubber sealant were identified using the FE model of the sandwich plate together with the measured responses. The model incorporated the silicon rubber properties such as density, Young's modulus and complex shear modulus, expressed as a combination of the storage G_r' and loss G_r'' moduli ($G_r^* = G_r' + i\,G_r''$). While the density (1460 kg/m^3) was obtained through direct measurements of the volume and the weight, the Young's modulus was considered negligible since the flexural rigidity of the silicon rubber is significantly lower than that of the face layers. Repeated simulations of the FE model were performed using varying values of the storage and loss moduli of the silicon rubber until reasonably good agreements were obtained between the predicted first six natural frequencies and the corresponding half power bandwidths and the measured data. The results suggested a constant value of the storage modulus ($G_r' = 1340000$ Pa), while the loss modulus revealed a quadratic relation with the excitation frequency ω (Hz), such that:

$$G_r'' = 152511 + 68.31\,\omega + 0.475\,\omega^2 \qquad (4.17)$$

The first six natural frequencies and the half power bandwidths (HP) corresponding to the first and third modes of the structure obtained from the FE model are compared with the measured values in Table 4.1.

Table 4.1 The first six natural frequencies (Hz) and the half power bandwidths (%) corresponding to the first and third modes of the PET sandwich plate without fluid.

		First	Second	Third	Fourth	Fifth	Sixth
Natural frequency	FE model	52.59	112.15	270.85	316.89	381.14	498.22
	Experiment	53.10	115.00	280.10	329.30	394.40	500.10
% Deviation		*1.0*	*2.5*	*3.3*	*3.8*	*3.3*	*0.4*
HP*	FE model	3.90	-	2.50	-	-	-
	Experiment	4.22	-	2.90	-	-	-
% Deviation		*7.6*		*13.7*			

HP: Half Power bandwidth

The results show reasonably good agreements between the computed and measured values (deviations less than 4% in the natural frequencies and 15% in the half power bandwidths). The measured natural frequencies and half power bandwidths were identified from the FRF measured at one of the free corners of the plate. It was further noted that the second, fourth, fifth and sixth modes of the plate were not significantly excited by the vertical support excitation at the root section of the plate. The half power bandwidths corresponding to these modes thus could not be reliably measured. The complexity associated with identification of the half power bandwidth has

also been reported by Oyadiji (1996). The natural frequencies of the plate were also identified using the impact hammer excitation together with the MEscopVES modal analysis software. These frequencies were very close to those obtained from the FRF (Table 4.1).

4.3.2 Characterization of the MR fluids

The complex shear moduli of the candidate MR fluids were identified using similar experimental and simulation methods. Two 150 *mm* long and 12 *mm* wide cantilever beams consisting of two 1 *mm* thick aluminum and 0.8 *mm* thick copper face layers and selected MR fluids as the core layer sealed by the silicon rubber sealant were fabricated for the experimental characterizations. The sealant bonded the two face layers of each beam and provided a gap of 2 *mm* between the face layers. The selected MR fluid (MRF 132DG or MRF 122EG) was carefully injected within the core layer of each sandwich beam using a syringe. Two high-temperature ceramic rectangular magnet bars were located at the top and bottom of the sandwich structure to provide uniform magnetic flux over the entire length of each sandwich beam. The density of the magnetic flux was varied by changing the vertical position of the magnets with respect to the face layers. The sandwich beam mounted on the electro-dynamic shaker in a cantilever configuration was subject to harmonic excitation in the 0 to 500 Hz frequency range. The natural frequencies and half power bandwidths corresponding to the first three modes were identified from the FRF of the response acceleration measured on the beam (30 *mm* from the clamped edge). The measurements were conducted under different vertical gaps between the magnets and the beam and thus the different magnetic flux densities, which was measured using a Gauss meter. The measurements conducted on both the beams without the MR fluid were used to further verify the properties of the rubber sealant described in Eq. (4.17). The simulation results obtained from the FE model of the MR sandwich beams revealed nearly identical moduli of the sealant.

The FE models of the beams incorporating the known sealant rubber moduli were used to identify the complex shear moduli of the candidate MR fluids, using the methodology described above. It is worth noting that the measurements obtained with the aluminum structure were used to identify the pre-yield shear moduli of the two MR fluids and the data acquired with the copper sandwich structure were applied for verification of the pre-yield model of the MR fluids. The results suggested nonlinear dependence of the loss and storage moduli on the excitation frequency and the magnetic flux density *B*, which has also been reported in (Mohammadi et al, 2010). Both

the storage and loss moduli increased with increasing magnetic flux density and excitation frequency, while saturation was observed with frequency for both the fluids, as seen in Figure 4.3. Consequently, the storage and loss moduli of the MR fluids were expressed by the following general relation in ω and B:

$$\bar{G} = (a_0 + a_1 B + a_2 B^2)\left(1 - e^{-a_3\omega}\right) \tag{4.18}$$

where $\bar{G}$ represents the storage or loss modulus, and a_0, a_1, a_2 and a_3 are unknown constants, which were identified through an error minimization problem. In the above equation, ω is taken in Hz and B is in mT. Table 4.2 summarizes the identified model coefficients for the MRF 122EG and MRF 132DG fluids.

Table 4.2 The identified coefficients of the storage and loss moduli models of MRF 122EG and MRF 132DG fluids

MR fluid	Modulus	a_0	a_1	a_2	a_3
MRF 122EG	Storage	97905.69	6744.595	92.75970	0.007328
	Loss	41281.45	1807.337	8.470100	0.006500
MRF 132DG	Storage	192160.6	30663.56	243.6247	0.004080
	Loss	45524.40	6757.977	6.441200	0.007416

It is worth noting that the squared dependence of the storage or loss modulus on the magnetic flux density is attributed to the fact that the rheological behavior of the MR fluids depends on dipole-dipole interactions. On the other hand, dipole-dipole interactions are proportional to product of the magnetic flux density, B, and dipole moment, P. As long as MR fluid is not saturated, the dipole moment is proportional to B, consequently, the rheological parameters of MR fluid such as loss and storage moduli and yield stress are proportional to B^2 (Choi et al., 1990).

(a)

(b)
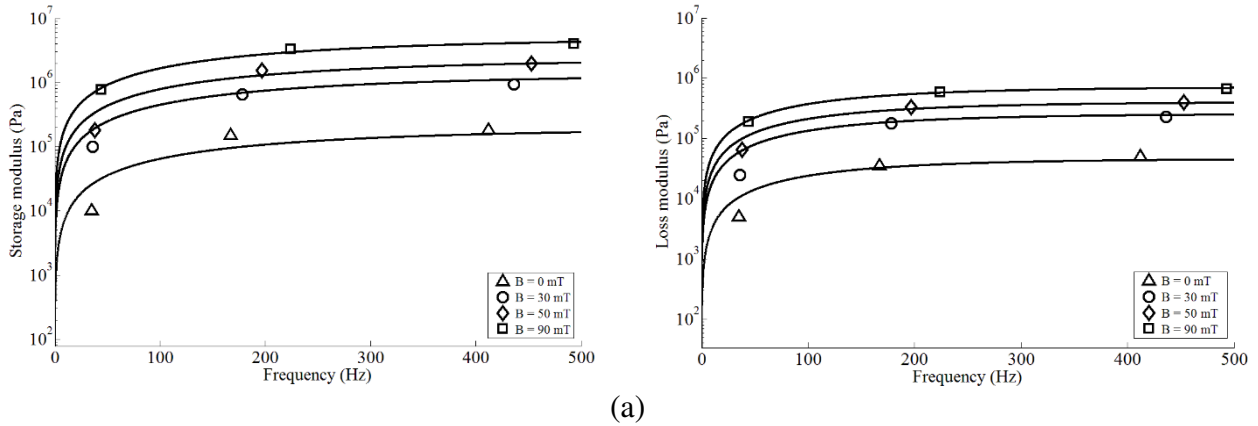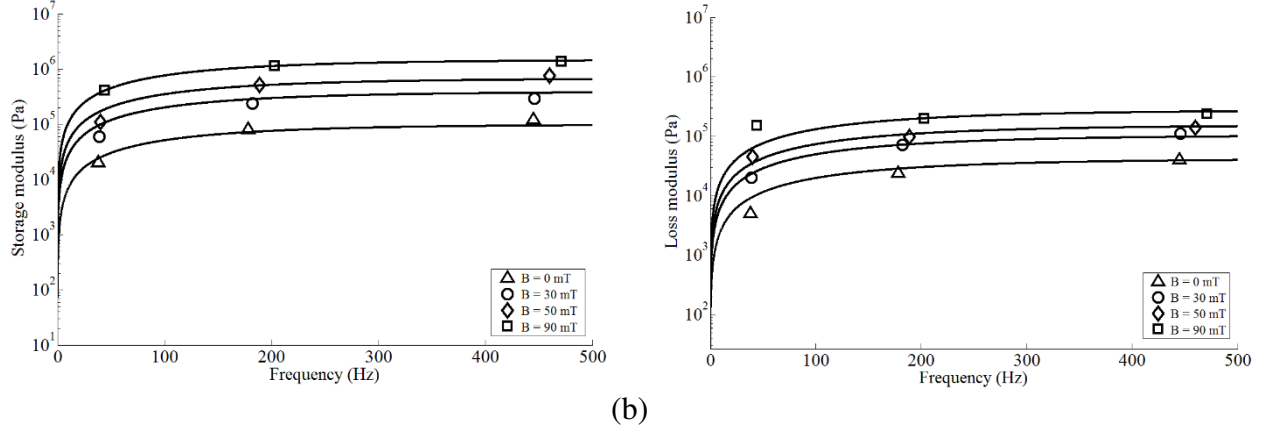
Figure 4.3 Variations in the storage and loss moduli of (a) MRF 132DG and (b) MRF 122EG fluids with increasing frequency, under different magnetic flux densities. (The moduli obtained from the model are shown by the solid lines).

4.3.3 Vibration analysis of the MR based sandwich plate

The second series of experiments were conducted to study the vibration characteristics of the MR plates under varying magnetic flux density. The selected MR fluid was injected into the core cavity of the sandwich plate using a hypodermic syringe through the silicon rubber spacer. A miniature hole near the free edge of the top layer permitted venting of the air from the core layer. The uniformity of the core layer (absence of air bubbles) was also ensured by visual inspection through the transparent PET face layers.
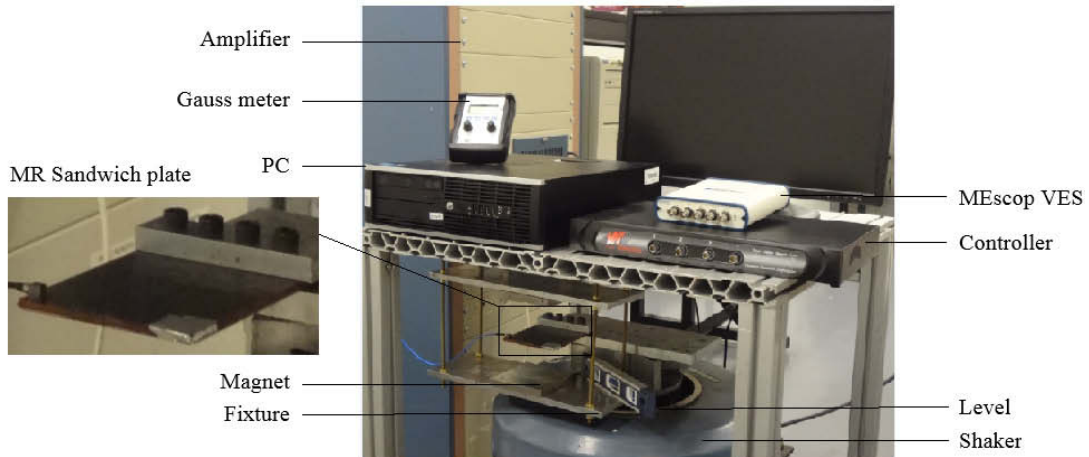
Figure 4.4 Experimental setup

Each sandwich plate was firmly fixed on the electrodynamic shaker via the root section. Two rectangular neodymium magnets, as depicted in Figure 4.4, were located above and below the plate using a specially-designed aluminum and brass fixture to realize nearly uniform magnetic flux

over the entire surface of the face layers. The vertical positions of the permanent magnets with respect to the sandwich plate were adjusted to achieve four different levels of average magnetic flux density (0, 30, 50 and 90 mT). The magnetic flux measurements through a hand-held Gauss meter revealed nearly uniform flux (up to ±20%) on the plate surfaces but lower intensity near the edges and higher intensity near the mid-section. The light weight three-axis accelerometer was installed at one of the free corner of the sandwich plate for measuring the vibration response, while a single axis accelerometer was installed at the support to measure the excitation. The support acceleration also served as the feedback for the vibration controller. The structure was excited using a constant acceleration (0.5 m/s^2 peak) harmonic vibration swept in the 1 to 500 Hz frequency range at the rate of 1 octave/min. The measured acceleration signals were used to obtain the FRFs of the plates with two different MR fluids subject to different average flux densities. The FRFs were subsequently analyzed to identify the natural frequencies and corresponding half power bandwidths of the sandwich plates. The repeated measurements revealed gradual reductions (about 50%) in the loss and storage moduli of the silicon rubber, which was attributed to absorption of the fluid by the sealant rubber.

4.4. Results and discussion

4.4.1. Validation of the FE model

The validity of the FE model is examined by comparing its responses in terms of lower six natural frequencies and the half power bandwidths corresponding to the first and third modes with the respective measured values for the four different flux densities. Table 4.3 summarizes the comparisons of the lower six natural frequencies of the plates with MRF 122EG and MRF 132DG fluids subject to four different values of the average magnetic flux density (0, 30, 50 and 90 mT). The comparisons show reasonably good agreements between the model and experimental results for all the frequencies, irrespective of the applied magnetic flux density and the type of MR fluid. The results also show substantial increase in the natural frequencies with increasing magnetic flux density, which has also been reported for MR sandwich beams (Rajamohan et al., 2010; Sun et al., 2003). The lower six frequencies of the plate with MRF 122EG fluid subject to 90 mT are 44.5%, 31.4%, 33.6%, 35.9%, 33.4% and 1.1%, respectively, higher compared to those obtained in the absence of the magnetic field. For the plate with 132DG fluid, the respective increases in the frequencies are 63.7%, 49.05%, 61.43%, 61.89%, 61.0% and 3.2%.

Table 4.3 Comparisons of lower six natural frequencies (Hz) of the PET sandwich plate obtained from the model and the measured data under different magnetic flux densities.

Flux (mT)		First	Second	Third	Fourth	Fifth	Sixth
		MRF 122EG					
0	Model	43.92	95.47	234.99	277.00	330.08	449.11
	Measured	43.90	98.90	233.10	289.10	345.10	465.40
30	Model	49.98	104.82	257.97	307.55	360.85	450.14
	Measured	47.52	102.50	245.90	316.50	353.90	467.20
50	Model	54.69	111.82	276.11	330.93	386.58	451.16
	Measured	52.92	111.10	276.00	348.40	390.30	467.20
90	Model	63.69	125.49	314.00	376.53	440.39	453.97
	Measured	62.49	119.20	302.00	363.00	452.00	473.70
		MRF 132DG					
0	Model	42.43	92.73	228.41	272.58	322.07	438.78
	Measured	41.73	91.00	226.10	260.80	325.90	445.90
30	Model	54.08	111.46	282.86	344.99	402.69	442.24
	Measured	49.03	114.90	280.40	360.90	401.10	459.10
50	Model	60.60	121.88	315.08	383.15	445.28	448.56
	Measured	57.11	129.20	314.70	398.00	431.20	462.70
90	Model	69.49	138.22	368.73	441.29	518.53	453.08
	Measured	71.11	147.31	370.21	455.50	526.31	476.51

The effect of the magnetic flux on the natural frequency depends on the mode shape, particularly the shear deformation of the core layer, which could cause substantial variations in the effective stiffness and damping property of the structure. As an example, Figure 4.5 illustrates the mode shapes of the sandwich plate with MRF 132DG fluid. For this purpose, the transverse displacement amplitude of the bottom layer, $w^{(3)}$, was computed.

First mode   Second mode
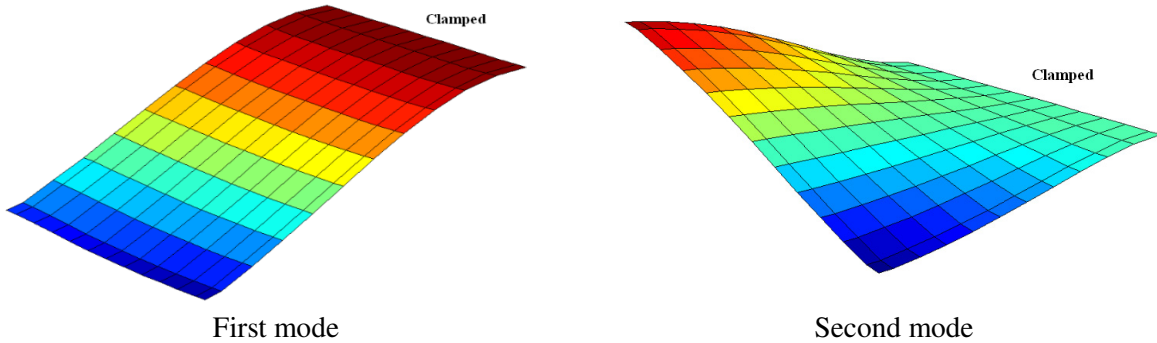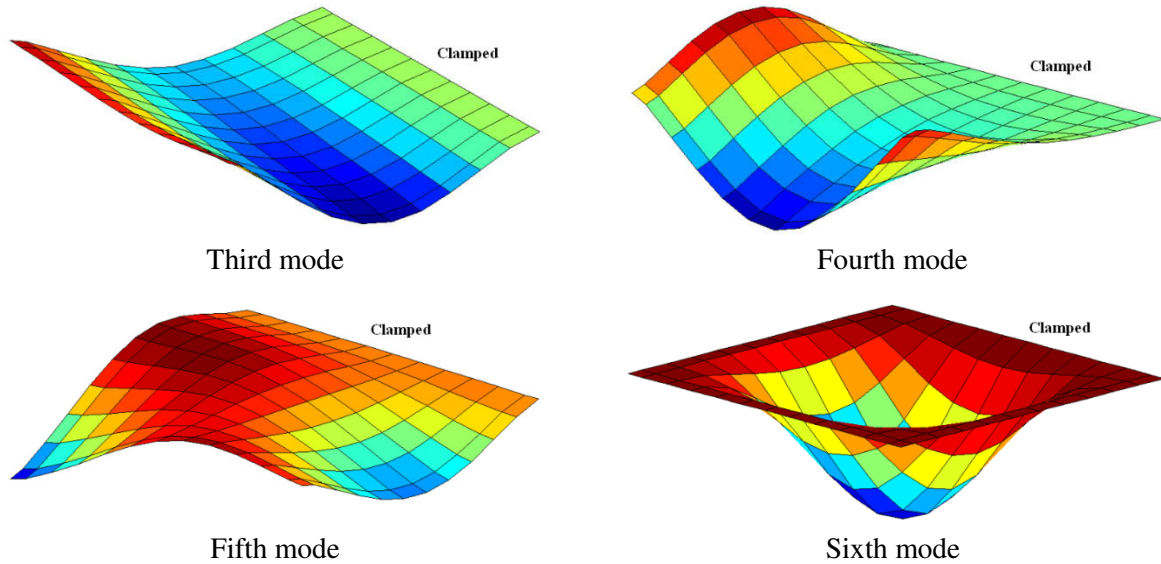
Figure 4.5 Deflection modes of the cantilever sandwich plate with MRF132DG fluid corresponding to the lower six natural frequencies.

The deflection modes suggest considerable shear deformations of the core layer corresponding to the first five frequencies. The effect of magnetic field on the lower five frequencies is thus significant. The considerably lower effect of the magnetic field on the sixth frequency is attributable to relatively low shear deformation in the sixth mode (in this mode, the top layer is deformed in opposite direction). The models developed by Hasheminejad and Maleki (2009) and Yeh (2013) could not capture the sixth mode, which was likely due to lack of consideration of the visco-elastic property of the sealant and assumption of uniform transverse displacement through the thickness of the sandwich plate. The results in the present study suggest that such assumptions could contribute to notable errors in the frequencies. For instance, in the absence of magnetic flux, the computed lower six natural frequencies of MRF 132DG based PET sandwich plate neglecting the effect of silicon rubber spacer are 35.6, 82.7, 218.48, 255.5, 309.9 and 438.8 Hz which show relatively significant discrepancy with the results presented in Table 4.3.

The first and third mode half power (HP) bandwidths of the FE model of the sandwich plate with two MR fluids are also compared with the measured values in Table 4.4. The results are presented for four different magnetic flux densities (0, 30, 50 and 90 mT). For the plate with 122EG fluid, the percent half power bandwidths corresponding to both the modes generally increased with increasing magnetic flux density. This trend, however, was not evident for the plate with 132DG fluid. Increasing the magnetic flux would yield higher energy dissipation, although it may not

necessarily cause higher percent half power bandwidth of the structure. This is due to the fact that half power bandwidth represents the ratio of dissipated energy to the stored energy in the structure. In the MR fluid sandwich plate, increasing the magnetic flux leads to increase in both the energies simultaneously. The half power bandwidth of the structure would thus depend on the relative rates of increase in the dissipated and stored energies.

Table 4.4 Comparisons of first- and third-mode half power bandwidths (%) obtained from the FE model with the measured data under different magnetic flux densities.

Flux (mT)		MRF 122EG		MRF 132DG	
	Mode	First	Third	First	Third
0	Model	6.42	4.39	6.95	4.52
	Measured	7.40	3.50	6.30	4.80
30	Model	7.80	6.14	11.19	8.33
	Measured	8.00	5.60	10.00	-
50	Model	7.60	6.60	9.85	8.27
	Measured	10.10	7.40	17.50	13.40
90	Model	6.14	6.86	6.68	6.81
	Measured	11.90	8.80	11.00	12.40

The results in Tables 4.3 and 4.4 also show considerable differences between the vibration properties of the plates with two different MR fluids with regard to the effect of magnetic flux on the natural frequencies and HP bandwidths. In the absence of the magnetic field, the natural frequencies of the sandwich structure with MRF 132DG as the core layer are relatively lower than those of the structure with MRF 122EG fluid. This is due to relatively higher mass density of the MRF 132DG fluid compared to the MRF 122EG fluid. The plate with MRF 132DG fluid also reveals relatively stronger effect of the magnetic field on all of the natural frequencies. This is attributable to the fact that MRF 132DG fluid constitutes relatively larger size magnetizable particles in the carrier fluids, which improves the magnetic permeability of the MR fluid. MRF 132DG thus provides greater magnetic flux density within the fluid resulting in greater changes in the rheological properties of the fluid (Mazlan et al., 2007). This, as seen in Figure 4.3, is also evident from relatively higher increase in the storage modulus of the MRF 132DG fluid with increasing the magnetic flux. Figure 4.6 illustrates variations of the first six frequency ratios and half power bandwidths corresponding to the first and third modes of the PET sandwich plate with MRF 122EG and MRF 132DG as the core layer, under different magnetic flux densities. The

frequency ratio is defined as the ratio of the natural frequency in a specific magnetic flux density to that of the structure in the absence of magnetic field.

(a)

(b)
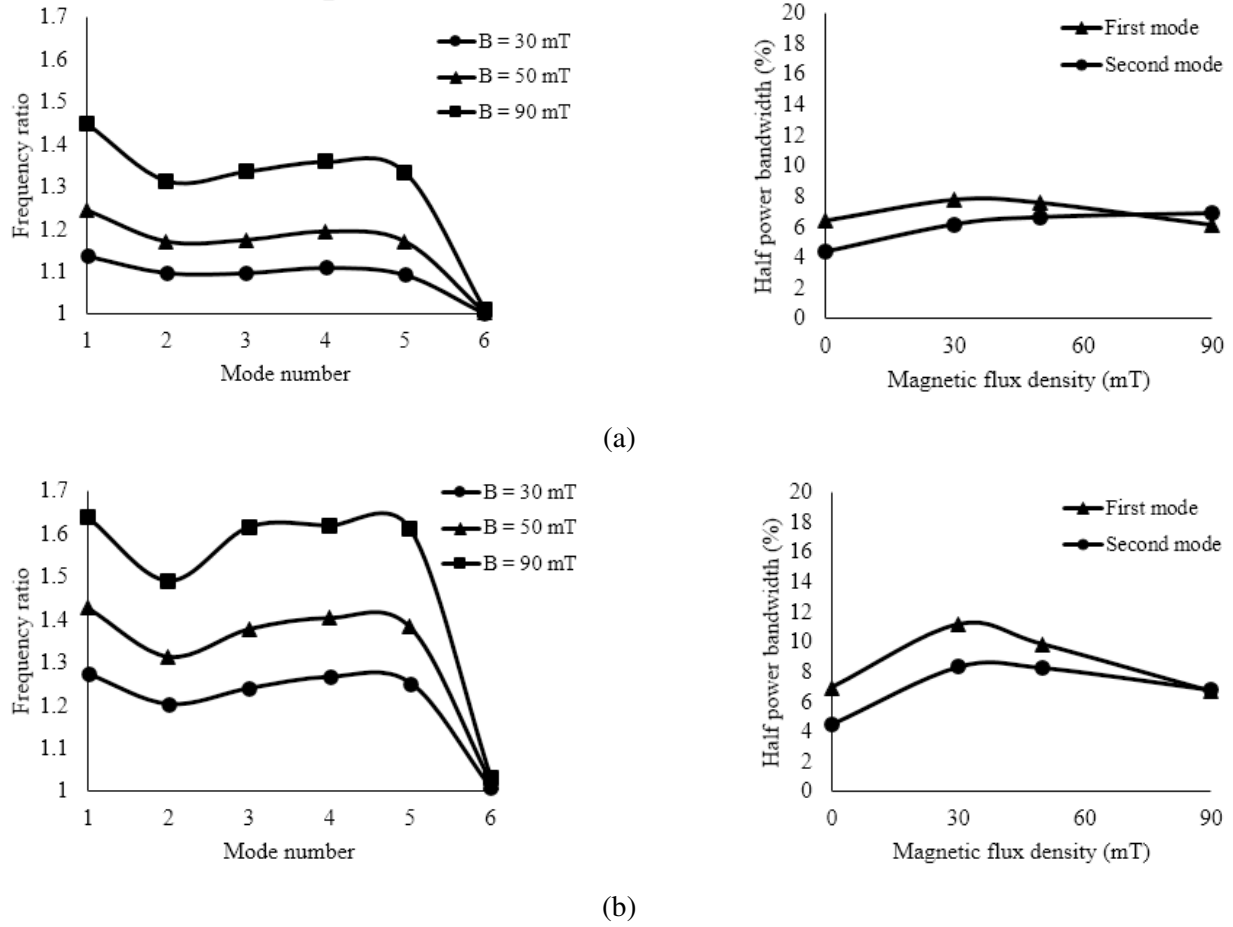
Figure 4.6 The effect of magnetic flux density on the natural frequency ratios and half power bandwidths: (a) MRF 122EG; and (b) MRF 132DG.

While the results in Table 4.3 show reasonable good agreements between the simulation and experimental results in terms of the natural frequencies, notable discrepancies are evident in the half power bandwidth, particularly under higher magnetic flux levels. The simulation and experimental results, however, exhibit similar trends. The differences may be attributed to the non-uniformity of the magnetic flux over the structure, which was observed to vary within the $\pm 20\%$ range. Since the magnetic flux variations affect both the storage and loss moduli significantly, the effect of magnetic flux non-uniformity is more pronounced on the half power bandwidth of the structure, particularly under higher magnetic flux densities. The effect of magnetic flux non-uniformity, however, is less significant on the natural frequencies of the structure, which may be

attributed to the fact that the resonant frequencies mostly depend on the storage modulus of the fluid. The MRF 132DG fluid was relatively more sensitive to the magnetic flux compared to the MRF 122EG one, thus the non-homogeneity of the magnetic flux yields more noticeable discrepancy in the computed and measured results of the MRF 132DG based plate compared to MRF 122EG one. It should be noted that the half power bandwidth corresponding to the third mode of the structure subjected to the magnetic flux density of 30 mT could not be captured from the measured FRF.

4.4.2. Effects of design parameters

The vibration response characteristics of the MR based sandwich structure are strongly dependent upon various design parameters such as boundary conditions, plate aspect ratio, MR fluid thickness, MR fluid type and applied magnetic field. The effects of variations in these parameters on the dynamic characteristics of the MR fluid sandwich plate are investigated using the developed finite element model so as to build some knowledge on the design guidance. The analyses are performed considering a l_1 ($0.4m$) $\times$ l_2 ($0.3m$) plate with aluminum elastic layers and five different boundary conditions: (i) CFFF- one edge (length=l_1) clamped, while others being free; (ii) SFSF- two edges (length=l_1) simply supported and two being free; (iii) SSSS- all edges simply supported; (iv) SCSC- two edges (length=l_1) simply supported and others being clamped; and (v) CCCC- all edges being clamped. The geometry boundary conditions for the clamped and simply supported edges are given, such that:

Clamped $\qquad\qquad\qquad\qquad\qquad w^{(i)} = u_0^{(i)} = v_0^{(i)} = \theta_x^{(i)} = \theta_y^{(i)} = 0$

$$(4.19)$$

Simply supported $\qquad\qquad\qquad w^{(i)} = 0, \qquad i = 1\, and\, 3$

 The density, Young's modulus and Poisson's ratio of the face layers were taken as 2700 kg/m^3, 70 Gpa and 0.3, respectively. In order to provide a uniform gap of 0.001 m between the elastic layers, a silicon rubber spacer was employed. The density and complex shear modulus of the silicon rubber were taken as those identified in Section 3.1. The acceleration response of the plate for each boundary condition was evaluated at a point (x=0.32 m, y=0.24 m). Table 4.5 illustrates variations in the first three natural frequencies and corresponding modal loss factors (η) of the sandwich plates with MRF 122EG as the core layer under different magnetic flux densities and boundary conditions.

Table 4.5 Variations in the first three natural frequencies (Hz) and corresponding modal loss factors of the aluminum sandwich plate with MRF 122EG fluid and different boundary conditions.

Magnetic flux density	Boundary condition	First mode		Second mode		Third mode	
		ω	η	ω	η	ω	η
	CFFF	18.370	0.0219	36.090	0.0193	87.280	0.0185
	SFSF	49.660	0.0147	69.580	0.0114	130.26	0.0116
B=0 mT	SSSS	77.000	0.0104	157.97	0.0076	221.54	0.0066
	SCSC	97.510	0.0074	208.17	0.0050	231.90	0.0060
	CCCC	140.43	0.0044	233.94	0.0041	329.51	0.0033
	CFFF	19.150	0.0342	37.510	0.0300	91.350	0.0329
	SFSF	51.190	0.0250	71.170	0.0192	134.53	0.0227
B=30 mT	SSSS	79.220	0.0204	161.64	0.0160	225.85	0.0137
	SCSC	99.780	0.0158	211.65	0.0115	236.09	0.0130
	CCCC	142.76	0.0107	237.45	0.0100	333.39	0.0080
	CFFF	19.930	0.0420	38.800	0.0358	95.200	0.0413
	SFSF	52.680	0.0319	72.690	0.0246	138.57	0.0296
B=50 mT	SSSS	81.390	0.0273	165.15	0.0220	229.96	0.0189
	SCSC	102.00	0.0218	215.07	0.0162	240.18	0.0181
	CCCC	145.04	0.0154	240.88	0.0143	337.16	0.0115
	CFFF	21.960	0.0529	41.970	0.0433	104.97	0.0528
	SFSF	56.790	0.0447	76.830	0.0351	148.67	0.0407
B=90 mT	SSSS	87.190	0.0397	174.63	0.0336	241.00	0.0295
	SCSC	107.97	0.0332	224.30	0.0258	251.21	0.0284
	CCCC	151.25	0.0250	250.33	0.0235	347.36	0.0190

The results in Table 4.5 suggest that the higher order constrained structure yields higher natural frequencies, as it would be expected. The CCCC condition yields the highest natural frequencies, while the CFFF condition shows the lowest natural frequencies, irrespective to the magnetic flux density. The CFFF structure also shows the highest shift in the natural frequencies in response to the applied magnetic field. In contrast, the lowest shift occurs in the CCCC structure. The relative percentage increase in the fundamental frequency of the MR sandwich plates (MRF 122EG) with CFFF, SFSF, SSSS, SCSC and CCCC conditions are 19.5%, 14.3%, 13.0%, 10.7% and 7.7%, respectively, when a 90 mT flux density is applied. The corresponding increases in the second mode frequency are 16.3%, 10.3%, 10.5%, 7.8% and 7.0%, respectively. The plate with CFFF condition undergoes the highest shear deformation and thereby yields the highest percent increase in the natural frequencies. Significant shear deformation enables CFFF plate to adjust its stiffness significantly, in response to the applied magnetic field. Such variations in the frequencies are far more significant for the plates with 132DG fluid. The plate with CFFF boundary condition also shows the highest loss factors corresponding to all the selected modes, irrespective to the magnetic flux density. The lowest loss factor is achieved for the CCCC plate due to insignificant shear

deformation. The modal loss factors also increase with increasing applied magnetic flux, as it was observed for the natural frequencies. The increasing loss factors, however, suggest relatively higher rate of increase in the structure damping with increasing magnetic flux density.
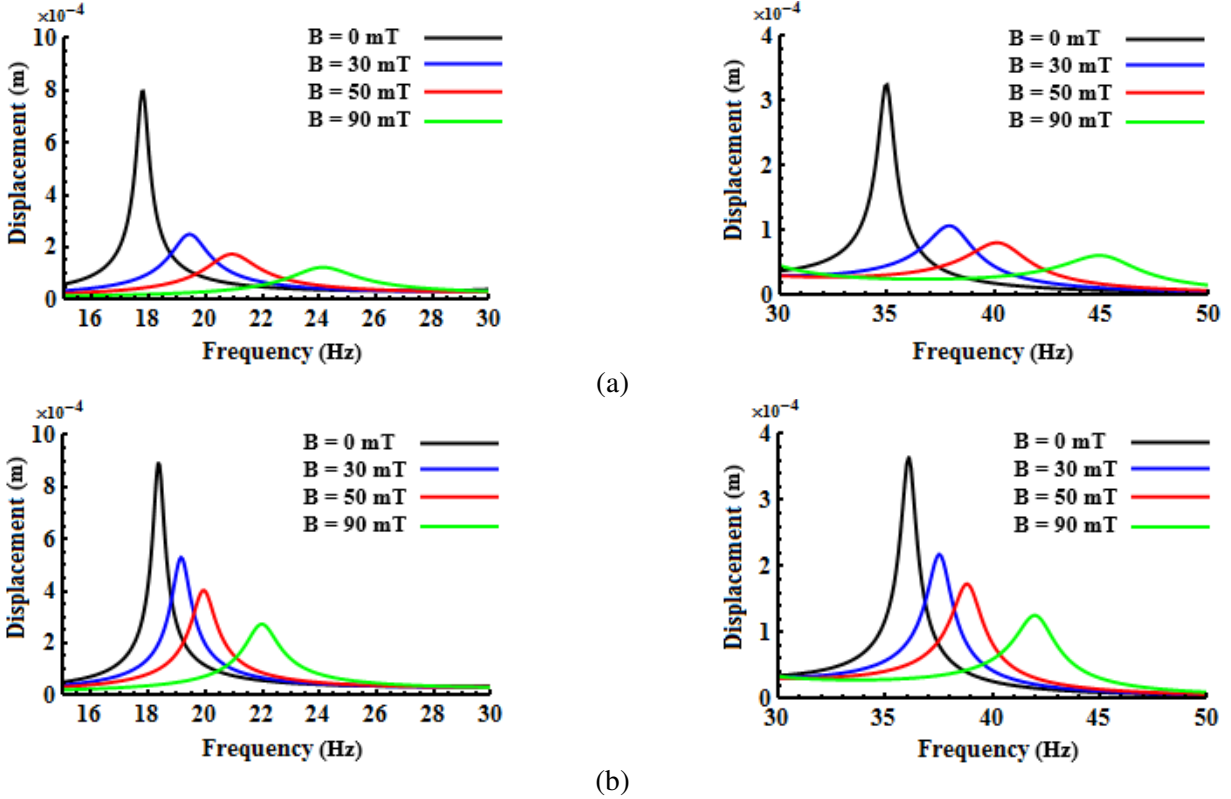
Figure 4.7 The effect of magnetic flux density on transverse vibration response of the CFFF sandwich plate in the vicinity of the first and second mode resonant frequencies (a): MRF 132DG; (b): MRF 122EG

Figures 4.7(a) and (b) illustrate the effect of magnetic flux intensity on the spectra of the transverse displacement responses of the CFFF plates with MRF 132DG and 122EG fluids, respectively, subjected to a unit harmonic point load ($x = 0.08\ m$; $y =0.06\ m$). The displacement responses obtained near the free end ($x = 0.32\ m$; $y =0.24\ m$) are presented only in the vicinity of the first and second mode frequencies. The results suggest that increasing the applied magnetic flux density decreases the displacement amplitude considerably and causes a notable rightward shift in the resonant frequencies. These clearly suggest that both the stiffness and damping of the sandwich plate can be substantially varied by varying the applied magnetic field. The monotonic decrease in the displacement amplitude can be directly attributed to increase in both the stiffness and damping of the structure with increasing magnetic field. It can also be noted that a higher magnetic flux reduces the sharpness of the peak which is attributed to increase in the damping of

the structure. The results also show relatively greater reductions in the peak magnitudes with the MRF 132DG fluid compared to the plate with 122EG fluid.

Table 4.6 The effects of plate aspect ratio (l_1/l_2) and core layer thickness ratio (h_2/h_1) on the first two natural frequencies and corresponding loss factors of the cantilever sandwich plates with MRF 122EG and 132DG fluids.

Mode	h_2/h_1	l_1/l_2	B=0 mT		B=30 mT		B=50 mT		B=90 mT	
			ω	η	ω	η	ω	η	ω	η
MRF 122EG Plate										
First	1	1	16.84	0.0211	17.43	0.0318	18.05	0.0395	19.76	0.0523
		2	65.23	0.0131	67.29	0.0239	69.32	0.0312	74.82	0.0445
	4	1	12.51	0.0271	13.02	0.0396	13.57	0.0485	15.14	0.0638
		2	47.75	0.0171	49.54	0.0294	51.35	0.0381	56.40	0.0540
Second	1	1	40.78	0.0191	42.35	0.0298	43.84	0.0360	47.41	0.0439
		2	99.60	0.0116	102.17	0.0205	104.65	0.0266	111.29	0.0379
	4	1	30.21	0.0262	31.74	0.0416	33.22	0.0508	37.38	0.0658
		2	72.97	0.0153	75.30	0.0263	77.61	0.0334	84.04	0.0490
MRF 132DG Plate										
First	1	1	15.93	0.0227	17.09	0.0596	18.24	0.0804	20.61	0.0976
		2	61.87	0.0145	66.44	0.0507	70.45	0.0685	80.35	0.0881
	4	1	11.20	0.0285	12.12	0.0705	13.11	0.0960	15.17	0.1180
		2	42.90	0.0181	46.44	0.0595	49.61	0.0807	567.87	0.1060
Second	1	1	38.63	0.0206	41.85	0.0560	44.39	0.0686	49.70	0.0774
		2	94.61	0.0126	100.55	0.0422	105.71	0.0569	117.95	0.0730
	4	1	27.16	0.0278	29.91	0.0767	32.50	0.0997	38.61	0.1186
		2	65.72	0.0225	70.50	0.0524	74.88	0.0720	85.94	0.0965

Table 4.6 shows the effects of magnetic flux density on the first two natural frequencies and corresponding modal loss factors of the CFFF plates with different aspect ratios (l_1/l_2=1 and 2) and core layer thicknesses ratio (h_2/h_1= 1 and 4). The results are presented for the plates with both MR fluids. The length l_1 (clamped edge) and thickness of the face layers are taken as 0.3 *m* and 0.002 *m*, respectively. Table 4.6 suggests that increasing the aspect ratio increases the natural frequency which is attributed to higher stiffness of the structure. The shear deformation is correlated to the aspect ratio of the sandwich plate so that the higher aspect ratio, the lower shear deformation. Thus, increasing the aspect ratio decreases the modal loss factor of the structure. The sandwich plates with thicker core layer (h_2/h_1= 4) show lower natural frequencies due to increase in the kinetic energy of the structure and higher modal loss factor, irrespective to the magnetic flux density. The percentage increase in the natural frequencies of the sandwich plates with the core layer of 8 *mm* is more significant than that of 2 *mm* thick core layer. For instance, in response to increase of the

magnetic flux density up to 90 mT, the right shift in the fundamental frequency of the sandwich plate (l_1/l_2=1) containing MRF 122EG with h_2/h_1=4 is 21.0% while that of the structure with h_2/h_1=1 is 17.3%.

4.5. Conclusions

The effects of variations in the magnetic flux on the vibration properties of a sandwich plate with two different MR fluids are investigated considering different boundary conditions. The results shows substantial increases in the lower mode frequencies and the corresponding loss factors with increasing magnetic field. It is further shown that the contributions of the rubber sealant can be accounted more by integrating the sealant properties in the FE model of the sandwich plate. Application of the MR fluid in an adaptive plate subject to the magnetic field can significantly alter the stiffness and damping properties of the structure under a noticeable shear strain. Furthermore, it was observed that the face layers may vibrate independently at higher modes. The assumption of uniform transverse displacement through the thickness of the structure may thus lead to significant errors in the responses at higher modes. The MRF 132DG fluid with relatively larger magnetizable particles resulted in higher percent increase in the resonant frequencies with increasing magnetic field compared to the MRF 122EG fluid. The sandwich plate with only one of its edges clamped (CFFF) showed greatest increase in the natural frequencies and loss factors with increasing magnetic field and the highest modal loss factor compared to the other boundary conditions. Increasing the plate aspect ratio resulted in relatively higher natural frequencies but lower loss factors of the structure. Increasing in the core layer thickness, on the other hand, resulted in lower natural frequencies but higher loss factors.

CHAPTER 5

ANALYTICAL AND EXPERIMENTAL FREE VIBRATION ANALYSIS OF MULTI-LAYER MR-FLUID CIRCULAR PLATES UNDER VARYING MAGNETIC FLUX

5.1. Introduction

Viscoelastic materials have been widely employed in sandwich structures to achieve improved vibration suppression (Wang and Chen, 2003). Such structures with fixed parameter viscoelastic materials, however, exhibit limited vibration attenuation performance. Alternatively, sandwich structures with smart fluids/elastomers with varying rheological properties in response to an applied field are known to yield superior performance. Sandwich structures coupled with controllable magnetic field yield continually vary stiffness and damping properties, and thereby could provide enhanced vibration isolation in a wide frequency range. Nayak et al. (2011) reported 30% greater attenuation of vibration of a cantilever sandwich beam containing a MR elastomer compared to that of the structure with viscoelastic core layer. Moreover, the MR elastomer provided a higher stability region of the structure under axial loads compared to the viscoelastic material sandwich beam.

The concepts of sandwich structures containing ER and MR fluids as the core layer were introduced by Carlson et al. (1990) and Weiss et al. (1996), respectively. These were followed by a number of analytical and experimental studies on dynamic characteristics of MR/ER sandwich structures. The majority of these, however, focused on multi-layer sandwich beams (Lara-Proeto et al, 2010; Rajamohan et al, 2010), likely due to their relatively simple mathematical formulations. These studies have invariably shown increase in structure stiffness and damping properties with increasing magnetic or electric field intensity. Only a few studies have investigated the dynamic characteristics of sandwich plates containing MR/ER fluids as the core layer, and majority of these focused only on ER-fluid sandwich plates (Oyadiji, 1996; Cho et al., 2005). The dynamic properties of MR based sandwich plates have been reported in even fewer studies (Pranoto et al., 2004; Yeh, 2013). These have invariably shown that appropriate applications of MR/ER core layers increase the controllability (Cho et al., 2005) and stability (Rahiminasab and

Rezaeepazhand, 20013) of the sandwich plates, with significant reductions in the vibration amplitude (Hasheminejad and maleki, 2009).

MR/ER fluids in the adaptive structures tend to operate in the pre-yield region (Nayak et al., 2011), where the MR/ER fluids exhibit predominantly viscoelastic behavior. The reported analytical models for sandwich structures with viscoelastic material may thus also be applicable to MR/ER-fluid adaptive structures. Rose et al. (Ross et al., 1959) proposed a model of a viscoelastic sandwich structure, known as RKU, for analysis of dynamic responses and effects of viscoelastic layers on the vibration performance of the structure. DiTaranto et al. (1965) investigated free vibration analysis of a three layered viscoelastically coupled plate structure considering the transverse inertia effect and simply supported boundary condition. Subsequently, Mead and Markus (Mead and Markus, 1969; 1970) modified the DiTaranto's model so as to investigate the sandwich structure responses under different geometry boundary conditions. The above-reported models for the viscoelastic sandwich structure have also been applied for characterizing vibration behavior of the MR/ER based sandwich structures (Yalcintas and Coulter, 1995; Yeh and shin, 2005; Hu et al., 2006). Coulter et al. (1989) and Coulter and Duclos (1990) employed the RKU model to investigate dynamic responses of ER sandwich beam structures. Mahjoob et al. (1993) compared the dynamic responses obtained from the RKU model reported by Rose et al. (1959) and the Mead and Markus (MM) model (Mead and Markus, 1969; 1970) for an ER based sandwich structure with the laboratory-measured responses and concluded that the MM model can predict more realistic dynamic behavior of the structure.

Finite element methods have been more commonly used for vibration analysis of MR/ER sandwich structures (Yeh, 2007; Rajamohan et al., 2010). A number of studies have also employed Hamilton energy method (Yeh et al., 2004; Sun et al., 2003). The solutions generally assumed insignificant normal stress in the core layer due to negligible Young's modulus of the MR/ER fluids compared to that of the elastic layers. The studies considered fluid layer thickness to be very small compared to its length, negligible slippage between the elastic and fluid layers, negligible shear strain and stress components in the elastic layers, uniform transverse displacement through the structure and negligible damping due to elastic layers (Hasheminejad and Maleki, 2009; Rajamohan et al., 2010). The classical plate theory (CPT) assumptions were considered applicable due to very small thickness of the elastic layers compared to the length.

The reported studies on MR/ER sandwich plates have invariably shown increase in resonant frequencies with increasing intensity of the applied magnetic/electric field (Choi et al., 1999; Hasheminejad and Maleki, 2009). The effect of field strength was particularly more pronounced on the lower mode frequencies compared to the higher mode frequencies (Hasheminejad and Maleki, 2009). Similar trend, however, was not observed in the loss factors associated with different modes. Hasheminejad and Maleki (2009) showed that the loss factor corresponding to a given mode of an ER sandwich plate increased with field strength when subject to relatively low electric field strength, while an opposite effect was observed under higher field strength. Highest loss factor was observed under intermediate levels of the field strength. The MR sandwich plates also revealed similar tendency in the los factor (Yeh, 2013). Other studies have shown important effects of different parameters on modal properties of the sandwich plates such as face layer geometry (Narayana and Ganesan, 2007), core layer thickness (Yeh, 2013), boundary conditions (Narayana and Ganesan, 2007) and excitation frequency (Lu and Meng, 2006). It has been reported that the face layer geometry or boundary condition that results in higher flexibility of the sandwich structure yields more pronounced effect of MR/ER fluids on the natural frequencies and damping of the structure under the applied field (Narayana and Ganesan, 2007). Yeh (2013) reported that increasing the core layer thickness of an ER sandwich plate yields lower natural frequencies but higher loss factors.

While rectangular sheets have been widely employed as the constraining and base layers in ER sandwich plates, only a few studies have investigated dynamic responses of annular circular plates containing ER fluids as the core layer (Yeh, 2007, 2007b, 2010). Many engineering applications, however, employ circular plates such as bulkheads in submersible vehicles, end caps of pressure vessels and baffles in road tankers. The vibration analyses of circular/annular plates with MR fluid as the core layer have not yet been reported. This study investigates dynamic characteristics of annular circular sandwich plates using analytical and experiment methods. The experiments were conducted on a sandwich plate comprising two circular face layers separated by silicone rubber spacer, and containing MR fluid in the core layer. The modal parameters of the plate with free boundary condition were obtained under different levels of magnetic flux using MEscop. Ritz method based on classical plate theory was utilized to evaluate dynamic characteristics of the structure in terms of natural frequencies and loss factors. The model validity was examined under a range of applied magnetic field intensity using the laboratory-measured modal properties for the

free boundary condition. The model was subsequently employed to investigate the effects of magnetic flux density, boundary conditions and core layer thickness on vibration suppression properties of the annular circular MR fluid sandwich plate.

5.2. Mathematical formulations

Consider a multi-layer annular circular plate (inner radius = R_i and outer radius = R_o), as shown in Figure 5.1. The plate comprises a MR fluid core layer sandwiched between the elastic material base and top constraining layers. The core layer is separated from the elastic material layers via a rubber sealant spacer, which helps contain the MR fluid within the core layer.
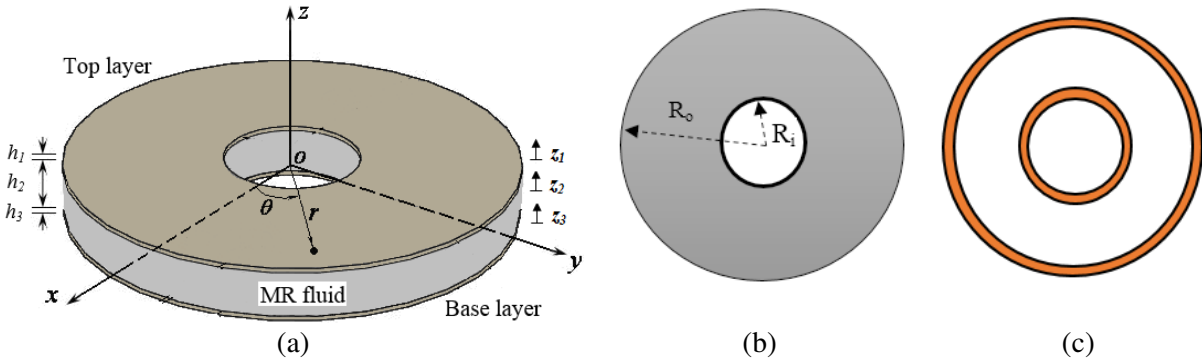
Figure 5.1 (a) Schematic of the three-layer annular circular sandwich plate; (b) top view; and (c) rubber sealant spacers

The thickness of the top, core and base layers are denoted by h_1, h_2 and h_3, respectively. It should be noted that the annular plate can be regarded as uniform circular plate when R_i approaches zero. Owing to very small thickness to radius ratio of the face layers, the classical plate theory is employed to identify displacement fields of the face layers. The transverse shear deformation and rotary inertia of the face layers are considered negligible considering the Kirchhoff assumptions (Leissa, 1969). The displacement functions of the elastic layers ($i=1, 3$) are thus obtained as:

$$u^{(i)}(r,\theta,z,t) = \left(u_0^{(i)}(r,\theta) - z_i \frac{\partial w(r,\theta)}{\partial r} \right) e^{j\omega t}$$

$$v^{(i)}(r,\theta,z,t) = \left(v_0^{(i)}(r,\theta) - z_i \frac{\partial w(r,\theta)}{r\partial \theta} \right) e^{j\omega t}, \qquad i=1,3 \qquad (5.1)$$

$$w(r,\theta,z,t) = w(r,\theta) e^{j\omega t}$$

where u and v denote the in-plane radial and circumferential displacements in r and θ directions, respectively, as shown in Figure 5.1. In the above equation, t denotes time, ω is the natural

frequency and $j = \sqrt{-1}$. u_0 and v_0 are the in-plane radial and circumferential displacements of the mid-plane in r and θ directions, and w represents the transverse displacement. The superscript $i = 1,3$ refers to top and bottom layers, respectively, and z_i is the transverse coordinate in the local coordinate system of each layer with origin located at mid plane of each layer. Considering the circumferential symmetry of annular plate about the coordinate θ, the radial and circumferential displacements of the mid-plane (u_0 and v_0), and transverse displacement w can be expressed as:

$$
\begin{aligned}
u_0^{(i)}(r,\theta) &= \bar{u}_0^{(i)}(r)\cos(m\theta) \\
v_0^{(i)}(r,\theta) &= \bar{v}_0^{(i)}(r)\sin(m\theta); \qquad i = 1,3 \\
w(r,\theta) &= \bar{w}(r)\cos(m\theta)
\end{aligned}
\tag{5.2}
$$

where the non-negative integer m identifies the circumferential wavenumber of corresponding mode shape, and $m = 0$ represents the axisymmetric vibration. $\bar{u}_0$, $\bar{v}_0$ and $\bar{w}$ are the displacement amplitude functions. Considering negligible slippage between the three layers, the compatibility conditions between layers through the structure thickness may be written as:

$$
\begin{aligned}
u^{(1)}\Big|_{z_1 = -h_1/2} &= u^{(2)}\Big|_{z_2 = h_2/2} \quad \& \quad v^{(1)}\Big|_{z_1 = -h_1/2} = v^{(2)}\Big|_{z_2 = h_2/2} \\
u^{(2)}\Big|_{z_2 = -h_2/2} &= u^{(3)}\Big|_{z_3 = h_3/2} \quad \& \quad v^{(2)}\Big|_{z_2 = -h_2/2} = v^{(3)}\Big|_{z_3 = h_3/2}
\end{aligned}
\tag{5.3}
$$

where the superscript (2) refers to the core layer. The above compatibility conditions are employed to describe displacement field of the core layer in terms of those of the top and bottom elastic layers. The normal and in-plane shear strain components in the face layers and transverse shear strain components in the core layer can now be evaluated from:

$$
\varepsilon_r^{(i)} = \frac{\partial u^{(i)}}{\partial r}; \quad \varepsilon_\theta^{(i)} = \frac{u^{(i)}}{r} + \frac{\partial v^{(i)}}{r\partial \theta}; \quad \varepsilon_{r\theta}^{(i)} = \frac{\partial v^{(i)}}{\partial r} + \frac{\partial u^{(i)}}{r\partial \theta} - \frac{v^{(i)}}{r}, \qquad i = 1,3
$$

$$
\gamma_{rz}^{(2)} = \left(\frac{u_0^{(1)} - u_0^{(3)}}{h_2} + \frac{d}{h_2}\frac{\partial w}{\partial r} \right)e^{j\alpha}; \quad \gamma_{\theta z}^{(2)} = \left(\frac{v_0^{(1)} - v_0^{(3)}}{h_2} + \frac{d}{h_2}\frac{\partial w}{r\partial \theta} \right)e^{j\alpha};
\tag{5.4}
$$

where $d = h_1/2 + h_2 + h_3/2$. Using the Hooke's law, the stress components in the face and core layers are obtained as:

$$\sigma_r^{(i)} = \frac{E_i}{\left(1-v_i^2\right)}\left(\varepsilon_r^{(i)} + v_i\varepsilon_\theta^{(i)}\right); \quad \sigma_\theta^{(i)} = \frac{E_i}{\left(1-v_i^2\right)}\left(\varepsilon_\theta^{(i)} + v_i\varepsilon_r^{(i)}\right); \quad \tau_{r\theta}^{(i)} = G\gamma_{r\theta}^{(i)}; \qquad i = 1 \, and \, 3$$

(5.5)

$$\tau_{rz}^{(2)} = \tilde{G}\gamma_{rz}^{(2)}; \quad \tau_{\theta z}^{(2)} = \tilde{G}\gamma_{\theta z}^{(2)}$$

where E, v and G are the Young's modulus, Poisson's ratio and shear modulus of the face layers, respectively. σ and τ denote the normal and shear stresses, respectively and $\tilde{G}$ is homogenized complex shear modulus of the mid-layer. The effect of silicon rubber on the complex shear modulus of the core layer is also considered using the 'rule-of-mixture'. The homogenized complex shear modulus of the mid-layer $\tilde{G}$ is thus evaluated from:

$$\tilde{G} = G_r \left(\frac{Area\ covered\ by\ rubber}{Total\ area\ of\ the\ core}\right) + G^* \left(\frac{Area\ covered\ by\ MR\ fluid}{Total\ area\ of\ the\ core}\right)$$

(5.6)

where G_r and G^* are complex shear moduli of the rubber and the MR fluid, respectively. In MR-fluid based sandwich structures, the MR fluid typically functions within the pre-yield regime. The fluid can thus be characterized as a linear viscoelastic material, where the shear stress and shear strain are proportional in terms of the complex modulus G^* given by (Li et al., 1999):

$$G^* = G' + iG''$$

(5.7)

where G' and G'' are the storage and loss moduli, which describe the average energy stored and dissipated, respectively, per unit volume of the material over a deformation cycle.

The total strain and kinetic energy of the annular sandwich plate in terms of stress and strain components can be expresses as:

$$V = V_1 + V_2 + V_3; \qquad T = T_1 + T_2 + T_3 + T_4$$

(5.8)

where V_1 and V_3 are the total strain energy associated with the top and bottom layers, respectively and V_2 represents the shear strain energy in the core layer including both the MR fluid and the rubber. T_1 and T_3 are the kinetic energy associated with the transverse and in-plane deformations in the top and bottom layers, respectively, T_2 denotes the kinetic energy due to rotational deformation of the core layer, and T_4 is the kinetic energy due to the silicon rubber. These energy functions can be expresses as:

$$V_i = \frac{1}{2}\int_{R_i}^{R_o}\int_0^{2\pi}\int_{-h_i/2}^{h_i/2}\left(\sigma_r^{(i)}\varepsilon_r^{(i)} + \sigma_\theta^{(i)}\varepsilon_\theta^{(i)} + \tau_{r\theta}^{(i)}\gamma_{r\theta}^{(i)}\right)r\,dz\,d\theta\,dr$$

(5.9)

$$V_2 = \frac{1}{2} \int_{R_i}^{R_o} \int_0^{2\pi} \int_{-h_2/2}^{h_2/2} \left(\tau_{rz}^{(2)} \gamma_{rz}^{(2)} + \tau_{\theta z}^{(2)} \gamma_{\theta z}^{(2)} \right) r \, dz \, d\theta \, dr$$

$$T_i = \frac{1}{2} \int_{R_i}^{R_o} \int_0^{2\pi} \int_{-h_i/2}^{h_i/2} \rho_i \left(\left(\dot{u}^{(i)} \right)^2 + \left(\dot{v}^{(i)} \right)^2 + \left(\dot{w}^{(i)} \right)^2 \right) r \, dz \, d\theta \, dr \qquad i = 1, 3$$

$$T_2 = \frac{1}{2} \int_{R_i+b_{ri}}^{R_o-b_{ro}} \int_0^{2\pi} \left(\rho_2 h_2 \left(\dot{w} \right)^2 + I_2 \left(\left(\dot{\gamma}_{rz}^{(2)} \right)^2 + \left(\dot{\gamma}_{\theta z}^{(2)} \right)^2 \right) \right) r \, d\theta \, dr$$

$$T_4 = \frac{1}{2} \left(\int_{R_i}^{R_i+b_{ri}} \int_0^{2\pi} \int_{-h_2/2}^{h_2/2} \rho_r \, Y \, r \, dz \, d\theta \, dr + \int_{R_o-b_{ro}}^{R_o} \int_0^{2\pi} \int_{-h_2/2}^{h_2/2} \rho_r \, Y \, r \, dz \, d\theta \, dr \right)$$

where ρ_r is mass density of the silicon rubber, b_{ri} and b_{ro} denote the sealant widths at the inner and other edges, respectively, $I_2 = \rho_2 h_2^3 / 12$ and $Y = \left(\dot{u}^{(2)} \right)^2 + \left(\dot{v}^{(2)} \right)^2 + \left(\dot{w} \right)^2$.

The Ritz method employs admissible basis functions to describe displacement of the structure, which satisfy the geometry boundary conditions. The displacement amplitude functions are described by polynomial functions multiplied by the boundary functions, such that:

$$\bar{u}_0^{(i)} (r) = F_1(r) H_1(r) \sum_{k=0}^N b_k \, r^k$$

$$\bar{v}_0^{(i)} (r) = F_2(r) H_2(r) \sum_{k=0}^N c_k \, r^k \qquad\qquad (5.10)$$

$$\bar{w}(r) = F_3(r) H_3(r) \sum_{k=0}^N l_k \, r^k$$

where b_k, c_k and l_k are unknown coefficients of the polynomial functions and $F_i(r)$ and $H_i(r)$ are boundary functions describing the inner and outer edges of the annular plate, respectively. The boundary functions are defined according to the given geometry boundary conditions. k is an integer and N denotes the highest degree of polynomials representing the displacement amplitude functions. The boundary functions $F_i(r)$ and $H_i(r)$ corresponding to different combinations of boundary conditions at the inner and outer edges are given in Table 1. In the table, notations F, S and C denote the free, simply supported and clamped condition, respectively. Furthermore, the first letter refers to the condition at the inner edge, while the outer edge condition is denoted by the second letter. It should be noted that for convenience of notation, the geometry boundary conditions at inner and outer edges of annular plate are described in a concise form (F = free, S =,

and C = clamped). For example, C-S annular plate is constrained by clamped and simply supported boundary conditions at inner and outer edges, respectively.

Table 5.1 Boundary functions for different combinations of boundary conditions

B.C.	$F_1(r)$	$F_2(r)$	$F_3(r)$	$H_1(r)$	$H_2(r)$	$H_3(r)$
F-F	1	1	1	1	1	1
F-C	1	1	1	$(r-R_o)$	$(r-R_o)$	$(r-R_o)^2$
F-S	1	1	1	$(r-R_o)$	$(r-R_o)$	$(r-R_o)$
C-F	$(r-R_i)$	$(r-R_i)$	$(r-R_i)^2$	1	1	1

The equations of motion for the multi-layer plate are subsequently obtained through minimization of the Lagrangian energy function, given by:

$$\Pi = V_{max} - T_{max} \tag{5.11}$$

where V_{max} and T_{max} are maximum potential and kinetic energy of the structure. The Lagrangian energy function is minimized with respect to the arbitrary coefficients b_k, c_k and l_k to formulate the eigenvalue problem, such that:

$$\frac{\partial \Pi}{\partial b_k} = 0, \quad \frac{\partial \Pi}{\partial c_k} = 0, \quad \frac{\partial \Pi}{\partial l_k} = 0, \tag{5.12}$$

Equation (5.12) yields the system equations of motion describing free vibration of the structure in the following form:

$$(K - \omega^2 M)C = 0 \tag{5.13}$$

where K and M are stiffness and mass matrices, and C is the vector of arbitrary coefficients. The nth natural frequency, ω_n, and the corresponding loss factor, η_n are subsequently obtained from the complex eigenvalue, $\lambda_n = \lambda_{n,1} + j\lambda_{n,2}$:

$$\omega_n = \sqrt{\lambda_{n,1}} \quad \text{and} \quad \eta_n = \lambda_{n,2}/\lambda_{n,1} \tag{5.14}$$

5.3. Experimental methods

A uniform circular MR-fluid sandwich plate was fabricated for experimental characterizations of its dynamic characteristics under varying levels of the magnetic flux. The sandwich structure comprised of circular PETG (Polyethylene Terephthalate Glycol) host and top layers (diameter =

100 *mm*, thickness = 0.5 *mm*) and MR fluid as the core layer (thickness = 0.5 mm). PETG is a light material with negligible magnetic permeability, which permits more uniform distribution of the magnetic flux over the structure. Silicon rubber, which is oil resistant, was employed to seal the core layer containing the MR fluid. An electromagnet was designed and fabricated to provide variable magnetic flux. The electromagnet comprised a hollow aluminum cylinder (diameter = 0.115 m) and copper wire (18 AWG) wrapped around the cylinder (number of turns = 4200). A power supply of 2A and 100 V was employed to energize the electromagnet to generate a uniform magnetic flux over the structure up to 30 mT. The flux density over the entire plate surface was measured at several positions using a gauss meter, which revealed nearly uniform flux distribution with peak variations of ±5%.

(a)   (b)

Figure 5.2 (a) Experimental setup; and (b) circular sandwich MR plate
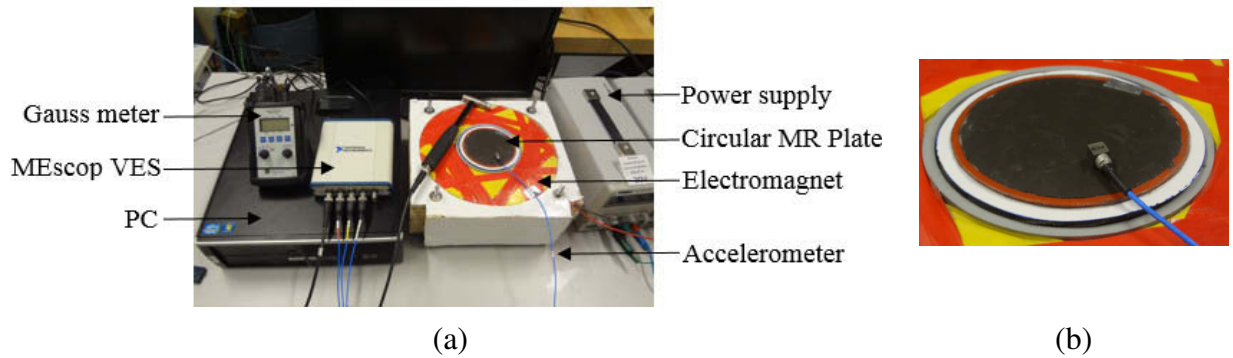
The experiment was designed to measure free vibration responses of the MR sandwich plate under different levels of the magnetic flux. The hollow core section of the electromagnet was filled with acoustic foam wall panels to support the MR sandwich circular plate and simulate free boundary condition. MEscop VES modal analyzer together with the modal hammer was used to identify modal parameters of the structure, as shown in Figure 5.2. A miniature three-axis accelerometer (PCB Piezotronics, model: 356A01), weighing 2.5 grams, was installed on the sandwich plate (at r = 30 mm). The input and output signals from the hammer and the accelerometer, respectively, were acquired and analyzed in the MEscopVES to obtain frequency response functions (FRF) and natural frequencies of the structure under different magnetic flux densities.

The experimental plate employed MRF 122EG manufactured by Lord Corporation as the core layer. The viscosity at room temperature, solid content by weight and density of the fluid were taken as 0.042 Pa-s, 72% and 2500 kg/m³, respectively. The storage and loss moduli of the MR

fluid is expressed by the following general relation in frequency ω and flux density B (Eshaghi et al., 2015):

$$\bar{G} = (a_0 + a_1 B + a_2 B^2)\left(1 - e^{-a_3\omega}\right)$$ (5.15)

where $\bar{G}$ represents the storage or loss modulus of the fluid, and a_0, a_1, a_2 and a_3 are constants. In the above equation, ω is taken in Hz and B in mT. Table 2 summarizes the identified model coefficients for the MRF 122EG fluid (Eshaghi et al., 2015).

Table 5.2 Coefficients of storage and loss moduli models for the MRF 122EG fluid (Eshaghi et al., 2015)

MR fluid	Modulus	a_0	a_1	a_2	a_3
MRF 122EG	Storage	97905.69	6744.595	92.75970	0.007328
	Loss	41281.45	1807.337	8.470100	0.006500

5.4. Results and discussions

5.4.1. Validation of the Ritz model

The validity of the analytical model of the plate was examined for the uniform plate only by letting $R_i = 0$. Three lower natural frequencies of the model, obtained under different levels of magnetic flux density, were compared with those identified from the measured FRFs. The model was analyzed considering MRF 122EG fluid as the core layer, while the properties of PETG face layers were taken as: $\rho_1 = \rho_3 = 1600\ kg/m^3$; $E_1 = E_3 = 2.2\ GPa$; $\nu_1 = \nu_3 = 0.35$. The mass density of the 0.5 mm thick and 2 mm wide silicon rubber was taken as $\rho_r = 1460\ kg/m^3$, while its frequency dependent complex shear modulus was evaluated from, $G_r = 1.34 \times 10^5 + j\left(152511 + 68.31\omega + 0.475\omega^2\right)$, as reported in (Eshaghi et al., 2015). The mass of accelerometer was considered as a lumped mass in Ritz model.

Table 3 presents comparisons of three lower natural frequencies of the circular sandwich plate subjected to four different levels of magnetic flux density (0, 10, 20 and 30 mT). Reasonably good agreements between the model and experimental frequencies are evident, irrespective of the applied magnetic flux density. Furthermore, the results suggest an increase in resonant frequencies of the sandwich plate with increasing magnetic flux, which is attributed to increase in complex shear modulus of the MR fluid. The lower three frequencies of the plate subjected to 30 mT magnetic flux are 44.0%, 45.8 and 35.3%, respectively, higher than those obtained in the absence of magnetic field.

Table 5.3 Comparison of lower three natural frequencies (Hz) of the PETG circular sandwich plate obtained from the model and the measured data under different magnetic flux densities

B (mT)	First mode		Second mode		Third mode	
	Model	Experiment	Model	Experiment	Model	Experiment
0	67.60	64.40	118.26	127.20	203.81	204.60
10	78.80	70.90	137.35	140.60	226.55	220.20
20	89.07	80.10	155.90	152.40	250.95	240.30
30	97.37	93.20	172.48	167.80	275.84	261.60

The peaks in the measured FRFs of the MR-fluid plate under the hammer impacts were not sufficiently distinct to perform curve fitting for identifying the damping properties with reasonable accuracy. This was attributed to free boundary conditions and light weight of the plate. The verification of the Ritz model in obtaining damping properties of the sandwich structure was thus conducted using the reported damping properties of an ER-fluid annular sandwich plate (Yeh, 2007).

Table 5.4 Comparison of three lower natural frequencies (rad/s) and corresponding loss factors of the ER-fluid annular sandwich plate, obtained from the Ritz model with those reported in (Yeh, 2007).

Mode		E=1 kV mm^{-1}		E=2 kV mm^{-1}		E=3 kV mm^{-1}	
		ω	η	ω	η	ω	η
First	Ref (Yeh, 2007)	96.1	0.050	105.6	0.016	110.2	0.007
	Ritz	95.4	0.050	104.3	0.016	111.2	0.007
Second	Ref (Yeh, 2007)	118.1	0.038	127.5	0.022	141.6	0.012
	Ritz	117.4	0.037	128.8	0.022	140.9	0.012
Third	Ref (Yeh, 2007)	167.4	0.060	190.0	0.030	210.4	0.012
	Ritz	166.5	0.059	190.3	0.029	211.6	0.013

The study reported the three lower natural frequencies and corresponding loss factors of an ER-fluid annular plate (R_o=0.15 m; R_i =0.01 m) with clamped-free (C-F) boundary condition and three different intensities of the electric field using the finite element model. The Ritz model formulated in this study was analyzed considering the same geometric parameters of the ER-fluid sandwich plate with aluminum elastic material layers (ρ_1=ρ_3=2700 kg/m^3; E_1=E_3 = 70 Gpa; v_1=v_3 = 0.29). The thickness of the top, core and bottom layers were 0.1, 0.25 and 0.5 mm, respectively. The storage and loss moduli of the ER fluid were defined as functions of electric field strength E, as 15000 E^2 and 6900 E, respectively, with ρ_2 =1700 kg/m^3. In the model, the effects of accelerometer mass, and the sealant spacer properties were neglected, as in case of the reported finite element (FE) model (Yeh, 2007). Table 4 compares the three lower mode frequencies and corresponding

loss factors, obtained from the Ritz model, with those reported in (Yeh, 2007). The comparisons are presented for three different magnitudes of the electric field, $E=$ 1, 2 and 3 kV-mm^{-1}. The results show good agreements between the results from the Ritz model and the reported FE model.

5.4.2. Effect of boundary conditions

The verified model is subsequently utilized to investigate the effect of geometric boundary condition on dynamic characteristics of the annular sandwich plates under different intensities of the magnetic flux. The simulations are performed for the annular sandwich plate with 1mm thick aluminum host and constraining layers, enveloping 1mm thick MRF 132DG fluid core layer. The viscosity at room temperature, solid content by weight and density of the MRF 132DG were taken as 0.112 Pa-s, 80.98% and 3500 kg/m^3, respectively. Table 5 summarizes the identified model coefficients for the MRF 132DG fluid (Eshaghi et al., 2015). The inner and outer radii of the plate are taken as 0.05 m and 0.25 m, respectively. The properties of the silicon rubber at the inner and outer edges are also incorporated in the simulation model. The results are obtained for different boundary conditions at the inner and outer edges, namely, F-F, F-S, C-F and F-C.

Table 5.5 Coefficients of storage and loss moduli models for the MRF 132DG fluid (Eshaghi et al., 2015)

MR fluid	Modulus	a_0	a_1	a_2	a_3
MRF 132DG	Storage	192160.6	30663.56	243.6247	0.004080
	Loss	45524.40	6757.977	6.441200	0.007416

Figure 5.3 illustrates the effect of boundary condition on the free vibration response in terms of lower three natural frequencies and corresponding loss factors, under different intensities of the magnetic flux in the 0 to 90 mT range. The results suggest that the resonant frequencies of the MR sandwich plate increase nearly linearly with the applied magnetic flux, irrespective of boundary condition. This trend, however, is not evident in the loss factors. The loss factors strongly depend on the boundary condition. For the annular sandwich plate with F-F and C-F boundary condition, the loss factors corresponding to all the three modes increase with increase in the magnetic flux up to certain limit, and then decrease with further increase in the magnetic flux density, as seen in Figures. 5.3(a) and 5.3(b). The trend suggests the existence of an optimal magnetic flux density that would yield highest loss factor for a given mode of vibration. For the F-S and F-C sandwich annular plates, the loss factors increase nearly linearly with increasing magnetic flux up to about 30 mT, and tend to saturate with further increase in the magnetic flux. This trend is evident for all

three mode and could be justified considering that the loss factor is proportional to the energy dissipation but inversely proportional to stiffness of the structure. The magnetic field applied to the structure causes increase in both the damping and stiffness of the structure, while their rates differ. The changes in the loss factor directly related to relative rates of change in the structure stiffness and damping properties.
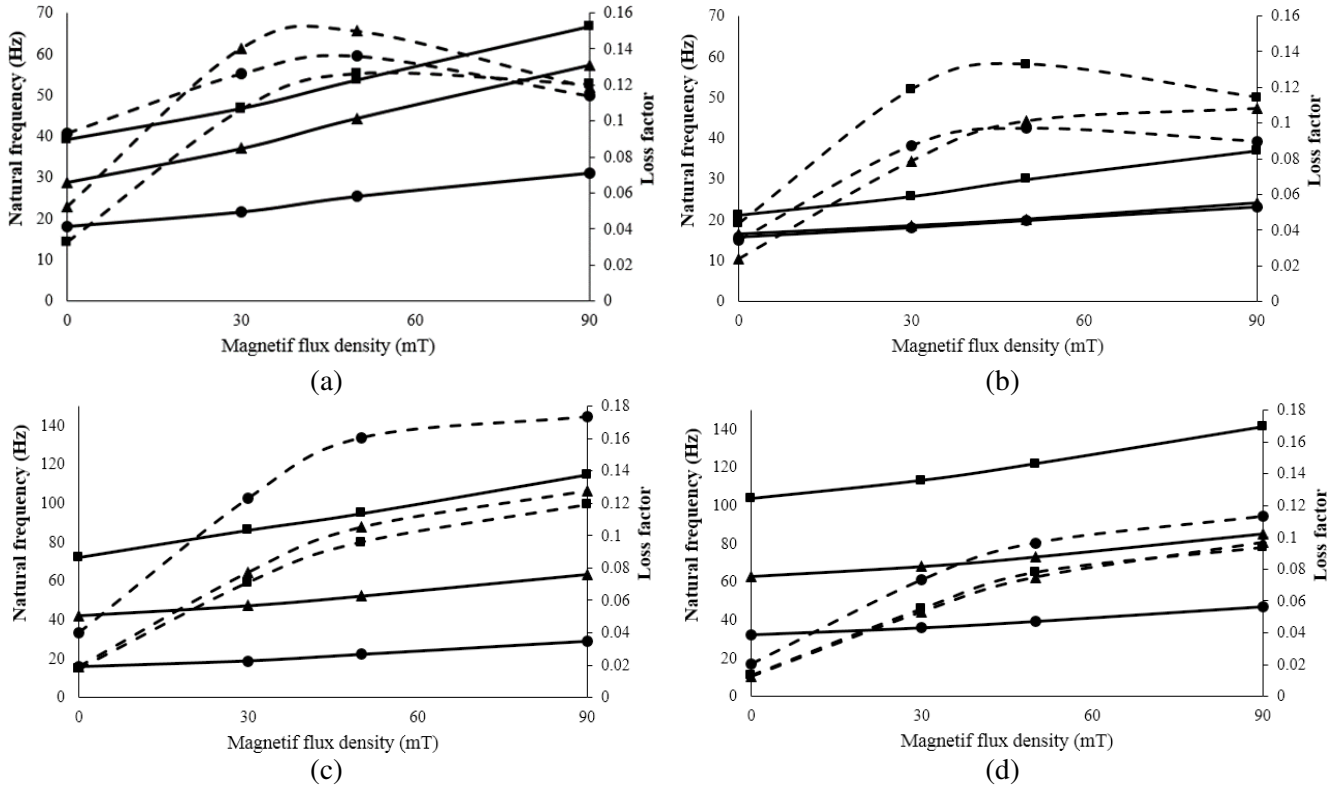
Figure 5.3 Influence of variations in the magnetic flux density on the lower three natural frequencies (solid lines) and corresponding loss factors (dashed lines) of the MR fluid (a) F-F; (b) C-F; (c) F-S; and (d) F-C annular plate $(\bullet\ldots\omega_1; \ldots\omega_2; \blacksquare\ldots\omega_3)$

The influence of variation in the magnetic flux on the natural frequencies of the MR-fluid annular sandwich plate is further evaluated in terms of percent change in the frequency. It can be observed that the maximum shift in the resonant frequencies occurs for the F-F boundary condition, while the F-C annular plate shows the lowest change in natural frequencies. The relative change in the frequencies with applied magnetic field is strongly related to flexibility of the structure. The boundary condition leading to higher flexibility of the structure causes relatively higher change in the resonant frequencies with increasing the magnetic field, as seen in case of F-F and C-F conditions. This is attributed to relatively larger shear deformation in the MR-fluid core layer of the relatively flexible plate. The boundary condition leading to higher stiffness, namely F-

115

S and F-C, yield largest change in the fundamental frequency, while the more flexible conditions (F-F and C-F) yield greatest change in the either second or third natural frequencies.

(a)

(b)

(c)

(d)
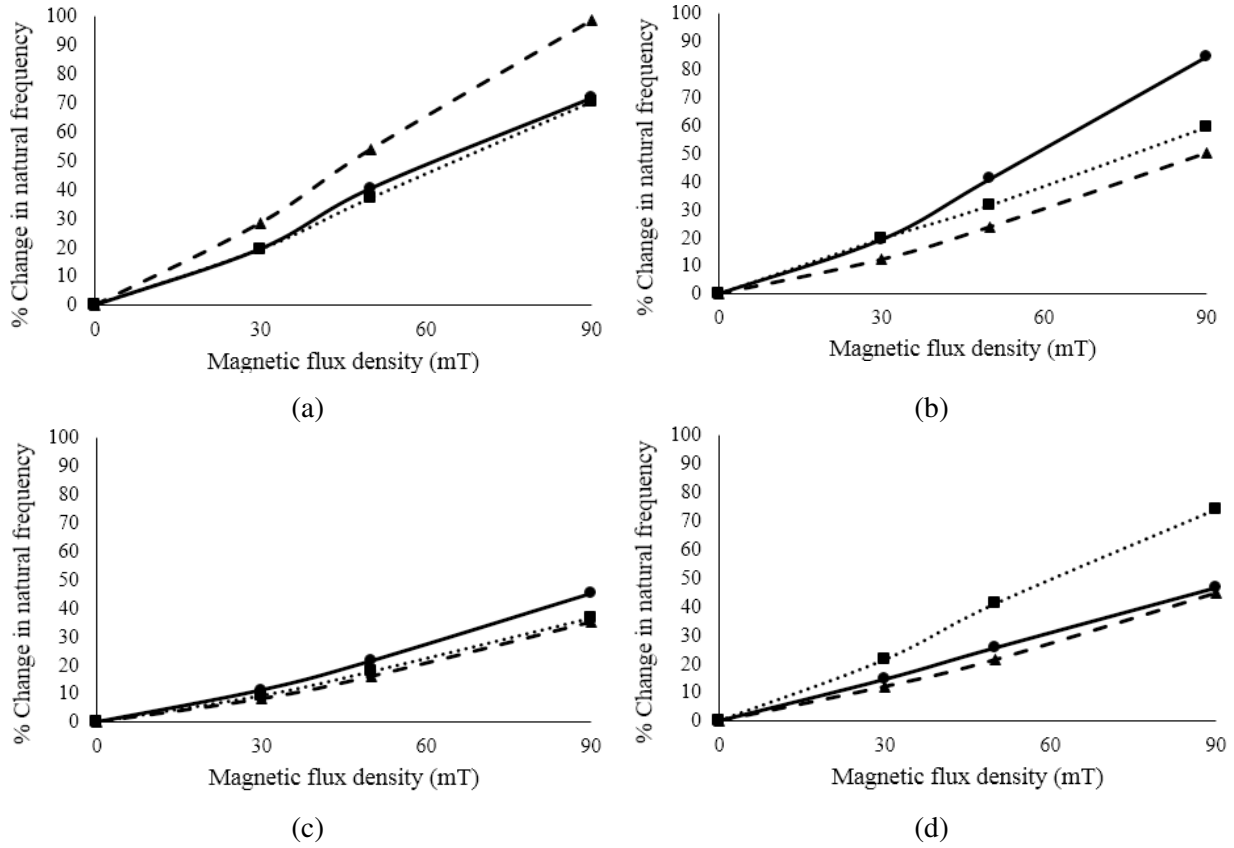
Figure 5.4 Influence of increasing magnetic flux density on percent changes in natural frequencies of the MR-fluid (a) F-F; (b) F-S; (c) F-C; and (d) C-F annular plate with different boundary conditions ($\bullet \ldots \omega_1$; $\blacktriangle \ldots \omega_2$; $\blacksquare \ldots \omega_3$).

The results in Figure 5.4 suggests that the relative change in the frequencies with increasing magnetic flux is dependent on the shear deformation of MR-fluid core layer and thereby the deflection mode of the plate. Figure 5.5 illustrates the deflection modes of the F-C and F-F sandwich annular plates. It can be observed that the deflection mode corresponds to ω_2 of the F-F sandwich plate is similar to the first mode of the F-C plate. The significant shear deformation of MR-fluid core layer attributed to this deflection shape thus causes largest variation in ω_1 and ω_2 of the F-C and F-F plates, respectively.
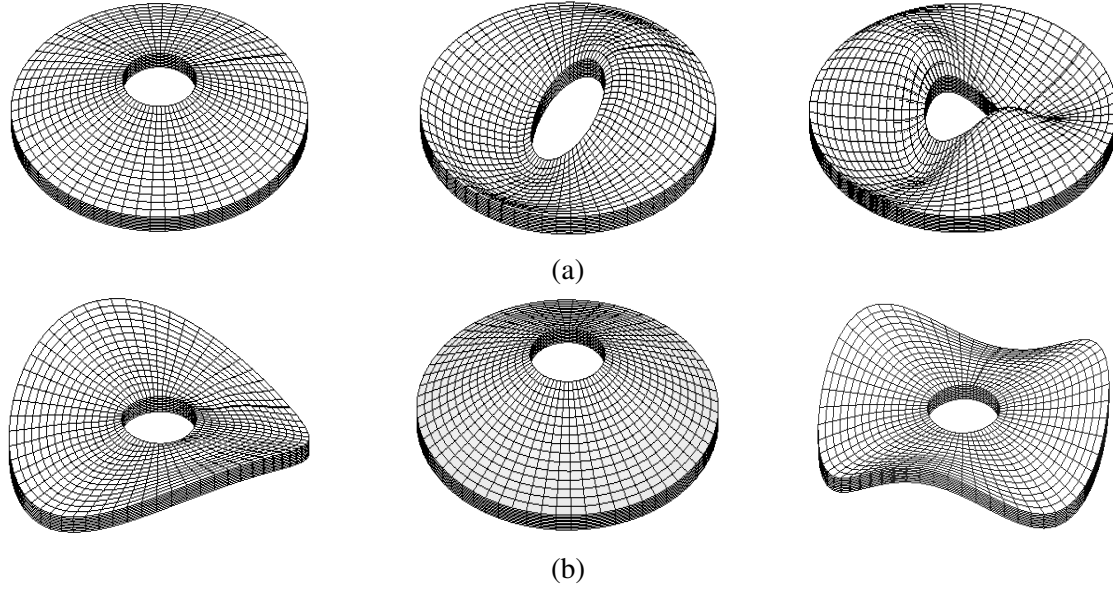
Figure 5.5 Deflection modes of the three lower natural frequencies of (a) F-C; and (b) F-F sandwich annular plates

5.4.3. Effect of inner/outer radius ratio

The free vibration responses of the annular plate are directly related to the inner and outer radius ratio (R_i/R_o), which affects both the mass and stiffness of the plate. Figure 5.6 illustrates the effect of variations in the radius ratio on changes in the fundamental frequency and corresponding loss factor of the annular plate under two different boundary conditions (F-F and F-C), when the magnetic field intensity is varied from 0 to 90 mT. The geometry and material properties of the sandwich plate are identical to those used in section 4.2, while the inner radius of the structure is varied from 0 to 0.2 m in increment of 0.05 m. Since varying the radius ratio affects both the mass and stiffness of the structure, fundamental frequency and corresponding loss factor of the plate may increase or decrease depending on geometric boundary condition. Increasing the radius ratio decreases mass of the MR annular plates, which would likely yield an increase in the natural frequency. The stiffness of the structure, however, varies with the radius ratio and the boundary conditions. For instance, the fundamental frequency of F-C plate tends to increase substantially only when the radius ratio approaches 0.6, while the changes in the loss factor are very small up to radius ratio of 0.6, as seen in Figure 5.6 (a). The natural frequency, however, increases sharply when the ratio exceeds 0.6, which is attributed to substantial increase in the stiffness and decrease in the mass. The loss factor also decreases due to reduced volume of MR fluid in the core layer.

117

Moreover, stiffening of the structure, however, causes lower shear strain in the MR fluid core layer leading to reduced energy dissipation and thereby loss factor with increasing radius ratio. The fundamental frequency of the F-F sandwich plate decreases substantially with radius ratio, particularly under the higher magnetic flux, as seen in Figure 5.6 (b). In this case, increasing the radius ratio lowers both the stiffness and mass of the structure. The fundamental frequency, however, decreases due to more pronounced stiffness effect. The corresponding loss factor also decreases due to reduced volume of the MR fluid in the core layer.

(a)   (b)
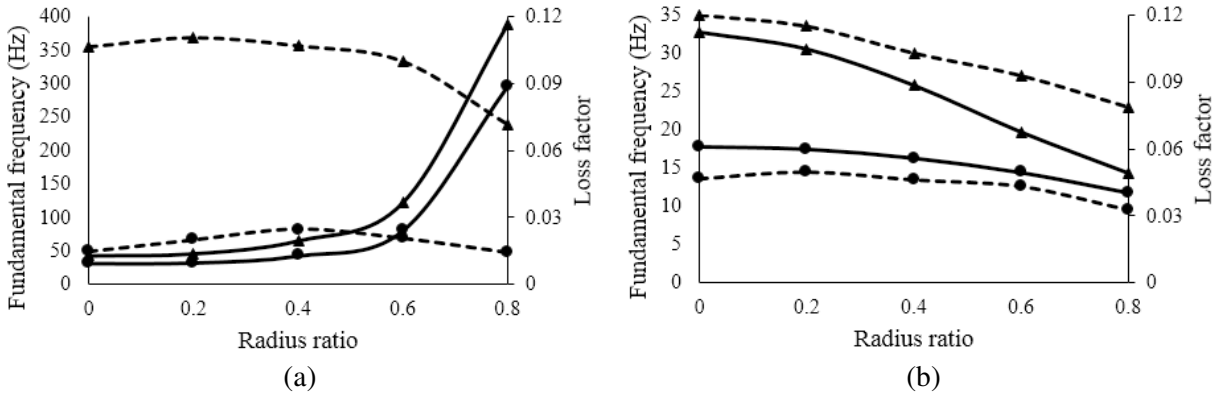
Figure 5.6 Influence of variations in the radius ratio on change in fundamental frequency (solid line) and corresponding loss factor (dashed line) of the MR-fluid annular plate with different boundary conditions ((a) F-C; and (b) F-F), under two levels of magnetic flux density ($\bullet \dots 0 \ and \ \blacktriangle \dots 90 \ mT$).

5.4.4. Effect of core layer thickness

Figure 5.7 illustrates the effect of thickness ratio of the core layer (h_2/h_3) on the fundamental frequency and corresponding loss factor of the plate with F-F and F-C conditions. The results are presented for two different intensities of the magnetic flux (0 and 90 mT). The geometry and material properties of the annular sandwich plate are identical to those described in section 4.2, while the core layer thickness is varied from 0.5 mm to 2.5 mm in increments of 0.5 mm. The results suggest that increasing the thickness ratio of the core layer leads to decrease in the fundamental frequency but increase in the loss factor, irrespective of boundary condition considered in the study. Increasing the MR-fluid layer thickness causes the structure mass to increase leading to lower natural frequency, while higher fluid volume contributes to greater energy dissipation and thereby the loss factor. The results also show that increasing the thickness ratio yields more pronounced effect of MR fluid on the resonant frequency of the F-F annular plate in response to the applied magnetic field, compared to the F-C plate. For instance, the fundamental

frequency of the F-F plate with thickness ratio of 1.5 and exposed to 90 mT magnetic flux is nearly 84% higher when compared to that of the plate in the absence of the magnetic field. The corresponding increase in the frequency of the F-C plate is near 43%. The relative higher increase the frequency of the F-F is due to its greater flexibility compared to F-C plate, which yields greater shear deformation of the core layer. The greater shear deformation also contributes to larger increase in the loss factor of the F-F plate compared to the F-C plate. Variations in the thickness ratio, however, yield only minimal effect on loss factor of the plate in the absence of magnetic field, for both the boundary conditions considered.
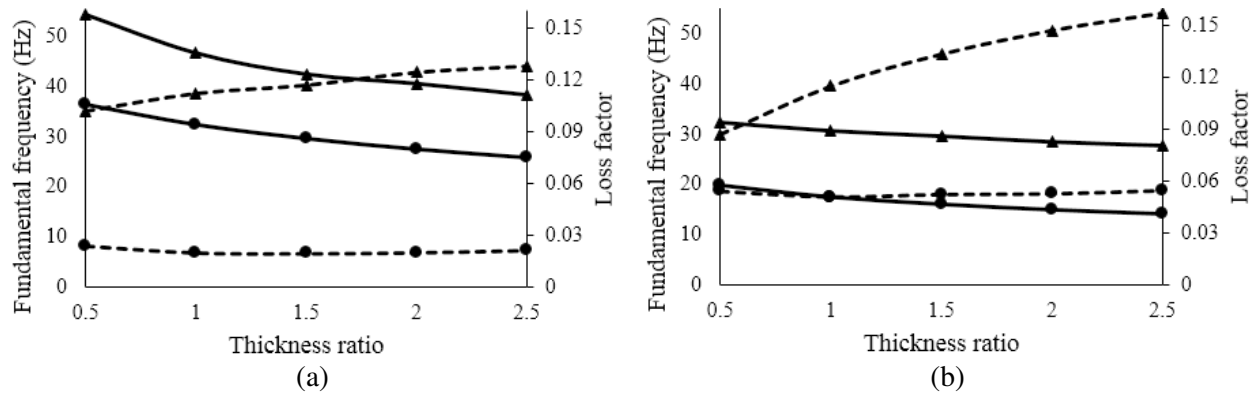
Figure 5.7 Influence of variations in the core layer thickness ratio (h_2/h_3) on fundamental frequency (solid line) and corresponding loss factor (dashed line) of the MR-fluid annular plate with different boundary conditions ((a) F-C; and (b) F-F), under two levels of magnetic flux density ($\bullet …0\ and\ \blacktriangle …90\ mT$).

5.5. Conclusions

The study investigated dynamic characteristics of the annular circular sandwich plates with MR-fluid core layer considering different boundary conditions. The effects of variations in magnetic flux intensity, MR-fluid core layer thickness and radius ratio are evaluated on free vibration properties of the plates in terms of natural frequencies and loss factors. The results obtained from analytical model based on Ritz method showed good agreements with the laboratory measured properties of the MR-fluid sandwich plate under a wide range of magnetic flux intensity and free-free boundary condition. The simulation results suggested increase in natural frequencies of the sandwich annular plates with increasing magnetic flux density, irrespective of the boundary conditions considered in the study. The rate of increase in the frequencies, however, was more pronounced for boundary conditions causing higher flexibility of the structure, e.g. free-free condition, which was attributed to relatively higher shear deformation of the core layer of the

flexible plate. The boundary condition leading to higher stiffness of the plate revealed largest increase in the fundamental frequency with increasing magnetic field. The conditions leading to higher flexibility, however, showed greatest changes in the higher modes frequencies. This tendency was not evident in the loss factors, which was attributed to its definition. The loss factor showed strong dependence on the boundary condition apart from the magnetic field. For the F-F and C-F boundary condition, the loss factors corresponding to the three lower modes increased with increase in magnetic flux up to certain limit, and then decreased with further increase in magnetic flux density. The trend suggested the existence of an optimal magnetic flux density that would yield highest loss factor for a given mode of vibration. Increasing the radius ratio of annular plate resulted in lower mass, while variations in stiffness and thus the natural frequencies were strongly related to boundary conditions. Increasing the core layer thickness lowered the natural frequency due to increasing mass of the structure, with only minimal variations in the loss factor in the absence of the magnetic field. Applications of the magnetic flux resulted in substantial increases in the fundamental frequency and the los factor. The relative increases in frequency and loss factor were substantially higher for free-free boundary condition due to relatively higher shear deformation of the core layer.

CHAPTER 6

VIBRATION ANALYSIS AND OPTIMUM DESIGN OF MULTI-LAYER PLATES PARTIALLY TREATED WITH THE MR FLUID

6.1. Introduction

A number of studies have shown that the magnetorheological (MR) fluids offer promising potentials for active and semi active control of vibration in systems and structures, which mostly derive from the rapid and reversible variations in the rheological properties (elasticity, plasticity and viscosity) of the fluids to an applied magnetic field (Jolly et al., 1998; Chen and Hansen, 2005; 1998; Rajamohan et al., 2010; Yeh, 2013). A number of studies have applied MR fluid as a damping treatment layer in sandwich beam and plate structures to achieve variable damping and stiffness properties as a function of the applied magnetic field (Rajamohan et al., 2010; Yeh, 2013). These have invariably shown substantial increase in the stiffness and damping properties of the sandwich structure fully treated with the MR fluid layer with increasing magnetic field. The fully treated sandwich structures, however, result in higher mass due to high weight density of the MR fluid, and pose some practical challenges in implementing the MR fluid layer (Jolly et al., 1998). Furthermore, the application of a uniform magnetic field over the entire structure poses difficult challenges. A partial MR fluid treatment of the structure would thus be desirable, particularly when applied to optimal locations to achieve controllable damping and stiffness of the structure with relatively small size electro-magnets.

The optimal designs of multi-layer structures with viscoelastic materials as the core layer have been widely investigated to achieve enhanced damping performance. Lifshitz and Leibowitz (1987) used an equality constrained minimization technique to seek optimal dimensions of a sandwich structure comprising two elastic layers and a viscoelastic mid-layer so as to maximize the visco-elastic damping. The model proposed by Mead and Markus (1969) was employed to determine the loss factor of the structure. Wang and Chen (2003) presented a free vibration analysis on a sandwich structure comprising annular Mindlin plate as the host layer, partially or fully treated viscoelastic core layer and a top constraining layer. The study considered the longitudinal normal stress and in-plane/transverse shear stress of the elastic layers, while the transverse normal stress was assumed negligible. It was shown that a partial damping treatment may yield more noticeable

vibration attenuation of the host layer compared to the fully treated damping layer. Zheng et al. (2004) employed the Genetic Algorithm (GA) to minimize vibrational energy of a sandwich cantilever beam with only partial viscoelastic treatment to determine the optimal length, location and shear modulus of the viscoelastic material. The study concluded that the maximum structural damping may be achieved when the viscoelastic patches are applied to the free end and closed to the beam center, which was attributed to greater shear deformations of the viscoelastic treatment in the considered mode of vibration. Mohammadi and Sedaghati (2012d) investigated the vibration characteristics of a sandwich cylindrical shell with partial viscoelastic treatment considering the slippage between the layers using the higher order Taylor's expansions of the displacement fields in the core layer. The study suggested that optimal distributions of the damping treatments could yield higher loss factors of the structure, particularly for the higher modes.

Applications of MR and ER (Electro-rheological) fluids in sandwich beams, plates and shells have also been explored in a few studies, although the vast majority have focused on beam structures (Rajamohan et al., 2010, 2010b and 2010c). Only a few studies, however, have investigated the responses of the partially treated structures. Cho et al. (2005) investigated the vibration responses of a fully- and a partially-treated ER plate, and concluded that the partially treated plate yields superior ratio of vibration suppression to consumed energy compared to a fully treated ER plate. Mohammadi and Sedaghati (2012c) presented vibration analysis of sandwich cylindrical structures with ER fluid as the core layer. The study considered different configuration of ER fluid treatments, electric field intensities, and thickness ratios of the elastic layers and the ER fluid layer as the design parameters to maximize the damping corresponding to the first two modes of transverse vibration. Rajamohan et al. (2010b) investigated the effect of partial MR fluid treatments on the vibration characteristics of multi-layer beam. It was shown that partial damping treatment may be more effective than a fully treated damping layer to attenuate the vibration. The optimal number and locations of the MR treatments in a multi-layer beam structure were identified to achieve maximum modal damping factors of the sandwich beam corresponding to the first five modes (Rajamohan, 2011). The optimal location of the MR fluid treatment was found to be strongly dependent on the vibration mode, irrespective of the boundary condition. Snamina (2011) employed the classical plate theory and energy method to find optimal number and locations of the MR segments in the core layer of a sandwich plate structure to maximize the energy dissipation

in the structure. This study revealed greater number of optimal MR fluid treatments for the higher modes of vibration.

From the review of reported studies, it is evident that the dynamic responses of the multi-layer beam structures with ER and MR fluids have been widely investigated. The dynamic responses of sandwich plates with MR fluid as the core layer, however, have been addressed in only a few studies (Snamina, 2011; Yeh, 2013). In particular, an experimental study on the vibration analysis of sandwich plates with partial MR fluid treatments could not be found. The present study is focused on the dynamic responses analyses of partially treated MR sandwich plates and identifications of optimal treatment locations to achieve greater vibration attenuation. The response characteristics of an aluminum cantilever sandwich plate with a localized MR fluid treatment were experimentally evaluated under harmonic excitations at the fixed support. A finite element model based on the classical plate theory is developed to formulate the governing equations of motion of the multi-layer plate with partial MR fluid treatments considering the effect of slippage between the elastic layers. The validity of the finite element model is demonstrated on the basis of the laboratory-measured responses. An optimization problem is formulated and solved to identify optimal locations of the MR fluid treatments so as to maximize the attenuation of the support vibration.

6.2. Mathematical formulations

6.2.1. Finite element model of a partially treated multi-layer plate

A multi-layer sandwich plate (length = l_1; width = l_2), consisting of an isotropic host layer (thickness = h_2+h_3) with m (along the length) $\times$ n (along the width) equal cavities of height h_2 and a constraining layer, is considered for developing the FE model. The MR fluid is applied to one or more cavities within the core layer to achieve a partially treated MR sandwich plate. Figure 6.1 illustrates the host layer with $m=n=3$ equal cavities and the constraining layer.
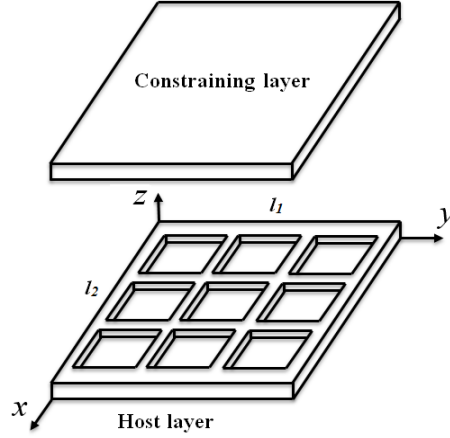
Figure 6.1 Schematics of the host layer with $m=n=3$ cavities and the constraining layer

The finite element model of the partially treated sandwich plate is developed using two types of two-dimensional elements. The edges of the host layer on the boundaries and between the cavities are modeled using the 'type 1' elements, as shown in Figure 6.2. In these elements, the host layer is attached to the constraining layer using an adhesive, which also serves as the sealant for the MR fluid contained in the cavity. This type of element is thus a two-layer plate element comprising the bottom and top elastic layers bonded with an adhesive layer. Each element, which discretizes the walls surrounding a cavity, includes four nodes with ten-degrees-of-freedom (DoF) per node (longitudinal and transverse displacements, and slopes about the x- and y-axis for both the top and the bottom layers). The second type of element is used to model the remaining region containing the MR fluid layer sandwiched between the host and the constraining layers.
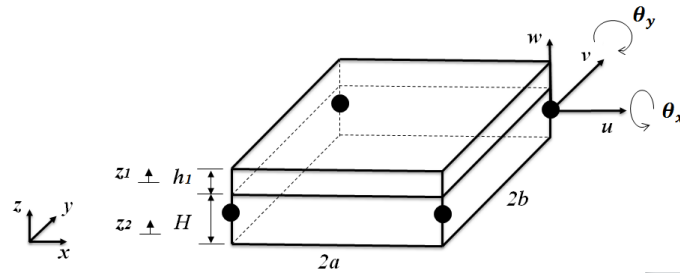
Figure 6.2 Two-dimensional plate element ('type 1') with 4 nodes and 10-DoF for each node.

In order to develop the mass and stiffness matrices of the 'type 1' element, it is assumed that the adhesive layer cannot provide a perfect bond between the two face layers. The slippage may thus occur between the two elastic layers due to longitudinal displacement discontinuity at the interface of the layers (Bai and Sun, 1995). The FE model is thus formulated considering the effect

124

of this slippage. The first-order shear deformation theory (FSDT), which is a simple and accurate theory for moderately thick plates, is used to define the displacement field of an arbitrary point in the domain of element, such that (Mindlin, 1951):

$$u^{(j)}(x,y,z,t) = u_0^{(j)}(x,y,t) + z_j \, \psi_x^{(j)}(x,y,t)$$

$$v^{(j)}(x,y,z,t) = v_0^{(j)}(x,y,t) + z_j \, \psi_y^{(j)}(x,y,t), \qquad j = 1,2 \tag{6.1}$$

$$w^{(j)}(x,y,z,t) = w^{(j)}(x,y,t)$$

where u and v represent the displacements along the x- and y-axis, respectively, and w is the transverse displacement. u_0 and v_0 denote the in-plane displacements at the mid-plane along the x- and y-axis, respectively. z_1 and z_2 are the transverse coordinates of the top and bottom layers, respectively, which are defined in the local coordinate systems. The origin of z_1 is at $z = H + h_1/2$, where $H = h_2 + h_3$, and that of z_2 is located at $z = h_3/2$. ψ_x and ψ_y are the slope rotations about the y-z and x–z planes, respectively, at $z_j = 0$, and t is the time. The superscript $j = 1, 2$ refers to the top and bottom layers, respectively. The strain components, associated with the displacements in Eq. (6.1) are obtained assuming small deformations, as:

$$\varepsilon_x^{(j)} = \frac{\partial u_0^{(j)}}{\partial x} + z_j \frac{\partial \psi_x^{(j)}}{\partial x}; \quad \varepsilon_y^{(j)} = \frac{\partial v_0^{(j)}}{\partial y} + z_j \frac{\partial \psi_y^{(j)}}{\partial y}; \quad \gamma_{xz}^{(j)} = \psi_x^{(j)} + \partial w^{(j)}/\partial x;$$

$$\gamma_{yz}^{(j)} = \psi_y^{(j)} + \partial w^{(j)}/\partial y; \quad \gamma_{xy}^{(j)} = \frac{\partial u_0^{(j)}}{\partial y} + \frac{\partial v_0^{(j)}}{\partial x} + z_j \left(\frac{\partial \psi_x^{(j)}}{\partial y} + \frac{\partial \psi_y^{(i)}}{\partial x} \right), \qquad j = 1,2 \tag{6.2}$$

where ε_x and ε_y are the normal strains, γ_{xy} is the plane shear strain and γ_{xz} and γ_{yz} are the transverse shear strains in the element. The stress components in the top and host layers are subsequently obtained using the Hooke's law, as:

$$\sigma_x^{(j)} = \frac{E_j}{\left(1 - v_j^2\right)} \left(\varepsilon_x^{(j)} + v_j \varepsilon_y^{(j)} \right); \quad \sigma_y^{(j)} = \frac{E_j}{\left(1 - v_j^2\right)} \left(\varepsilon_y^{(j)} + v_j \varepsilon_x^{(j)} \right)$$

$$\tau_{xy}^{(j)} = G \gamma_{xy}^{(j)}; \quad \tau_{xz}^{(j)} = \kappa G \gamma_{xz}^{(j)}; \quad \tau_{yz}^{(j)} = \kappa G \gamma_{yz}^{(j)} \qquad j = 1,2 \tag{6.3}$$

where E, v and G are Young's modulus, Poisson's ratio and shear modulus of the elastic layers, respectively. σ_x and σ_y are the normal stresses, τ_{xy} is the plane shear stress, and τ_{xz} and τ_{yz} are the

125

transverse shear stresses. It should be noted that the FSDT method assumes constant transverse shear stress through the thickness of the element, which would violate the zero shear stress condition at the free surfaces of the element. A shear correction factor κ is thus used to compensate for the resulting error in transverse shear stresses, as proposed by Mindlin (1951).

The slippage between the two layers is described by the discontinuity in the longitudinal displacement at the interface of the top and bottom layers. The compatibility condition can be expressed as (Bai and Sun, 1995):

$$\tau_{xz}^{(j)} = k^* \left(u^{(1)}\left(x, y, -h_1/2, t\right) - u^{(2)}\left(x, y, h_2 + h_3/2, t\right) \right)$$

$$\tau_{yz}^{(j)} = k^* \left(v^{(1)}\left(x, y, -h_1/2, t\right) - v^{(2)}\left(x, y, h_2 + h_3/2, t\right) \right)$$

(6.4)

where k^* is the complex shear stiffness parameter of the adhesive layer, referred to as the adhesive interface stiffness (Bai and Sun, 1995). An adhesive layer with a low value of k^* would yield soft and poor bonding, and thereby greater slippage, while a higher value of k^* signifies a stronger bonding and lower slippage between the layers. Assuming identical transverse shear stresses in the two layers at the interface, $\tau_{xz}^{(1)} = \tau_{xz}^{(2)}$ and $\tau_{yz}^{(1)} = \tau_{yz}^{(2)}$, yields;

$$\left(\psi_x^{(1)} + \partial w^{(1)}/\partial x\right) - \left(\psi_x^{(2)} + \partial w^{(2)}/\partial x\right) = 0; \quad \left(\psi_y^{(1)} + \partial w^{(1)}/\partial y\right) - \left(\psi_y^{(2)} + \partial w^{(2)}/\partial y\right) = 0$$

(6.5)

Using Eqs. (6.4) and (6.5), ψ_x and ψ_y of the top and bottom layers can be represented in terms of the in-plane displacements and slopes, such that:

$$\psi_x^{(1)} = \frac{-\theta_x^{(1)}\left(k^*\left(2h_2 + h_3\right) + 2G\kappa\right) + k^*\left(\theta_x^{(2)}\left(2h_2 + h_3\right) + 2u_0^{(1)} - 2u_0^{(2)}\right)}{k^*\left(h_1 + 2h_2 + h_3\right) + 2G\kappa}$$

$$\psi_y^{(1)} = \frac{-\theta_y^{(1)}\left(k^*\left(2h_2 + h_3\right) + 2G\kappa\right) + k^*\left(\theta_y^{(2)}\left(2h_2 + h_3\right) + 2v_0^{(1)} - 2v_0^{(2)}\right)}{k^*\left(h_1 + 2h_2 + h_3\right) + 2G\kappa}$$

$$\psi_x^{(2)} = \frac{\theta_x^{(1)}h_1 k^* - \theta_x^{(2)}\left(h_1 k^* + 2G\kappa\right) + 2k^*\left(u_0^{(1)} - u_0^{(2)}\right)}{k^*\left(h_1 + 2h_2 + h_3\right) + 2G\kappa}$$

(6.6)

$$\psi_y^{(2)} = \frac{\theta_y^{(1)}h_1 k^* - \theta_y^{(2)}\left(h_1 k^* + 2G\kappa\right) + 2k^*\left(v_0^{(1)} - v_0^{(2)}\right)}{k^*\left(h_1 + 2h_2 + h_3\right) + 2G\kappa}$$

where $\theta_x = \partial w/\partial x$ and $\theta_y = \partial w/\partial y$. In the FE modeling, the transverse and longitudinal displacements of the element are expressed in terms of the nodal displacement vector,

$q(t) = \left\{ u_{0i}^{(1)}, v_{0i}^{(1)}, u_{0i}^{(2)}, v_{0i}^{(2)}, w_i^{(1)}, w_i^{(2)}, \theta_{xi}^{(1)}, \theta_{xi}^{(2)}, \theta_{yi}^{(1)}, \theta_{yi}^{(2)} \right\}^T$; $i=1,2,3,4$, and the shape function vectors

$N_{u1}(x), N_{v1}(x), N_{u2}(x), N_{v2}(x), N_{w1}(x)$ and $N_{w2}(x)$, such that:

$$w^{(j)}(x,y,t) = N_{wj}(x,y)q(t); \quad u_0^{(j)}(x,y,t) = N_{uj}(x,y)q(t); \quad v_0^{(j)}(x,y,t) = N_{vj}(x,y)q(t) \quad (6.7)$$

The shape function vectors derived for the model are presented in the Appendix.

The total potential and kinetic energy of the ($2a \times 2b$) element is obtained from the sum of those of the individual layers, such that:

$$V = V_1 + V_2; \qquad T = T_1 + T_2 \tag{6.8}$$

where V_1 and V_2 represent the total strain energy of the top and bottom layers, respectively and T_1 and T_2 denote the kinetic energy associated with the transverse motion and axial deformations of the respective layers. These energy terms can be expressed as:

$$V_j = \frac{1}{2} \int_{-a}^{a} \int_{-b}^{b} \int_{-h_{lj}}^{h_{uj}} \left(\sigma_x^{(j)} \varepsilon_x^{(j)} + \sigma_y^{(j)} \varepsilon_y^{(j)} + \tau_{xy}^{(j)} \gamma_{xy}^{(j)} + \tau_{xz}^{(j)} \gamma_{xz}^{(j)} + \tau_{yz}^{(j)} \gamma_{yz}^{(j)} \right) dz\, dy\, dx$$

$$T_j = \frac{1}{2} \int_{-a}^{a} \int_{-b}^{b} \int_{-h_{lj}}^{h_{uj}} \rho_j \left(\left(u^{(j)} \right)^2 + \left(v^{(j)} \right)^2 + \left(w^{(j)} \right)^2 \right) dz\, dy\, dx; \quad j=1,2 \tag{6.9}$$

where ρ_j is the weight density of layer j. $h_{l1} = h_{u1} = h_1/2$, $h_{l2} = h_3/2$ and $h_{u2} = h_2 + h_3/2$.

The governing equations of motion of the plate element in the finite element form can be derived using the Lagrange's equation, as:

$$\frac{d}{dt}\left(\frac{\partial T}{\partial \dot{q}_l} \right) - \frac{\partial T}{\partial q_l} + \frac{\partial V}{\partial q_l} = Q_l, \qquad l = 1,...,s \tag{6.10}$$

where Q_l denotes the generalized force component and s represents total DoF of the element ($s=40$). The governing equations of motion for 'type 1' plate element are obtained upon substituting for the energy functions in Eq. (6.9) into the Lagrange's equation, as:

$$\left[m^e \right]\{\ddot{q}\} + \left[k^e \right]\{q\} = \{ f^e \} \tag{6.11}$$

where $[m^e]$ and $[k^e]$ are the element mass and stiffness matrices, respectively, and $\{f^e\}$ is the nodal force vector.
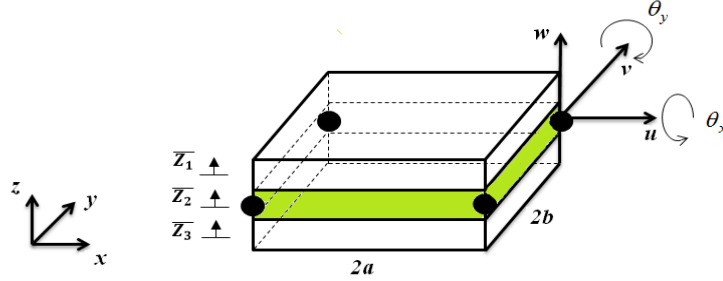
Figure 6.3 Two-dimensional sandwich plate element ('type 2')

The second type of the element ('type 2'), as depicted in Figure 6.3, is a two dimensional sandwich plate element (length = $2a$, width = $2b$), which consists of the two elastic face layers and a core layer of the MR fluid. This element also includes four nodes with ten-DoF for each node (longitudinal and transverse displacements, and slopes about x- and y-axis of the top and bottom layers). The thickness of the top, core and bottom layers are h_1, h_2 and h_3, respectively. Considering very low thickness to length ratio of the face layers, the Kirchhoff-Love assumptions are applicable so that the transverse shear deformation and rotary inertia can be neglected. The displacement functions of the 'type 2' plate element, based on the Kirchhoff assumptions, are expressed as (Brush and Almroth, 1975):

$$\bar{u}^{(i)}(x,y,z,t)=\bar{u}_0^{(i)}(x,y,t)-\bar{z}_i\frac{\partial \bar{w}^{(i)}(x,y,t)}{\partial x}$$

$$\bar{v}^{(i)}(x,y,z,t)=\bar{v}_0^{(i)}(x,y,t)-\bar{z}_i\frac{\partial \bar{w}^{(i)}(x,y,t)}{\partial y}, \qquad i=1\,and\,3 \qquad (6.12)$$

$$\bar{w}^{(i)}(x,y,z,t)=\bar{w}^{(i)}(x,y,t)$$

The superscripts $i = 1$ and 3 refer to the top and bottom layers, respectively and $\bar{z}_1, \bar{z}_2$ and $\bar{z}_3$ denote the transverse coordinates of the top, middle and bottom layers of the element, respectively, which are defined in the local coordinate systems with origins located at the mid x-y planes of the respective layers. Assuming negligible slippage between the three layers leads to continuous displacement profiles through the thickness of the element, given by:

$$\left. \overline{u}^{(1)} \right|_{\overline{z}_1=-h_1/2} = \left. \overline{u}^{(2)} \right|_{\overline{z}_2=h_2/2} \quad \& \quad \left. \overline{v}^{(1)} \right|_{\overline{z}_1=-h_1/2} = \left. \overline{v}^{(2)} \right|_{\overline{z}_2=h_2/2} \quad \& \quad \left. \overline{w}^{(1)} \right|_{\overline{z}_1=-h_1/2} = \left. \overline{w}^{(2)} \right|_{\overline{z}_2=h_2/2}$$

$$\left. \overline{u}^{(2)} \right|_{\overline{z}_2=-h_2/2} = \left. \overline{u}^{(3)} \right|_{\overline{z}_3=h_3/2} \quad \& \quad \left. \overline{v}^{(2)} \right|_{\overline{z}_2=-h_2/2} = \left. \overline{v}^{(3)} \right|_{\overline{z}_3=h_3/2} \quad \& \quad \left. \overline{w}^{(2)} \right|_{\overline{z}_2=-h_2/2} = \left. \overline{w}^{(3)} \right|_{\overline{z}_3=h_3/2}$$

(6.13)

The superscript '2' in the above equations refers to the core layer of the element. Based on the compatibility condition, the displacement field of the core layer can be formulated with respect to those of the top and bottom layers. Assuming negligible transverse shear strain in the elastic layers and in-plane shear strain in the core layer (Yeh, 2013), the expressions for the linear strains of the 'type 2' element corresponding to the displacement fields, are obtained as:

$$\overline{\varepsilon}_x^{(i)} = \frac{\partial \overline{u}_0^{(i)}}{\partial x} - \overline{z}_i \frac{\partial^2 \overline{w}^{(i)}}{\partial x^2}; \quad \overline{\varepsilon}_y^{(i)} = \frac{\partial \overline{v}_0^{(i)}}{\partial y} - \overline{z}_i \frac{\partial^2 \overline{w}^{(i)}}{\partial y^2}; \quad \overline{\gamma}_{xy}^{(i)} = \frac{\partial \overline{u}_0^{(i)}}{\partial y} + \frac{\partial \overline{v}_0^{(i)}}{\partial x} - 2\overline{z}_i \frac{\partial^2 \overline{w}^{(i)}}{\partial x \partial y}, \quad i=1 \, and \, 3$$

$$\overline{\gamma}_{xz}^{(2)} = \frac{\overline{u}_0^{(1)} - \overline{u}_0^{(3)}}{h_2} + \frac{h_1}{2h_2} \frac{\partial \overline{w}^{(1)}}{\partial x} + \frac{h_3}{2h_2} \frac{\partial \overline{w}^{(3)}}{\partial x} + \frac{\partial \overline{w}^{(2)}}{\partial x}$$

$$\overline{\gamma}_{yz}^{(2)} = \frac{\overline{v}_0^{(1)} - \overline{v}_0^{(3)}}{h_2} + \frac{h_1}{2h_2} \frac{\partial \overline{w}^{(1)}}{\partial y} + \frac{h_3}{2h_2} \frac{\partial \overline{w}^{(3)}}{\partial y} + \frac{\partial \overline{w}^{(2)}}{\partial y}$$

(6.14)

Using the Hooke's law, the stress components of the element in the face and core layers are obtained as:

$$\overline{\sigma}_x^{(i)} = \frac{E_i}{\left(1-v_i^2\right)} \left(\overline{\varepsilon}_x^{(i)} + v_i \overline{\varepsilon}_y^{(i)} \right); \quad \overline{\sigma}_y^{(i)} = \frac{E_i}{\left(1-v_i^2\right)} \left(\overline{\varepsilon}_y^{(i)} + v_i \overline{\varepsilon}_x^{(i)} \right); \quad i=1 \, and \, 3$$

$$\overline{\tau}_{xy}^{(i)} = G \overline{\gamma}_{xy}^{(i)}; \quad \overline{\tau}_{xz}^{(2)} = G^* \overline{\gamma}_{xz}^{(2)}; \quad \overline{\tau}_{yz}^{(2)} = G^* \overline{\gamma}_{yz}^{(2)}$$

(6.15)

where G^* is the complex shear modulus of the core layer. It should be noted that in the pre-yield region, MR fluid behaves visco-elastically, and the shear stress and shear strain are proportional in terms of the complex shear modulus G^*, given by (Li et al., 1995):

$$G^* = G' + iG''$$

(6.16)

where G' is the storage modulus, which determines the average energy stored per unit volume of the material over a deformation cycle, and G' is the loss modulus, defined as the dissipated energy per unit volume of the material during a deformation cycle.

For the FE model, the transverse and longitudinal displacements of the element are expressed in terms of the nodal displacement vector $\bar{q}(t) = \left\{ \bar{u}_{0i}^{(1)}, \bar{v}_{0i}^{(1)}, \bar{u}_{0i}^{(3)}, \bar{v}_{0i}^{(3)}, \bar{w}_i^{(1)}, \bar{w}_i^{(3)}, \bar{\theta}_{xi}^{(1)}, \bar{\theta}_{xi}^{(3)}, \bar{\theta}_{yi}^{(1)}, \bar{\theta}_{yi}^{(3)} \right\}^T$; $i=1,2,3,4$, and the shape function vectors, $N_{u1}(x)$, $N_{v1}(x)$, $N_{u3}(x)$, $N_{v3}(x)$, $N_{w1}(x)$ and $N_{w3}(x)$. For the sandwich plate element the potential and kinetic energies can be evaluated as:

$$\bar{V} = \bar{V}_1 + \bar{V}_2 + \bar{V}_3 ; \qquad \bar{T} = \bar{T}_1 + \bar{T}_2 + \bar{T}_3 \tag{6.17}$$

where $\bar{V}_1$ and $\bar{V}_3$ are the total strain energy of the top and bottom layers, respectively and $\bar{V}_2$ represents the shear strain energy in the core layer. $\bar{T}_1$ and $\bar{T}_3$ are the kinetic energy associated with the transverse motion and axial deformation in the top and bottom layers, respectively and $\bar{T}_2$ denotes the kinetic energy due to rotational deformation of the core layer. The energy functions can be given by:

$$\bar{V}_i = \frac{1}{2} \int_{-a}^{a} \int_{-b}^{b} \int_{-h_i/2}^{h_i/2} \left(\bar{\sigma}_x^{(i)} \bar{\varepsilon}_x^{(i)} + \bar{\sigma}_y^{(i)} \bar{\varepsilon}_y^{(i)} + \bar{\tau}_{xy}^{(i)} \bar{\gamma}_{xy}^{(i)} \right) dz \, dy \, dx$$

$$\bar{V}_2 = \frac{1}{2} \int_{-a}^{a} \int_{-b}^{b} \int_{-h_2/2}^{h_2/2} \left(\bar{\tau}_{xz}^{(2)} \bar{\gamma}_{xz}^{(2)} + \bar{\tau}_{yz}^{(2)} \bar{\gamma}_{yz}^{(2)} \right) dz \, dy \, dx$$

$$\qquad\qquad\qquad\qquad\qquad\qquad\qquad\qquad\qquad\qquad\qquad i = 1 \, and \, 3 \tag{6.18}$$

$$\bar{T}_i = \frac{1}{2} \int_{-a}^{a} \int_{-b}^{b} \int_{-h_i/2}^{h_i/2} \rho_i \left(\left(\bar{u}_0^{(i)} \right)^2 + \left(\bar{v}_0^{(i)} \right)^2 + \left(\bar{w}^{(i)} \right)^2 \right) dz \, dy \, dx$$

$$\bar{T}_2 = \frac{1}{2} \int_{-a}^{a} \int_{-b}^{b} \left(\rho_2 h_2 \left(\dot{\bar{w}}^{(2)} \right)^2 + I_2 \left(\left(\dot{\bar{\gamma}}_{xz}^{(2)} \right)^2 + \left(\dot{\bar{\gamma}}_{yz}^{(2)} \right)^2 \right) \right) dy \, dx$$

where $I_2 = \rho_2 h_2^3 / 12$. The governing equations of motion of the plate element ('type 2') are subsequently formulated in the FE form upon substituting for the kinetic and potential energy functions for the face and core layers in the Lagrange's equation:

$$\left[\bar{m}^e \right] \{ \ddot{\bar{q}} \} + \left[\bar{k}^e \right] \{ \bar{q} \} = \{ \bar{f}^e \} \tag{6.19}$$

where $\left[\bar{m}^e \right]$ and $\left[\bar{k}^e \right]$ are the element mass and stiffness matrices, respectively, and $\{ \bar{f}^e \}$ is the nodal force vector. The governing equations of motion for the system are then obtained by assembling the stiffness and mass matrices of the elements ('type 1' and 'type 2') discretizing the structure and considering compatibility condition to ensure identical transverse and axial displacements and slopes at the interfaces of the two elements, such that:

$$\bar{u}_0^{(1)} = u_0^{(1)}, \; \bar{u}_0^{(3)} = u_0^{(2)}, \; \bar{v}_0^{(1)} = v_0^{(1)}, \; \bar{v}_0^{(3)} = v_0^{(2)}, \; \bar{w}^{(1)} = w^{(1)},$$

$$\bar{w}^{(3)} = w^{(2)}, \; \bar{\theta}_x^{(1)} = \theta_x^{(1)}, \; \bar{\theta}_x^{(3)} = \theta_x^{(2)}, \; \bar{\theta}_y^{(1)} = \theta_y^{(1)}, \; \bar{\theta}_y^{(3)} = \theta_y^{(2)}$$

(6.20)

While the adhesive layer in 'type 1' elements cannot provide a perfect bonding between the top and bottom layers, it ensures constant transverse deformations of the walls surrounding the cavities. The Lagrange multiplier technique is used to incorporate this constraint in the FE model, which yields following system governing equations:

$$[M]_{p \times p} \{\ddot{d}\}_{p \times 1} + [K]_{p \times p} \{d\}_{p \times 1} + [B]_{p \times r}^T \{\lambda\}_{r \times 1} = \{F\}_{p \times 1}$$

$$[B]_{r \times p} \{d\}_{p \times 1} = \{0\}_{r \times 1}$$

(6.21)

where $[M]$, $[K]$ and $[B]$, are the system mass, stiffness and constraint coefficient matrices, respectively, and $[d]$, $\{F\}$ and $\{\lambda\}$ are the displacement, force and Lagrange multiplier vectors, respectively. p and r denote the number of total DoF of the structure and the constraints, respectively. The natural frequencies and loss factors of the structure may be evaluated through solutions of the following system of equations:

$$\begin{bmatrix} -[M]\omega^2 + [K] & [B]^T \\ [B] & 0 \end{bmatrix} \begin{Bmatrix} d \\ \lambda \end{Bmatrix} = \begin{Bmatrix} 0 \\ 0 \end{Bmatrix}$$

(6.22)

6.2.2. Optimal locations of the MR fluid treatments

An optimization problem is formulated to seek optimal locations of MR fluid treatments in a plate structure with $m \times n$ MR fluid cavities so as to enhance the control flexibility in terms of stiffness and damping properties corresponding to the three lower modes. The problem is formulated to seek optimal partial treatments considering three different objective functions. In the first case, the optimization goal is to maximize variations in the stiffness of the structure (case 1), evaluated in terms of increase in the first three natural frequencies, when the applied magnetic field is varied from 0 to 90 mT, such that:

$$\textit{Maximize } F_1^{(r)}(X) = \frac{f_{@B=90mT}^{(r)} - f_{@B=0mT}^{(r)}}{f_{@B=0mT}^{(r)}}; \qquad r = 1, 2, 3 \quad \text{subject to} \quad 0 < P \leq N \qquad (6.23)$$

where $F_1^{(r)}$ is the objective function and $f_{@B}^{(r)}$ represents the natural frequency corresponding to mode r and a specific magnetic flux density B. The design vector X, defines the locations of the treated cavities (P) in the core layer and N is the maximum number of fluid-filled cavities.

The objective in the second case was to maximize the loss factor corresponding to the first three vibration modes of the structure under a magnetic flux density of 90 mT (case 2):

$$Maximize\ F_2^{(r)}(X)=\eta^{(r)}; \quad r=1,2,3 \quad \text{subject to} \quad 0<P\leq N \tag{6.24}$$

The loss factor corresponding to mode r is defined as $\eta^{(r)} = Im(\lambda^{(r)})/Re(\lambda^{(r)})$, where λ is complex eigenvalue, and 'Im' and 'Re' denote the imaginary and real components of the eigenvalue, respectively. The final optimization problem (case 3) is formulated so as to maximize the energy dissipation of the partially treated structure corresponding to each mode, which is expressed by the imaginary component of the eigenvalue, such that:

$$Maximize\ F_3^{(r)}(X) = Im(\lambda^{(r)}); \quad r=1,2,3 \quad \text{subject to} \quad 0<P\leq N \tag{6.25}$$

Although both the loss factor and the energy dissipation used in cases 2 and 3 relate to damping of the structure, the two objective functions differ. The solutions of the problem in case 3 would yield optimal locations of the MR fluid treatments for maximizing the energy dissipation of the structure, while that in case 2 may not converge to maximum energy dissipation, as implied by the definition of the loss factor. The above optimization problems are solved using the genetic search algorithm (GA) (Rajamohan et al., 2010) considering two different boundary conditions: (i) the plate clamped along one of the edges (CFFF); and (ii) the plate simply-supported along all the edges (SSSS). The geometry boundary conditions for the clamped and simply supported edges are given by (Hasheminejad and Maleki, 2009):

$$\text{CFFF:} \quad w=u_0=v_0=\theta_x=\theta_y=0 \quad \text{and} \quad \text{SSSS:} \quad w=0 \tag{6.26}$$

The repeated solutions obtained considering different population sizes, crossover fractions, mutation functions, generations and function tolerances were examined to ensure globally optimal locations of the MR fluid treatments.

6.3. Experimental study

A laboratory experiment was designed to characterize response characteristics of a cantilevered sandwich plate partially treated with MR fluid, when subjected to harmonic vibration at the fixed

132

support (Ali et al., 2013). The plate was fabricated using aluminum elastic layers due to the light weight and negligible magnetic permeability of aluminum, which also helped realizing more uniform magnetic flux over the plate surface. The host layer ($300 \times 300 \times 2$ *mm*) was designed with nine 1 *mm* deep cavities (*m*=3 and *n*=3) of identical size (93.34×93.34 *mm*). The width of the walls surrounding the cavities was 5 *mm*. The constraining top layer ($300 \times 300 \times 1$ *mm*) was bonded to the host layer using silicon-based adhesive. The oil resistant silicon-based adhesive also served as the sealant for the MR fluid in a cavity. One of the edges of the sandwich plate was firmly clamped to an electrodynamic vibration exciter. Two square neodymium magnets, mounted on a nonmagnetic materials fixture, were positioned symmetrically above and below the sandwich plate to impose a nearly uniform magnetic flux over the plate surface. The experiments were performed with four different levels of gaps between the magnets and the sandwich plate to achieve flux density near 0, 30, 50 and 90 mT. A gauss meter was used to measure the magnetic flux density over the plate surfaces. The measurements revealed lower flux density near the edges of the plate but nearly uniform density over rest of the plate surface. The peak deviation in the flux density was in the order of 20%.

The experiments were conducted with the untreated and partially treated sandwich plates. The partial treatment was realized by filling the corner cavity near the free edge of the plate with the MR fluid (MRF 132DG, Lord Corporation; viscosity at room temperature = 0.112 Pa-s, solid content by weight = 80.98% and mass density = 3500 kg/m^3). The fluid was assumed to remain in the pre-yield region, where the storage and loss moduli of the MR fluid could be described by the following general relation in frequency ω (Hz) and flux density B (mT):

$$\bar{G} = \left(a_0 + a_1 B + a_2 B^2\right)\left(1 - e^{-a_3 \omega}\right) \tag{6.27}$$

where $\bar{G}$ is the storage or loss modulus of the fluid, and a_0, a_1, a_2 and a_3 are unknown constants, which are presented in Table 6.1.

Table 6.1 The identified coefficients of the storage and loss moduli model

MR fluid	Modulus	a_0	a_1	a_2	a_3
MRF 132DG	Storage	192160.6	30663.56	243.6247	0.004080
	Loss	45524.40	6757.977	6.441200	0.007416

The sandwich structure was subjected to harmonic vibration swept in the 1 to 250 Hz frequency range at the rate of 1 octave/min with constant acceleration magnitude (0.5 m/s^2). A miniature

three-axes accelerometer (PCB Piezotronics, model: 356A01), weighing 2.5 grams, was installed on the constraining layer of the plate at $x = 200\ mm$ and $y = 100\ mm$ with respect to the origin of the coordinate system (Figure 6.1). The acceleration due to excitation was also measured using a single axis accelerometer installed at the support, which also served as the feedback for the vibration controller. The H_1 function was used to characterize the frequency response function of the structure under four different levels of the magnetic flux density: 0, 30, 50 and 90 mT.

6.4. Results and discussion

6.4.1. Validation of the FE model

The validity of the FE model of the partially treated sandwich structure was examined by comparing the resulting natural frequencies and the corresponding half power bandwidths with the measured values. For this purpose, the simulations were performed for the aluminum sandwich plate (E= 65 Gpa; v = 0.33; ρ = 2650 kg/m³) with nine cavities ($m=n=3$). One of the cavities in the core layer positioned at the corner of the free end was treated with the MR fluid as in the experimental study. The interface stiffness k^* due to the silicon based adhesive layer and the shear correction factor κ were taken as 22×10^{10} (1+0.067i) and π²/12, respectively (Bai and Sun, 1995). Table 6.2 presents a comparison of the lower seven modes natural frequencies obtained from the FE models of the treated and untreated sandwich plates with the measured frequencies. For the treated plate, the frequencies were obtained under four different levels of the magnetic flux density (0, 30, 50 and 90 mT). A reasonably good agreement between the computed and measured natural frequencies can be observed for the vibration modes and magnetic flux densities considered in the study. The maximum deviation between the computed and measured frequencies is about 15.3%, which occurs in the 2nd mode frequencies. The results suggest that in the absence of magnetic flux, the MR fluid treatment yields relatively lower natural frequencies compared to those of the untreated plate, which is simply due to higher mass of the MR fluid treated plate. Increasing the magnetic flux resulted in increase in the natural frequencies, although the rate of increase is not significant. Increasing the field density from 0 to 90 mT caused an increase in the lower two frequencies in the order of only 1%, and 6-7% in the higher mode frequencies. This is attributable to the treatment applied only to a single cavity and relatively thick walls around the cavities, and thereby very low shear deformation experienced by the MR fluid. The shear deformation of the

fluid could be enhanced by reducing the thickness of the walls or by implementing low elasticity material walls such as rubber.

Table 6.2 Comparisons of the first seven natural frequencies (Hz) obtained from the FE models of the untreated and partially treated MR sandwich plates with the measured frequencies under different levels of magnetic flux density.

Flux (mT)	Method	First	Second	Third	Fourth	Fifth	Sixth	Seventh
Without MR-fluid								
	FE	20.42	40.97	86.20	111.96	119.10	190.70	203.94
	EXP	19.04	42.70	87.42	109.00	124.20	186.80	204.00
With MR-fluid in only one cavity								
B=0	FE	19.23	38.43	84.68	108.01	116.28	187.34	198.69
	EXP	18.07	42.79	86.30	107.10	123.90	183.10	203.50
B=30	FE	19.27	38.55	85.53	110.30	117.41	189.11	200.71
	EXP	18.16	43.00	86.55	111.80	125.70	184.50	205.00
B=50	FE	19.30	38.63	86.13	111.92	118.26	190.38	202.03
	EXP	18.20	43.66	87.20	114.90	127.60	185.90	206.50
B=90	FE	19.36	38.83	87.25	114.85	120.06	192.88	204.30
	EXP	18.07	44.77	88.08	117.50	130.20	188.30	208.10

The half power bandwidths obtained from the measured responses of the untreated and partially treated plates are also compared with those obtained from the models in Table 6.3. The results are presented only for the bending modes (first and third). The half power bandwidths corresponding to the other modes could not be accurately identified since the vertical excitation at the root section of the plate could not adequately excite the second, fourth, fifth, sixth and seventh modes of the plate. The complexity associated with identification of the half power bandwidths for some of the modes has also been reported by Oyadiji (1996).

Table 6.3 Comparisons of the first and third modes half power bandwidths (%) obtained by the FE models of the untreated and partially treated MR sandwich plates with the measured values under different levels of magnetic flux.

Method	Untreated plate		Partially treated plate							
			$B = 0$ mT		$B = 30$ mT		$B = 50$ mT		$B = 90$ mT	
	First	Third	First	Third	First	Third	First	Third	First	Third
FE	5.00	3.80	5.00	3.90	5.05	4.15	5.01	4.21	5.08	4.10
EXP	5.20	2.50	5.30	2.60	5.35	2.70	5.15	2.80	5.30	2.90

The results suggest relatively small variations in the half power bandwidths corresponding to the lower bending modes with increasing magnetic flux, as it was observed for the natural frequencies.

This can in-part be attributed to low shear deformation experienced by the MR fluid, and in-part to partial damping treatment applied to only a small fraction of the plate.

Figure 6.4 illustrates the percentage increase in the lower seven natural frequencies and half power bandwidths corresponding to the first and third modes of the partially treated sandwich plate, under different magnetic flux densities, compared to the those of the structure in the absence of magnetic field. The results show largest increase in the fourth mode natural frequency in response to the applied magnetic field, which is caused by larger shear deformation experienced by the MR fluid.
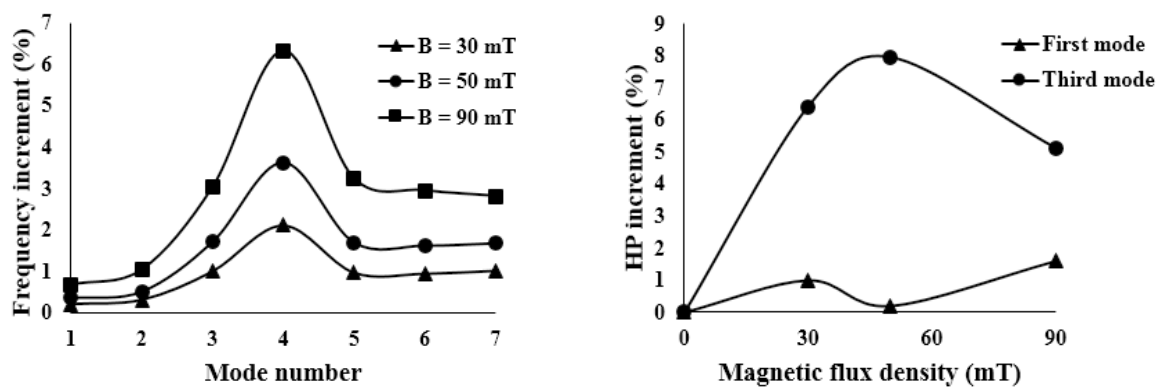
Figure 6.4 Percent variations in (a) first seven natural frequencies and (b) first and third modes half power bandwidths (HP) of the partially treated MR sandwich plate under different magnetic densities.

Figure 6.5 illustrates the four lower deflection modes of the partially treated sandwich plate that was configured for the experiments. It can be observed that the fourth mode corresponds to torsional deformation of the plate, which causes notable shear deformation of the MR fluid located at free corners of the structure. The shear deformation of the MR fluid cavity is relatively small in all the other modes. The application of the magnetic flux thus caused relatively more significant shift in the fourth natural frequency compared to the other modes. Depending on relative changes in both the stiffness and damping properties with the applied magnetic field, the half power bandwidth may increase or decrease.

First mode   Second mode

136

| Third mode | Fourth mode |
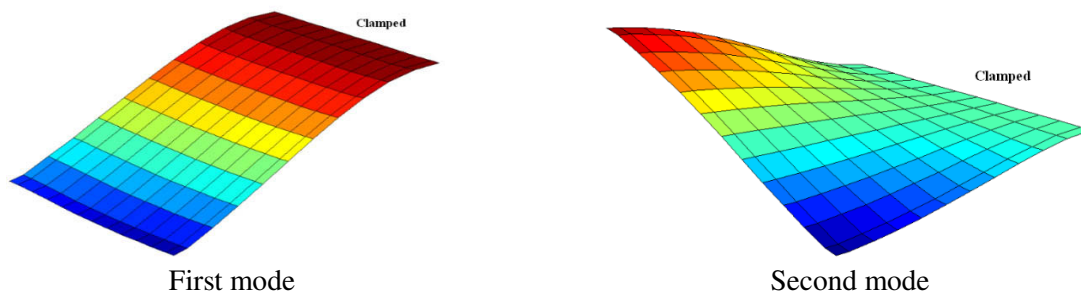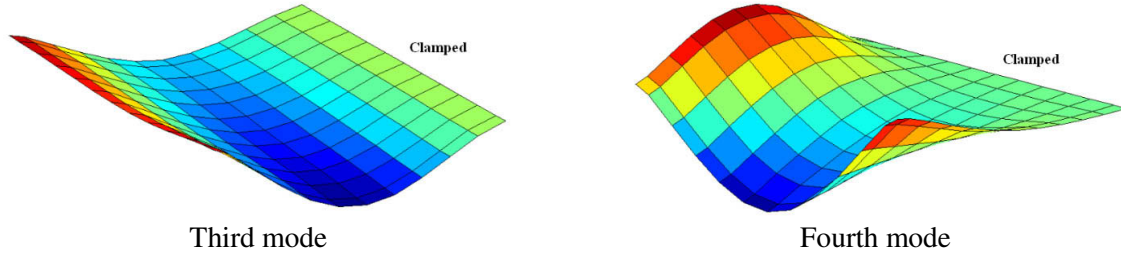
Figure 6.5 Deflection modes of the partially treated cantilevered sandwich plate corresponding to the lower four natural frequencies.

6.4.2. Effect of number and locations of the MR fluid treatments

The dynamic response characteristics of a partially treated sandwich plate are strongly dependent upon the number and locations of the localized MR fluid treatments, apart from the boundary conditions. The effects of the number and locations of partial treatments are thus investigated considering CFFF and SSSS boundary conditions. The simulations are performed using the sandwich plate model with aluminum host and constraining layers, each measuring $300 \times 200 \times 1$ mm. The cantilever configuration is realized by clamping the sandwich plate along one of the 300 mm long edges. The 4 mm thick core layer of the structure was partitioned using silicon rubber to obtain 25 equal cavities (57.6 *mm* $\times$ 37.6 *mm*) for MR fluid applications, which were arranged in 5 rows and 5 columns ($m=n=5$). The thickness of the walls surrounding each cavity was 2 *mm*. The mass density of the sealant was taken as 1460 kg/m^3 with frequency dependent complex shear modulus $G_r^* = 1340000 + i\left(152511 + 68.31\,\omega + 0.475\,\omega^2\right)$, as reported in chapter 3. Owing to the very low flexural rigidity of the silicon rubber compared to that of aluminum, negligible slippage between silicon rubber and the aluminum face layers is assumed ($k^* \rightarrow \infty$). Simulations were initially conducted considering the cavities within the first row (along the length of the plate and close to the clamped edge) filled with MR fluid. The natural frequencies and corresponding loss factors of the structure were evaluated under two different levels of magnetic flux density (B=0 and 90 mT). The simulations were subsequently repeated by shifting the MR fluid treatments to second, third, fourth and fifth rows in a sequential manner.

Tables 6.4 and 6.5 illustrate the effects of variations in the location of the MR fluid treatment and the flux density on the natural frequencies (ω) and the loss factors (η) corresponding to the first 3 modes for the CFFF and SSSS sandwich plates, respectively. The results show substantially lower natural frequencies of the CFFF sandwich plate compared to those of the SSSS plate, as it

137

would be expected. The loss factors of the cantilevered plate, however, are higher than those of the simply supported structure. This is due to the relatively higher flexibility of the CFFF plate compared to the SSSS structure leading to relatively higher shear strain in the core layer of the of CFFF plate. The location of the MR fluid row in the plates alters the stiffness and the mass distribution and thereby strongly affects the natural frequencies, as seen in Tables 6.4 and 6.5. For the CFFF plate, treating the cavities away from the constrained boundary decreases the natural frequencies in the absence of the magnetic flux, which is attributed to higher kinetic energy of the structure. The natural frequencies and corresponding loss factors of the plates with both the boundary conditions increase with increasing the magnetic flux density, irrespective of the MR fluid location, which is attributable to increase in the storage moduli of the MR fluid in the presence of the magnetic flux. The changes in the loss factors, however, are influenced by variations in both the loss and storage moduli of the MR fluid.

Table 6.4 Variations in the first three natural frequencies (Hz) and corresponding loss factors of the CFFF sandwich plate with varying MR treatment locations and magnetic flux density (0 and 90 mT)

Row	Mode	$B=0$ mT		$B=90$ mT		Frequency increment (%)	Loss factor increment (%)
		ω	η	ω	η		
	First	26.65	0.0514	27.34	0.0612	2.59	19.06
1	Second	43.65	0.0418	44.65	0.0500	2.29	19.62
	Third	90.58	0.0311	92.19	0.0367	1.78	18.00
	First	26.20	0.0534	29.24	0.0888	11.60	66.29
2	Second	42.56	0.0433	46.76	0.0728	9.87	68.13
	Third	86.99	0.0326	94.55	0.0557	8.69	70.86
	First	24.25	0.0532	28.49	0.0969	17.48	82.14
3	Second	39.02	0.0438	45.04	0.0851	15.43	94.29
	Third	79.19	0.0345	94.01	0.0808	18.71	134.20
	First	21.29	0.0536	24.50	0.0839	15.07	56.53
4	Second	34.77	0.0456	41.33	0.0896	18.87	96.49
	Third	72.32	0.0374	93.46	0.1024	29.21	173.80
	First	18.33	0.0568	20.68	0.0780	12.82	37.32
5	Second	30.84	0.0495	38.20	0.0957	23.86	93.33
	Third	65.75	0.0415	92.27	0.1129	40.33	172.05

The largest variations in the fundamental frequencies of the SSSS and CFFF sandwich plates are achieved when the MR fluid is applied in the first and third rows, respectively. The results presented for the CFFF plate are in agreement with those reported for a partially activated ER fluid

cantilever plate by Cho et al. (2005). Treating the third and fifth rows yields the maximum shift in the second natural frequencies of the SSSS and CFFF sandwich plates, respectively. The same trend was observed for the third natural frequencies of both the plates. Owing to the symmetric configuration of the SSSS sandwich plate, treating the first or fifth and second or fourth rows showed identical trends. The results are thus not presented for the MR fluid treatments in the fourth and fifth rows of the SSSS sandwich plate. In general, the MR fluid location that yields greatest shift in a particular natural frequency also shows the highest loss factor under $B= 90$ mT. This is attributed to the fact that a larger shear deformation of the core layer in the presence of the magnetic flux causes both the storage and dissipated energy to increase and thus the frequency and the loss factor. An exception, however, is evident for the first mode of the SSSS sandwich plate, which is likely due to definition of the loss factor, the ratio of the dissipated energy to the stored energy. In this case, the change in the stored energy is relatively greater compared to dissipative energy.

Table 6.5 Variations in the first three natural frequencies (Hz) and corresponding loss factors of the SSSS sandwich plate with varying MR treatment locations and magnetic flux density (0 and 90 mT)

Row	Mode	$B = 0$ mT		$B = 90$ mT		Frequency increment (%)	Loss factor increment (%)
		ω	η	ω	η		
1	First	82.63	0.0244	89.94	0.0443	8.85	81.56
	Second	150.82	0.0148	162.7	0.0337	7.88	127.70
	Third	217.75	0.0105	227.94	0.0233	4.68	121.90
2	First	69.27	0.0216	75.00	0.0480	8.27	122.22
	Second	125.79	0.0147	142.83	0.0551	13.55	274.83
	Third	209.93	0.0101	217.85	00207	3.77	104.95
3	First	64.37	0.0208	69.39	0.0485	7.80	133.17
	Second	118.24	0.0150	136.22	0.0611	15.21	307.33
	Third	206.58	0.0113	241.49	0.0562	16.90	397.34

The shear strain associated with each node in the finite element model was further evaluated using Eq. (6.14). For this purpose, the sandwich plate was discretized to a mesh of 21×21 elements and a total of 400 nodes with nodes being numbered from A to B, as shown in Figure 6.6. The figure also illustrates the variations in the nodal shear strain amplitudes in the core layer of the untreated SSSS plate for the first three modes of vibration. Furthermore the nodes with the highest shear strain in the core layer are indicated by bold dots. First 80 nodes with the highest shear strain amplitude in the core layer (number of nodes contained in the five cavities) are identified on the discretized plate FE model for the lower three modes, as shown in the Figure 6.6. The logic behind

choosing number of nodes contained in the five cavities is to compare the results with those of Table 6.5.
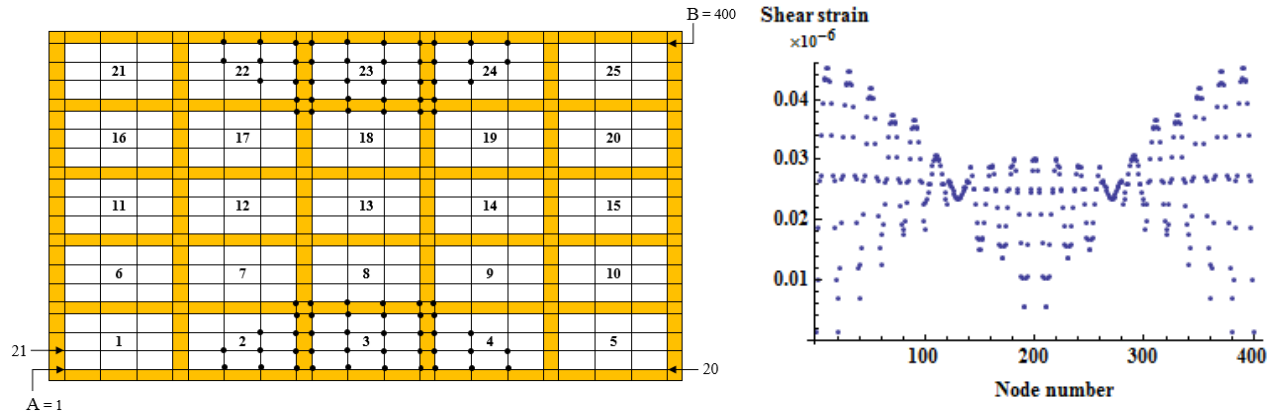
First mode
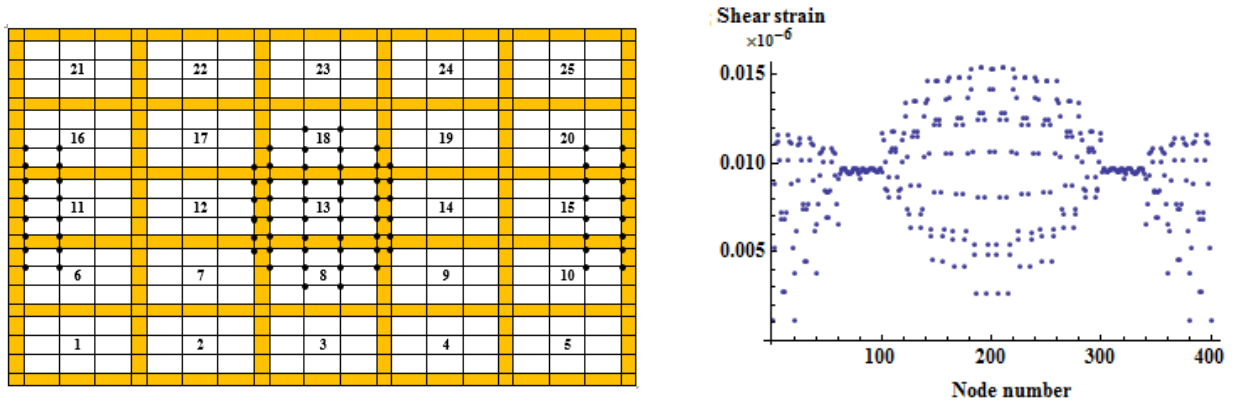
Second mode
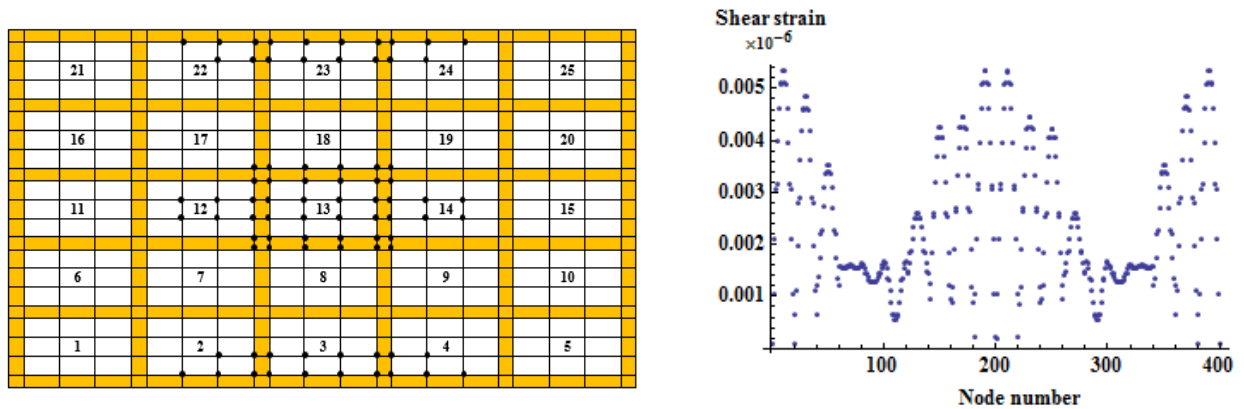
Third mode

Figure 6.6 Shear strain distribution in the core layer of the untreated SSSS plate

The results suggest greatest shear strain in the first and fifth rows in the first mode (nodes 1 to 80 and 321 to 400). The third row of the structure experiences the highest shear strain in the core layer in the second and third modes (nodes 161 to 240). The nodes in the first and the fifth rows also incur higher strains in the third mode. These results demonstrate the effect of MR fluid locations on variations in the stiffness and damping of the SSSS sandwich plate in response to different levels of magnetic flux, as presented in Table 6.5. From the results, it is evident that treating the MR fluid in the cavities with noticeable shear deformation would yield greater variations in the stiffness and damping of the structure under an applied magnetic field.

Figure 6.7 illustrates the variations in the natural frequencies and loss factors of the CFFF and SSSS plates when the MR fluid is applied to cavities in a single column. The results are presented in terms of percent changes when the magnetic flux is increased from 0 to 90 mT. The observed variations in the natural frequencies under an applied magnetic flux may also be related to the shear strain distribution in the core layer, as presented in Figure 6.6. For instance, the significant shift in the third resonant frequency of the SSSS plate is achieved when the third column of the structure (cavities # 3, 8, 13, 18 and 23) is treated with the MR fluid. This is attributable to distribution of the shear strain in the core layer of the structure, which is noticeable around the third column.

(a)

141

(b)
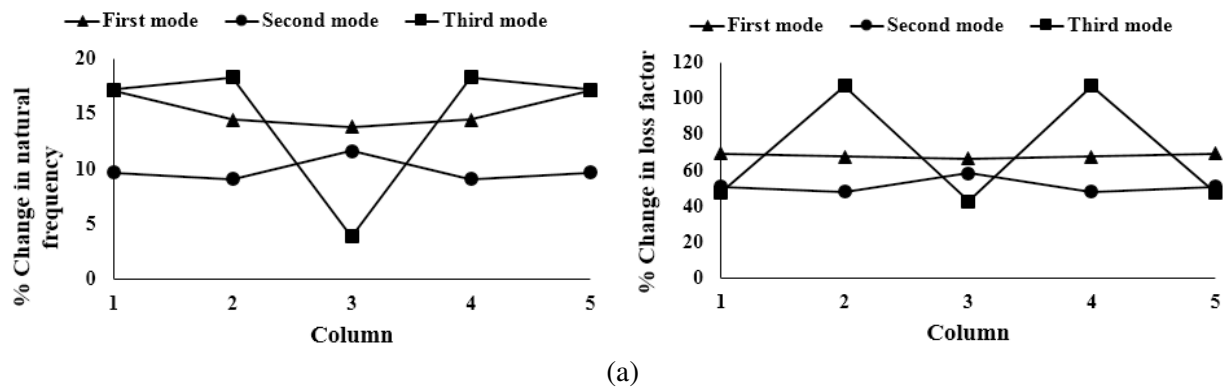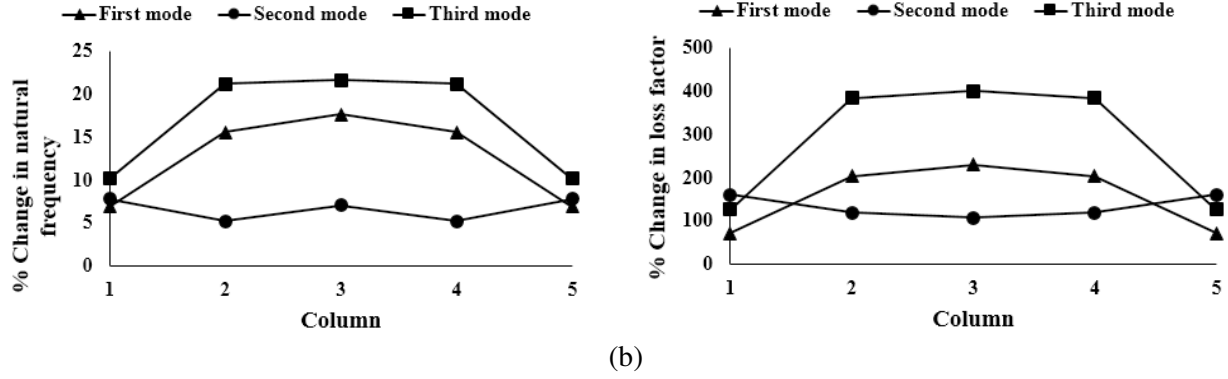
Figure 6.7 The effect of treating different columns of (a) CFFF and (b) SSSS sandwich plates on natural frequencies and loss factors of the structures, when *B* increases from 0 to 90 mT.

6.4.3. Identification of optimal MR fluid treatment locations

6.4.3.1. Optimal locations for maximizing variations in the natural frequencies (Case 1)

The optimization problem in Eq. (6.23) was initially solved considering a total of 25 cavities for MR fluid applications (*m*=5, *n*=5) and *N*=5 so as to compare the results with trends observed from Tables 6.4 and 6.5. Table 6.6 illustrates the optimal locations in terms of treated cavities numbers for the three lower modes frequencies of the CFFF and SSSS plates together with the frequencies and the corresponding loss factors for *B*=0 and *B*= 90 mT. The table also shows percent changes in the frequencies ($\Delta \omega$) and the loss factors ($\Delta \eta$), when *B* is varied from 0 to 90 mT.

Table 6.6 Optimal locations of five treated cavities in the core layer of the CFFF and SSSS sandwich plates resulting in maximum variations in the three lower mode frequencies under an applied magnetic flux of 90mT.

B.C.	Mode	Optimal cavities	B=0 mT		B=90 mT		$\Delta \omega$ (%)	$\Delta \eta$ (%)
			ω	η	ω	η		
CFFF	First	11,12,16,17,21	20.61	0.0543	24.62	0.0916	19.46	68.70
	Second	11,18,22,23,24	37.80	0.0481	47.44	0.0994	25.50	106.65
	Third	16,21,22,24,25	69.58	0.0443	101.86	0.1157	46.40	161.17
SSSS	First	2,3,4,23,24	80.96	0.0251	102.99	0.0907	27.21	261.35
	Second	8,11,13,15,18	138.09	0.0170	165.77	0.0687	20.04	304.12
	Third	3,8,13,18,23	181.19	0.0133	220.32	0.0663	21.60	398.50

The results show that the optimal locations of the MR treatments strongly depend on the mode of vibration, irrespective of the boundary condition. The results suggest that the optimal treated cavities are generally located in regions where the core layer experienced notable shear

deformation (Figure 6.6). Some differences, however, are evident, which could be attributed to changes in the mass distribution of the treated plates and thus the shear deformations. For instance, the solution for the third mode frequency of the SSSS sandwich plate converged to treatments along the mid-column (cavities 3, 8, 13, 18, 23), while the results in Figure 6.6 revealed greater shear strains around cavities 3, 12, 13, 14 and 23.

The solutions were also obtained by varying the number of treated cavities (N) from 0 to 25. The results suggested complex effects of relaxing the number of cavities due to varying mass distribution, and increasing loss and storage moduli. Relaxing the number of cavities generally resulted in greater variation in the three lower mode frequencies of both the plates, as seen in Figure 6.8. The figure illustrates the percent increase in the frequencies when the applied magnetic flux density is increased from 0 to 90 mT. The effect of relaxing the number of cavities is quite significant on the higher mode frequency of the CFFF plate, while the effect on the frequencies of the SSSS plate is relatively modest, which has also been reported by Rajamohan et al (2010b) for a cantilever beam. The results also show diminishing rate of increment in the frequencies with increasing number of treated cavities. These suggest that relaxing N beyond 15 may not be beneficial for realizing greater variations in the three lower mode frequencies. It is further seen that the optimally treated CFFF plate with $N = 20$ can yield a larger shift in the third mode frequency compared to the fully treated plate (N=25). This is also evident in the fundamental mode frequency of the SSSS plate.
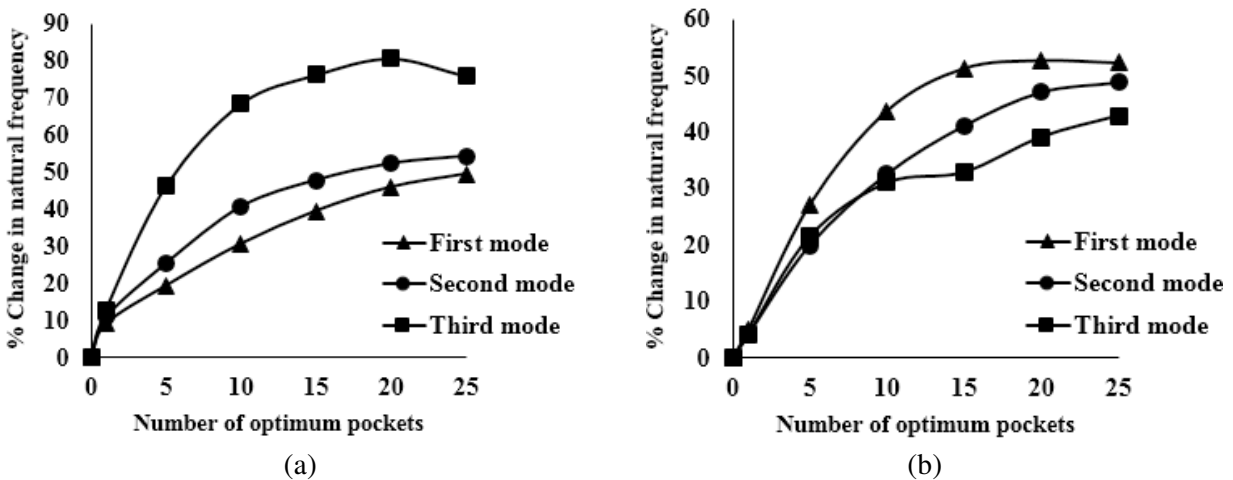

Figure 6.8 The effect of relaxing limit of constraint on variations in the lower three resonant frequencies of (a) CFFF and (b) SSSS sandwich plates treated under case 1.

6.4.3.2. Optimal locations based on maximizing the loss factor and energy dissipation (Cases 2 & 3)

The optimization problems in Eqs. (6.24) and (6.25) were solved to identify optimal locations of the treated cavities so as to realize maximum loss factors and energy dissipation respectively, for the three lower modes of the CFFF and SSSS plates. The solutions were obtained for varying limits on the maximum number of cavities ($N= 1,2,…10$), while the results are presented only for the CFFF plate. Tables 6.7 and 6.8 summarize the optimal locations of the treated cavities and the resulting loss factors and energy dissipation in terms of *Im* (λ), respectively, corresponding to the lower three modes of the partially treated CFFF sandwich plate.

Table 6.7 Optimal locations of the MR fluid cavities leading to highest loss factors corresponding to the lower three modes of the CFFF sandwich plate ($B = 90$ mT and $1 \leq N \leq 10$)

	First mode		Second mode		Third mode	
N	Optimal cavities	η	Optimal cavities	η	Optimal cavities	η
1	21	0.061	23	0.061	22	0.057
2	11, 21	0.074	22, 24	0.074	21, 25	0.075
3	11, 16, 21	0.080	22, 23, 24	0.088	21, 24, 25	0.095
4	6,11,16,21	0.089	21,22,23,24	0.092	21,22,24,25	0.111
5	6,11,12,16,21	0.096	15,21,22,23,24	0.100	19,21,22,24,25	0.117
6	6,11,12,13,16 21	0.102	10,15,21,22,23, 24	0.108	17,19,21,22,24, 25	0.123
7	6,11,12,13,16, 19,21	0.104	6,10,15,21,22, 23,24	0.114	17,19,20,21,22, 24,25	0.128
8	6,7,11,13,16, 17,21,22	0.109	6,10,11,15,21, 22,23,24	0.118	16,17,19,20,21 22,24,25	0.132
9	6,7,11,12,13, 16,17,21,22	0.113	6,10,11,15,18, 21,22,23,24	0.121	12,16,17,19,20, 21,22,24,25	0.135
10	6,7,8,11,12, 13,16,17,21,22	0.118	6,9,10,11,15, 18,21,22,23,24	0.124	12,14,16,17,19, 20,21,22,24,25	0.136

In both cases, the results also show that the optimal locations of the treated segments are strongly dependent on the mode of vibration. The two optimization problem solutions tend to converge to quite different solutions for the fundamental mode but somewhat comparable solutions for the higher modes. The highest loss factor corresponding to the fundamental mode is obtained by applying the treatments around the first column (near free edge), while the treatment around the middle row yields the highest energy dissipation. Moreover, the solutions in case 2 are also similar

to those obtained in case 1 focusing on greatest variations in the frequencies (Table 6.6). The solutions also follow the trends observed in Figure 6.7, suggesting that treating the first and second columns yields largest variations in the fundamental frequency of the structure under an applied magnetic field.

Table 6.8 Optimal locations of MR fluid cavities leading to maximum energy dissipation corresponding to the lower three modes of the CFFF sandwich plate ($B = 90$ mT and $1 \le N \le 10$)

N	First mode		Second mode		Third mode	
	Optimal cavities	$Im(\lambda)$	Optimal cavities	$Im(\lambda)$	Optimal cavities	$Im(\lambda)$
1	13	1855	23	5190	22	20536
2	12, 14	2238	10, 23	6399	22, 24	28600
3	11, 13, 15	2554	6, 10, 23	7798	21, 22, 25	36550
4	8,11,13,15	2866	6,10,18,23	8748	21,22,24,25	44890
5	7,9,12,13,15	3265	6,10,18,23,24	9760	19,21,22,24,25	48870
6	6,8,10,11,13, 15	3707	6,10,18,19,22, 23	10643	17,19 ,21,22,24 25	52860
7	6,8,9,10,11, 13,15	3990	6,10,13,18,22, 23,24	11200	17,19,20,21,22, 24,25	55690
8	6,7,8,9,10, 11,13,15	4281	6,10,17,18,19, 22,23,24	11390	16,17,19,20,21 22,24,25	58200
9	6,7,8,9,10, 11,12,14,15	4528	5,6,7,10,15, 18,22,23,24	12090	12,16,17,19,20, 21,22,24,25	59680
10	6,7,8,9,10, 11,12,13,14,15	4750	6,9,10,11,13 15,18,22,23,24	12230	12,14,16,17,19, 20,21,22,24,25	61120

The results in Tables 6.7 and 6.8 show similar locations for the loss factor and energy dissipation corresponding to the third mode, which is likely due to the loss factor definition. The optimization problem aimed at maximizing the loss factor (case 2) would yield optimal locations for realizing higher energy dissipation together with lower natural frequency of the structure. The solutions in this case are thus similar to those obtained in case 3. The solutions corresponding to the first and second vibration modes, however, do not converge to maximum dissipated energy and minimal natural frequencies simultaneously. The two optimization problems thus yield somewhat different solutions. The optimal solutions for the maximum loss factors revealed lower first and second mode frequencies compared to those for the maximum energy dissipation, while the third mode frequencies in both cases were quite comparable.

6.4.4. Resonant responses of the optimal structures

The displacement responses of the three optimal configurations of the sandwich plate (N=5) are evaluated under a harmonic point load applied at $x = 0.062$ m and y =0.042 m. The results are presented for the partially treated CFFF sandwich plate under $B = 0$ and 90 mT. The partial treatment is applied in accordance with the solutions obtained from the optimization problems formulated in Eqs. (6.23) to (6.25) with objectives to maximize variations in the natural frequencies, loss factors and the energy dissipation corresponding to the three lower modes (Tables 6.6 to 6.8). The displacement responses of the three optimal configurations, obtained near the free end ($x = 0.238$ m; y =0.158 m), are presented in the 20 to 34 and 33 to 55 Hz ranges in Figure 6.9 to assess the effects of optimal MR fluid treatments on the first and second modes resonant responses. The results suggest significant reductions in the resonant response amplitudes in the presence of 90 mT magnetic field in all the optimal configurations. The application of the magnetic field yields 39.5%, 42.7% and 57.7 % reductions in the fundamental frequency amplitudes of the optimally-treated CFFF plates as per the cases 1, 2 and 3, respectively. Even larger reductions are evident in the second mode resonant responses. The lower resonant responses can be directly attributed to increases in both the stiffness and damping of the structure under the applied magnetic flux, which are evident from the higher resonant frequencies and reduced sharpness of the peaks, when compared to those under B=0. The half power bandwidths of the peaks around the fundamental mode resonance of the three optimal configurations are in the order of 5% under B=0 mT. These increase to 9-10% under B=90 mT. The optimal treatments corresponding to cases 1, 2 and 3 yield 19.5, 18.1 and 17.1 % increases in the respective fundamental frequencies, respectively, when B is increased from 0 to 90 mT. The energy dissipation expressed in terms of the imaginary part of the eigenvalues corresponding to three cases were obtained as 2189, 2465 and 3265, respectively. The results suggest nearly similar resonant amplitudes and loss factors of the three partially-treated CFFF plates for B=90 mT, while optimal configuration realized in case 3 yields significantly higher energy dissipation compared to those in cases 1 and 2. Furthermore, the MR layout based on case 3 yields highest natural frequencies of the sandwich plate, irrespective of the applied magnetic field.
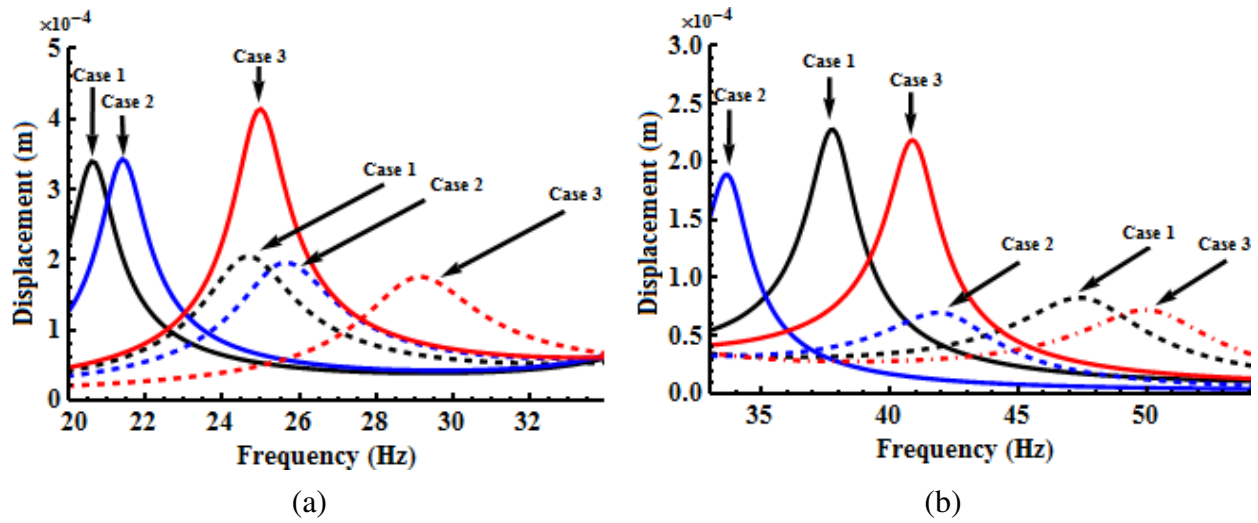
Figure 6.9 The effect of MR configurations on transverse vibration response of the CFFF sandwich plate under $B = 0$ mT (solid lines) and $B = 90$ mT (dashed line) in the vicinity of the (a) first and (b) second mode resonant frequencies.

6.5 Conclusions

This study investigated dynamic responses of the partially treated cantilever and simply-supported MR sandwich plates through experiment and finite element analysis. The stiffness variations in response to the applied magnetic field were identified in terms of natural frequencies while the loss factor and energy dissipation were considered to represent the damping properties of the structures. The results showed complex effects of mass distribution due to MR fluid treatments, and increase in loss and storage moduli of the fluid with increasing magnetic field. Increasing the MR fluid treatment area resulted in greater variations in the three lower mode frequencies and the loss factors under a given magnetic field. Increasing the treatment beyond 50-60% of the plate surface area, however, was not beneficial for realizing greater variations in the three lower mode frequencies. The solutions of the optimization problems aimed at maximizing the changes in the three lower modes frequencies and the corresponding loss factors resulted in similar optimal locations of the MR fluid treatments, irrespective of the boundary condition and mode of vibration. The optimal solutions converged to locations with relatively higher shear strains under the applied magnetic field. The optimization problem aimed at maximizing the energy dissipation, however, resulted in quite different optimal locations of the partial MR-fluid treatments, particularly for the fundamental mode. The solutions obtained for maximizing the loss factors of the partially treated structure, however, revealed relatively lower natural frequencies compared to other optimal configurations. The half-power bandwidths and amplitude responses

147

around the two lower modes frequencies were quite similar for all the optimal configurations of the partially-treated cantilevered plates under a 90 mT magnetic field.

CHAPTER 7

CONTRIBUTION, CONCLUSIONS AND FUTUR WORK

7.1. Major Contributions

This research dissertation presents a comprehensive investigation on the pre-yield characterization of the MR fluids, analysis and design optimization of MR fluid based adaptive plates. The major contributions of the dissertation research are summarized below:

1. The state-of-the-art development in multi-layered controllable MR/ER fluid structures is presented through review of reported studies on pre-yield characterizations of MR/ER fluids, dynamic responses of partially and fully treated sandwich beams, plates, shells and panels containing MR/ER fluids as the core layer and control strategies applied to the structures. The review included different fabrication techniques, experimental methods, mathematical modeling, methods of solution and critical analysis of assumptions employed in different studies. The effects of different parameters such as applied field, geometry, elastic layer material, boundary conditions, excitation frequency, temperature and external disturbances on dynamic responses of the structures were thoroughly investigated. Furthermore, the complexities associated with experimental studies and sources of disagreements between theoretical and experimental studies were addressed.

2. An experimental method for pre-yield characterization of MR fluids was developed. The complex shear moduli of MR fluids (122EG and 132DG) were characterized as a function of excitation frequency and applied magnetic flux density. MR based aluminum sandwich beam was employed for characterizing and developing of phenomenological models representing complex shear moduli of the MR fluids in the pre-yield region, while copper sandwich beam containing MR fluid was used to demonstrate validity of the proposed models. Both the loss and storage moduli of the fluids were characterized through composition of an exponential function in frequency and a quadratic function in magnetic flux density. Accurate pre-yield complex shear models of the two MR fluids were identified on the basis of the measurement-based moduli as opposed to the sandwich structure response, namely the natural frequencies and/or the frequency response magnitude peaks. The finite element model of the sandwich structure in conjunction with

the measured frequency responses provided the target storage and loss moduli for model parameters identifications.

3. Analytical models of rectangular and circular sandwich plates are developed for free and forced vibration analyses under varying magnetic field. The effects of variations in the magnetic flux and plate parameters on the vibration properties of a sandwich plate with two different MR fluids were investigated considering different boundary conditions. Numerical models based on finite element and Ritz methods were developed and validated using the experimental data. The dynamic characteristics of the structures were explored in terms of natural frequencies and loss factors. The dynamic responses of the fully as well as partially treated cantilever and simply-supported MR sandwich plates were investigated through experiments and finite element analysis. The stiffness variations of the structure in response to the applied magnetic field were identified in terms of natural frequencies, while the loss factor and energy dissipation were considered to represent the damping properties of the structures. Finally, three optimization problems were formulated to identify optimal locations for the MR fluid treatments so as to maximize variations in the natural frequencies and damping ratios in response to the magnetic field.

7.2. Major Conclusions

The major conclusions extracted from the present dissertation research are summarized below:

- Although rheometers have been widely used to characterize MR/ER fluids in terms of applied field and excitation frequency, treating MR/ER sandwich beam structures as SDOF systems ensured accurate pre-yield characterization of the fluids associated with relatively small strain amplitude of the fluids in sandwich structures compared to the rheometers.

- Application of MR/ER fluids in sandwich structures subject to magnetic/electric field could significantly alter the stiffness and damping properties of the structures only under noticeable shear strains.

- Solid models are more appropriate to identify pre-yield characteristics of the MR/ER fluids than the fluid models.

- Although, fully treated sandwich structures generally yield superior vibration control performance compared to the partially treated ones, optimal MR/ER fluid treatment could

150

yield damping properties comparable to those of the fully treated structures with relatively lower mass.

- The consideration of viscoelastic properties of the sealant rubber found to be important for accurate characterization of the fluid and for vibration response analysis of the MR filled structures.

- The models representing loss and storage moduli of MR fluids revealed that the pre-yield loss and storage moduli of the MR fluids increase with frequency but approach saturation at frequencies above 200 to 300 Hz. Both the moduli, however, increased with the magnetic flux density in a quadratic manner. Moreover, the stiffening effect of the magnetic field was far more pronounced in the fundamental mode frequency.

- Increasing the magnetic flux density increased natural frequencies of the MR sandwich structures, irrespective of the boundary conditions. The rate of increase, however, was more pronounced when the core layer experienced more significant shear deformation. A similar trend, however, was not observed in the loss factors under increasing the magnetic flux density.

- The MRF 132DG fluid with relatively larger magnetizable particles resulted in higher percent increase in resonant frequencies of the sandwich structures with increasing magnetic field compared to the MRF 122EG fluid.

- Since the face layers of sandwich structures may vibrate independently at higher modes, the assumption of uniform transverse displacement through the thickness of the structure may lead to significant errors in the responses at higher modes.

- The rectangular sandwich plate with only one of its edges clamped (CFFF) showed greatest increase in natural frequencies and loss factors with increasing magnetic field and the highest modal loss factor compared to the other boundary conditions.

- Increasing the plate aspect ratio resulted in relatively higher natural frequencies but lower loss factors of the sandwich structure.

- Increasing the core layer thickness in the sandwich plate resulted in lower natural frequencies but higher loss factors.

- Increasing the radius ratio in the annular sandwich plates decreased mass of the plate and altered stiffness of the structure, and thereby the natural frequencies and loss factors.

- In the partially treated sandwich plate, increasing the MR fluid treatment area resulted in greater variations in the three lower mode frequencies and corresponding loss factors under a given magnetic field. Increasing the treatment beyond 50-60% of the plate surface area, however, was not beneficial for realizing greater variations in three lower mode frequencies.

- In the partially treated sandwich plate, the solutions of the optimization problems aimed at maximizing changes in the three lower modes frequencies and the corresponding loss factors resulted in similar optimal locations of the MR fluid treatments, irrespective of the boundary condition and mode of vibration. The optimal solutions converged to locations with relatively higher shear strains under the applied magnetic field. The optimization problem aimed at maximizing the energy dissipation, however, resulted in relatively different optimal locations of the partial MR-fluid treatments, particularly for the fundamental mode.

- In the partially treated sandwich plate, the solutions obtained for maximizing the loss factors of the structure revealed relatively lower natural frequencies compared to other optimal configurations. The half-power bandwidths and amplitude responses around the two lower modes frequencies were quite similar for all the optimal configurations of the partially-treated cantilevered plates under a 90 mT magnetic field.

7.3. Recommendation for the future works

In this dissertation, vibration characteristics of fully and partially treated MR sandwich plate structures were systematically investigated. The models formulated for characterizing MR fluids and analysis of fully and partially treated MR fluid structures provide important design tools for adaptive sandwich structures. The models and the methods, however, need to be further refined so as to extend applications of MR fluid to general structures. In particular, further efforts in controllable design and design of practically implementable electro-magnets are highly desirable. Some of the recommended studies are suggested below:

- Designing semi-active controllers through various control strategies such as ON-OFF control law, linear quadratic regulator, sliding mode or real time control to improve vibration suppression of MR sandwich plate structures. The performance of the

controllers can be demonstrated by suppressing external disturbances such as sinusoidal signal, random signal, impulse or white noise.

- Vibration analysis methods need to be developed for MR sandwich plates with fluid operating in either post-yield region or combined pre- and post-yield region.

- Study on noise control and sound transmission properties of MR adaptive structures under varying magnetic flux.

- Supersonic flutter control of magnetorheological fluid-based sandwich plate structures.

- Application of MR fluid in shear mode dampers which is applicable for vibration suppression of large flexible structures such as aircraft wings.

- Study on applications of MR sandwich plates as adaptive tunable vibration absorbers.

- Designing small and implementable electro-magnets for generating strong magnetic flux over the MR based sandwich structures.

References

Ali G, Borsa K, Kaur Chahal R, Singh Kaloti H and Shingari R (2013) Design, fabrication and testing of a MR fluid based adaptive structure. Capstone Project, Concordia University.

Allahverdizadeh A, Eshraghi I, Mahjoob MJ and Nasrollahzadeh N (2014) Nonlinear vibration analysis of FGER sandwich beams. *International Journal of Mechanical Sciences* 78; 167-176.

Allahverdizadeh A, Mahjoob MJ, Eshraghi I and Asgharifard SP (2012) Effects of electrorheological fluid core and functionally graded layers on the vibration behavior of a rotating composite beam. *Meccanica* 47(8); 1945-1960.

Allahverdizadeh A, Mahjoob MJ, Eshraghi I and Nasrollahzadeh N (2013b) On the vibration behavior of functionally graded electrorheological sandwich beams. *International Journal of Mechanical Sciences* 70; 130-139.

Allahverdizadeh A, Mahjoob MJ, Nasrollahzadeh N and Eshraghi I (2013) Optimal parameters estimation and vibration control of a viscoelastic adaptive sandwich beam incorporating an electrorheological fluid layer. *Journal of Vibration and Control* 0(0); 1-14.

Allahverdizadeh A, Mahjoob MJ, Maleki M, Nasrollahzadeh N and Naei MH (2013c) Structural modeling, vibration analysis and optimal viscoelastic layer characterization of adaptive sandwich beams with electrorheological fluid core. *Mechanics Research Communications* 51; 15-22.

ASTM (2002) Standard Test Method for Measuring Vibration-Damping Properties of Materials Designation: E756 – 05.

Bai JM and Sun CT (1995) The effect of viscoelastic adhesive layers on structural damping of sandwich beams. *Journal of Structural Mechanics* 23 (1); 1-16.

Berg CD, Evans LF and Kermode PR (1996) Composite structure analysis of a hollow cantilever beam filled with electro-rheological fluid. *Journal of intelligent material systems and structures* 7(5); 494-502.

Bird RB, Armstrong R and Hassager O (1987) Dynamics of polymeric liquids vol. 1 fluid mechanics. John Wiley & Sons, New York.

Bishay PL, Tawfik M and Negm HM (2010) Experimental and finite element models of an adaptive magnetorheological sandwich beam. *The 17th International Congress on Sound and Vibration*, Cario.

Brush DO and Almroth BO (1975) Buckling of Bars Plates and Shells (New York: McGraw-Hill).

Carlson JD, Coulter JP and Duclos TG (1990) Electrorheological Fluid Composite Structures US Patent No. 4, 923, 057.

Chen L and Hansen CH (2005) Active vibration control of magnetorheological sandwich beam. *Australian Acoustical Society*, Busselton.

Chen L and Tian J (2006) Distributed magnetorheological (MR) fluid damper for active structural vibration control. *In International Symposium on Active Control of Sound and Vibration*. Adelaide, Australia.

Chen Y, Yuan FG and Conard H (1994) Damping characteristics of laminate composites containing electrorheological (ER) fluids. Proceedings of the 2nd International Conference on Intelligent Material, edited by Rogers CA and Wallace GG. Technomic Publishing CO. Inc., Lancaster, Pennsylvania, pp 328-339.

Cho KD, Lee I and Han JH (2005) Dynamic characteristics of ER fluid-filled composite plate using multielectrode configuration. *Journal of intelligent material systems and structures* 16(5); 411-419.

Choi SB (2000) Electric field-dependent vibration characteristics of a plate featuring an electrorheological fluid. *Journal of sound and vibration* 234(4); 705-712.

Choi SB, Gandhi MV and Thompson BS (1989) An active vibration tuning methodology for smart flexible structures incorporating Electro-Rheological fluids: a proof-of-concept investigation. *In American Control Conference*, 694-703.

Choi SB and Park YK (1994) Active vibration control of a cantilevered beam containing an electro-rheological fluid. *Journal of Sound and Vibration* 172; 428–32.

Choi SB, Park YK and Cheong CC (1996) Active vibration control of intelligent composite laminate structures incorporating an electro-rheological fluid. *Journal of Intelligent Material Systems and Structures* 7(4); 411-419.

Choi SB, Park YK and Kim JD (1993) Vibration characteristics of hollow cantilevered beams containing an electro-rheological fluid. *International journal of mechanical sciences* 35(9); 757-768.

Choi SB, Park YK and Jung SB (1999) Modal characteristics of a flexible smart plate filled with electrorheological fluids. *Journal of aircraft* 36(2); 458-464.

Choi SB, Park YK and Suh MS (1994) Elastodynamic characteristics of hollow cantilever beam containing an electro-rhoelogical fluid: Experimental results. *AIAA Journal* 32 (2); 438-440.

Choi SB, Thompson BS and Gandhi MV (1989b) Smart structures incorporating electro-rheological fluids for vibration-control and active-damping applications: an experimental investigation. *Proceedings of the 12th Biennial ASME Conference on Mechanical Vibration and Noise*, Montreal, Canada.

Choi SB Thompson BS and Gandhi MV (1989c) An experimental investigation on the active damping characteristics of a class of ultra-advanced intelligent composite materials featuring electro-rheological fluids. *Damping 89*, Ohio, 1-14.

155

Choi SB, Seo JW, Kim JH and Kim KS (2001) An electrorheological fluid-based plate for noise reduction in a cabin: experimental results. *Journal of sound and vibration* 239(1); 178-185.

Choi WJ, Xiong YP and Shenoi RA (2008) Characterization of magnetorheological elastomer materials for the core of smart sandwich structures. *Proceedings of the 8th International Conference on Sandwich Structures*, Porto Portugal 818–826.

Choi WJ, Xiong YP and Shenoi RA (2010) Vibration characteristics of sandwich beams with steel skins and magnetorheological elastomer cores. *Advances in Structural Engineering* 13 (5): 837-847.

Choi Y, Sprecher AF and Conrad H (1990) Vibration characteristics of a composite beam containing an electrorheological fluid. *Journal of Intelligent Materials and Structures* 1; 91–104.

Choi Y, Sprecher AF and Conrad H (1992) Response of electrorheological fluid-filled laminate composites to forced vibration. *Journal of intelligent material systems and structures* 3(1); 17-29.

Claracq J, Sarrazin J and Montfort J (2004) Viscoelastic properties of magnetorhelogical fluids. *Rheologicl Acta* 43; 38-49.

Coulter JP and Duclos TG (1990) Applications of electro-rheological materials in vibration control. In Proceedings of Second International Conference on ER Fluids, JD Carlson, Lancaster.

Coulter JP, Duclos TG and Acker DN (1989) The usage of electrorheological materials in viscoelastic layer damping applications. *In Proceedings of Damping* 89.

Coulter JP, Weiss KD and Carlson JD (1993) Engineering applications of electrorheological materials. *Journal of Intelligent Material Systems and Structures* 4(2); 248-259.

Coulter JP, Don DL, Yalcintas M and Biermann PJ (1993c) Experimental investigation of electro-rheological material based adaptive plates. *ASME Aerospace Div. Publ. AD: Adaptive Structures and Material Systems* 35; 287–96.

Coulter JP, Don DL, Yalcintas M and Biermann P (1993b) An experimental investigation of ER material based adaptive plates. ASME Winter Annual, New Orleans, LA.

Deng HX, Gong XL and Zhang PQ (2006) Tuned vibration absorber based on magnetorheological elastomer. *Journal of Functional Materials* 37(5); 790.

Deng HX and Gong XL (2007) Adaptive tuned vibration absorber based on magnetorheological elastomer. *Journal of intelligent material systems and structures* 18(12); 1205-1210.

Deng HX and Gong XL (2008) Application of magnetorheological elastomer to vibration absorber. Communications in nonlinear science and numerical simulation 13(9); 1938-1947.

Deng HX, Gong XL and Wang LH (2006b) Development of an adaptive tuned vibration absorber with magnetorheological elastomer. *Smart Materials and Structures* 15(5); N111-16.

DiTaranto RA (1965) Theory of vibratory bending for elastic and viscoelastic layered finite-length beams. *Journal of Applied Mechanics* 32(4); 881-886.

Don DL (1993) An investigation of electrorheologial material adaptive structures. Master's thesis, Lehigh University, Bethlehem, Pennsylvania.

Don DL and Coulter JP (1995) An analytical and experimental investigation of electrorheological material based adaptive beam structures. *Journal of intelligent material systems and structures* 6(6); 846-853.

Dong XM, Yu M, Liao CR and Chen WM (2009) A new variable stiffness absorber based on magneto-rheological elastomer. Transactions of Nonferrous Metals Society of China 19; 611-615.

Dwivedy SK and Srinivas M (2008) Parametric instability regions of a soft cored sandwich beam with magnetorheological elastomer and non-conductive skins. Proceedings of the 52nd Congress of the Indian Society of Theoretical and Applied Mechanics, 117–123.

Dwivedy SK and Srinivas M (2011) Dynamic instability of MRE embedded soft cored sandwich beam with non-conductive skins. *Shock and Vibration* 18; 759–788.

Dwivedy SK, Mahendra N and Sahu KC (2009) Parametric instability regions of a soft and magnetorheological elastomer cored sandwich beam. *Journal of Sound and Vibration* 325; 686–704.

Ehrgott R and Masri S (1992) Experimental studies of electrorheological materials for application in adaptive structures. Proceedings of the Third International Conference on Adaptive Structures, Lancaster. PA: Technomic Publishing Co; 161-175.

Farjoud A, Cavey R, Ahmadian M and Craft M (2009) Magneto-rheological fluid behavior in squeeze mode. *Smart Materials and structures* 18; 95001-18.

Ferry JD (1980) Viscoelastic Properties of Polymers 3rd edn (New York: Wiley)

Fukuda T, Takawa T and Nakashima K (2000) Optimum vibration control of CFRP sandwich beam using electro-rheological fluids and piezoceramic actuators. Smart materials and structures 9(1); 121-125.

Gamota DR and Filisko FE (1991) Dynamic mechanical studies of electrorheological materials: moderate frequencies. *Journal of Rheology* 35(3); 399–425.

Gandhi F and Bullough WA (2005) On the phenomenological modeling of electrorheological and magnetorheological fluid pre-yield behavior. *Journal of Intelligent Material Systems and Structures* 16; 237.

Gandhi MV and Thompson BS (1990) Dynamically-tunable smart composites featuring electro-rheological fluids. International Society for Optics and Photonics 294-304.

Gandhi MV, Thompson BS and Choi SB (1988) Ultra-advanced composite materials incorporating electro-rheological fluids *Proc. 4th Japan–US Conf. on Composite Materials* (Lancaster, PA: Technomic) 875–84.

Gandhi MV, Thompson BS and Choi SB (1989) A new generation of innovative ultra-advanced intelligent composite materials featuring electro-rheological fluids: an experimental investigation. *Journal of composite materials* 23(12); 1232-1255.

Gavin HP (2001) Multi-duct ER dampers. *Journal of Intelligent Material Systems and Structures* 12 (5); 353-366.

Genc S and Phule PP (2002) Rheological properties of magnetorheological fluids. *Smart Materials and Structures* 11; 140-146.

Ginder JM, Davis LC and Elie LD (1995) Rheology of magnetorheological fluids: models and measurements. *5th Int. Conf. on ER Fluids and MR Suspensions* (Singapore: World Scientific) 504–14.

Ginder JM, Schlotter WF and Nichols ME (2001) Magnetorheological elastomers in tunable vibration absorbers. In SPIE's 8th Annual International Symposium on Smart Structures and Materials. International Society for Optics and Photonics; 103-110.

Han L, Voloshin AS, Yalcintas M and Coulter JP (1994) Electrorheological adaptive structures with embedded sensing and control. North American Conference on Smart Structures and Materials. International Society for Optics and Photonics; 2-12.

Haiqing G and King LM (1997) Vibration characteristics of sandwich beams partially and fully treated with electro-rheological fluid. *Journal of intelligent material systems and structures* 8(5); 401-413.

Haiqing G, King LM and Cher TB (1993) Influence of a locally applied electro-rheological fluid layer on vibration of a simple cantilever beam. *Journal of intelligent material systems and structures* 4(3); 379-384.

Harland NR, Mace BR and Jones RW (2001) Adaptive-passive control of vibration transmission in beams using electro/magnetorheological fluid filled inserts. *Control Systems Technology* 9(2); 209-220.

Hasheminejad SM and Maleki M (2009) Free vibration and forced harmonic response of an electrorheological fluid-filled sandwich plate. Smart Materials and Structures 18(5); 1-16.

Hasheminejad SM and Motaaleghi MA (2014) Supersonic flutter control of an electrorheological fluid-based smart circular cylindrical shell. *International Journal of Structural Stability and Dynamics* 14(02); 1350064-88.

Hasheminejad SM and Shabanimotlagh M (2010) Magnetic-field-dependent sound transmission properties of magnetorheological elastomer-based adaptive panels. *Smart Materials and Structures* 19(3); 1-13.

Hasheminejad SM, Nezami M and Panah MA (2013) Flutter suppression of an elastically supported plate with electro-rheological fluid core under yawed supersonic flows. *International Journal of Structural Stability and Dynamics*, 13(01); 1250073-97.

Hirunyapruk C, Brennan MJ, Mace BR and Li WH (2010) A tunable magneto-rheological fluid-filled beam-like vibration absorber. *Smart Materials and Structures* 19: 055020-30.

Hu B, Wang D, Xia P and Shi Q (2006) Investigation on the vibration characteristics of a sandwich beam with smart composites-MRF. *World Journal of Modelling and Simulation* 2(3); 201-206.

Hu G, Guo M, Li W, Du H and Alici G (2011) Experimental investigation of the vibration characteristics of a magnetorheological elastomer sandwich beam under non-homogeneous small magnetic fields. *Smart Materials and Structures* 20; 127001-8.

Huang SC, Inman DJ and Austin EM (1996) Some design considerations for active and passive constrained layer damping treatments. *Smart Materials and Structures* 5(3); 301-13.

Jianting R and Jiesheng J (2003) Active vibration control of an electrorheological sandwich beam. *Mechanics of Electromagnetic Solids* 3; 163-172.

Jolly MR, Bender JW and Carlson JD (1998) Properties and applications of commercial magnetorheological fluids. Thomas Lord Research Center Lord Corporation.

Joshi SB (2012) Vibration study of magnetorheological fluid filled sandwich beams. *International Journal of Applied Research in Mechanical Engineering* 2(2); 100-104.

Kamath GM and Wereley NM (1997) A nonlinear viscoelastic- plastic model for electrorheological fluids. *Smart Materials and Structures* 6; 351–359.

Kang YK, Kim J and Choi SB (2001) Passive and active damping characteristics of smart electro-rheological composite beams. *Smart materials and structures* 10(4); 724-729.

Kciuk M and Turczyn R (2006) Properties and application of magnetorheological fluids. *Journal of Achievements in Materials and Manufacturing Engineering* 18 (1); 127-130.

Kela L and Vähäoja P (2009) Recent studies of adaptive tuned vibration absorbers/neutralizers. Applied Mechanics Reviews 62(6); 060801.

Kim, Y., Wang, K., Lee, H. (1992) Feedback control of ER-fluid-based structures for vibration suppression, *Smart materials and structures* 1; 139.

Kim YK, Koo JH, Kim KS and Kim SH (2011) Suppressing harmonic vibrations of a miniature cryogenic cooler using an adaptive tunable vibration absorber based on magneto-rheological elastomers. Review of Scientific Instruments 82(3); 035103-6.

Kim YK, Koo JH, Kim KS and Kim SH (2011b) Developing a real time controlled adaptive MRE-based tunable vibration absorber system for a linear cryogenic cooler. In Advanced Intelligent Mechatronics (AIM), IEEE/ASME; 287-290.

Kordonsky W, Mastepuro A, Demchuk S and Novikova Z (1994) Electrorheological fluid-based composite materials properties for vibration control in distributed systems. In ICIM'94-International Conference on Intelligent Materials, Colonial Williamsburg, VA; 743-750.

Lara-Prieto V, Parkin R, Jackson M, Silberschmidt V and Kesy Z (2010) Vibration characteristics of MR cantilever sandwich beams: experimental study. *Smart Materials and Structures* 19; 15005-14.

Lee C (1995) Finite element formulation of a sandwich beam with embedded electro-rheological fluids. *Journal of intelligent material systems and structures* 6(5); 718-728.

Lee CY (1992) Dynamic characteristics of a smart beam featuring embedded electro-rheological fluids. 9th International Conference on Mechanical Engineering, CSME, Taiwan; 441-448.

Lee BC and Kim KJ (1999) Shear and normal strain effects of core layers in vibration of square sandwich plates under clamped boundary conditions. *Journal of Sound and Vibrations*. 228 (4); 845-856.

Lee CY and Cheng CC (1998) Dynamic characteristics of sandwich beam with embedded electro-rheological fluid. *Journal of intelligent material systems and structures* 9(1); 60-68.

Lee CY and Cheng CC (2000) Complex moduli of electrorheological material under oscillatory shear. *International journal of mechanical sciences* 42(3); 561-573.

Leissa AW (1969) Vibration of plates, NASA SP-169, Office of Technology Utilization, Washington.

Leng J, Liu Y and Du S (1997) Dynamic characteristics of a beam specimen featuring electrorheological fluids. *Experimental Mechanics* 37; 1–4.

Li W and Zhang X (2008) Research and applications of MR Elastomers. *Recent Patents on Mechanical Engineering* 1; 161-166.

Li WH, Chen G and Yeo SH (1999) Viscoelastic properties of MR fluids. *Smart Materials and Structures* 8; 460–8.

Li JF, Gong XL, Zhang XZ, Xu ZB and Zhang PQ (2005b) Study of adaptive tuned vibration absorber and Its dynamic properties. *Journal of Experimental Mechanics*, 4; 1-10.

Li WH, Du H, Chen G, Yeo SH and Guo N (2003) Nonlinear viscoelastic properties of MR fluids under large-amplitude-oscillatory-shear. *Rheol Acta* 42; 280–286.

Li WH, Zhang PQ, Gong XL and Kosasih (2005) Linear viscoelasticity of MR fluids: dependence on magnetic fields. *International Journal of Modern Physics* 19 (7,8,9); 1198-1204.

Li WH, Zhou Y and Tian TF (2010) Viscoelastic properties of MR elastomers under harmonic loading. *Rheologica acta* 49(7); 733-740.

Liao GJ, Gong XL, Kang CJ and Xuan SH (2011) The design of an active–adaptive tuned vibration absorber based on magnetorheological elastomer and its vibration attenuation performance. *Smart Materials and Structures* 20(7); 1-10.

Liao GJ, Gong XL, Xuan SH, Kang CJ and Zong LH (2012) Development of a real-time tunable stiffness and damping vibration isolator based on magnetorheological elastomer. *Journal of Intelligent Material Systems and Structures* 23(1); 25-33.

Librescu L and Hause T (2000) Recent developments in the modeling and behavior of advanced sandwich constructions: a survey. *Composite structures* 48(1); 1-17.

Lifshitz JM and Leibowitz M (1987) Optimal sandwich beam design for maximum viscoelastic damping. *International Journal of Solids and Structures* 23 (7); 1027-1034.

Lu H and Meng G (2006) An experimental and analytical investigation of the dynamic characteristics of a flexible sandwich plate filled with electrorheological fluid. *The International Journal of Advanced Manufacturing Technology* 28(11-12); 1049-1055.

Lu J and Li Q (2007) Dynamic performance of cantilever mortar beams with embedded Electro-rheological fluids.

Mahjoob MJ, Martin HR and Ismail F (1993) Distributed vibration control using electrorheological fluids. In International Modal Analysis Conference (IMAC) Kissimmee; 68-774.

Mazlan SA, Ekreem NB and Olabi AG (2007) The performance of magnetorheological fluid in squeeze mode. *Smart Materials and Structures*16; 1678-82.

Mead DJ and Markus S (1969) The forced vibration of a three-layer, damped sandwich beam with arbitrary boundary conditions. *Journal of sound and vibration* 10(2); 163-175.

Mead DJ and Markus S (1970) Loss factors and resonant frequencies of encastre damped sandwich beams. *Journal of Sound and Vibration* 12(1); 99-112.

Mikhasev GI, Botogova MG and Korobko EV (2011) Theory of thin adaptive laminated shells based on magnetorheological materials and its application in problems on vibration suppression. In Shell-like Structures; 727-750.

Mindlin RD (1951) Influence of rotary inertia and shear in flexural motion of isotropic elastic plates. *Journal of Applied Mechanics* 18; 31-38.

Mohanty SC (2013) Dynamic stability of a sandwich beam with an Electrorheological fluid core. Asia-pacific international congress on engineering and natural sciences (APICENS-2013), Bangkok, Thailand.

Mohammadi F and Sedaghati R (2012) Dynamic mechanical properties of an electrorheological fluid under large amplitude oscillatory shear strain. *Journal of Intelligent Materials and Structures* 23(10); 1093–1105.

Mohammadi F and Sedaghati R (2012b) Nonlinear free vibration analysis of sandwich shell structures with a constrained electrorheological fluid layer. *Smart Materials and Structures* 21(7); 1-18.

Mohammadi F and Sedaghati R (2012c) Vibration analysis and design optimization of sandwich cylindrical panels fully and partially treated with electrorheological fluid materials. *Journal of Intelligent Material Systems and Structures* 23(15); 1679-1697.

Mohammadi F and Sedaghati R (2012d) Vibration analysis and design optimization of viscoelastic sandwich cylindrical shell. *Journal of Sound and Vibration* 331; 2729–2752.

Mohammadi N, Mahjoob MJ, Kaffashi B, Malakooti S (2010) An experimental evaluation of pre-yield and post-yield rheological models of magnetic field dependent smart materials. *Journal of Mechanical Science and Technology* 24 (9); 1829-1837.

Murata H (2012) Polymerization. In: Gomes AS (ed) InTech, Chapter 17.*DOI: 10.5772/2750*

Narayana VG and Ganesan N (2007) Critical comparison of viscoelastic damping and electrorheological fluid core damping in composite sandwich skew plates. *Composite structures* 80(2); 221-233.

Nashif AD, Jones DIG and Henderson JP (1985) Vibration Damping. New York: John Wiley.

Nayak B, Dwivedy SK and Murthy KSRK (2011) Dynamic analysis of magnetorheological elastomer-based sandwich beam with conductive skins under various boundary conditions. *Journal of Sound and Vibration* 330; 1837–59

Nayak B, Dwivedy SK and, Murthy KSRK (2010) Free vibration control of MRE embedded viscoelastic cored sandwich beam with time varying magnetic field. ASME 10th Biennial Conference on Engineering Systems Design and Analysis, Istanbul, Turkey.

Nayak B, Dwivedy SK and, Murthy KSRK (2012b) Multi-frequency excitation of magnetorheological elastomer-based sandwich beam with conductive skins. *International Journal of Non-Linear Mechanics* 47; 448–460.

Nayak B, Sastri JBS, Dwivedy SK and, Murthy KSRK (2012) A comparative study of the classical and higher order theory for free vibration analysis of MRE cored sandwich beam with composite skins using finite element method. IEEE-International Conference on Advances in Engineering, Science and Management.

Ni YQ, Ying ZG and Chen ZH (2010) Magneto-rheological elastomer (MRE) based composite structures for micro-vibration control. *Earthquake Engineering and Engineering Vibration* 9(3); 345-356.

Ni YQ, Ying ZG and Chen ZH (2011) Micro-vibration suppression of equipment supported on a floor incorporating magneto-rheological elastomer core. *Journal of Sound and Vibration* 330; 4369–4383.

Oyadiji SO (1996) Applications of electro-rheological fluids for constrained layer damping treatment of structures. *Journal of intelligent material systems and structures* 7(5); 541-549.

Panah MA and Hasheminejad SM (2010) Vibration suppression of an elastic plate by use of an electrorheological patch and constraining layer. *The International Journal of Structural Changes in Solids* 2(2); 65-76.

Park YK, Choi SB and Cheong CC (1994) Dynamic modelling and vibration control of smart structures incorporating electro-rheological fluids. Fifth International Conference on Adaptive Structures, Sendai, Japan; 228-237.

Park YK, Choi SB and Jung SB (1998) Shape control of an electrorheological fluid-based smart plate. *In 5th Annual International Symposium on Smart Structures and Materials* (pp. 824-835). International Society for Optics and Photonics.

Phani SA and Venkatraman K (2003) Vibration control of sandwich beams using electro-rheological fluids. *Mechanical systems and signal processing* 17(5); 1083-1095.

Phani SA and Venkatraman K (2005) Damping characteristics of electro-rheological fluid sandwich beams. *Acta mechanica* 180(1-4); 195-201.

Philips RW (1969) Engineering applications of fluid with a variable yield stress PhD thesis

Mechanical Engineering, University of California at Berkeley.

Pranoto T, Nagaya K and Hosoda A (2004) Vibration suppression of plate using linear MR fluid passive damper. *Journal of sound and vibration* 276(3); 919-932.

Qiu J, Tani J and Hajika T (1999) Damping effect of multi-layer beams with embedded electro-rheological fluid. *Journal of intelligent material systems and structures* 10(7); 521-529.

Rahiminasab J and Rezaeepazhand J (2013) Aeroelastic stability of smart sandwich plates with electrorheological fluid core and orthotropic faces. *Journal of Intelligent Material Systems and Structures* 24(5); 669-677.

Rahn C and Joshi S (1998) Modeling and control of an electrorheological sandwich beam. *Journal of Vibration and Acoustics* 120; 221.

Rajamohan V (2013) Vibration analysis of a rotating axially non-homogeneous Magnetorheological fluid sandwich beam. *Transaction of Control and Mechanical Systems* 2(2); 83-91.

Rajamohan V and Natarajan P (2012) Vibration analysis of a rotating Magnetorheological fluid sandwich beam. International Conference on Advanced Research in Mechanical Engineering, Trivendum.

Rajamohan V and Ramamoorthy M (2012) Dynamic characterization of non-homogeneous Magnetorheological fluids based multi-layer beam. *Applied Mechanics and Materials* 110; 105-112.

Rajamohan V, Rakheja S and Sedaghati R (2010b) Vibration analysis of partially treated multi-layer beam with magnetorheological fluid. *Journal of Sound and Vibration* 329; 3451-3469.

Rajamohan, V., Sedaghati, R., Rakheja, S. (2011) Optimal vibration control of beams with total and partial MR-fluid treatments, *Smart materials and structures,* 20 (11); 115016.

Rajamohan V, Sedaghati R and Rakheja S (2010) Vibration analysis of a multi-layer beam containing magnetorheological fluid. *Smart Materials and Structures* 19; 015013-25.

Rajamohan V, Sedaghati R and Rakheja S (2010c) Optimum design of a multilayer beam partially treated with magnetorheological fluid. *Smart Materials and Structures* 19; 0650002-17.

Rajamohan V, Sundararamanb V and Govindarajanb B (2013) Finite element vibration analysis of a Magnetorheological fluid sandwich beam. *Procedia Engineering* 64; 603 – 612.

Rezaeepazhand J and Pahlavan L (2008) Transient response of sandwich beams with electrorheological core. *Journal of Intelligent Material Systems and Structures* 20; 171-179.

Rezaeepazhand J and Pahlavan L (2008b) Transient response of three layer sandwich plate with electrorheological core and orthotropic faces. In 13th European Conference on Composite Materials-ECCM-13.

Ross D, Ungar EE and Kerwin EM (1959) Damping of plate flexural vibrations by means of viscoelastic laminea. *Structural Damping* 3, Ruzicka, ASME.

Sapiński B and Snamina J (2008) Vibration control capabilities of a cantilever beam with a magnetorheological fluid. *Mechanics* 27(2); 70-75.

Sapiński B and Snamina J (2009) Modeling of an adaptive beam with MR fluid. *Solid State Phenomena* 147; 831-838.

Sapiński B, Snamina J and Romaszko M (2010) Identification of model parameters of a sandwich beam incorporating magnetorheological fluid. *Vibration in Physical Systems* 24; 349-354.

Sepehrinour M and Nezami M (2012) Dynamic Response of an Electro-Rheological Sandwich Beam with Different Elastic Layers Subjected to Simultaneous Impact Loads. *Applied Mechanics and Materials* 232; 117-121.

Sinko R, Karnes M, Koo JH, Kim YK and Kim KS (2012) Design and test of an adaptive vibration absorber based on magnetorheological elastomers and a hybrid electromagnet. *Journal of Intelligent Material Systems and Structures* 0(0); 1-10.

Simon TM, Reitich F, Jolly MR, Ito K and Banks HT (2001) The effective magnetic properties of magnetorheological fluids. *Mathematical Computational Modelling* 33; 273-84.

Sims ND, Wereley NM (2003) Modelling of Smart Fluid Dampers. *Smart Materials and Structures, Conf., Passive Damping and Isolation*, SPIE Vol. 5052.

Sims ND, Holmes NJ and Stanway R (2004) A unified modelling and model updating procedure for electrorheological and magnetorheological vibration dampers. *Smart Materials and Structures* 13; 100–121.

Shaw J (2000) Hybrid control of a cantilevered ER sandwich beam for vibration suppression, *Journal of Intelligent Material Systems and Structures* 11(1); 26-31.

Shiang AH and Coulter JP (1994) Controllability and reliability issues related to electrorheological materials adaptive structures. Proceedings of the Second International Conference on Intelligent Materials, Lancaster. PA: Technomic Publishing CO; 1117-1130.

Shiang AH and Coulter JP (1996) A comparative study of AC and DC electrorheological material based adaptive structures in small amplitude vibration. *Journal of intelligent material systems and structures* 7(4); 455-469.

Snamina J (2011) Optimal location of an active segment of magnetorheological fluid layer in a sandwich plate. In Carpathian Control Conference (ICCC), 12th International; 362-365.

Sprecher AF, Carlson JD and Conrad H (1987) Electrorheology at small strains and strain rates of suspensions of silica particles in silicone oil. *Material Science and Engineering* 95; 187–197.

Sprecher AF, Choi Y and Conrad H (1991) Mechanical behavior of ER fluid-filled composites in forced oscillation. In US/Japan Conference on Adaptive Structures, Session E; 560-579.

Stanway R, Sproston JL and El-Wahed AK (1996) Applications of electro-rheological fluids in vibration control: a survey. *Smart Materials and Structures* 5(4); 464-482.

Stevens NG, Sproston, JL and Stanway R (1987) On the mechanical properties of electro-rheological fluids. *Journal of applied mechanics* 54(2); 456-458.

Sun JQ, Jolly MR and Norris MA (1995) Passive, adaptive and active tuned vibration absorbers—a survey. *Journal of mechanical design* 117(B); 234-242.

Sun Q, Zhou J X and Zhang L (2003) An adaptive beam model and dynamic characteristics of magnetorheological materials. *Journal of Sound and Vibration* 261; 456-481.

Tabassian R and Rezaeepazhand J (2011) Stability of smart sandwich beams with cross-ply faces and electrorheological core subjected to axial loads. *Journal of Reinforced Plastics and Composites* 31(1); 55-64.

Tabassian R and Rezaeepazhand J (2013) Dynamic stability of smart sandwich beams with electro-rheological core resting on elastic foundation. *Journal of Sandwich Structures and Materials* 15(1); 25-44.

Tang X and Conrad H (1996) Quasistatic measurements on a magnetorheological fluid. *Journal of Rheology* 0(6);1167–1178.

Tylikowski A (2000) Dynamic stability of electrorheological fluid-filled laminate. *Journal of Theoretical and Applied Mechanics* 38(2); 417-428.

Tylikowski A (2002) Analytical modelling of electrorheological material based adaptive shells. *Journal of Theoretical and Applied Mechanics* 40; 761-773.

Vaicaitis R, Liu S and Jotautienė E (2007) Vibrations of a double wall plane adaptive to electrorheological materials. *Journal of Vibroengineering*, 9(3); 26-30.

Vaičaitis R, Liu S and Jotautienė E (2008) Nonlinear random vibrations of a sandwich beam adaptive to electrorheological materials. *Mechanika.-Kaunas: Technologija* 3(71); 38-44.

Wang DH and Liao WH (2011) Magnetorheological fluid dampers: a review of parametric modelling. *Smart Materials and Structures* 20; 23001-35.

Wang HJ and Chen LL (2003) Vibration and damping analysis of annular plates with constrained damping layer treatments. *Journal of Sound and Vibrations* 264; 893-910.

Wang X and Gordaninejad F (1999) Flow analysis of field-controllable, electro- and magneto-rheological fluids using Herschel-Bulkley model. *Journal of Intelligent Materials and Structures* (10); 601-608.

Wei K, Bai Q, Meng G and Ye L (2011) Vibration characteristics of electrorheological elastomer sandwich beams. *Smart Materials and Structures* 20(5); 1-8.

Wei K, Meng G, Lu H and Zhu S (2005) Dynamic analysis of rotating electrorheological composite beams. International Journal of Modern Physics B 19(07n09); 1236-1242.

Wei K, Meng G, Zhang W and Zhou S (2007) Vibration characteristics of rotating sandwich beams filled with electrorheological fluids. *Journal of Intelligent Material Systems and Structures* 18; 1165-73.

Wei K, Meng G, Zhang W and Zhou S (2008) Experimental investigation on vibration characteristics of sandwich beams with magnetorheological elastomers cores. *Journal of Central South University of Technology* 15; 239-242.

Wei K, Meng G, Zhou S and Liu J (2006) Vibration control of variable speed/acceleration rotating beams using smart materials. *Journal of sound and vibration* 298(4); 1150-1158.

Weiss KD, Carlson JD and Nixon DA (1994) Viscoelastic properties of magneto- and electro-rheological fluid. *Journal of intelligent materials and structures* 5; 772–5.

Weiss KD, Duclos TG and Carlson JD (1993) High strength magneto- and electro-rheological fluids. *SAE Technical Paper Series* 932451; 425–30.

Weiss KD, Duclos TG, Chrzan MJ and Yanyo LC (1996) Magnetorheological fluid composite structures US Patent Specification 5,547,049.

Whittle M, Atkin RJ and Bullough WA (1995) Fluid dynamic limitations on the performance of an Electrorheological clutch. *Journal of Non-Newtonian Fluid* 57; 61-81.

Wilhelm M (2002) Fourier-transform rheology. *Macromolecular Materials and Engineering* 287; 83–105.

Xu Z, Gong X, Liao G and Chen X (2010) An active-damping-compensated magnetorheological elastomer adaptive tuned vibration absorber. *Journal of Intelligent Material Systems and Structures* 21; 1039-47.

Yalcintas M and Coulter JP (1995) An adaptive beam model with electrorheological material based applications. *Journal of Intelligent Material Systems and Structures* 6; 498-507.

Yalcintas M and Coulter JP (1995b) Analytical modeling of electrorheological material based adaptive beams. *Journal of intelligent material systems and structures* 6(4); 488-497.

Yalcintas M and Coulter JP (1995c) Electrorheological material based adaptive beams subjected to various boundary conditions. *Journal of intelligent material systems and structures* 6(5); 700-717.

Yalcintas M and Coulter JP (1998) Electrorheological material based non-homogeneous adaptive beams. *Smart materials and structures* 7(1); 128-143.

Yalcintas M and Dai H (1998) Performance comparison of magnetorheological and electrorheological materials in adaptive structural applications. *Adaptive structures and material systems*, 49-61.

Yalcintas M and Dai H (1999) Magnetorheological and electrorheological materials in adaptive structures and their performance comparison. *Smart Materials and Structures* 8; 560-573.

Yalcintas M and Dai H (2004) Vibration suppression capabilities of magnetorheological materials based adaptive structures. *Smart Materials and Structures* 13; 1-11.

Yalcintas M, Coulter JP and Don DL (1995) Structural modeling and optimal control of electrorheological material based adaptive beams. *Smart Materials and Structures* 4(3); 207.

Yanju L, Hejun D and Dianfu W (2001) ER fluid based on inorganic/ polymer blend particles and its adaptive viscoelastic properties. *Colloids and Surfaces A: Physicochemical and Engineering Aspects* 189; 203–210.

Yao GZ, Yap FF, Chen G, Li WH and Yeo SH (2002) MR damper and its application for semi-active control of vehicle suspension system. *Mechatronics*. 12; 963-973.

Yeh JY (2007) Vibration analyses of the annular plate with electrorheological fluid damping treatment. *Finite Elements in Analysis and Design* 43(11); 965-974.

Yeh JY (2007b) Vibration control of a sandwich annular plate with an electrorheological fluid core layer. *Smart Materials and Structures* 16(3); 837.

Yeh JY (2010) Vibration and damping characteristics analysis of a rotating annular plate with electrorheological treatment. *Smart Materials and Structures* 19(8); 1-8.

Yeh JY (2010b) Dynamic stability control analysis of sandwich annular plate with electrorheological core treatment. *Journal of Engineering Technology and Education* 7(4); 618-627.

Yeh JY (2011) Free vibration analysis of rotating polar orthotropic annular plate with ER damping treatment. *Composites Part B: Engineering* 42(4); 781-788.

Yeh JY (2011b) Vibration and damping analysis of orthotropic cylindrical shells with electrorheological core layer. *Aerospace Science and Technology* 15(4); 293-303.

Yeh JY (2012) Active dynamic instability control analysis of polar orthotropic sandwich annular plate with electrorheological fluid damping treatment. *Journal of Engineering Technology and Education* 9(3); 290-299.

Yeh JY (2013) Vibration analysis of sandwich rectangular plates with magnetorheological elastomer damping treatment. *Smart Materials and Structures* 22(3); 1-8.

Yeh JY and Chen LW (2004) Vibration of a sandwich plate with a constrained layer and electrorheological fluid core. *Composite structures* 65(2); 251-258.

Yeh JY and Chen LW (2005) Dynamic stability of a sandwich plate with a constraining layer and electrorheological fluid core. *Journal of sound and vibration* 285(3); 637-652.

Yeh JY and Chen LW (2006) Dynamic stability analysis of a rectangular orthotropic sandwich plate with an electrorheological fluid core. *Composite structures* 72(1); 33-41.

Yeh JY and Chen LW (2007) Finite element dynamic analysis of orthotropic sandwich plates with an electrorheological fluid core layer. *Composite structures* 78(3); 368-376.

Yeh JY, Chen LW and Wang CC (2004) Dynamic stability of a sandwich beam with a constrained layer and electrorheological fluid core. *Composite structures* 64(1); 47-54.

Yeh JY, Chen JY, Lin CT and Liu, CY (2009) Damping and vibration analysis of polar orthotropic annular plates with ER treatment. *Journal of Sound and Vibration* 325(1); 1-13.

Yeh ZF and Shih YS (2005) Critical load, dynamic characteristics and parametric instability of electrorheological material-based adaptive beams. *Computers & structures* 83(25); 2162-74.

Yeh ZF and Shih YS (2006) Dynamic characteristics and dynamic instability of Magnetorheological material-based adaptive beams. *Journal of Composite Materials* 40: 1333-58.

Yeh ZF and Shih YS (2006b) Dynamic stability of a sandwich beam with Magnetorheological core. *Mechanics Based Design of Structures and Machines* 34; 181–200.

Yen WS and Achorn PJ (1991) A Study of the Dynamic Behavior of an Electrorheological Fluid. *Journal of Rheology* 35; 1375–1384.

Yin HM, Sun LZ and Chen JS (2006) Magneto-elastic modeling of composites containing chain-structured magnetostrictive particles. *Journal of the Mechanics and Physics of Solids* 54(5); 975–1003.

Ying ZG and Ni YQ (2009) Micro-vibration response of a stochastically excited sandwich beam with a magnetorheological elastomer core and mass. *Smart Materials and Structures* 18; 95005-18.

Ying ZG, Chen H and Ni Y (2012) Magnetorheological visco-elastomer and its application to suppressing microvibration of sandwich plates. In Third International Conference on Smart Materials and Nanotechnology in Engineering. International Society for Optics and Photonics.

Ying ZG, Ni YQ and Ye SQ (2014) Stochastic micro-vibration suppression of a sandwich plate using a magneto-rheological visco-elastomer core. *Smart Materials and Structures* 23(2); 1-11.

Zhang X and Li W (2009) Adaptive tuned dynamic vibration absorbers working with MR elastomers. *Smart Structures and Systems* 5(5); 517-529.

Zheng H, Cai C and Tan XM (2004) Optimization of partial constrained layer damping treatment for vibrational energy minimization of vibrating beams. *Computers and Structures* 82; 2493-2507.

Zhou GY and Li JR (2003) Dynamic behavior of a magnetorheological elastomer under uniaxial deformation: I. Experiment. *Smart Materials and Structures* 12; 859-872.

Zhou GY and Wang Q (2005) Magnetorheological elastomer-based smart sandwich beams with nonconductive skins. *Smart Materials and Structures* 14; 1001-1009.

Zhou GY and Wang Q (2006) Study on the adjustable rigidity of magnetorheological-elastomer-based sandwich beams. *Smart Materials and Structures* 15; 59-74.

Zhou GY and Wang Q (2006b) Use of magnetorheological elastomer in an adaptive sandwich beam with conductive skins. Part II: Dynamic properties. *International Journal of Solids and Structures* 43; 5403–5420.

Zhou GY and Wang Q (2006c) Use of magnetorheological elastomer in adaptive sandwich beam with conductive skins—part I: magnetoelastic loads in conductive skins. *International Journal of Solids and Structures* 43; 5386–5402.

Zhou GY, Lin KC and Wang Q (2006) Finite element studies on field-dependent rigidities of sandwich beams with magnetorheological elastomer cores. *Smart Materials and Structures* 15; 787-791.

Appendix

Shape functions:

$$N_w(x, y) = [w_1, w_2, w_3, w_4]$$ $$\qquad N_{u_1}(x, y) = [u_{11}, u_{12}, u_{13}, u_{14}]$$ (A.1-2)

$$N_{v_1}(x, y) = [v_{11}, v_{12}, v_{13}, v_{14}]$$ $$\qquad N_{u_3}(x, y) = [u_{31}, u_{32}, u_{33}, u_{34}]$$ (A.3-4)

$$w_i = [0, 0, 0, 0, n_i(x, y), n_{i+4}(x, y), n_{i+8}(x, y)], \quad i = 1, ..., 4$$ $$\qquad N_{v_3}(x, y) = [v_{31}, v_{32}, v_{33}, v_{34}]$$ (A.5-6)

$$u1i = [n_{12+i}(x, y), 0, 0, 0, 0, 0, 0], \quad i = 1, ..., 4$$ $$\qquad u3i = [0, 0, n_{12+i}(x, y), 0, 0, 0, 0], \quad i = 1, ..., 4$$ (A.7-8)

$$v1i = [0, n_{12+i}(x, y), 0, 0, 0, 0, 0], \quad i = 1, ..., 4$$ $$\qquad v3i = [0, 0, 0, n_{12+i}(x, y), 0, 0, 0], \quad i = 1, ..., 4$$ (A.9-10)

$$n_1(x, y) = \frac{1}{8}\left(1 - \frac{x}{a}\right)\left(1 - \frac{y}{b}\right)\left(2 - \frac{x}{a} - \frac{x^2}{a^2} - \frac{y}{b} - \frac{y^2}{b^2}\right)$$ $$\qquad n_2(x, y) = \frac{1}{8}\left(1 + \frac{x}{a}\right)\left(1 - \frac{y}{b}\right)\left(2 + \frac{x}{a} - \frac{x^2}{a^2} - \frac{y}{b} - \frac{y^2}{b^2}\right)$$ (A.11-12)

$$n_3(x, y) = \frac{1}{8}\left(1 + \frac{x}{a}\right)\left(1 + \frac{y}{b}\right)\left(2 + \frac{x}{a} - \frac{x^2}{a^2} + \frac{y}{b} - \frac{y^2}{b^2}\right)$$ $$\qquad n_4(x, y) = \frac{1}{8}\left(1 - \frac{x}{a}\right)\left(1 + \frac{y}{b}\right)\left(2 - \frac{x}{a} - \frac{x^2}{a^2} + \frac{y}{b} - \frac{y^2}{b^2}\right)$$ (A.13-14)

$$n_5(x, y) = \frac{1}{8}b\left(1 - \frac{x}{a}\right)\left(1 - \frac{y}{b}\right)\left(1 - \frac{y^2}{b^2}\right)$$ $$\qquad n_6(x, y) = \frac{1}{8}b\left(1 + \frac{x}{a}\right)\left(1 - \frac{y}{b}\right)\left(1 - \frac{y^2}{b^2}\right)$$ (A.15-16)

$$n_7(x, y) = -\frac{1}{8}b\left(1 + \frac{x}{a}\right)\left(1 + \frac{y}{b}\right)\left(1 - \frac{y^2}{b^2}\right)$$ $$\qquad n_8(x, y) = -\frac{1}{8}b\left(1 - \frac{x}{a}\right)\left(1 + \frac{y}{b}\right)\left(1 - \frac{y^2}{b^2}\right)$$ (A.17-18)

$$n_9(x, y) = \frac{1}{8}a\left(1 - \frac{x}{a}\right)\left(1 - \frac{y}{b}\right)\left(1 - \frac{x^2}{a^2}\right)$$ $$\qquad n_{10}(x, y) = -\frac{1}{8}a\left(1 + \frac{x}{a}\right)\left(1 - \frac{y}{b}\right)\left(1 - \frac{x^2}{a^2}\right)$$ (A.19-20)

$$n_{11}(x, y) = -\frac{1}{8}a\left(1 + \frac{x}{a}\right)\left(1 + \frac{y}{b}\right)\left(1 - \frac{x^2}{a^2}\right)$$ $$\qquad n_{12}(x, y) = \frac{1}{8}a\left(1 - \frac{x}{a}\right)\left(1 + \frac{y}{b}\right)\left(1 - \frac{x^2}{a^2}\right)$$ (A.21-22)

$$n_{13}(x, y) = \frac{1}{4}\left(1 - \frac{x}{a}\right)\left(1 - \frac{y}{b}\right)$$ $$\qquad n_{14}(x, y) = \frac{1}{4}\left(1 + \frac{x}{a}\right)\left(1 - \frac{y}{b}\right)$$ (A.23-24)

$$n_{15}(x, y) = \frac{1}{4}\left(1 + \frac{x}{a}\right)\left(1 + \frac{y}{b}\right)$$ $$\qquad n_{16}(x, y) = \frac{1}{4}\left(1 - \frac{x}{a}\right)\left(1 + \frac{y}{b}\right)$$ (A.25)